COMPARATIVE STUDY OF PHOTOGENERATED ISOMERIC QUINONE METHIDES AND INNOVATIVE SOLUTIONS FOR POLYESTER PLASTIC POLLUTION

by

AYESHA SIDDIKA MOHAMED MOHIDEEN NISATHAR

(Under the Direction of Vladimir V. Popik)

ABSTRACT

Quinone methides (QM) are analogs of quinones with a benzylic methylene group in place of one of the carbonyl oxygens. Isomeric ortho- and para-quinone methides, while possessing similar electronic structures, show very different properties. o-Quinone methides (oQM) are more reactive towards nucleophiles and undergo efficient inverse electron-demand-Diels-Alder (IEDDA) reaction with electron-rich alkenes. p-Quinone methide (pQM), while also acting as Michael acceptors, is not reactive in IEDDA. Chapter One is an overview of reactions, generation methods, types of QMs, their applications, and the goals of the research projects.

Our research group is interested in exploring applications of o-naphthoquinone methides (o-NQMs) that are photochemically generated from (3-hydroxynaphthalen-2-yl)methanol (o-NQMP) derivatives using UV-A light. Chapter two describes the photochemistry of a novel QM system that can produce both o-NQM and p-QM upon irradiation with UV-A light. These photogenerated QMs are conjugated to an aromatic system at the methide position, and the reactivity of such conjugated QMs has not been

explored previously. Herein, a detailed study of the photophysical properties and photoreactivity of novel Quinone methide precursor (QMP) , as well as their comparison with two structural analogs is reported. Additionally, chapter two discusses the potential applications of the novel QMP and its structural analogs as fluorophores for imaging techniques.

Polyethylene terephthalate (PET) is one of the world's most widely used plastics. While PET is thermoplastic, and therefore, is potentially recyclable, the recycling rate is low. Huge quantities of this non-biodegradable polymer end up in the environment casing significant damage. Chapter three elaborates on our effort to develop a photodegradable analog of PET by incorporating a suitable o-NQMP-based photocleavable linker into the macromolecule. This “end-of-life” engineered PET analog can be depolymerized using powerful UV lamps for subsequent re-use and has faster rates of degradation in the environment under sunlight than PET.

The most preferred method for PET recycling is chemical depolymerization, where the polymer is cleaved back into original monomers. However, the process requires a catalyst for efficient and complete depolymerization. Chapters four and five describe the feasibility studies of using thiols and bases as inexpensive catalysts for PET recycling.

INDEX WORDS: Ortho-Naphthoquinone Methide, Kinetics of conjugated quinone methides, Fluorescent dyes, Photodegradable polymer, Poly(ethylene terephthalate)/PET recycling, Thiol catalyzed ester hydrolysis, PET alkaline solvolysis

COMPARATIVE STUDY OF PHOTOGENERATED ISOMERIC QUINONE METHIDES AND INNOVATIVE SOLUTIONS FOR POLYESTER PLASTIC POLLUTION

by

AYESHA SIDDIKA MOHAMED MOHIDEEN NISATHAR

BS, University of Peradeniya, Sri Lanka, 2017

A Dissertation Submitted to the Graduate Faculty of The University of Georgia in Partial Fulfillment of the Requirements for the Degree

DOCTOR OF PHILOSOPHY

ATHENS, GEORGIA

2023

COMPARATIVE STUDY OF PHOTOGENERATED ISOMERIC QUINONE METHIDES AND INNOVATIVE SOLUTIONS FOR POLYESTER PLASTIC POLLUTION

by

AYESHA SIDDIKA MOHAMED MOHIDEEN NISATHAR

Major Professor:	Vladimir V. Popik
Committee:	Robert S. Phillips
	Richard W. Morrison

Electronic Version Approved:

Ron Walcott
Vice Provost for Graduate Education and Dean of the Graduate School
The University of Georgia
May 2023

DEDICATION

I dedicate my Doctor of Philosophy (Ph.D.) work to all my family members, my Dad, Mohamed Mohideen Nisathar; my Mom, Lailathul Munawwara; my Sister, Fathima Razana, and my Brother, Mohamed Ajmal, who has had the most significant impact on my life because of their unwavering love and support.

ACKNOWLEDGEMENTS

First, I would like to express my profound gratitude to my research advisor, professor Vladimir Popik, for teaching me the fundamentals of advanced Photochemistry concepts and transferring knowledge without hesitance.

Second, I thank my research committee members, professor Robert Phillips, and Richard Morrison, for their time and valuable suggestions to improve my research work.

Third, I thank all past group members of the Popik research group, Dr. Mariia Sutton, Dr. Kun Wang, Dr. Shubham Sharma, Dr. Chris Molnar, Dr. Nannan Lin, Dr. Zichun Ren, Shrey Patel for teaching me the research skills that I was not familiar with before and helping me in troubleshooting instruments whenever needed. It was also a great pleasure working with all the current members of the Popik research group, Rohan Bhavsar, and Patric Foster.

Fourth, I would like to thank all UGA research facilities members who supported me in my experiments promptly. I want to acknowledge Dr. Jason Locklin and his research group member, Ryan Maynard, for their support and for allowing me to use the equipment for the PET recycling project. I want to thank Dr. Dennis Phillips, Dr. Chau-wen Chou, and Dr. Kevin Clark for their support in getting mass spectral analysis. I also thank Dr. Dongtao Cui, Dr. John Glushka, and Earle Raymond Adams for their support in NMR training and help with research.

Finally, I thank everyone at the University of Georgia and outside who encouraged and motivated me throughout the graduate school journey.

TABLE OF CONTENTS

Page

LIST OF TABLES

Page

LIST OF FIGURES

Page

LIST OF SCHEMES

Page

LIST OF ABBREVIATIONS

QMP/QM	Quinone methide precursor/quinone methide
NQMP/NQM	Naphthoquinone methide precursor/naphthoquinone methide
IEDDA	Inverse electron demand Diels-Alder
EVE	Ethyl vinyl ether
PET	Poly(ethylene terephthalate)
TPA	Terephthalic acid
EG	Ethylene glycol
2-ME	2-Mercaptoethanol
3-MPA	3-Mpercaptopropionic acid
4-MBA	4-Mercaptobenzoic acid
TP	Thiophenol
DEAET	Diethylaminoethanethiol
TC	Thiocholine
TFET	1,1,1-Trifluoroethanethiol
BHET	Bishydroxyethyl terephthalate
DMT	Dimethyl terephthalate
MHET	Monohydroxyethyl terephthalate
HEMT	Hydroxyethyl methyl terephthalate
MMT	Monomethyl terephthalic acid
HFIP	1,1,1,1,1,1-Hexafluroisopropanol

CHAPTER 1

INTRODUCTION

1.1. Quinone Methides: Background, Reactivity and Applications

Quinone methides (QM) are important intermediates in many biochemical processes and synthetic procedures.[1–4] QMs belong to the category of transient species due to its high reactivity, and short-lived nature. Therefore, QMs cannot be isolated, or stored and must be generated *in-situ*. The initial hypothesis for the existence of QM was reported by Fries et. al in 1907.[5,6] QMs structure contains cyclohexadiene core with exocyclic methylene and carbonyl moieties. There are two isomers of the parent quinone methide; *ortho*- (*o*QM) and *para*- (*p*QM) based on the relative position of the methylene and carbonyl groups.[7] Structurally, o- and pQM resonate between neutral (**1.1** and **1.2**) and zwitterionic forms (**1.1a** and **1.2a**) due to conjugation. (Scheme 1.1).

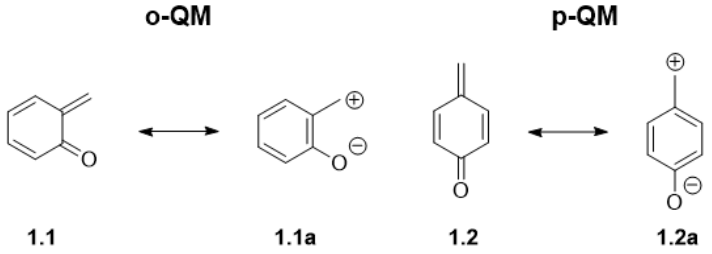

Scheme 1.1. Isomers of parent quinone methides.

Conjugation between the exocyclic double bond and the carbonyl group in oQM and pQM makes benzylic carbon very electrophilic. Both isomers of QM undergo Michael addition in direct analogy with α,β-unsaturated carbonyl compounds. However, the rate of nucleophilic addition is much higher for QM, as it is accompanied by the re-aromatization.

oQMs show 1,4-Michael addition and p-QM show 1,6-Michael addition with nucleophiles (NuH) leading to the products **1.3** and **1.4** respectively (Scheme 1.2). oQM is sterically more hindered and has a greater dipole moment compared to pQM.[5] Therefore, oQM is less stable and significantly more reactive in Michael addition than pQM. The lifetime of oQM and pQM in aqueous solution are $2x10^{-3}$ s and 0.3 s, respectively. The hydration reactivity rate constant for oQM is $2.6x10^{2}$ s^{-1} and that for pQM is 3.3 s^{-1}.[8–10]

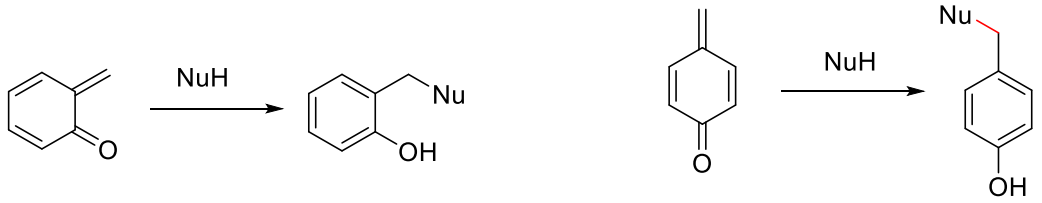

1.1 **oQM** **1.3** **1.2** **pQM** **1.4**

Scheme 1.2. Michael addition to the isomers of the parent quinone methide.

The main difference between the *ortho*- and *para*- isomers of quinone methide is the ability of oQM to undergo [4+2] cycloaddition or Inverse Electron Demand Diels-Alder reaction (IEDDA) with electron-rich polarized alkenes producing chroman derivatives, **1.5** (Scheme 1.3).

1.1 **1.5**

Scheme 1.3. Ortho-quinone methide (oQM) in IEDDA.

High reactivity of QMs towards nucleophiles has been successfully employed in organic synthesis and in biochemistry in broad range of organic reactions, specifically for building natural products.[11,2,12] The electrophilic nature of QMs has been utilized in

biological systems where QMs react with amino acids, proteins, nucleobases and DNA making them excellent antiproliferative agents. The ability of QMs to alkylate DNA has been utilized in DNA crosslinking agents, and reversible covalent modification of DNA by Rokita and co-workers. [13,14]

1.2. Generation Methods of o-QM

Numerous approaches to producing QMs from different precursors have been documented. In this section, examples of oQM generation methods will be discussed, where similar methods are used for pQM generation. oQM generation methods can be classified into two main categories, non-photochemical methods,[2,15,11] and photochemical methods (Scheme 1.4).[8] Non-photochemical methods include thermal,[16] oxidation,[17] acid[18] or base-catalyzed,[19] and β elimination in the presence of a nucleophile[20] using suitable Quinone Methide Precursors (QMPs). All of these methods often extremely high reaction temperature, long reaction time, difficulties in precursor synthesis and requirement of a catalyst.[21]

On the other hand, photochemical generation of QMs is a far more benign method that is especially applicable in biological systems due to temporal and spatial control.[22] Additionally, photo-generated QMs can be characterized and reaction kinetics can be studied spectroscopically to obtain more information about the existence and the formation mechanism of QMs.[23] Wan and coworkers were the first to describe the photochemical production of simple quinone methides by dehydration of (hydroxymethyl) phenols (**1.11**).[24] The other common photochemical methods use various leaving groups at the methyl position (**1.12**): alkoxy groups (OR), acetate groups (OCOR),[10] Mannich bases

(**1.13**),[25] quaternary ammonium salt derivatives (**1.14**)[26], hydroxystyrenes (**1.15**)[22] and lactones (**1.16**).[27]

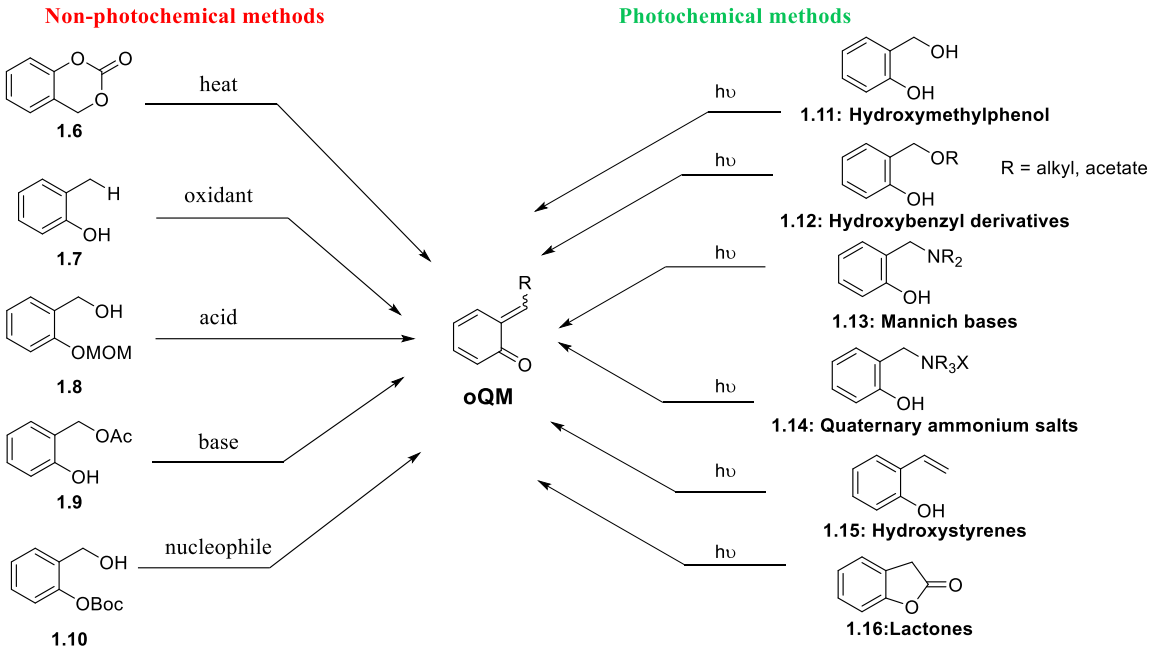

Scheme 1.4. oQM generation methods.

The efficiency of photogeneration is highly dependent on the leaving group. The main parameter that shows the efficiency of QM generation from QMPs is the quantum yield. Saito was the first to study photochemistry of QMPs with Mannich bases and found a high yield compared to that of phenol analogs in 50% aqueous acetonitrile solution (Φ = 0.57 vs 0.23).[25] Freccero, then developed QMPs with quaternary ammonium salt leaving group as a novel method and to reduce the side-effects associated with the leaving group, Mannich base such as nucleophilic nitrogen reacting with other electrophiles in biological media or reacting with transient QM itself. They reported 4-times higher quantum yield when the leaving group is quaternary ammonium salt (Φ = 0.98) compared to phenol (Φ = 0.23).[26] Additionally, the quantum yield is dependent on the substituents in the QMP. Hydroxybenzyl alcohol has a low quantum yield compared to α-phenylhydroxybenzyl

alcohol; Φ = 0.23 vs 0.46.[9] Photolysis of hydroxy styrene and lactones are also used to photo-generate QMs.[28,29] Among these methods, photodehydration of (hydroxymethyl)phenol is the most useful in oQM generation as it regenerates the starting material back in aqueous medium, and no loss of starting material (Scheme 1.5).[9]

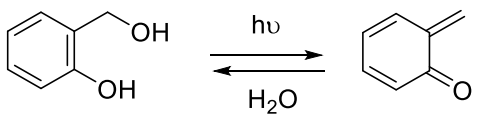

1.11 **1.1**

Scheme 1.5. Photochemical generation of o-QM from o-(hydroxymethyl)phenol.

1.3. Photochemical Generation and Importance of NQMP

An important parameter in photochemical reaction for the generation of QMs is the wavelength of light that is needed for the generation of QM. The precursor, o-(hydroxymethyl)phenol has maximum absorbance below 250 nm and is not suitable for biomedical applications. Quinone methides generated on a naphthoquinone methide precursor systems show red-shift in the absorption spectra compared to o-(hydroxylbenzyl) based systems. Two isomeric forms of o-naphthoquinone methide precursors (oNQMPs), and 3-hydroxy-2-naphthalenemethanol (**1.17**) and 2-hydroxy-1-naphthalenemethanol (**1.19**) to photogenerate o-naphthoquinone methides (oNQMs), 2,3-naphthoquinone-3-methide (**1.18**) and 1,2- naphthoquinone-1-methide (**1.20**) has been first studied and reported by Popik et. al (Scheme 1.6).[30] Both reactions occur upon irradiation with 300-350 nm light.

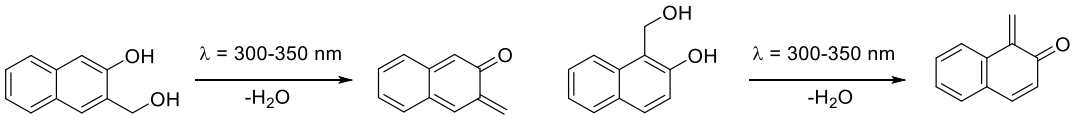

1.17 **1.18** **1.19** **1.20**

Scheme 1.6. Regioisomers of o-NQMPs and respective o-NQMs.

Apart from the benefit of long wavelength activation, oNQMP photochemistry can be used as photolabile protecting group (PPG) for alcohols, phenols, and carboxylic acids. Our research group has successfully demonstrated the use of 3-(Hydroxymethyl)-2-naphthol derivatives (**1.21-1.27**) in protecting simple groups such as ethanol, phenol and benzoic acid. Additionally, our research group has showed the release of some biologically important molecules such as progesterone, dimethyl thymidine, estrogen, and N-Boc protected phenyl alanine (Scheme 1.7). Substrate release and photogeneration of oNQM, **1.18** occurs rapidly with a good quantum yield, and high chemical yields. In aqueous medium, in the absence of other nucleophiles, oNQM undergoes rapid hydration (144 s^{-1}) to form **1.17**. In the presence of nucleophiles, thiols, or azides, o-NQM rapidly forms nucleophilic adducts, **1.28** and **1.29** with second-order rate constants $2.2x10^5$ $M^{-1}s^{-1}$, and $2x10^4$ $M^{-1}s^{-1}$ respectively. Additionally, oNQM reaction with ethyl vinyl ether (EVE) in IEDDA reaction to generate chroman adduct, **1.30** was experimentally proved by the authors and the rate constant for IEDDA reaction with ethyl vinyl ether is $4.1x10^4$ $M^{-1}s^{-1}$.[31]

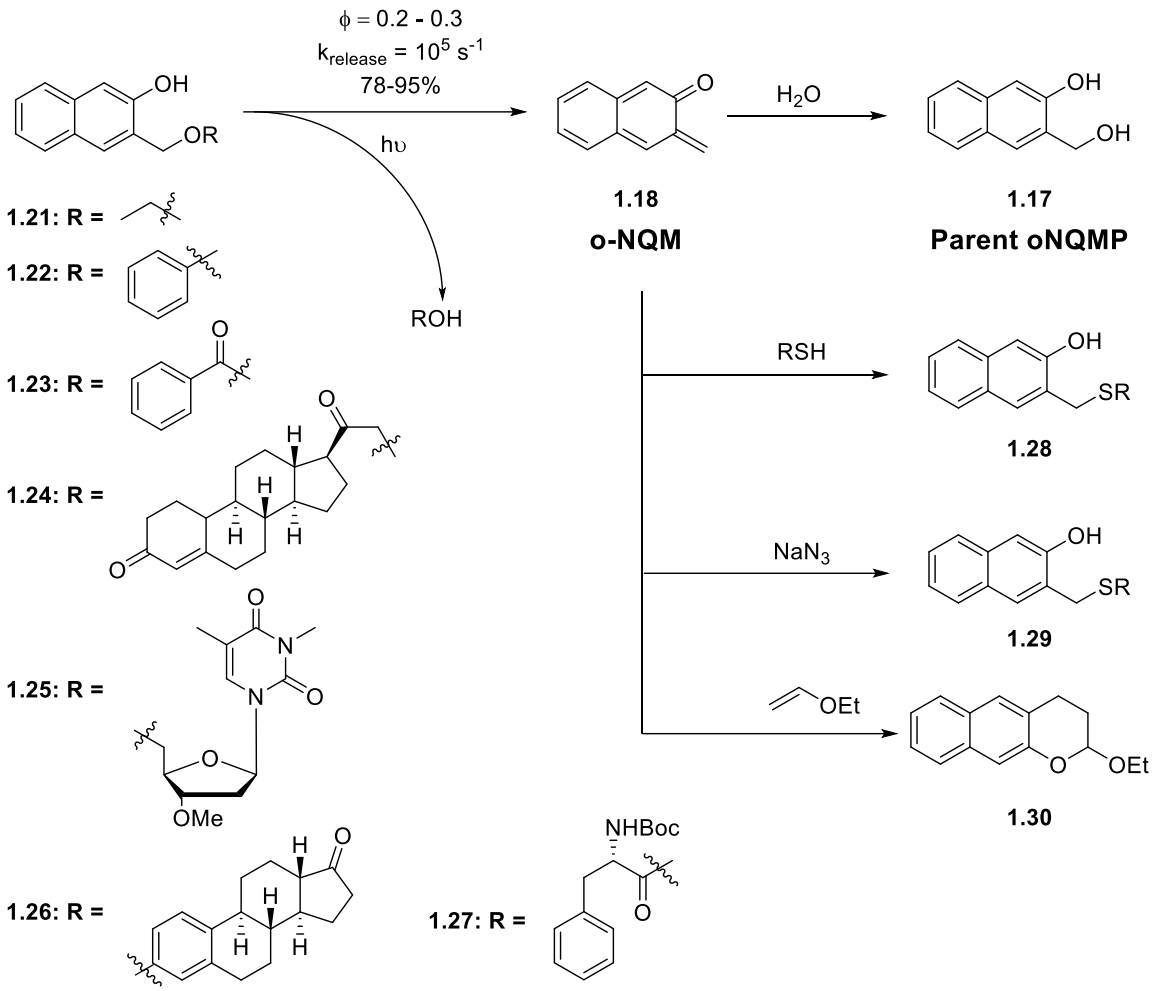

Scheme 1.7. The use of o-NQMP as a photolabile protecting group.

In 2010, Freccero and colleagues have reported the synthesis and the photochemical generation of pNQM or 2,6-naphthoquinone-6-methide, (**1.32**) from a pNQMP, (**1.31);** (Scheme 1.8).[32] The chromophore has a maximum absorbance of 310-330 nm, similar to oNQMP.

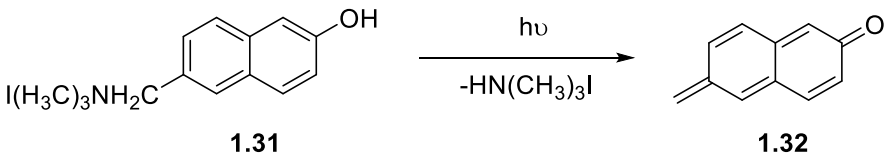

Scheme 1.8. p-NQM photogeneration from p-NQMP.

It should be noted that in 2004 Wan, Corrie and co-workers have reported the photogeneration of 1,5-naphthoquinone methide (1,5-NQM, **1.34**) derivative from 5-(1-hydroxyethyl)naphthalen-1-ol, **1.33** (Scheme 1.9A). 1,5-NQM cannot be classified as o-, or p-QM. However, authors have employed long wavelength (300-350 nm) for activation which is a feature of NQMPs, mentioned future perspective and benefits of NQMP for photogeneration of NQMs. Additionally, authors have attempted the photogeneration of 1,4-naphthoquinonemethide, **1.36** from 4-(1-hydroxyethyl)naphthalen-1-ol, **1.35** and were unsuccessful (Scheme 1.9B).[33]

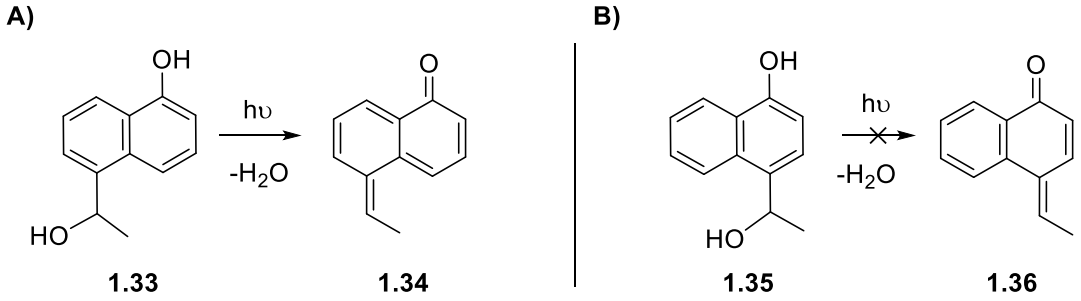

Scheme 1.9. Photochemical generation of other NQMs.

1.4. Mechanism of QM and NQM Photogeneration

The mechanism for oQM formation in aqueous medium was first proposed by Wan and co-workers based on quantum yield measurements for the formation of oQM, α-phenyl-o-quinone methide, **1.41** from oQMP, 2-(hydroxy(phenyl)methyl)phenol, **1.37** at different pH profile. At low pH (<8), oQMP is excited to **1.39** where it readily deprotonates to generate the excited state phenolate anion, **1.40** due to low pKa of excited state oQMP (pK_a = 2.5) in comparison to the ground state oQMP (pK_a = 9.8). At high pH (8-12), oQM, **1.41** formation occurs via photoexcitation of the readily available **1.38** to **1.40**. Loss of hydroxide ion from **1.40** results in the formation of the final product, oQM, **1.41**. The authors have also proposed the possibility of oQM formation via the carbocation, **1.42**. However, the effect of the latter path may not be significant (Scheme 1.10).[23,24] A concerted mechanism is possible in organic solvents; it was not observed in partially or wholly aqueous solution. However, a stepwise mechanism also cannot be eliminated.

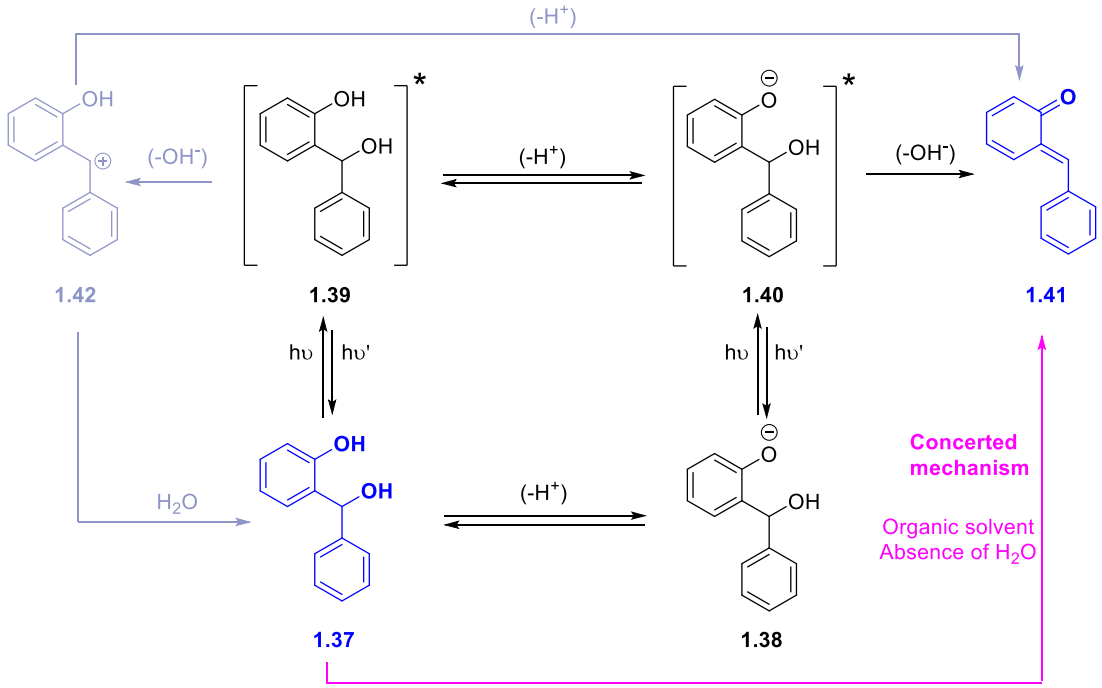

Scheme 1.10. Possible routes of oQM photogeneration.

The excited state deprotonation to form phenolate can occur via Excited State Intramolecular Proton Transfer (ESIPT) or via Excited State Proton Transfer (ESPT). In ESIPT, the phenolic proton in **1.37** is transferred to alkyl hydroxy group via intramolecular hydrogen bonding (Scheme 1.11 left). ESPT is a process where the phenolic proton in **1.37** is transferred to the protic solvent/water (Scheme 1.11 right). Wan and co-workers hypothesized that the ionization step is a water-assisted pathway based on their experiment results in various ratios of acetonitrile: water. Additionally, Wan reported inability to photo-generate pQM in neat acetonitrile is due to the distance between phenol and hydroxy groups are too large to undergo ESIPT and absence of water prohibits the occurrence of ESPT.[23] Therefore, ESIPT occurs in aprotic solvents where hydrogen bonding is minimal and ESPT is favored in polar protic solvents.[34]

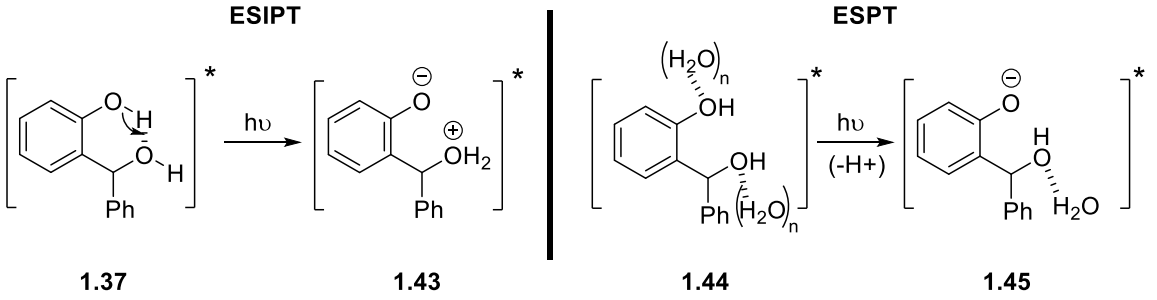

Scheme 1.11. ESIPT (left) vs ESPT (right).

In 2018, Basaric and co-workers reported a the mechanism of oQM, **1.1** formation from the parent oQMP, 2-(hydroxymethyl)phenol, **1.11** based on spectroscopic evidence and using computational analysis.[34] They have proved that QMs are formed via singlet excited states. They have attempted to observe any plausible precursor to oQM such as the naphthoxete, **1.40** analog in the photogeneration of oNQM from oNQM (*Vide infra*). Instead, they observed simultaneous photogeneration of a phenoxy radical, **1.48** from the

excited state oQMP, **1.46** via homolytic cleavage and the formation of oQM, **1.1** via elimination of water Scheme 1.12). Photogenerated phenoxy radical at 400 nm decayed very fast in comparison to oQM at 267 nm ($2x10^9$ M^{-1} s^{-1} vs $2.6x10^2$ s^{-1}) which were detected by nanosecond transient absorption spectroscopy (ns-TAS) and femtosecond (fs-TAS), respectively. Computational studies showed a high energy barrier between oQMP and the benzoxete, **1.47** (29.3 $kcalmol^{-1}$) in comparison to QMP and oQM (16.4 $kcalmol^{-1}$) which explains the reason for oQM formation without an intermediate. However, they claimed the possible equilibrium between oQM, **1.1** and the benzoxete, **1.47** (Scheme 1.13). They reported oQM, **1.1** is more stable than the benzoxete, **1.47**.

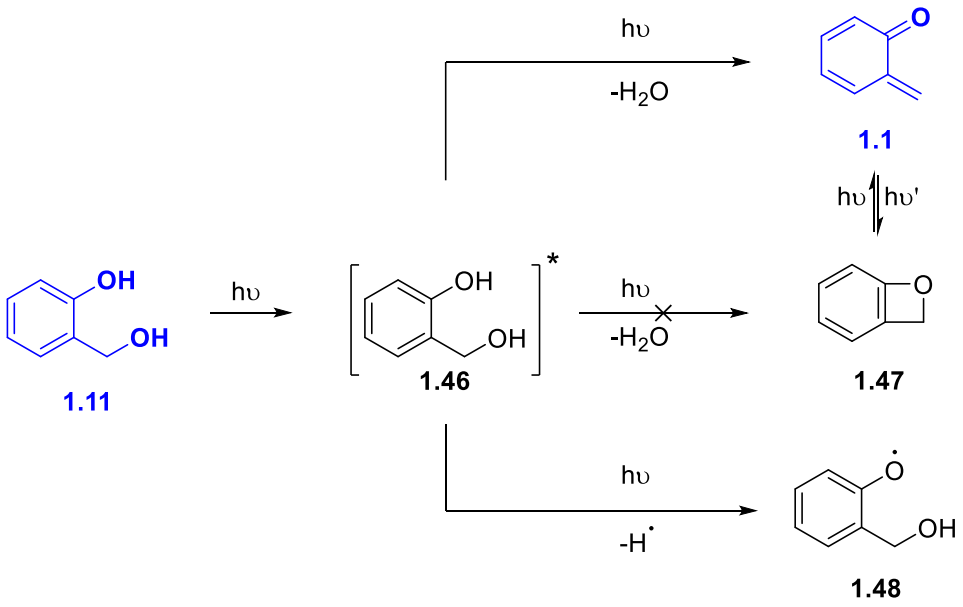

Scheme 1.12. Mechanism for the photolysis formation of parent oQM.

Prior to Basaric, in 2009, our research group has attempted to elucidate the mechanism of oNQM, **1.52** photo-generation from the precursor, oNQMP, **1.17** employing laser flash photolysis and density functional theory (DFT) calculations.[30] The parent oNQMP, **1.17** has a pK_a of 9.01 and the excited state has a pK_a of 0.77. We also proposed

the two-step mechanism of ionization of the excited state followed by dihydroxylation to generate oNQM, **1.52**. Furthermore, we reported the absence of ESIPT and a precursor to the oNQM which is naphthoxete intermediate, **1.51** (Scheme 1.13).

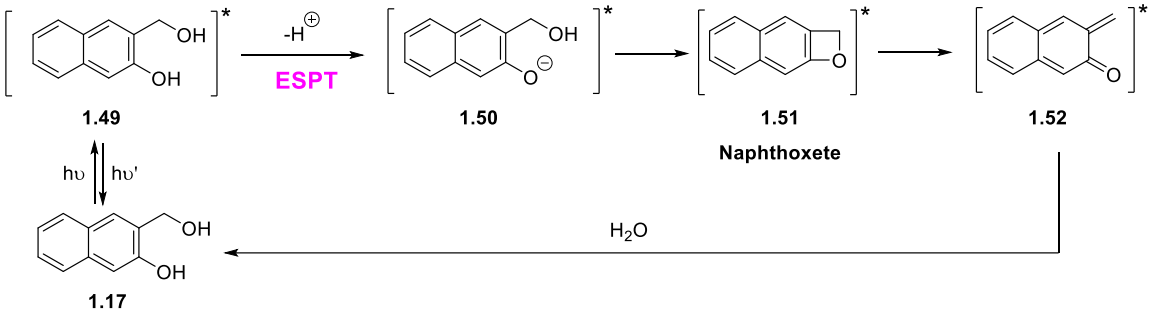

Scheme 1.13. oNQM photogeneration mechanism.

Many research groups have synthesized various derivatives of QMPs later and stated that the mechanism is highly dependent on the ring system of which the QM is generated (e.g., phenyl vs naphthyl) and substituents in the ring system. Therefore, a unique mechanism for the photogeneration of all oQM types cannot be provided and even the parent oQM formation mechanism is still under debate between the scholars.

1.5. Types of QMs, Reactivity and Stability

Characterization and studying reaction kinetics of QMs has been the key interest for physical organic chemist since a detailed study was first reported by Wan. Laser Flash Photolysis (LFP) enables the photochemical generation and the study of short-lived transient species. Attempts were made to improve photophysical properties such as activation/photolysis wavelength (λ_{max}), quantum yield (Φ), lifetime (τ), and photo-reactivity of QMs with quenchers (nucleophiles: thiols, azides, and electron rich alkenes: EVE). It is preferred to have long λ_{max}, high Φ, fast and selective rate constants for applications of QMs (*Vide infra*; see section 1.6) Therefore, several derivatives of the

parent hydroxybenzyl QMPs to generate QMs on the phenyl ring system, and other aromatic ring system have been reported. Wan, Rokita, Kresge, Doria, Freccero, Popik, and Basaric were the key contributors to the development of novel QM systems. In this section, QMs are classified based on the ring system in which they are generated, QM derivatives of each system, and the photophysical properties and photo-reactivity of each QM derivatives will be compared.

1.5.1. Benzyl Quinone Methides

The parent oQM, **1.1** is short-lived and more reactive towards nucleophiles compared to the parent pQM, **1.2**.[24] Parent oQM has a lifetime of 2 ms whereas the parent pQM has a lifetime of 0.3 s in aqueous phosphate buffer solution. Hydration rate constant for the parent oQM, **1.1** is 2.6×10^2 s^{-1} and for parent pQM, **1.2** is 3.3 s^{-1}. The effect of substituents at the methide position in both QMs has been studied (Scheme 1.14).

These substituents are methyl, phenyl and adamanthyl groups.[23,35] Having phenyl substituents at the methide position of QMs red-shifts the maximum absorbance of the QMs. The parent oQM, **1.1** has a λ_{max} of 400 nm, whereas as the monophenyl substituted oQM, **1.41** has a λ_{max} around 450 nm. The parent pQM, **1.2** has a λ_{max} of 380 nm and the phenyl pQM, **1.56** has a λ_{max} around 400 nm. Additionally, substituents at the methide position increases the life-time of the QMs in aqueous phosphate buffer solutions.[36,37] The life-time varies in the order of parent oQM, **1.1** (2.3 ms), monophenyl oQM, **1.41** (0.4 s), diphenyl oQM, **1.53** (5-10 s), and the adamanthyl oQM, **1.55** has a life-time of 0.5 s. As for the pQM series, the life-time difference between the parent pQM, **1.2** and monophenyl pQM, **1.56** is nearly 16-fold higher (0.3 s vs 5 s).[8, 38] The correlation between the rate constant and the number of phenyl groups at the methide position of pQM was well studied.

The rates for the parent pQM, **1.2** monophenyl pQM, **1.56** and biphenyl pQM, **1.57** are 110, 15, and 0.19 M^{-1} s^{-1} respectively. The values demonstrates an increase in the rate constant with the increasing number of stabilizing groups at the methide position.[39]

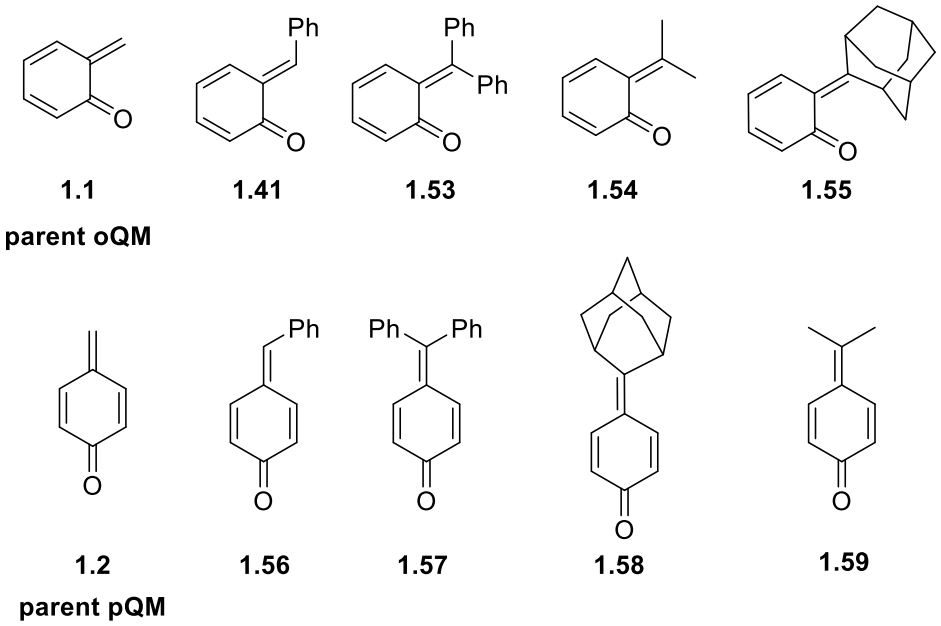

Scheme 1.14. Structures of o- and p-QM with substituents at the methide position.

The effect of substituent at the phenyl ring of oQMP on the stability and reactivity of photogenerated oQM was studied by Rokita and co-workers.[40] They have synthesized six different hydroxybenzyl-quaternary ammonium salt oQMPs with substituents at the 4-position of the phenyl ring with respect to the phenolic oxygen (Scheme 1.15). They tested the effect of varying functional groups (**1.60-1.65**); electron donating group (OMe), weak to strong electron withdrawing groups (Cl, COOMe, CN, and NO_2) at the 4-positionand compared with the parent oQM, **1.1**. rate constants and selected nucleophiles: an amine nucleophile – morpholine, and thiol nucleophile – 2-mercaptoethanol.

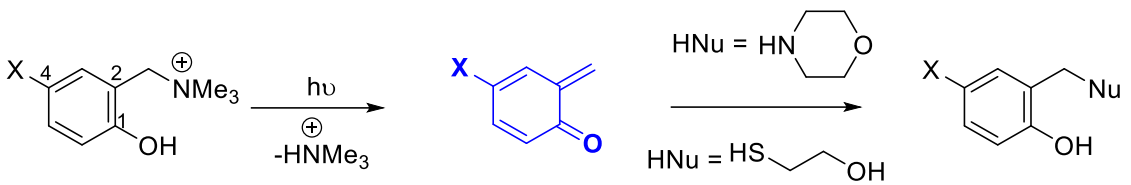

1.60: X = OMe
1.61: X = H
1.62: X = Cl
1.63: X = COOMe
1.64: X = CN
1.65: X = NO_2

1.60 QM: X = OMe
1.1 : X = H
1.62 QM: X = Cl
1.63 QM: X = COOMe
1.64 QM: X = CN
1.65 QM: X = NO_2

1.66: X = OMe
1.67: X = H
1.68: X = Cl
1.69: X = COOMe
1.70: X = CN
1.71: X = NO_2

Scheme 1.15. Ms with varying substituents in the phenyl ring.

The λ_{max}, and rate constants of each QM in water are summarized in the Table 1.1. All QMs have a maximum absorbance of around 400 nm. The stability of QMs can be interpreted based on the high hydration rate constant. A higher reactivity rate constant indicates short-life time. The lifetime of QMs varying in the order of when X = OMe > H > Cl > COOMe > CN > NO_2. The stability of oQMs with electron withdrawing groups (**1.62**, **1.63**, **1.64**, and **1.65** QM) are low compared to that of parent oQM, **1.1** and substituent with electron donating group, **1.60 QM** are more stable than parent oQM, **1.1**. Therefore, electron donating group in the phenyl 4-position increases the stability of parent oQM, **1.1**. Short-lived QMs are more prone to react with nucleophiles to regain stability which is apparent from the second-order rate constants. However, the difference of the rate constants of substituted QMs vs unsubstituted QMs was only a few orders of magnitude. The reactivity difference between electron donating OMe, **1.60 QM** vs parent oQM, **1.1** is only 4-5-fold and the difference between electron withdrawing **1.65 QM** vs unsubstituted **1.1** QM is only 20-fold.

Table 1.1. Reactivity of 1.60 QM to 1.65 QM towards nucleophiles.

QM	X	λ_{max} nm	k_2 (H_2O) M^{-1} s^{-1}	k_2 (morpholine) x10^5 M^{-1} s^{-1}	k_2 (2-mercaptoethanol) x10^5 M^{-1} s^{-1}
1.60 QM	OMe	410	1.9	5.5	0.40
1.1	H	400	7.8	23	1.9
1.62 QM	Cl	400	22.8	36	4.4
1.63 QM	COOMe	420	363	160	59
1.64 QM	CN	415	1999	505	501
1.65 QM	NO_2	435	25400	N.R.	N.R.

N.R.: Not Reported

Doria, Freccero and colleagues reported the design of oQMs with alkynyl substituents at the 4, or 5th position of the phenyl ring in an effort to achieve conjugated QM systems that can be activated using long wavelength (Scheme 1.16).[41]

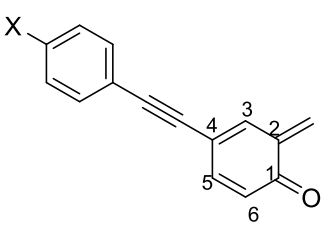

1.72: X = H
1.73: X = F
1.74: X = OCH_3
1.75: X = NMe_2
1.76: X = NMe_3I
1.77: X = NO_2

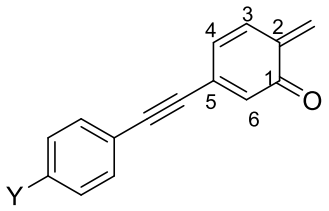

1.78: Y = H
1.79: Y = F
1.80: Y = OCH_3
1.81: Y = NO_2

Scheme 1.16. oQM structures with alkyne extension at 4- or 5-position.

The λ_{max} of QMs **1.72** to **1.81** and their rate constant in the absence of nucleophiles, and in the presence of thiol nucleophile (RSH), 2-mercaptoethanol in 50% aqueous

acetonitrile are listed in the Table 1.2. Having alkyne conjugation causes a bathochromic shift in the λ_{max} (340-485 nm) in all the alkyne conjugated QM series compared to the parent oQM (254 nm). The most electron-rich oQM, **1.75** is the longest-lived species in the 4-ethynyl series of oQM. The lifetime of oQM is evident based on the slow reactivity for hydration and the reaction with thiols. The most short-lived species in the same series is the oQM **1.77** with the nitrobenzene. Thus, it is clear that the lifetime of QM is dependent on the electronics and electron donating substituents increases the stability of oQM. Hydration rate constants varies in the order of X = NMe_2 $(2.0\pm0.3)x10^2$ < H $(5.9\pm0.1)x10^2$ < NO_2 $(3.4\pm0.08)x10^4$ M^{-1} s^{-1}.

Comparison of the reactivity of 4- vs 5-ethynyl extension with the same X substituent shows that 5-ethynyl conjugated QMs are less electrophilic than 4-alkenyl conjugated QMs. The hydration rate constant of unsubstituted 4-ethynyl QMs is more reactive compared to the 5-alkenyl conjugated QM. The rate constant of 4-ethynyl QM, **1.72** is X = H: $(5.9\pm0.1)x10^2$ M^{-1} s^{-1}, whereas the oQM isomer with 5-ethynyl, **1.78** is X = H: (9.8 ± 0.1) M^{-1} s^{-1}.

Table 1.2. Characteristic wavelength and rate constant of oQMs 1.72 to 1.81 with nucleophiles.

QM	**λ_{max} nm**	**k_{obs} (H_2O) s^{-1}**	**$k_{(RSH)}$ M^{-1} s^{-1}**
1.72	380	$(5.9\pm0.1)x10^2$	$(1.18\pm0.02)x10^5$
1.73	380, 540, 630	$(3.5\pm0.2)x10^2$	N.D.
1.74	410	$(2.6\pm0.2)x10^2$	$(1.29\pm0.1)x10^3$
1.75	440, 485	$(2.0\pm0.3)x10^2$	$(7.0\pm0.2)x10^2$

1.76	340, 350	$(1.8\pm0.05)\times10^3$	N.R.
1.77	420	$(3.4\pm0.08)\times10^4$	$(1.45\pm0.1)\times10^5$
1.78	350	9.8±0.1	N.D.
1.79	350	$(6.6\pm0.3)\times10^2$	$(7.7\pm0.1)\times10^2$
1.80	360	53.1±0.4	N.D.
1.81	400	$(4.4\pm0.08)\times10^4$	$(3.5\pm0.1)\times10^4$

N.D.: Not Determined.

Rokita and co-workers reported the photogeneration of two oQMs in the same phenyl ring as a tandem process and used the feature to crosslink Deoxyribonucleotide (DNA).[42] Photogeneration of DNA adduct, **1.76** from the QMP, **1.72** was proved using gel electrophoresis experiments which indicated mono-oQM, **1.73** formation followed by bis-oQM, **1.75** (Scheme 1.17). However, LFP or reactivity studies were not conducted to determine the lifetime, stability, or rate constants.[43]

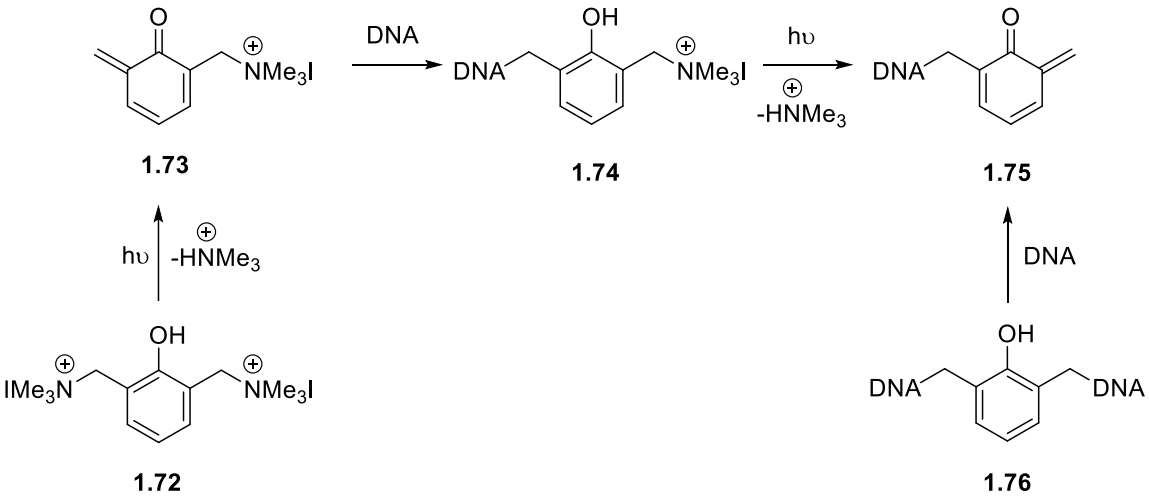

Scheme 1.17. Tandem oQM photogeneration.

Recently, Doria, Freccero and colleagues reported an extension of their alkyne conjugated oQM work to design a bifunctional oQMP, **1.77** by conjugating two of the

alkynyl oQMPs via a phenyl ring as a linker (Scheme 1.16 and Scheme 1.18). The aim of the design is to photo-generate oQMs with V-shaped geometry to facilitate binding and alkylation at G-quadruplex structures.[44] The key advantage of the system is the possibility of activating using long-wavelength of light, 327 – 410 nm. LFP experiments of the bifunctional QMP, **1.77** in 50% aqueous acetonitrile solution irradiated with Nd:YAG laser at 266 nm showed a transient at 370 nm with a life-time of 1 ms which was assigned as oQM as it was not quenched by oxygen. QMs are singlet exited state species and are not quenched by molecular oxygen. Only the triplet exited state species get quenched by oxygen. Authors have not reported hydration rate constants. However, the mono-hydration product, **1.78** and bis-hydration product, **1.79** was isolated in 62% and 8% yield, respectively. The formation of bis-hydration product, **1.79** confirms the bifunctional nature of the oQMP, **1.77**. oQM formation was further validated by the reaction of oQMP with EVE and isolating the oQMP-EVE adduct, **1.80** with a 60% yield.

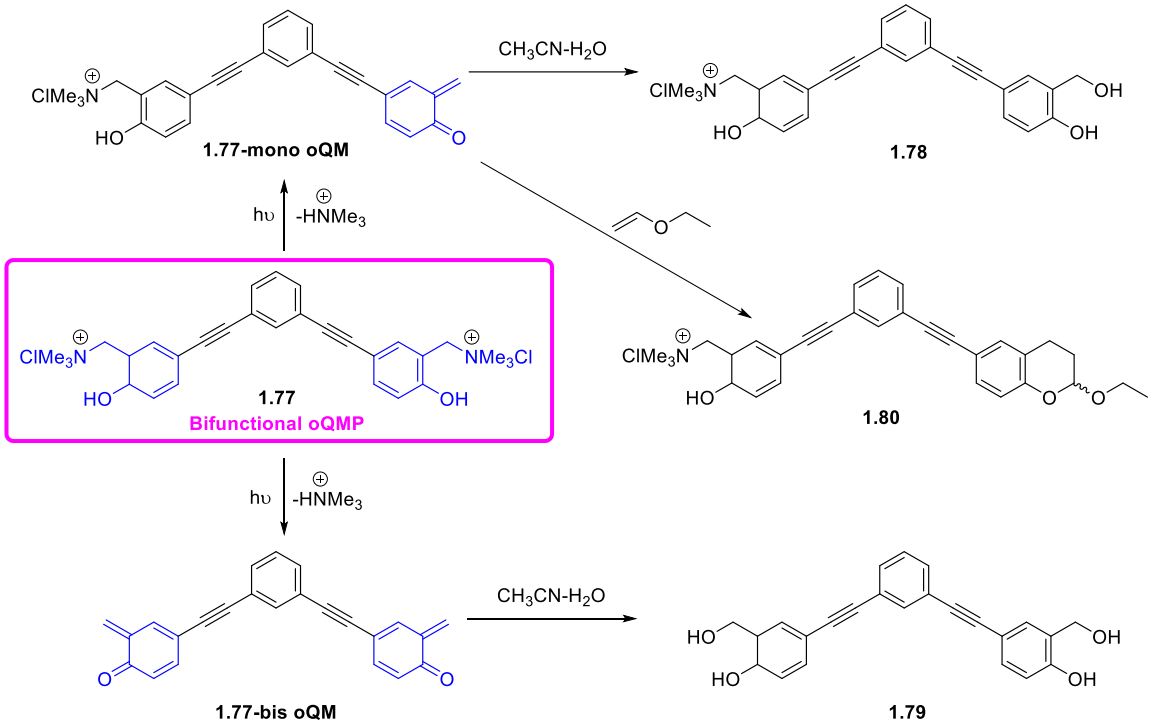

Scheme 1.18. Bifunctional oQM with a V-shaped geometry.

1.5.2. Naphthyl Quinone Methides

QMs in the naphthalene series are chromophores with 300-350 nm λ_{max} and has a Φ around 0.2-0.3. Both parent oNQMs, 2,3-naphthoquinone-3-methide, **1.18** and 1,2-naphthoquinone-1-methide, **1.20** show similar rate constants with quenchers such as nucleophiles and electron rich alkenes. Nucleophiles used are thiol, cysteamine, sodium azide and electron rich alkene was EVE despite they are regioisomers with very different electronic structures (Table 1.3).[31] Sterically congested adamanthyl-oNQMs are short-lived in comparison to parent oNQMs and more reactive with nucleophile sodium azide (~100-fold).[45,46] However, IEDDA rate constant of parent oNQM with EVE is ~1000-fold higher than adamantyl-oNQM, **1.81** due the effect of steric hindrance caused by the adamantyl group. The parent pNQM, **1.32** reactivity with thiols is much lower in comparison to parent oNQM (Scheme 1.19, Table 1.3).

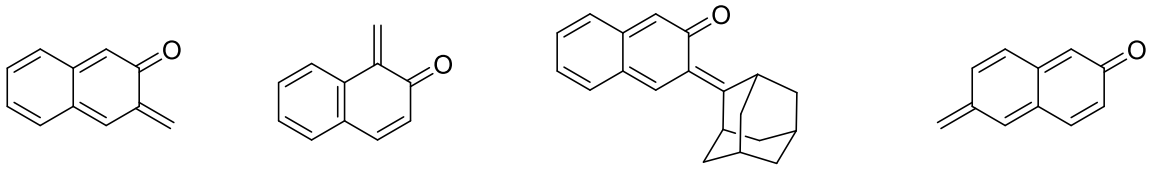

1.18 **1.20** **1.81** **1.32**

Scheme 1.19. Structures of different NQMs.

Table 1.3. Photophysical properties and reactivity of NQMs with quenchers.

QM	λ_{max} nm	τ ms	Second-order rate constant $M^{-1} s^{-1}$			Ref.
			Cysteamine	Sodium azide	EVE	
1.13	330	4-8	$(2.24\pm0.06)x10^5$	$(2.00\pm0.11)x10^4$	$(4.07\pm0.19)x10^4$	30
1.15			$(3.34\pm0.28)x10^5$	$(3.00\pm0.25)x10^4$	$(6.05\pm0.34)x10^4$	30
1.81	370	0.19	N.D.	$(3.7\pm0.5)x10^6$	85±10	45
1.22	310-330	>1	$1.3x10^3$ (a)	N.D.	N.D.	32

(a) Thiol group: ethanethiol. N.D.: Not Determined.

1.5.3. Anthracene Quinone Methides

Basaric and co-workers reported anthracene based oQMs and the first anthracene QMP 2-hydroxy-3-(diphenylhydroxymethyl)-anthracene, **1.82** in 2014.[47] Later in 2017 the same research group synthesized a series of 3-hydroxymethyl-2-anthrol derivatives to further understand photo-reactivity of anthracene QMs and explore their usage as long wavelength activatable antiproliferative agents(Scheme 1.20).[48,49]

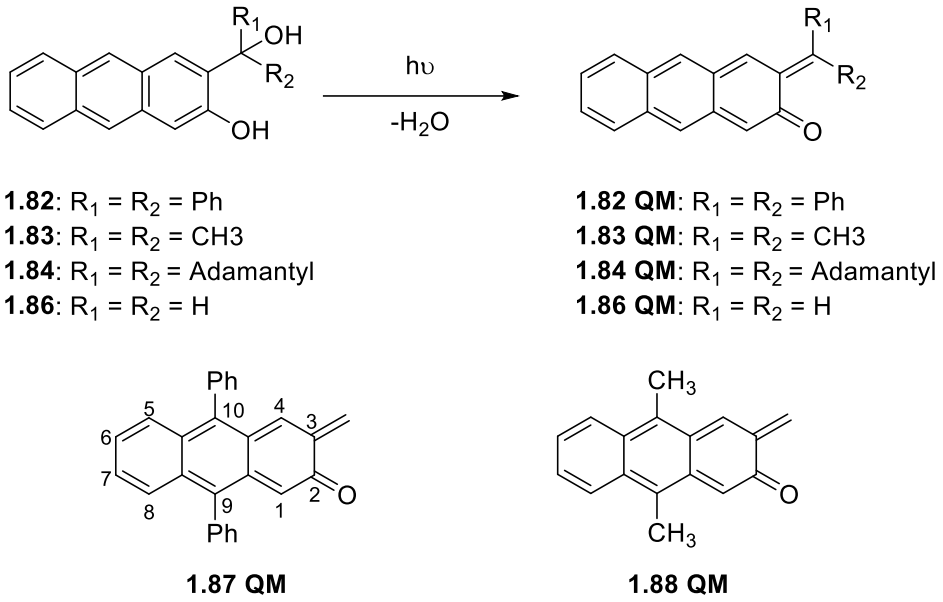

Scheme 1.20. Structures of anthracene QMPs and anthracene QMs.

Compounds **1.82** to **1.86** has λ_{max} above 400 nm. Authors have done a detailed LFP study on all the derivatives. However, the authors were skeptical is assigning the peak for oQMs, **1.82 QM** to **1.86 QM**. Therefore, neither lifetime, nor rate constant for **1.82 QM** to **1.86 QM** were reported. Interestingly, authors detected the quinone methide Anthracene-oQM structures with diphenyl or dimethyl substituents at the 9 and 10 position of the anthracene ring, **1.87 QM** and **1.88 QM**. The lifetime and rate constants of **1.87 QM** and **1.88 QM** reaction with azide, and ethanolamine are shown in Table 1.4. The rate constants of 1.87 QM and 1.88 QM with was reported are same as for unsubstituted oNQM (10^{5}-scale).

Table 1.4. Reactivity of anthracene oQMs.

QM	**τ**	**k (NaN_3)**	**k (ethanolamine)**
	μs	**M^{-1} s^{-1}**	**M^{-1} s^{-1}**

1.87 QM	550±50	(8±3) x10^5	(4.8±0.7) x10^3
1.88 QM	400±50	(4.8±0.8) x10^6	(5±1) x10^4

1.5.4. Binaphthyl Quinone Methides

Freccero and co-workers have developed the photogeneration of oQMs in binaphthyl system which can be considered as the dimer of 2,3-naphthoquinone-3methide, **1.18**. o-Binapthalene quinone methide precursor (oBQMP), **1.89** is a bifunctional oQMs designed for DNA crosslinking (Scheme 1.21).[50]

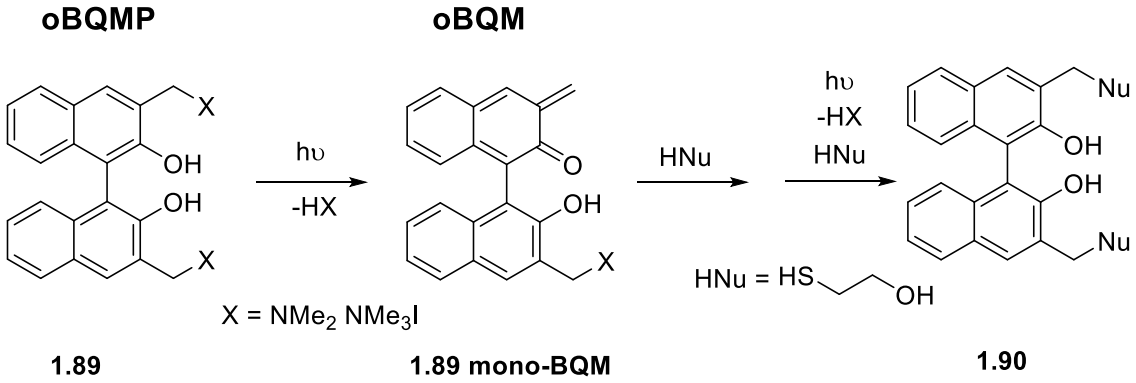

Scheme 1.21. Photogeneration of oBQM from oBQMP and its reaction with nucleophiles.

Authors have reported that the QM generation is a step-wise process similar to the report by Rokita.[42] oBQMP shows 30 nm red-shift in the absorbance spectra compared to parent oNQMP. Furthermore, o-Binaphthalene quinone methide (oBQM) is more reactive compared to oNQM. The hydration rate constant of oBQMP is 4.7x10^3 s^{-1} whereas for oNQMP/oNQM is 144 s^{-1}. The second-order constant with thiol (2-mercaptoethanol) for oBQMP is 5.5x10^6 M^{-1} s^{-1} and that oNQMP/oNQM with thiol (2-mercapethylaminehydrochloride is 2.24x10^5 M^{-1} s^{-1}.[30] The reason for oBQMP/oBQM high reactivity is ascribed to the presence of a naphthol group at 2' position in oBQMP that

could lead to a specific intramolecular acid-catalyzed mechanism in oBQM photo-generation.

Isomeric p-binaphthalene quinone methide precursors, **1.91** (pBQMP) was also developed by the same research group to photo-generate p-binaphthalene quinone methide (pBQM).[32] Absorbance spectra of pBQMP, **1.91** were similar to that of oBQMP, **1.89** and showed 30 nm bathochromic shift compared oNQMP or pNQMP. However, the binaphthyl analog showed high reactivity in comparison to the naphthyl precursor. The hydration rate constant of pBQMP/pBQM is $2x10^7$ M^{-1} s^{-1}, whereas that for pNQMP/pNQM 1.3x103 M^{-1} s^{-1} (Scheme 1.22)

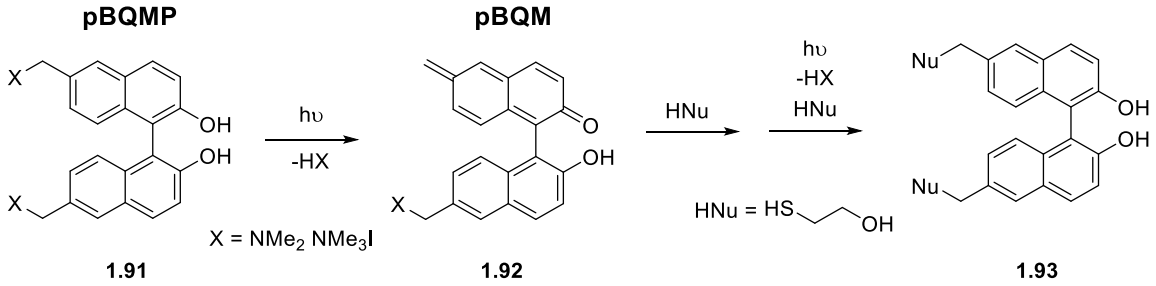

Scheme 1.22. pBQMP photochemistry and the reactivity of pBQM with nucleophiles.

1.5.5. Phenanthrene Quinone Methides

N,N-Dialkyl-9-aminomethyl-10-phenanthrols, **1.94** and **1.95** to photo-generate the phenanthrene quinone methide, 9-methylene-10-phenanthrone, **1.96** was reported (Scheme 1.23).[51] Both phenanthrol QMPs display identical fluorescence spectra and has maximum absorbance bands at 380 nm and 460 nm. Authors have proved the formation of phenanthrene quinone methide based on the reactivity with alkenes with electron donating groups, EVE, butyl vinyl ether, ethylene glycol vinyl ether and isolated the chroman products in moderate to high yields. However, neither the quantum yield nor rate constants for the reaction was mentioned.

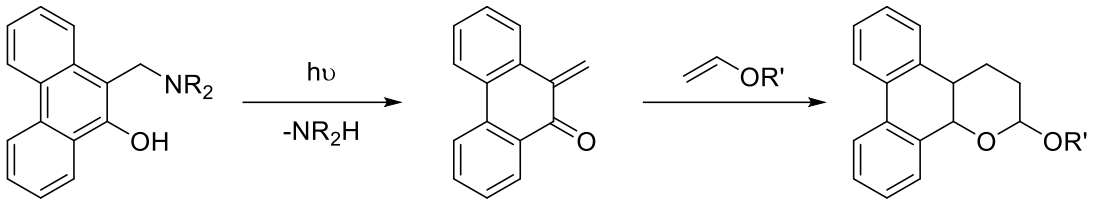

1.94: R = Me
1.95: R = Et

1.96

1.97: R' = Et
1.98: R' = *i*-Bu
1.99: R' = CH_2CH_2OH

Scheme 1.23. Photogeneration of phenanthrene oQM and its reactivity with EVE.

1.6. Applications of Photochemically Generated NQMs

Our research group is particularly interested in NQMP-based precursors and their applications. Since the discovery and photochemical reactivity of oNQMs by us, other research groups also have designed various oNQMP derivatives and explored applications. Herein, three examples for applications-based on o-NQMP photochemistry from our research group and two examples from other research groups will be described.

In the first example, oNQMP is derivatized for fast and efficient photo-release of calcium ions (Ca^{2+}). One of the common Ca^{2+} chelating agent, 1,2-bis(o-aminophenoxy)ethane-N,N,N′,N′-tetraacetic acid)Bis-aminophenoxyethane tetra acetic acid (BAPTA) is attached to the naphthyl/benzyl position of the parent oNQMP to generate o**QMP-BAPTA** which could form a chelated complex in the presence of Ca^{2+}. Upon irradiation of the chelated complex, photolabile benzylic ether bond is cleaved and releases Ca^{2+} along with free o-aminophenoxydiacetic acid and oNQM attached o-aminophenoxymethane diacetic acid (**oNQM-APDA**). The oNQM undergoes rapid hydration to generate oNQMP forming **oNQMP-APDA** (Figure 1.1). This method can be occupied in biomedical applications where regulation of physiological Ca^{2+} is important,

such as in neurological disorders. Unlike the conventional Ca^{2+} regulating drugs, usage of light to modulate Ca^{2+} has more control and non-invasive.[52]

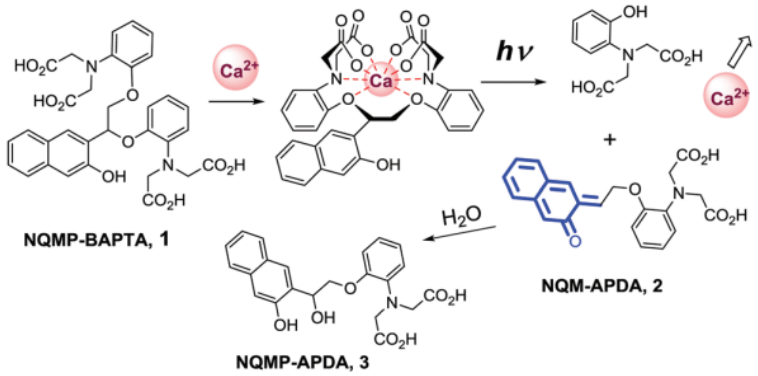

Figure 1.1. oNQMP as a calcium ion chelating agent (scheme adopted from ref. 52).

The second example demonstrates the use of extremely fast IEDDA reactivity of oNQM with electron rich olefins for patterned surface derivatization. oNQMP is attached to silicon oxide surfaces at the C5 position in the naphthalene ring. Upon irradiation, oNQMP photo-generates oNQM and undergoes reaction with an alkene labeled with a dye, azide, alkyne, or biotin group (Figure 1.2). The Diels-Alder photo-ligation at surfaces can be used for high-throughput analytical methods such as protein assays.[53]

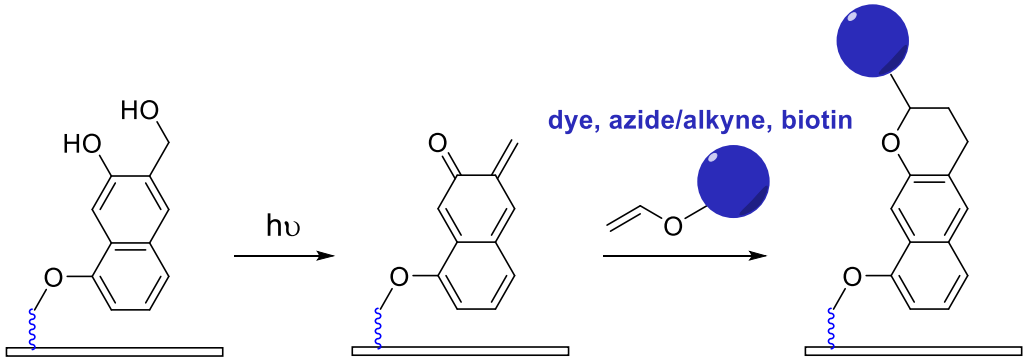

Figure 1.2. Diels-Alder reaction of oNQMP for patterned surface derivatization.

The third example illustrates a benefit of the efficient reaction of oNQM with nucleophiles/thiols to develop procedure for the protein and peptide labeling. The thioether bond in the immobilized or labeled protein is stable under ambient conditions and during proteolytic digestion for mass spectrometric analysis. However, the thioether bond can be photocleaved upon irradiation to release the protein on demand and regenerate oNQMP starting material. The authors have demonstrated the utilization of PEG, dye, biotin, alkyne/azide modified oNQMP for further decoration or fluorescent labeling of proteins (Figure 1.3).[54]

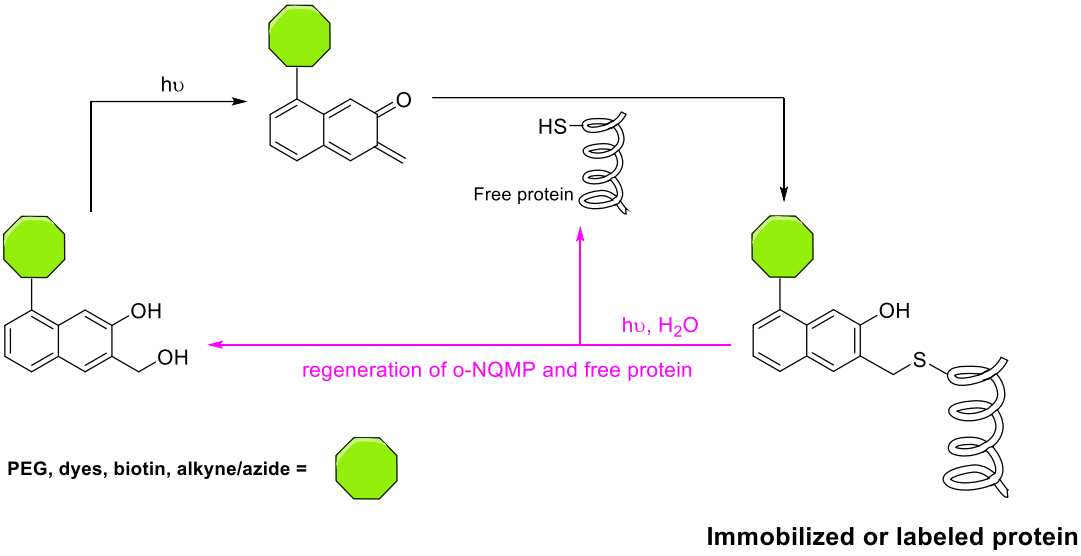

Figure 1.3. oNQMP for reversible derivatization of peptides/proteins.

As it was mentioned in section 1.1, QMPs are known to be active pharmacophores with antiproliferative properties due to the reaction of QM with proteins, nucleosides, or DNA. Basaric and co-workers developed six derivatives of oNQMs with adamanthyl group (**1.100-NQM** – **1.105-NQM**) attached at the methide position and measured the antiproliferative activity of each experimentally (Figure 1.4).[45] They attempted the photogeneration of each sterically hindered NQM using the respective hydroxynaphthol

precursors (**1.100 – 1.105**). Synthesis of the precursors **1.101** and **1.102** was not possible as it leads to the formation of stable **1.101-NQM** and **1.102-NQM** that were even able to be isolated and characterized by X-ray crystallography. UV spectra of rest of the synthesized precursors (**1.100, 1.103, 1.105**) showed maximum absorbance around 300-350 nm, which is a characteristic feature of naphthalene ring-based QMs. Increased antiproliferative effect was reported for **1.100-NQM** compared to other NQM derivatives.

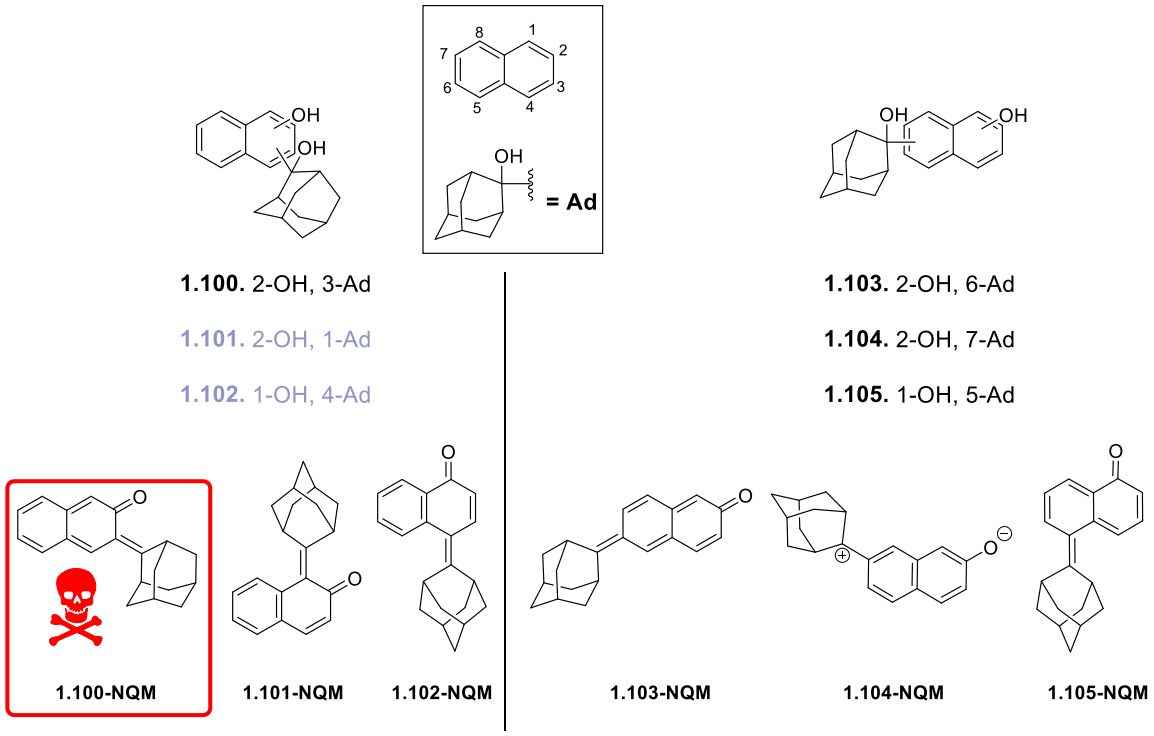

Figure 1.4. Adamanthyl NQMP and their NQMs.

In a separate study, Basaric and co-workers improved photophysical properties and antiproliferative activity of oNQMs by conjugating oNQMP with naphthalimide core via a hydrocarbon linker with varying (CH_2) length from 1-5 (Figure 1.5 left).[55] Naphthalimides are well known pharmacophores that exhibit anticancer properties and used as a versatile chromophores or electron acceptors in Foster resonance energy transfer (FRET). Authors have synthesized NQMP-naphthalimide conjugates which can facilitate NQM formation

via photoinduced electron transfer (PET) due to the presence of naphthalimide chromophore. Antiproliferative activity will be a combined effect from photogenerated oNQM and naphthalimide.

Later, the authors have further modified the system by conjugating aminonaphthalimide to the oNQMP system to convert the system to a fluorescent entity along with the antiproliferative properties upon irradiation (Figure 1.5 right).[56] Aminonaphthalimides are used as fluorescent probes compared to naphthalimide due to the presence of electron donating amino group that facilitates FRET. Upon irradiation, aminonaphthalimide can stain endoplasmic reticulum (ER) and lipid droplets, simultaneously destructing cancer cells via both aminonaphthalimide and photo-generated oNQM.

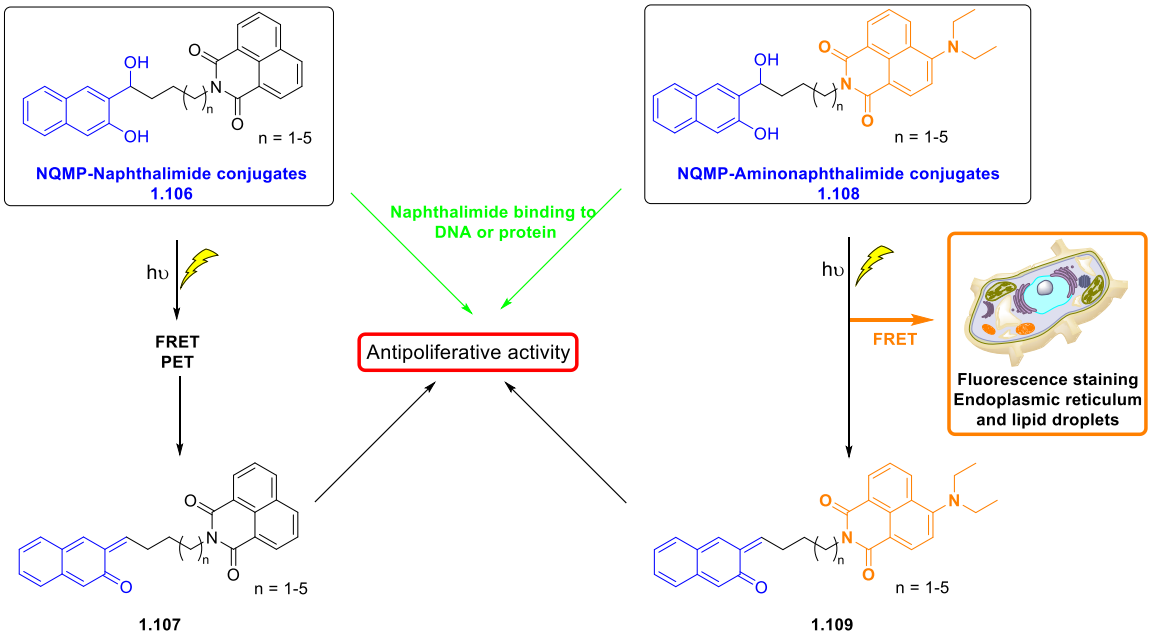

Figure 1.5. NQMP and derivatives of naphthalimide conjugates in cancer therapy.

In this thesis research study, we explored oNQMP application as a bioanalytical tool for in-situ generation of fluorescent dyes and to develop a novel photodegradable polymer analog.

1.7. *In-situ* Generation of Fluorescent Dyes

There are three main methods to generate fluorescent dyes *in-situ*. Photoactivatable fluorophores (PAF), photoswitchable fluorophores and photoconvertible fluorophores.[57] Our research work aims at the development of PAF and photoswitchable fluorophores. Therefore, photoconvertible fluorophores or examples therein will not be discussed in this dissertation.

1.7.1. Photoactivatable Fluorophores (PAF)

PAFs are weak or non-fluorescent molecules that can be photochemically converted to fluorescent dyes when excited at the appropriate wavelength. PAFs allow spatiotemporal emission control from fluorescent reporters and are helpful in cell tracing and microscopy.[58, 59] The most common strategy for making photoactivatable fluorophores is caging of a fluorescent molecule using photolabile protecting groups.[60] Common PPGs used o-nitrobenzyl[61] and coumarinyl groups.[62] We have demonstrated oNQMP as PPG for developing clickable caged fluorophores (Figure 1.6).[63] In this example, oNQMP is attached to the fluorescent molecule, fluorescein and the fluorescence is masked. The azide group facilitates tagging of a substrate of interest via azide-alkyne click reaction with substrate conjugated to Oxadibenzocyclooctyne (ODIBO) group. Upon irradiation, the photolabile C-O bond in oNQMP is cleaved and releases the fluorescein dye.

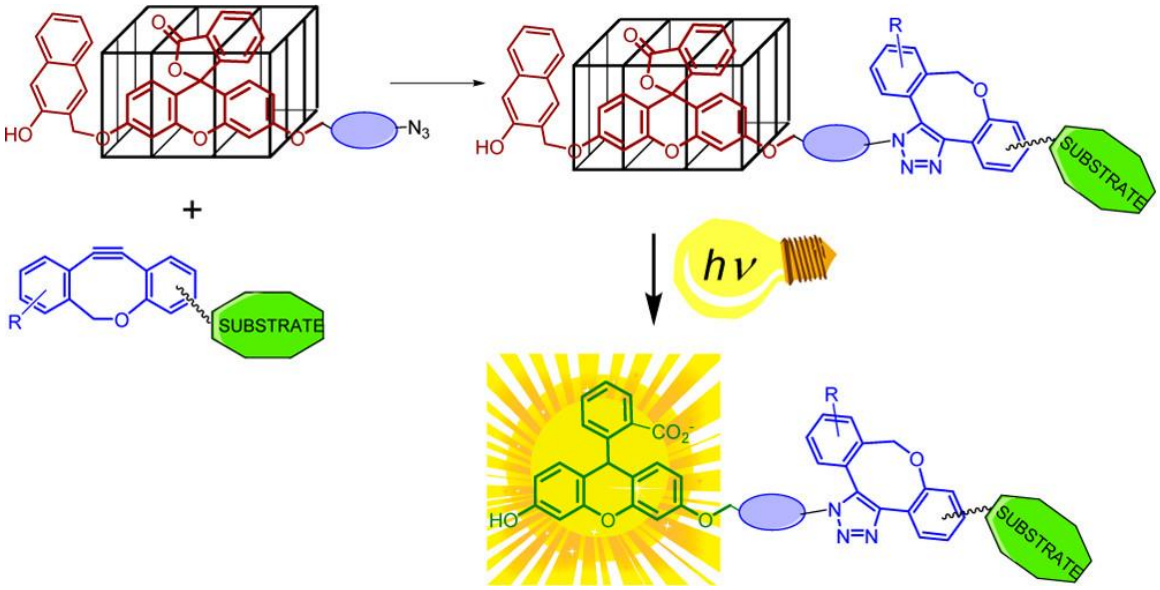

Figure 1.6. Photoactivatable fluorescein-oNQMP cage. (Diagram from ref. 63).

1.7.2. Photoswtichable Fluorophores

Photoswitchable fluorophores are molecules that toggle between fluorescent and non-fluorescent state when applied light and in the dark, respectively. These molecules are widely used in super-resolution microscopy.[64] Diarylethenes are the most common photochromic compound used as a photoswitchable fluorophore, but they are poorly soluble in water. Hence, it is not ideal for bioimaging or fluorescence nanoscopy. There's a demand for the development of novel photoswitchable fluorophores.[65] We designed QMPs that generates QMs with phenyl conjugation at the methide position that can be fluorescent which will be elaborated in chapter 2.

1.8. Poly(ethylene terephthalate)/PET Plastic Recycling

PET polyester is a popular choice for consumer plastic products such as bottles, fibers due to its numerous benefits, such as being lightweight, safe, durable, chemical resistant, recyclable, flexible, and low market price. However, plastic pollution has significantly burdened our environment over the last few decades as PET does not degrade

under natural environmental conditions. Additionally, monomers for PET synthesis are terephthalic acid and ethylene glycol (Scheme 1.24). The monomers are derived from petroleum sources and fossil fuels. There is a demand for alternatives for PET using renewable resources to alleviate the depletion of fossil resources. Treatment of plastic waste is a global issue, and the need for biodegradable alternatives to conventional PET is increasing.[66, 67]

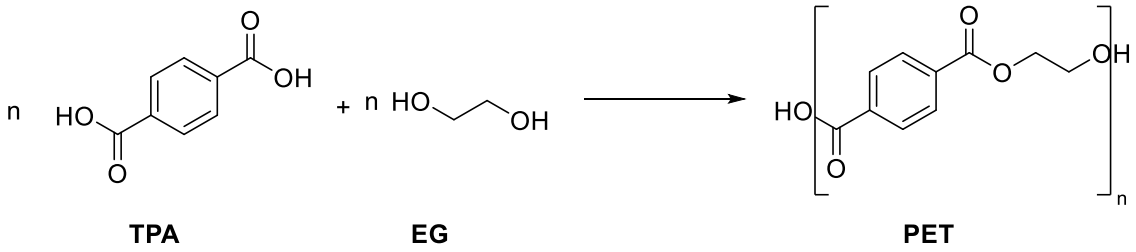

Scheme 1.24. PET synthesis reaction scheme.

Using natural light to degrade polymers is a convenient approach in comparison to traditional chemically degradable polymers, as it saves reagents, is easily tunable, and often shows fast degradation.[68] Ortho-nitrobenzyl group is the most widely used PPGs in the design of various photodegradable polymers. oNQMP was never used in creating a polymer before despite being an excellent PPG. Therefore, we explored the usage of oNQMP to design a novel polymer in chapter 3.

1.9. PET Plastic Recycling

PET is a recyclable polymer, and the most common PET plastic recycling methods are mechanical and chemical recycling. Mechanical recycling leads to low commodity value plastics, and chemical recycling has taken the attraction industrially as it is a sustainable method and can recover monomers.[69, 70] However, the rate of chemical recycling is slow compared to post-consumer PET waste. The USA recycled less than 30% of PET waste in 2015 due to deficiencies in existing chemical recycling methods.[71] More details on the types of chemical recycling pathways, pros, and cons will be elaborated in chapter 4. Therefore, novel chemical recycling methods that are industrially more robust and economical need to be developed. Two of the research projects in this dissertation focuses on exploring novel, cost-effective chemical recycling routes for PET (chapter 4 and 5).

1.10. Goals of the Research Projects

This dissertation describes four main projects where the first and second projects are based on NQMP photochemistry. Third and fourth projects are novel methods for Poly(ethylene terephthalate) (PET) plastic recycling.

1.10.1. Novel oNQMP based Design for *in-situ* Generation of Fluorescent Dye

We explored the application of o-NQMP for in-situ generation of fluorescent dyes from a novel Quinone Methide Precursor design (**QMP 1**). A detailed photochemistry study of the novel QMP system is described in chapter two (Scheme 1.25).

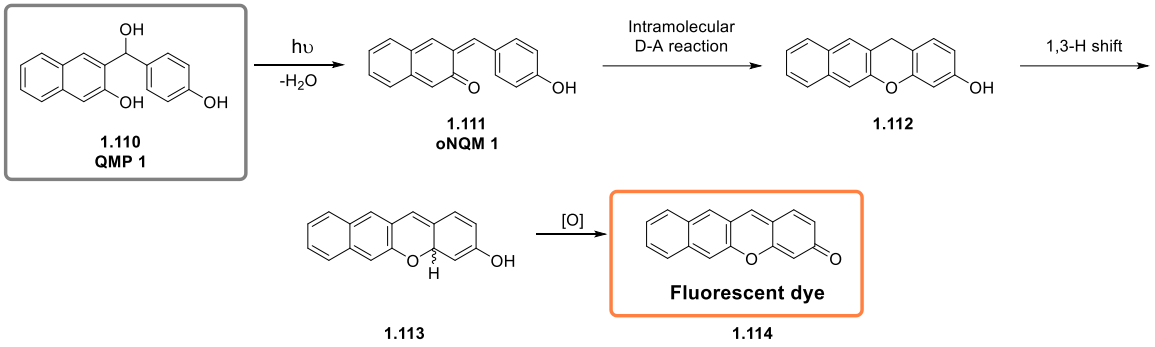

Scheme 1.25. Novel oNQMP design for photoactivatable fluorophores.

1.10.2. Novel oNQMP based Poly(ethylene terephthalate) Design and Importance

Chapter three details our approach towards the design of a photodegradable PET by utilizing the photochemistry of oNQMP (Scheme 1.26). UV-A light can be used to photochemically produce (oNQM) from derivatives of (3-hydroxynaphthalen-2-yl)methanol (o-NQMP).

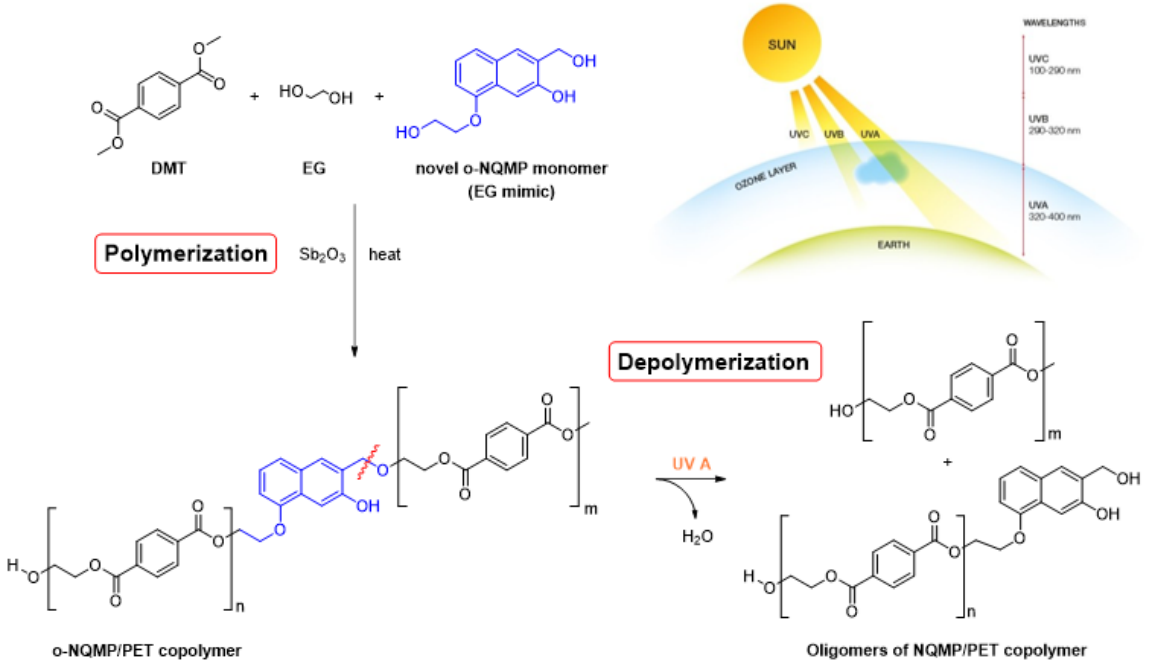

Scheme 1.26. Novel oNQMP design for photodegradable polymer.

1.10.3. Thiol-Catalyzed Hydrolysis of Esters: Investigation of the Mechanism

Chapter four describes the kinetic study of thiols for the hydrolysis of esters which can be used as catalyst to fasten the aqueous recycling of PET. p-nitrophenyl acetate (p-NPA) as a model aromatic ester and a series of thiols with different acidity (pK_a) was tested to find the best thiol catalyst and understand the mechanism of thiol catalyzed ester hydrolysis (Scheme 1.27).

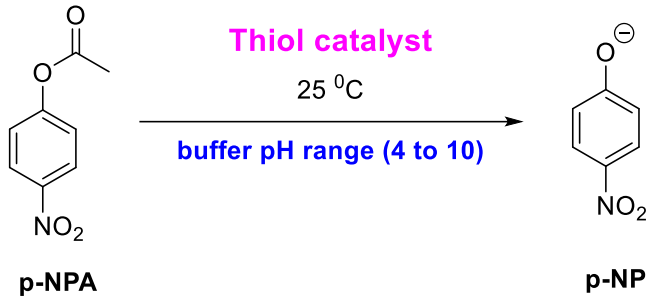

Scheme 1.27. Thiol-catalyzed hydrolysis of p-NPA reaction scheme.

1.10.4. Alakaline Solvolysis of PET as a Novel PET Chemical Recycling Method

Chapter five describes a method to recycle contaminated PET bottles under mild conditions without an expensive catalyst. Herein, we report an industrially convenient protocol for contaminated PET recycling using NaOH as the catalyst by taking the advantage of transesterification of PET in organic alcohol solvents (Scheme 1.28).

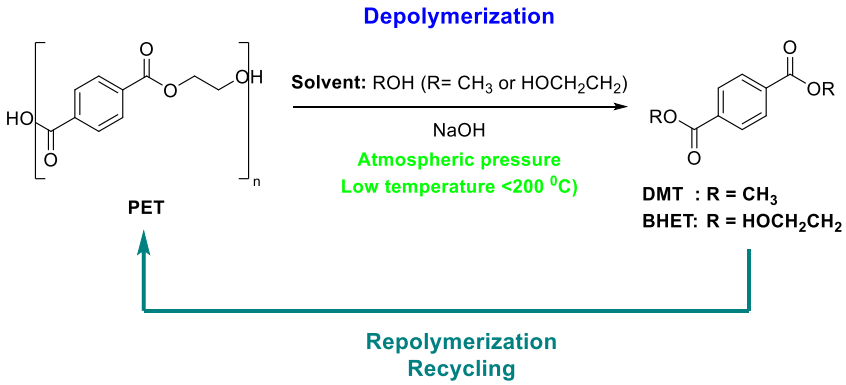

Scheme 1.28. Alkaline solvolysis of PET.

CHAPTER 2

PHOTO-DEHYDRATION OF (3-HYDROXYNAPHTHALEN-2-YL)(4-HYDROXYPHENYL)METHANOL IN AQUEOUS SOLUTION: A KINETIC STUDY OF CONJUGATED ORTHO- AND PARA-QUINONE METHIDE TAUTOMERS

2.1 Introduction: Objectives and Applications

We took a novel approach in designing a fluorescent dye by intramolecular cyclization of oNQMs with aryl substituents at the alkene terminus. The foundation for this research work is based on previous work reported by Padwa and co-workers. In 1975, Padwa reported the formation of 9H-xanthene (3% yield) upon photoirradiation of 3-phenylbenzofuran-2(3H)-one, **2.1.** Irradiation of **2.1** formed a conjugated oQM, **2.1 oQM** via photo-decarbonylation, which underwent intramolecular Diels-Alder reaction to generate **2.2**. Compound **2.2** followed by a hydride shift to form xanthene (Scheme 2.1).[27]

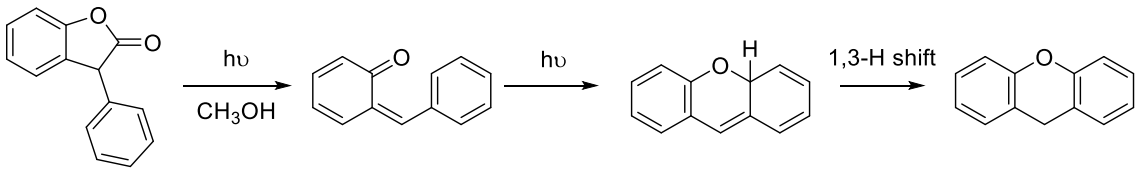

2.1 **2.1 oQM** **2.2** **Xanthene**

Scheme 2.1. Photogeneration of conjugated oQM and intramolecular cyclization.

We designed and synthesized **QMP 1** in this study to find the feasibility of Padwa's observations on oNQMP derivatives. Our goal is to achieve a novel approach in designing a fluorescent dye by intramolecular cyclization of oNQMs with aryl substituents at the

alkene terminus. We have introduced para phenolic group at the naphthyl position of the parent oNQMP as it can undergo an additional oxidation step to form the fluorescent final product, **2.5** upon formation of **oNQM 1**, intramolecular Diels-Alder cyclization and 1,3-hydride shift. (Scheme 2.2).

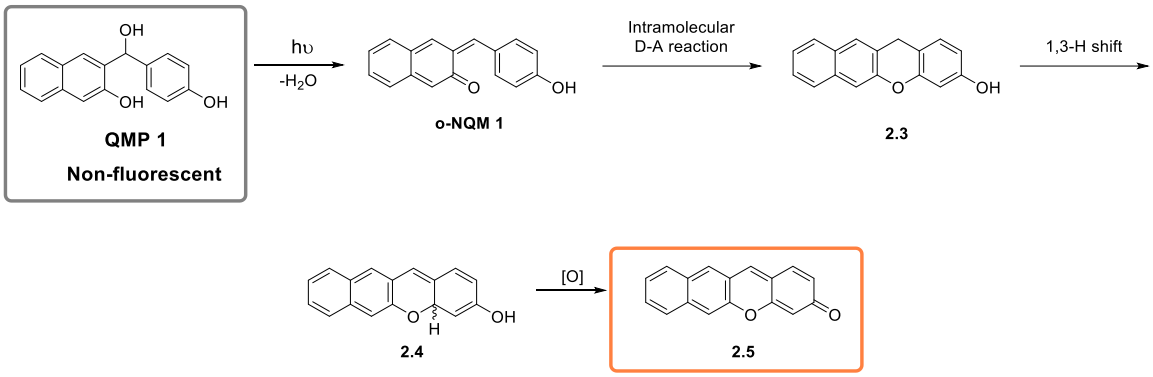

Scheme 2.2. QMP 1 for the in-situ photogeneration of a novel fluorescent dye.

Structure of the fluorescent final product, **2.5**: 3H-benzo[b]xanthen-3-one resembles the structure of well-known Seminaphthofluorone (SNAFR) dyes (Figure 2.1).[72,73] Thus, our approach is a novel design for the in-situ generation of fluorescent dyes/photoactivatable fluorophores. Additionally, we use a structural rearrangement concept for the design of photoactivatable fluorophore instead of the conventional caged fluorophore method described in Section 1.7.

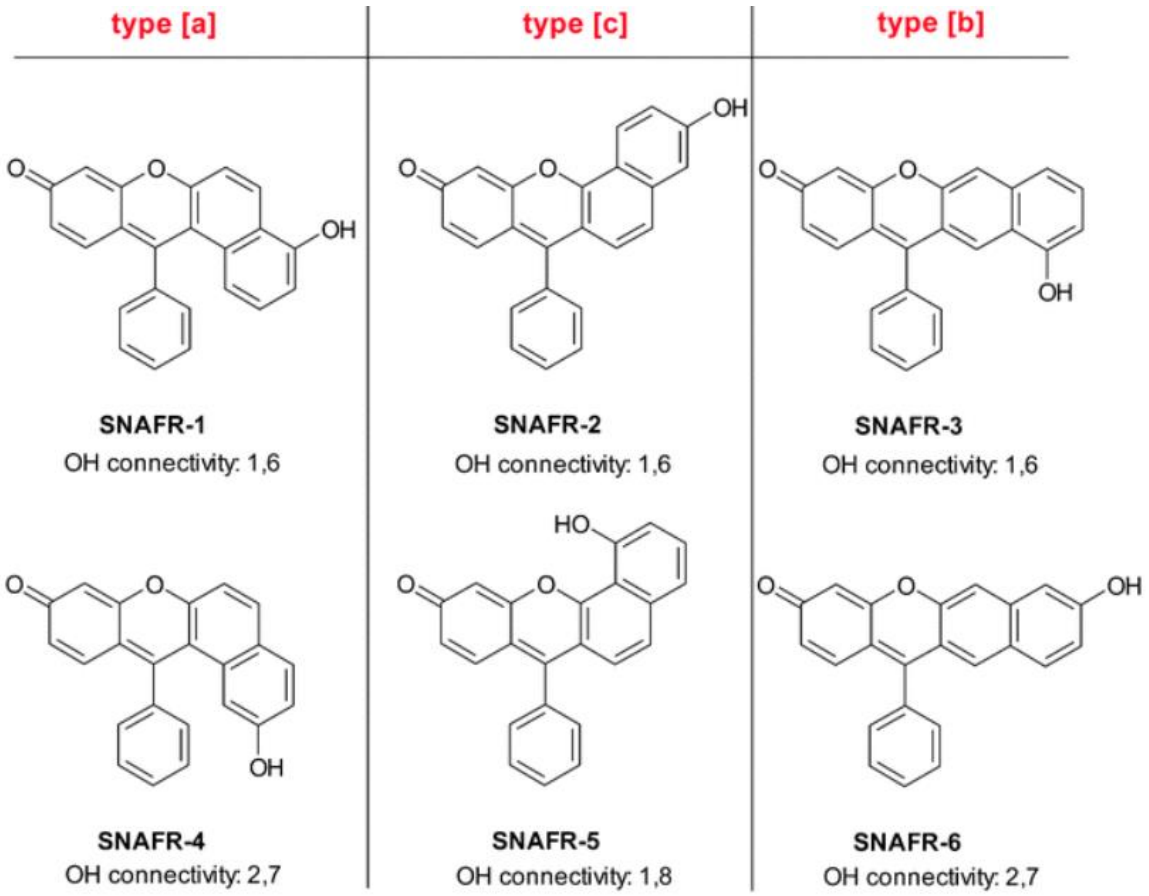

Figure 2.1. Structures of SNAFR dye series along with the labeling: ref 72.

A characteristic feature of the novel Quinone Methide Precursor, **QMP 1** in this study is the simultaneous photogeneration of isomeric quinone methides: ortho-naphthoquinone methide, **oNQM 1** and para-quinone methide, **pQM 1** (Scheme 2.3).

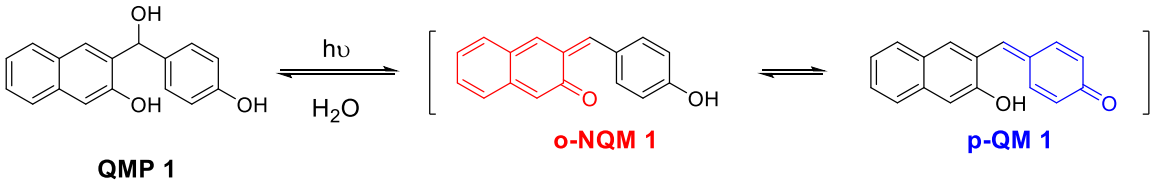

Scheme 2.3. Isomeric quinone methides generated from QMP 1.

Photochemical generation of bifunctional oQMs, their reactivity, kinetics and applications as DNA cross-linking agents have been reported by Rokita, Freccero and

Basaric research groups (Section 1.5.1). However, photochemical generation of different isomers of QMs simultaneously and the competition towards the generation of an oNQM vs. a pQM have never been reported to the best of our literature search. Thus, the initial goal of this project is to find the predominant form of QM whether **oNQM 1** or **pQM 1** in the competing **QMP 1** system. Herein, we report a complete photochemical reactivity and kinetic study of the novel **QMP 1** system. Nucleophilic addition reactions and inverse electron demand Diels-alder (IEDDA) reactions of **QMP 1** was studied. Both **oNQM 1** and **pQM 1** undergo nucleophilic addition with methanol, sodium azide, and cysteamine to form compounds **2.6**, **2.7**, and **2.8** respectively (Scheme 2.4A). **oNQM 1** undergoes intermolecular Diels-Alder reaction with EVE (Scheme 2.4B) and intramolecular Diels-Alder cyclization leading to naphthoxanthene, **2.4** which would oxidize to SNAFR analog, **2.5** (Scheme 2.4C).

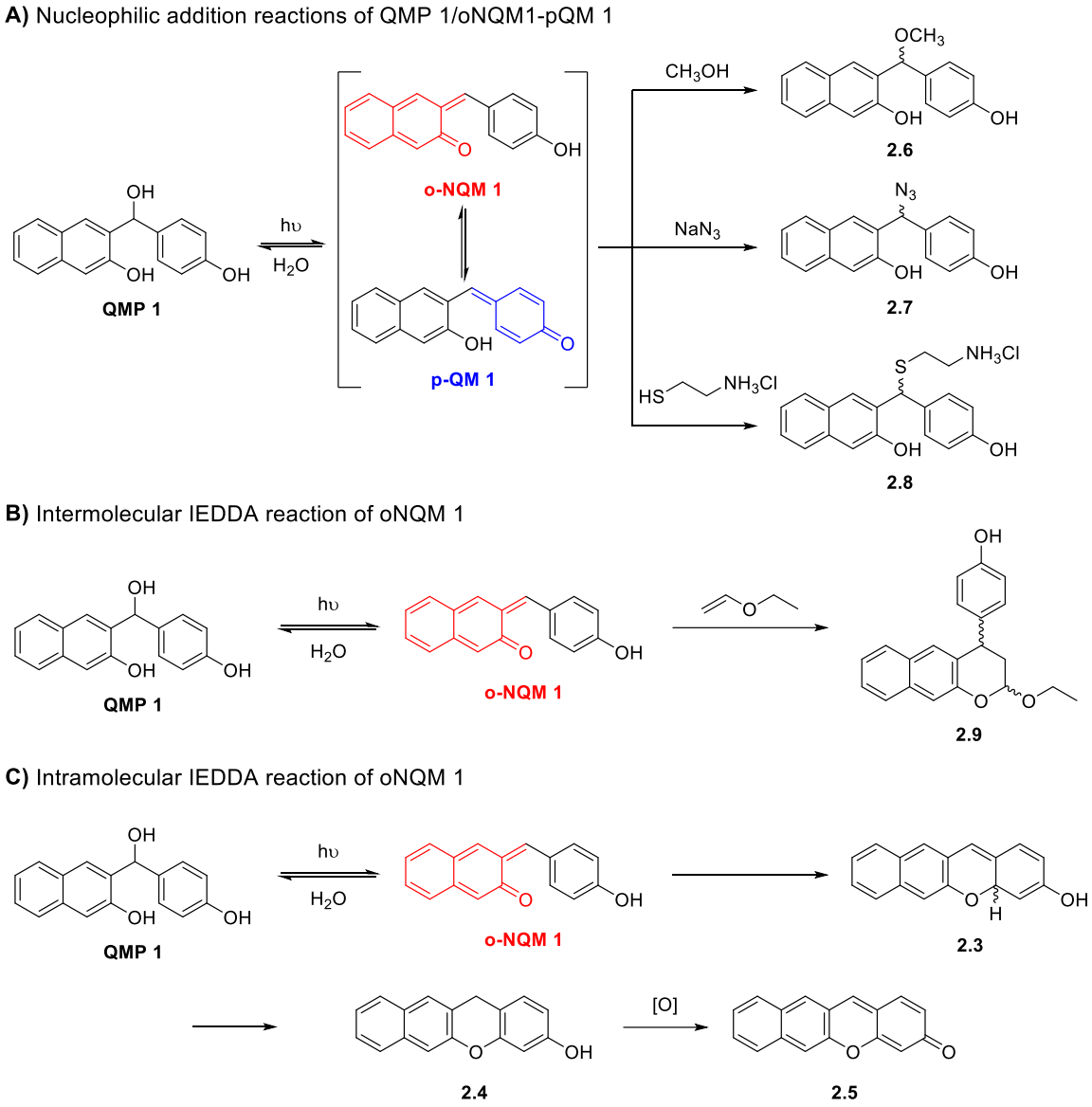

Scheme 2.4. Reactions of QMP 1 system.

The best evidence to find the predominant form of quinone methide in our system is the characteristic feature of **oNQM 1**, the ability of **oNQM 1** to undergo intermolecular or intramolecular IEDDA reaction and respective rate constants because **pQM 1** is unreactive in IEDDA reaction. Our experiments with EVE to monitor intermolecular IEDDA showed low-rate constants compared to the parent oNQM: 2,3-naphthoquinone-3-methide, **1.13**. Additionally, photoirradiation of **QMP 1** showed the formation of a novel

compound other than the expected xanthone-derivative, **2.5** (*Vide infra*). The results of IEDDA experiments prompted us to investigate additional evidence to confirm the predominant form of QM in the **QMP 1** system. Nucleophilic addition reactions with **oNQM 1** and **pQM 1** produce the same final product and therefore, identification or isolation of product is insufficient or not informative to determine the predominant form of QM. However, comparison of the rate constant values for the reaction between a nucleophile and **QMP 1** with the same nucleophile and an analog of **oNQM 1** or **pQM 1** is an excellent tool to find the predominant form of QM in the competing **QMP 1** system. **oNQM 1** has a para phenol group at the methide position and **pQM 1** had o-hydroxynaphthyl group at the methide position. Photochemical generation and the reactivity of oNQM or pQMs with exact or similar substituents as in our novel system have not been reported.

Therefore, we have designed and synthesized two structural analogs of the novel competing QMP that would only produce one type of QM in the QMP system. **QMP 2** only produces an analog of **oNQM 1**, **oNQM 2** and cannot generate pQM as the phenolic OH in **QMP 1** is blocked with a methoxy group in **QMP 2** (Scheme 2.5A). **QMP 3** is the methoxy protected-naphthol OH of **QMP 1** and **QMP 3** only generates **pQM 2** which is analogous to **pQM 1** (Scheme 2.5B).

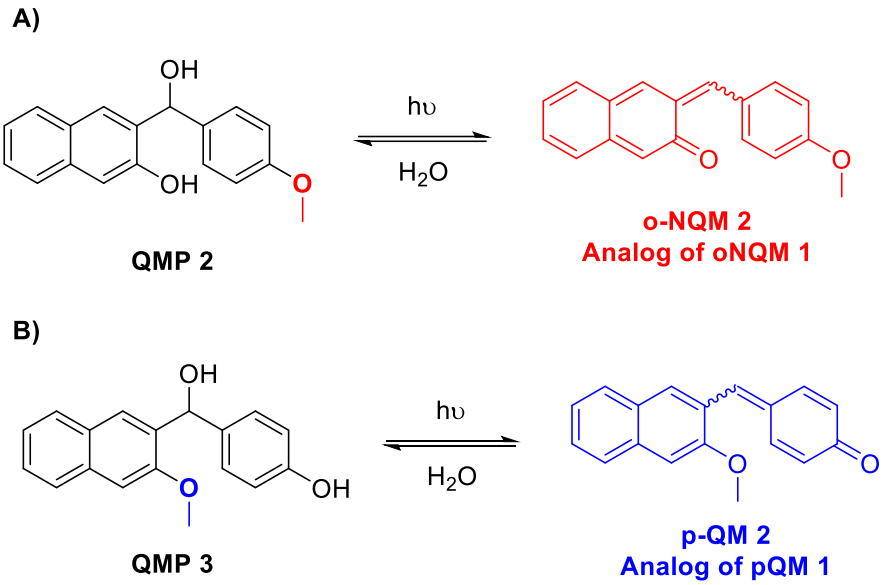

Scheme 2.5. Structural analogs of QMP 1: A) QMP 2 precursor, B) QMP 3 precursor.

Additionally, photogenerated QMs from **QMP 1, QMP 2 and QMP 3** are conjugated to a phenyl ring for **oNQM 1, and oNQM 2** or naphthyl ring for **pQM 1, and pQM 2** at the methide position. Photochemical generation and reactivity of conjugated o, m, and p-QM with a phenyl ring at the methide position was studied by Wan and co-workers which was described in Section 1.5.1.[23, 74] However, conjugated oNQM and naphthyl conjugated p-QM was not reported before. Herein, we report the photochemical reactivity and kinetics of conjugated oNQM and naphthyl conjugated pQM with quenchers (cysteamine; thiol nucleophile, EVE) for the first time in literature.

oNQM 2 undergoes nucleophilic addition with methanol, azide and thiol leading to the products **2.10**, **2.11**, and **2.12** respectively (Scheme 2.6A right). oNQM also undergo reactions with EVE and form **2.13** and intramolecular cyclization to form **2.14** (Scheme 2.6A left). On the other hand, **pQM 2** only undergo reactions with nucleophiles (Scheme 2.6B right) and does not undergo inter- or intramolecular DA reaction (Scheme 2.6 left).

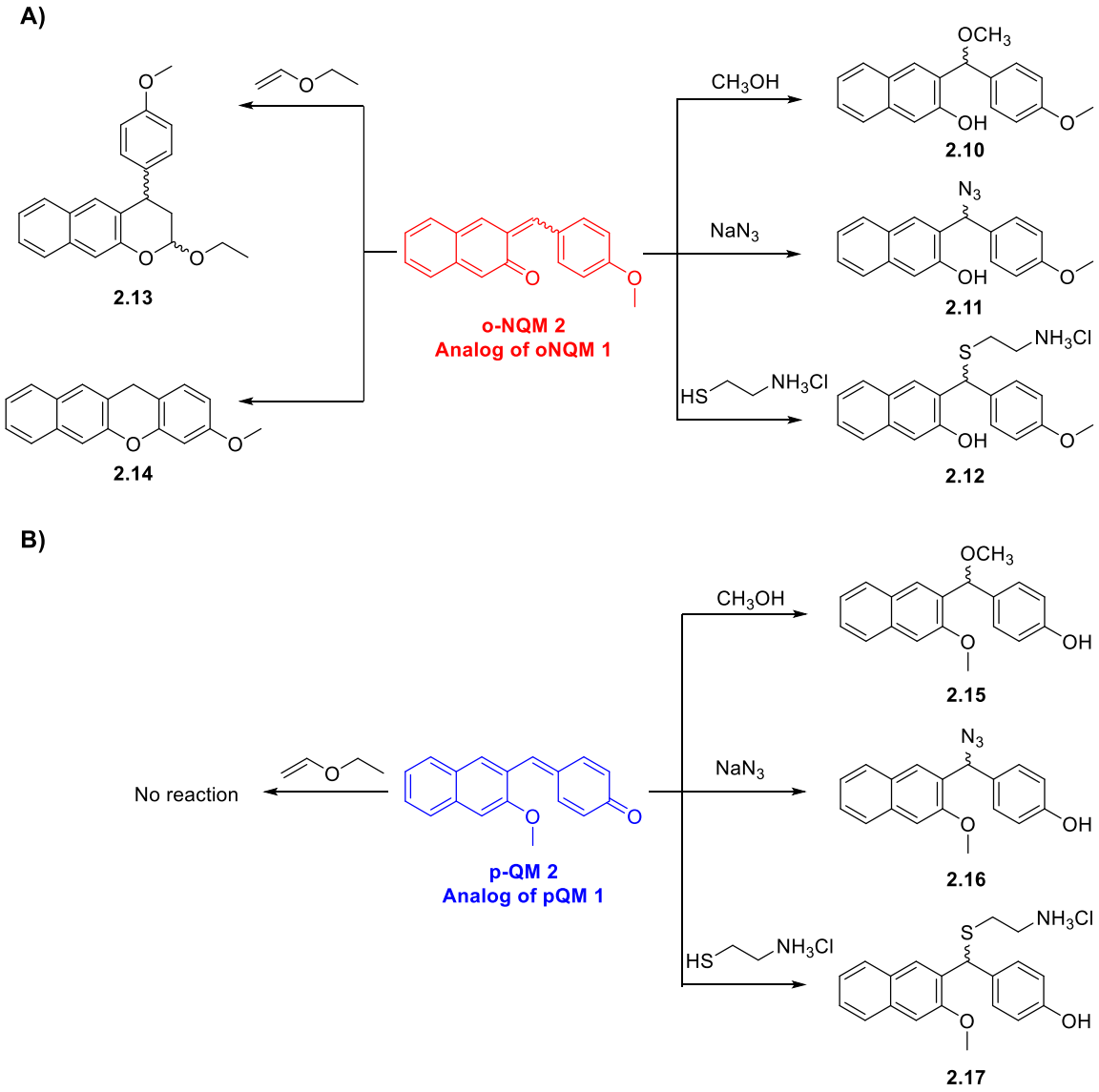

Scheme 2.6. A) Reactions of oNQM 2, B) reactions of pQM 2.

QMPs are non-fluorescent and photogenerated QMs in this research work are expected to be fluorescent due to conjugation. Irradiation of QMPs form QMs and the generated QMs re-hydrate back to QMP in aqueous medium. Therefore, conjugated QMP-QMs are novel photoswitchable fluorophores. Thus, we studied fluorescent properties of **oNQM 1** and **pQM 1** and explored the applicability of QMP systems as photoswitchable fluorophore.

2.2 Synthesis of QMPs

Synthesis of **QMP 1** was carried out according to Scheme 2.7. The synthesis starts from commercially available methyl 3-hydroxynaphthoate. Methyl ether protection of the phenolic hydroxyl groups was followed by lithium aluminum hydride reduction of the ester and produced compound **2.20** in high yield. The oxidation of **2.20** gave 3-methoxy-2-naphthaldehyde, **2.21** in 99% yield. The aldehyde was coupled with 4-bromoanisole in the presence of n-BuLi to obtain compound **2.22**. The deprotection of methyl groups in compound **2.22** was done via oxidation of **2.22** to ketone, **2.23** followed by BBr_3 deprotection and finally reduction of obtained compound 2.24 to obtain **QMP 1** in 99% yield.

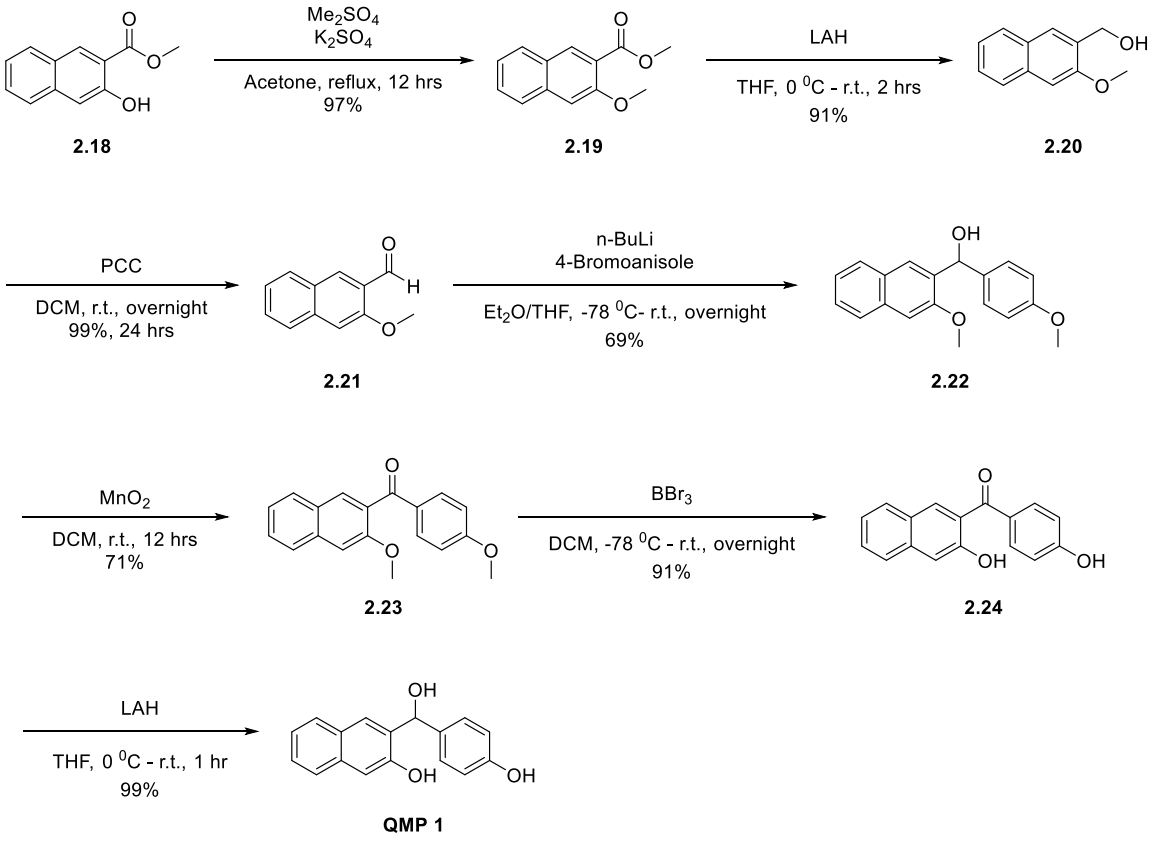

Scheme 2.7. Synthetic route of QMP 1.

Synthesis of **QMP 2** and **QMP 3** was carried out by selecting intermediates from the **QMP 1** synthetic pathway. Compound **2.24** was methylated to get the desired monomethylated compound **2.25** in 94% yield at 65% conversion. Reduction of **2.25** resulted in the formation of **QMP 2** (Scheme 2.8).

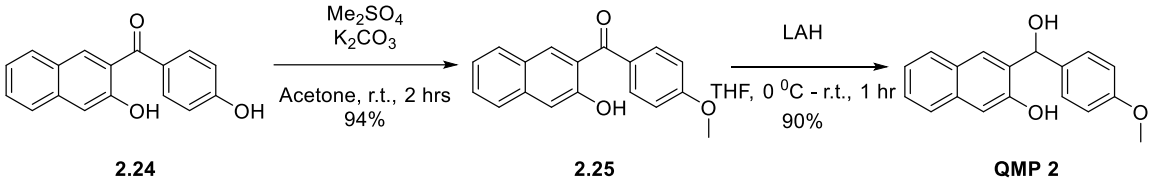

Scheme 2.8. Synthetic route of QMP 2.

The aldehyde, **2.21** was coupled with TBDMS protected 4-bromophenol in the presence of n-BuLi to get **QMP 3** in one step (Scheme 2.9).

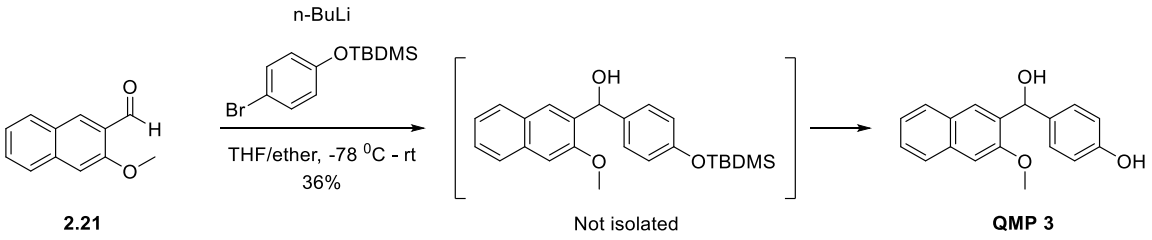

Scheme 2.9. Synthetic route of QMP 3.

2.3 Photophysical Properties of QMPs

Absorption spectra of all QMPs in aqueous acetonitrile (1:1) show three major absorbance bands at 230, 275 and 330 nm similar to the UV spectrum of the parent NQMP, 3-hydroxy-2-naphthalenemethanol[30,31] **(**Figure 2.2A**)**. The similarity is due to the presence of the same chromophore and all three major absorbance bands were found with similar molar extinction coefficients: 230 nm ($\varepsilon \sim 1x10^5$ M^{-1} cm^{-1}), 275 nm ($\varepsilon \sim 1x10^4$ M^{-1} cm^{-1}), and 330 nm ($\varepsilon \sim 6x10^3$ M^{-1} cm^{-1}). The concentration of each QMP is ~$2.5x10^{-5}$ M. Fluorescence emission spectra of QMPs recorded in aqueous acetonitrile (1:1) at the

excitation wavelength of 266 nm has one band at 325-415 nm region (Figure 2.2B). Concentrations of QMPs are, **QMP 1** ($3x10^{-5}$ M) **QMP 2** ($2.5x10^{-5}$ M), and **QMP 3** ($3x10^{-5}$ M) in aqueous acetonitrile 1:1 (λ_{ex} = 266 nm).

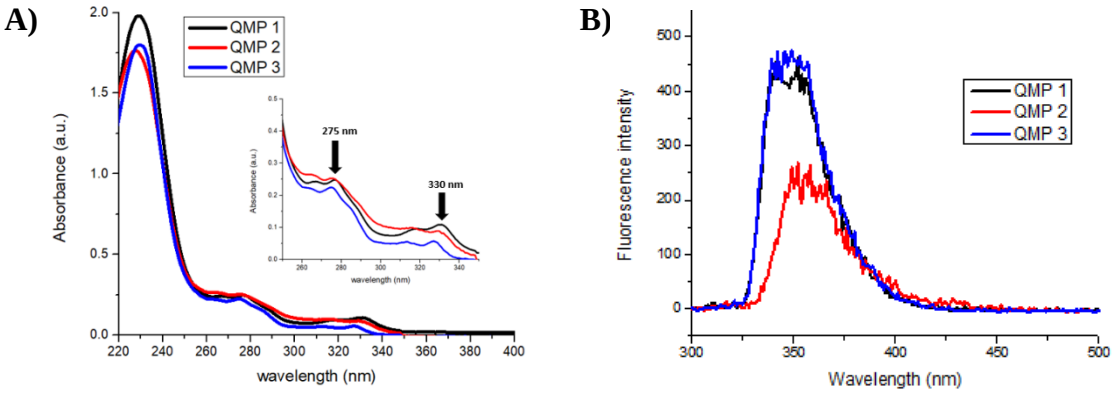

Figure 2.2. A) UV-Visible spectra of QMPs, B) Fluorescence spectra of QMPs.

Quantum efficiencies (Φ_R) of QMPs were measured for the photochemical reaction of each QM trapping with 2-mercaptoethylamine. 3,4-dimethoxynitrobenzene was used as the reference/actinometer (Φ=0.116±0.002 in aqueous KOH solution, wavelength range = 254-365 nm).[75] The quantum yield values for all QMPs, and the **parent o-NQMP**, 3-hydroxy-2-naphthalenemethanol are given in Table 2.1.

Table 2.1. Quantum efficiencies of QMP 1, 2, 3 and parent oNQMP.

	QMP 1	QMP 2	QMP 3	Parent oNQMP[30]
	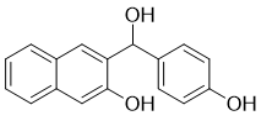 QMP 1	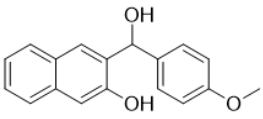 QMP 2	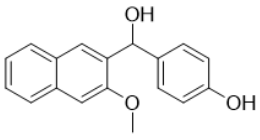 QMP 3	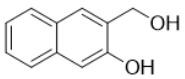 parent oNQMP
Φ_R	0.157±0.002	0.240±0.001	0.217±0.003	0.17±0.02

All the photochemical reactions were conducted in wholly aqueous phosphate buffer solutions (IS =0 .1 M, $[H_3PO_4]$ = 0.005 M, $[H_2PO_4^-]$ = 0.008 M, $[NaClO_4]$ = 0.07 M, BR= 0.6, calculated pH 7.00, final pH measured 7.02). Irradiation experiments were conducted using a Rayonet photoreactor equipped with ten 8W 300 nm fluorescent lamps unless otherwise specified. Qualitative analysis of each QMP photolysate with upon irradiation was done by HPLC (High-performance liquid chromatography). The formation of product peaks in HPLC was confirmed by comparing with a standard. Novel products were isolated by preparative photolysis and fully characterized.

2.4 Photoreactivity of QMPs in the Absence of a Quencher

Irradiation of **QMP 1** and **QMP 2** wholly aqueous phosphate buffer solution of pH 7 for a short time (<10 minutes) resulted in the formation of a novel compound that is not expected from a quinone methide precursor. Detailed experiments on unknown product identification and structure elucidation are described in section 2.10. **QMP 1** formed **NPQ 1** and **QMP 2** formed **NPQ 2** (Scheme 2.10.4.1). The primary photoproduct formed from **QMP 2** was stable compared to that of **QMP 1** (stability: **NPQ 1** < **NPQ 2**). This may be because of the possible reaction of phenolic OH in **NPQ 1** with the same molecule or quinone methide in the medium. Prolonged irradiation of both **QMP 1** and **QMP 2** leads to the decomposition of both QMPs and the primary photoproducts.

Attempts were taken to avoid the formation of **NPQ 2** by conducting the photoreactions of **QMP 2** under argon. **NPQ 2** percentage yield is 50% low in argon purged conditions compared to oxygen purged condition which indicates the process is clearly an oxidation (Table 2.2). However, complete removal of oxidized products, the **NPQ 1** or **NPQ 2** formation was not possible even under controlled conditions.

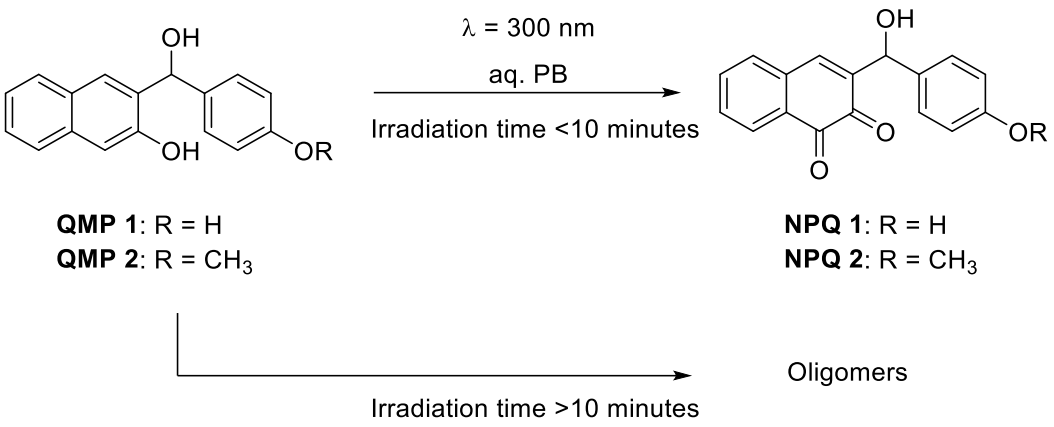

Scheme 2.10. Photoproducts formed from QMP 1 and QMP 2.

Table 2.2. Conversion of QMP 2 and NPQ 2 yield.

Condition	QMP 2 conversion (%)	NPQ 2 yield (%)
Argon purged	31	44
Aerated	54	75
Oxygen purged	66	82

QMP 2 (30 μm), 300 nm, 2 min irradiation.

Photoirradiation of **QMP 3** at short irradiation primarily generates **pQM 2** which hydrates back to **QMP 3** since the reactions were carried out in aqueous medium without any other nucleophiles. However, prolonged irradiation causes the **QMP 3** to cleave forming the 3-methoxy-2-naphthaldehyde, **2.21** (Scheme 2.11). Unlike **QMP 1** and **QMP 2**, aldehyde (**2.21**) is a secondary photoproduct for **QMP 3** as it was formed upon prolonged irradiation. Additionally, formation of the aldehyde, **2.21** was not observed under argon purged condition. Thus, it is evident that the mechanism of the secondary photoproduct formation from **QMP 3** also requires oxygen (*vide infra*).

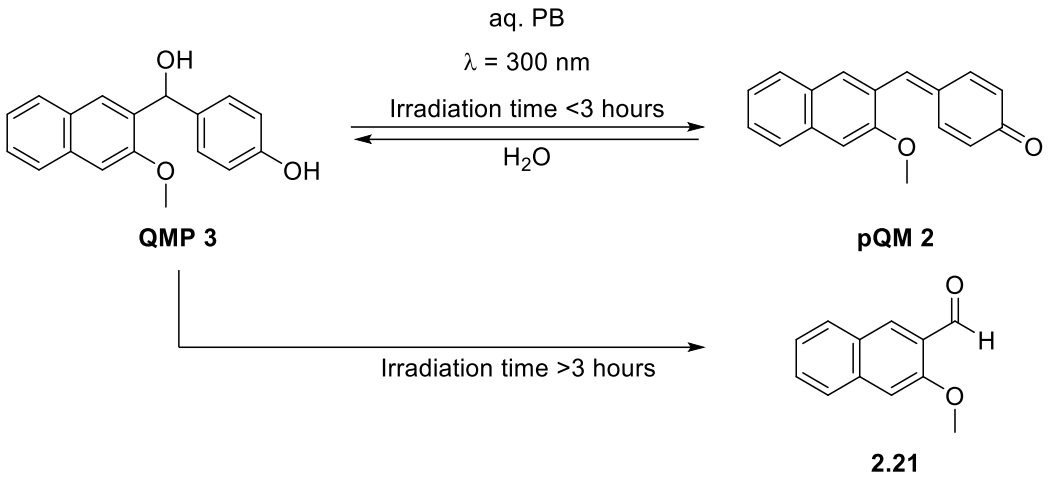

Scheme 2.11. Photoirradiation products of QMP 3 with time.

2.5 Photoreactivity of QMPs in the Presence of a Quencher

Photoirradiation of QMPs in methanol (photomethanolyis) showed only the formation of the respective methylated adduct, and the oxidative product/s was not observed. Irradiation of **QMP 1**, **QMP 2**, **QMP 3** in methanol for 2 minutes formed only the respective methylated adducts, **2.6**, **2.10**, and **2.15** respectively (Scheme 2.4 and 2.6). 20% of **QMP 1** was converted to **2.6,** 70% of QMP 2 to **2.10**, and 2% of **QMP 3** converted to **2.15** upon 2 minutes of irradiation. QMP percentage conversion after 2 minutes of irradiation varied in the order of **QMP 2** > **QMP 1** > **QMP 3.** Quantum efficiencies of **QMP 1**, **QMP 2**, **QMP 3** reaction with cysteamine in pH 7 aqueous phosphate buffer are 0.2, 0.7, and 0.02, respectively.

Photomethanolysis efficiency differences of QMPs can be explained based on the type of QM generated. Photomethanolysis quantum yield for oQMPs are higher than pQMPs. 2-hydroxymethylphenol (oQMP) has a quantum yield of 0.23, whereas 4-(hydroxymethyl)phenol (pQMP) has a quantum yield of 0.007. Similarly, **QMP 2** only generates **oNQM 2** and **QMP 3** only photogenerate **pQM 2** and the photomethanolysis

quantum yield of **QMP 2** is much higher than **QMP 3** (0.7 vs 0.02). In wholly organic solvent where Excited State Intramolecular Proton Transfer (ESIPT) mechanism predominates quinone methide formation. The distance between phenolic OH and hydroxy OH in 4-(hydroxymethyl)phenol is higher compared to that in 2-(hydroxymethyl)phenol. Therefore, slow formation of pQM compared to oQM. Similarly, the distance between hydroxyl and phenol group in **QMP 3** is larger **QMP 2** compared to to undergo effective ESIPT. Photomethanolysis efficiency of **QMP 1** is an average in between the analogs, however much closer to the value of **QMP 2**. Thus, it indicates that **oNQM 2** could be the predominant form of QM in the **QMP 1** system.

Irradiation of **QMP 1** in aqueous acetonitrile (1:1) in the presence of a nucleophile, sodium azide, cysteamine produced only the nucleophilic adduct **2.7**, and **2.8**, respectively. Additionally, the reactions of **QMP 1** with EVE produced only **2.9** (Scheme 2.4). However, photoirradiation of **QMP 2** in the presence of a nucleophile or EVE resulted in the formation of the expected nucleophilic adduct (**2.10 - 2.12**) or the chroman ring (**2.13**) and **NPQ 2** as the minor product even under controlled conditions (Scheme 2.12).

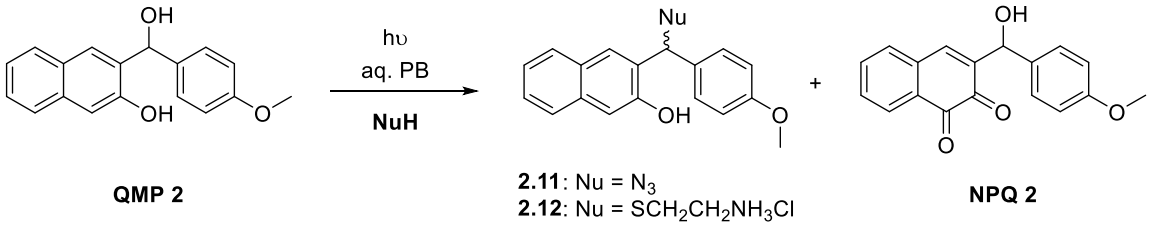

Scheme 2.12. Photoproducts of QMP 2 irradiation in the presence of a quencher.

Irradiation of **QMP 3** in the presence of a nucleophile resulted only in the formation of the adducts **2.16** with azide and **2.17** with cysteamine (Scheme 2.6B).

2.6 Detection of the Transient Species and Reactivity Kinetics of QMP/QMs

Irradiation of all three QMPs in fully aqueous solution with 300 nm light resulted in the formation of a new peak around 400 nm. UV spectra before and after irradiation along with the differential absorption spectra (inserts) of **QMP 1**, **QMP 2** and **QMP 3** are shown Figure 2.3A, B, and C respectively. Both oQM and pQM also exhibits characteristic maximum absorbance around 400 nm.[24] Therefore, we further inspected the new band at 400 nm and collected evidence of QM formation. As the first evidence, we collected irradiated and collected the absorbance spectra of the compound **2.23** which is methoxy protected at both naphthol and phenolic positions and therefore will not generate any type of QMs. Evidently, the compound did not show formation of a new band around 400 nm which confirms that the 400 nm band observed in QMPs to be their respective QM (Figure 2.3D).

We followed the kinetics of the new band at 400 nm for all QMPs soon after irradiation and in the dark. **QMP 1** showed a decay that fits well into a three-exponential function with three different half-lifetimes (~25, ~100, ~1500 s) indicating multiple processes involved (Figure 2.8A). The kinetic trace observed for **QMP 1** in UV spectrometer could be a combined effect of **oNQM 1** and/or **pQM 1** and formation of the oxidized product from **oNQM 1** and/or the decomposition of **NPQ 1** (Scheme 2.13). We excluded the possibility of **pQM 1** hydration regenerating the precursor because of our results from **QMP 3** and fast kinetic study of **QMP 1** which confirmed **oNQM 1** is the predominant form of QM in the **QMP 1** system.

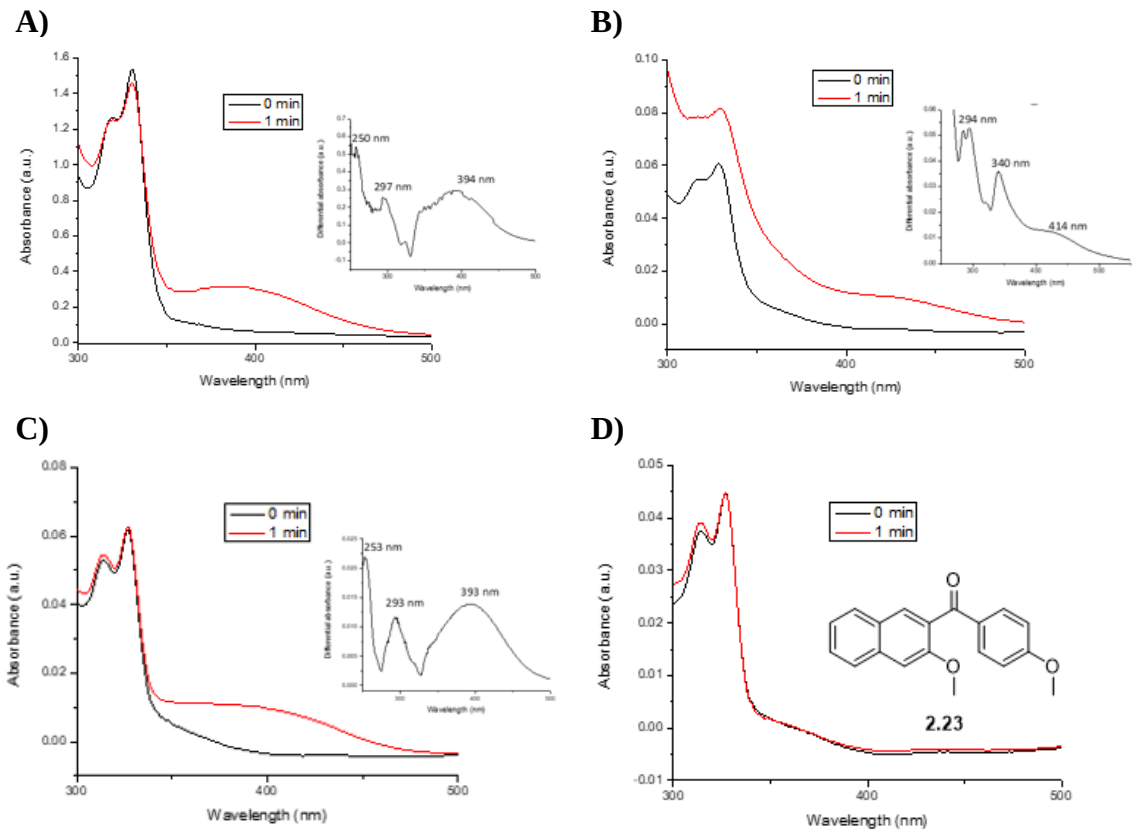

Figure 2.3. Change in UV spectra A) QMP 1, B) QMP 2, C) QMP 3, and D) 2.23. (Insert: differential absorbance).

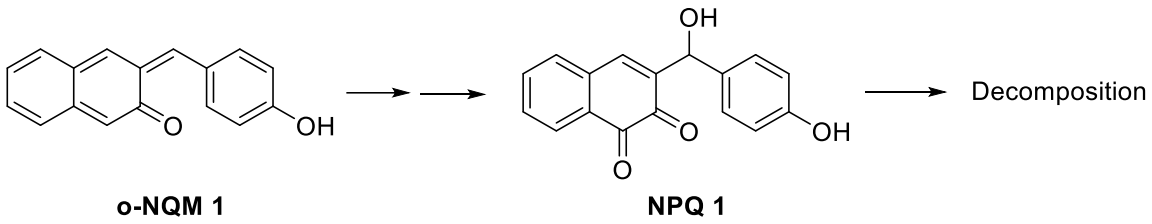

Scheme 2.13. oNQM 1 conversion to NPQ 1 and decomposition.

Transient absorbance spectra of **QMP 1** showed one peak at 370 nm which was confirmed as **oNQM 1** because it corresponds to the same wavelength we previously reported for 2,3-naphthoquinone-3-methide, compound **1.13** generated from parent oNQMP and the band.[30,31] Furthermore, the 370 nm peak was effectively quenched in the presence of a trapping agent, confirming it to be **oNQM 1** and not affected by oxygen

(Figure 2.4A, B). The reaction of **QMP 1** with thiol nucleophile, cysteamine and sodium azide showed quenching rate constants that are like that of parent o-NQMP.[30,31] Nevertheless, quenching of QMP 1 with ethyl vinyl ether (EVE) was significantly low (Figure 2.4C, and Table 2.3). [4+2] cycloaddition reaction of quinone methides belong to the category of IEDDA reaction and it requires a diene/QM with electron-rich groups and alkenes with electron-donating groups.[76,77] Additionally, Basarić and co-workers reported a lower rate constant for o-NQM-EVE reaction due to steric effect when an o-NQM with an adamantyl group at the methide position, compound **1.84 QM** (Table 2.3).[45] **QMP 1** having a phenolic group at the methide position, causes both electronic and steric barriers for Diels-Alder reactions with ethyl vinyl ether. Therefore, resulting in a low-rate constant for the reaction between oNQM 1-EVE, and not because of **pQM 1** formation in competing QM system, **QMP 1**.

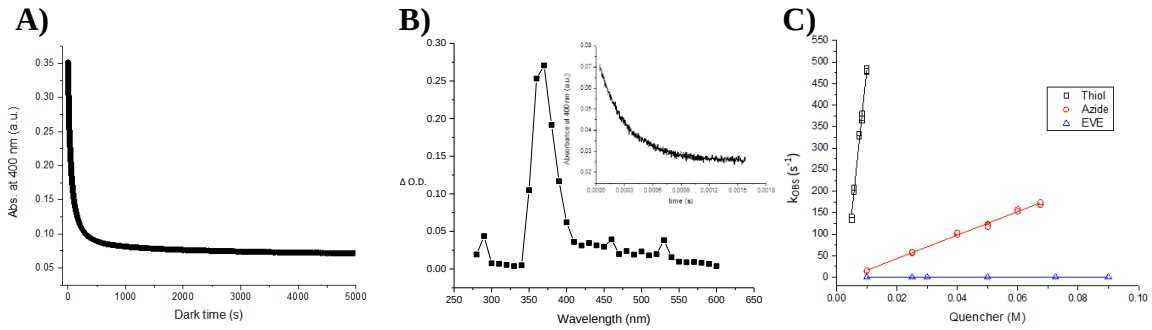

Figure 2.4. A) QMP 1 kinetics trace at 400 nm in the dark B) Transient spectra of oNQM 1 (inset: dark decay) C) oNQM 1 second-order kinetic plots.

Table 2.3. Second-order rate constants of oNQM 1, 1.13, and 1.84 QM with quenchers.

	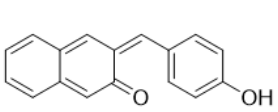 oNQM 1	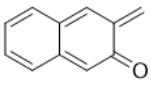 1.13	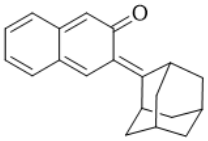 1.84 QM
Quencher	**Second-order rate constant $M^{-1} s^{-1}$**		
	oNQM 1	**1.13**[31]	**1.84 QM**[45]
RSH	$(6.7\pm0.3)\times10^{4}$	$(2.24\pm0.06)\times10^{5}$	$(1.08\pm0.05)\times10^{5}$
NaN_3	$(2.73\pm0.05)\times10^{3}$	$(2.00\pm0.11)\times10^{4}$	$(3.7\pm0.5)\times10^{4}$
EVE	(1.49±0.07)	$(4.07\pm0.19)\times10^{4}$	(85±10)

Additionally, o-NQM 1 generation from QMP 1 does not follow the benzoxete intermediate formation pathway that was previously reported by our group (Section 1.4). This is because the formation of respective benzoxete intermediate is too strained, sterically hindered, and energetically not favorable to form.

QMP 2 showed an increase in the absorbance at 400 nm in the dark/soon after irradiation. The absorbance reached a plateau which fits into a double exponential growth with two half-lives at 300 s and 1400 s (Figure 2.5). The double exponential growth of **oNQM 2** in the dark should be due to the formation of **NPQ 2** via sequential first-order kinetics/two steps. **QMP 2** in the presence of a quencher, did show the formation of a new band at 400 nm, which decreased in absorbance. Attempts were taken to study the quenching kinetics of **oNQM 2** using a modified LFP as we believe the lifetime of to be in the millisecond range, which is too slow to measure by LFP and too fast to be measured by UV spectrophotometer upon irradiation. However, complex kinetic results were

observed due to the formation of oxidized product along with the nucleophilic adducts (Scheme 2.12).

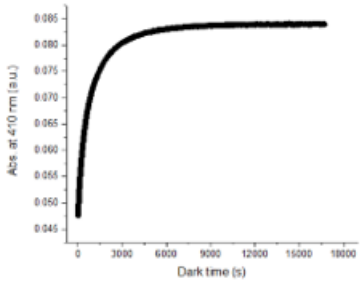

Figure 2.5. QMP 2 kinetics trace at 400 nm in the dark.

QMP 3 400 nm new band exhibited the expected single exponential decay in the dark with a half-lifetime of ~80 s (Figure 2.6A) and the peak was quenched in the presence of nucleophiles. Therefore, the observed 400 nm peak for **QMP 3** was assigned as **pQM 3**. Irradiation of **QMP 3** using a rayonet photoreactor and following kinetics by UV spectrophotometer was challenging as the cuvette transfer delay time caused measurement of incomplete kinetic trances. Therefore, a conventional UV spectrophotometer (Cary 60) was modified where the sample could be irradiated inside the cuvette compartment in the instrument and follow kinetics immediately upon irradiation. The pseudo first-order rate constants for **QMP 3** in the presence of excess quenchers were measured. The quenchers used are cysteamine (RSH-thiol), sodium azide and EVE. The second-order rate constant of **QMP 3**/**pQM 2** reactions with various quenching agents were calculated from a plot of pseudo first-order rate constants vs varying quencher concentration (Figure 2.6B).

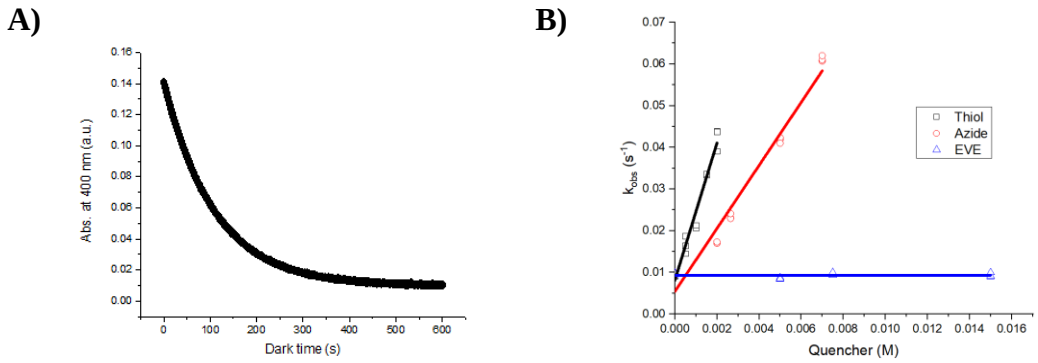

Figure 2.6. A) QMP 3 kinetics trace in the dark, B) quenching kinetics of pQM 2.

QMP 3 quenching rate constant with thiol are lower than that of parent pQM, 1,4-quinone-4-methide, compound 1.2 (~6-fold).[39] However, same rate constants were noted regardless of having naphthyl or phenyl at the methide position of pQM, compound 1.44 (Table 2.4).[39, 10]

Table 2.4. Second-order rate constants of pQM 2, 1.2, and 1.44 with quenchers.

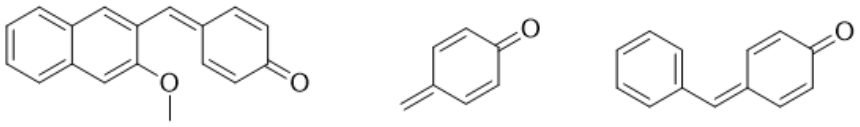

pQM 2 **1.2** **1.44**

Quencher	**Second-order rate constant M^{-1} s^{-1}**		
	pQM 2	**1,4-quinone-4-methide**[27]	**1,4-quinone-4-phenylmethide**[23]
RSH	(17.1±0.9)	110	15
NaN_3	(8.0±0.3)	N/A	N/A
EVE	~0	x	x

2.7 Applications of QMPs for in-situ Generation of Fluorescent Dyes

A characteristic feature of the QMPs in this study is that QMs generated are conjugated to a naphthyl or phenyl ring at the methide position. We explored an interesting application of conjugated QMs. QMPs are non-fluorescent. Photochemically generated-conjugated QMs are expected to be highly fluorescent. Since QMs are short-lived, and undergo rapid hydration, regenerating QMPs, QMP-QM system can be considered as photoswitchable fluorophores. Thus, we attempted to measure fluorescence of each QMP photolysate. A limitation of testing photoswitchable feature of QMP-QM is that the slow scanning speed of fluorimeter compared to QM lifetime. In this regard, justification of the photoswitch concept with o-NQMs was not achievable as the lifetime is 7-8 milliseconds. **QMP 3** is an ideal candidate test our hypothesis as the lifetime is sufficient to measure fluorescence. Irradiation of a **QMP 3** sample (0.2 mM in aq. Acetonitrile, λ_{ex} = 400 nm). using 300 nm showed a color change from colorless to bright yellow (Figure 2.7A), and fluorescence intensity enhancement at 500 and 535 nm (Figure 2.7B).

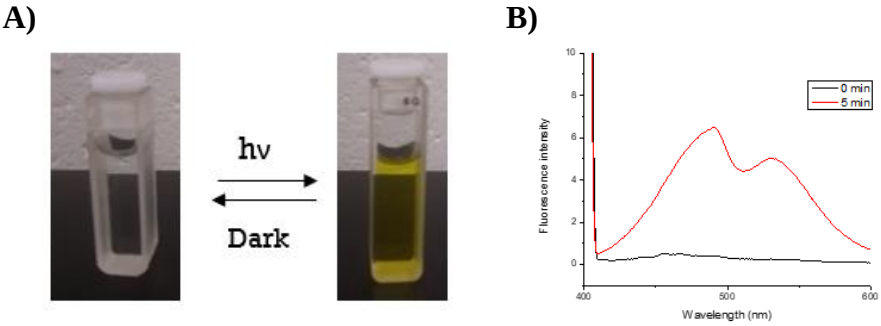

Figure 2.7. A) Photos, B) fluorescence spectra of QMP 3 before and after irradiation.

Irradiation of **QMP 2** showed an increase in the fluorescence intensity, which was a permanent change with emission at 455, 485, and 530 nm (Figure 2.8A). Fluorescence spectra of the primary photoproduct, **NPQ 2** showed the same maximum emission

wavelength bands suggesting **QMP 2** is a photoactivatable fluorophore (Figure 2.8B). Both spectra were collected in aqueous acetonitrile, λ_{ex} = 425 nm.

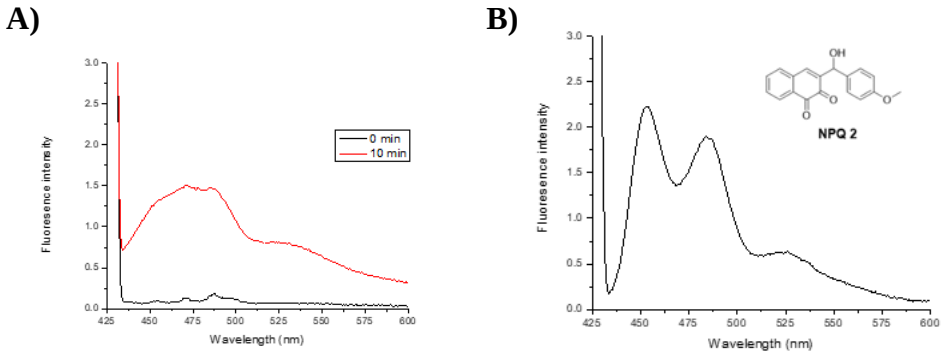

Figure 2.8. A) QMP 2 photolysate fluorescence, B) NPQ 2 fluorescence spectra.

2.8 Plausible Mechanisms for QMP 1, QMP 2 and QMP 3 Oxidation

Photooxidation of 1-naphthol,[78,79] dienes/polycyclic aromatic hydrocarbons (pentacene),[80] photooxygenation of 1,5-dihydroxynaphthalene to 5-Hydroxy-1,4-naphthoquinone (Juglone) are well known and the mechanism occur via 1,4-cycloaddition of singlet oxygen to the aromatic ring to form a stable endo-peroxide.[81,82] Basaric and co-workers have reported oxidation of anthracene-QMP, 3-(hydroxymethyl)anthracen-2-ol to 1,2-anthroquinone derivative, 2.27 (Scheme 2.14).[49] However, the mechanism of the reaction was not discussed.

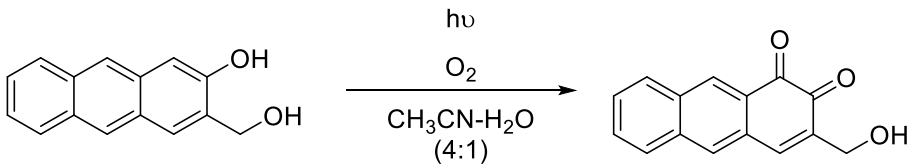

2.26 **2.27**

Scheme 2.14. Photooxidation of 3-(hydroxymethyl)anthracen-2-ol.

The observations reported for anthracene QMP is similar as we observed for **QMP 1** and **QMP 2**. However, photooxidation of **QMP 1**/**QMP 2** to **NQP 1**/**NPQ 2** as the

primary photoproduct and **QMP 3** to the aldehyde, **2.21** as the secondary photoproduct is the first reported feature for NQMPs and pQMPs, yet an interesting feature to explore mechanistically. This may be because naphthyl or phenyl conjugation at the methide position in this study are long-lived compared to non-conjugated QMs reported in the literature and the latter do not undergo oxidation.

In the case of **QMP 2**, irradiation in the presence of quenchers showed a competition to form the desired nucleophilic adduct and the oxidized product, **NPQ 2**. Thus, photooxidation could be due to the oxidation of respective NQMs which competes for oxygen and nucleophile (Scheme 2.15).

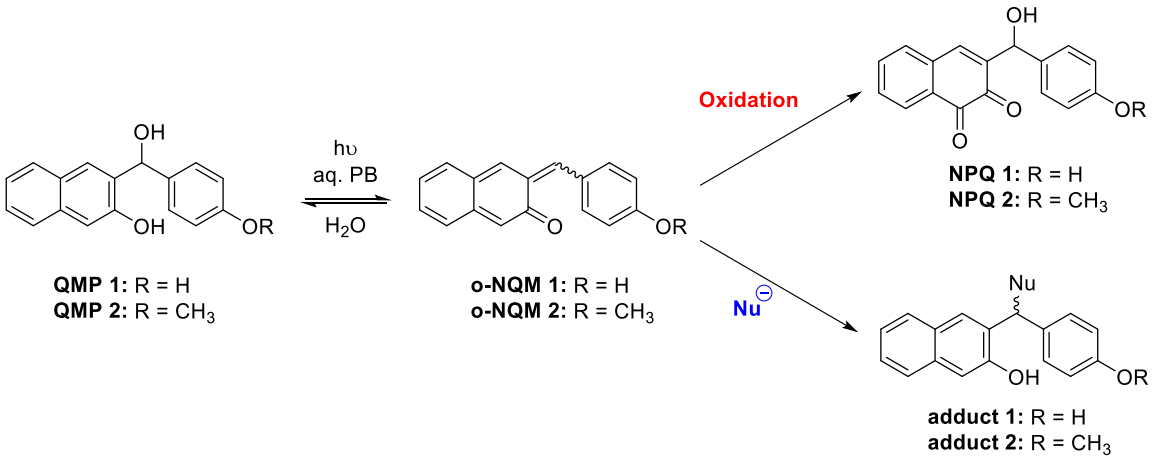

Scheme 2.15. Photogeneration of oNQMs from QMP 1, QMP 2, and their competing reactions.

On the basis of a literature precedent, we propose a similar mechanism as photogeneration of juglone to the oxidation of **QMP 2** to **NPQ 2** (Scheme 2.16).

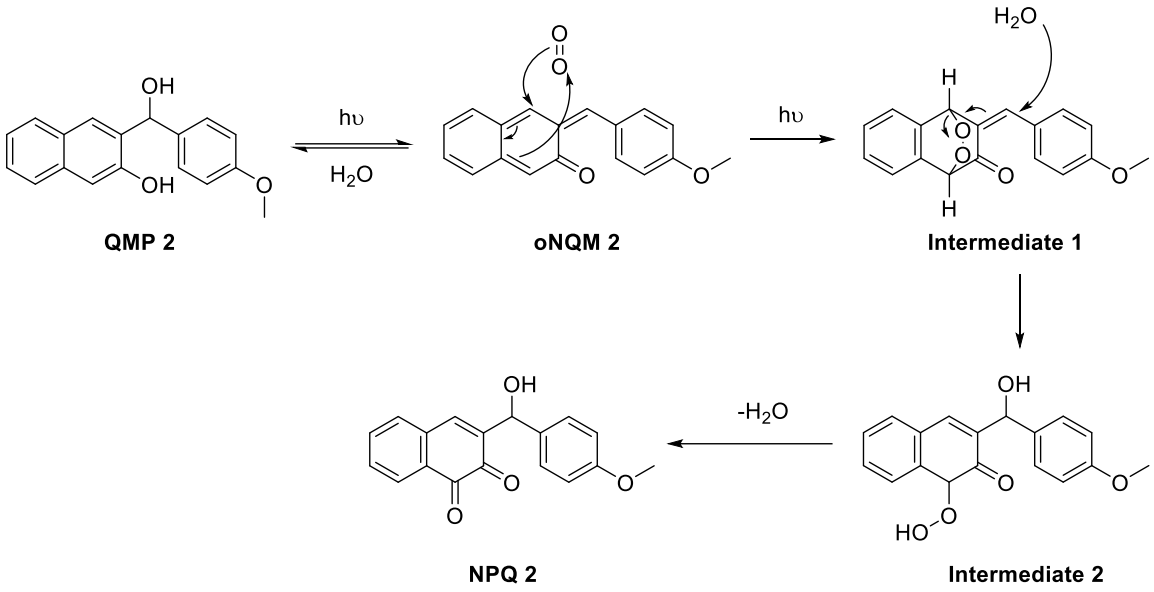

Scheme 2.16. Plausible oxidation mechanism for QMP 2.

Spiro epoxidation of QMs with oxygen was reported recently[83] and we propose a mechanism for **QMP 3/pQM 2** oxidation to aldehyde, 2.21 followed by Spiro epoxidation (Scheme 2.17).

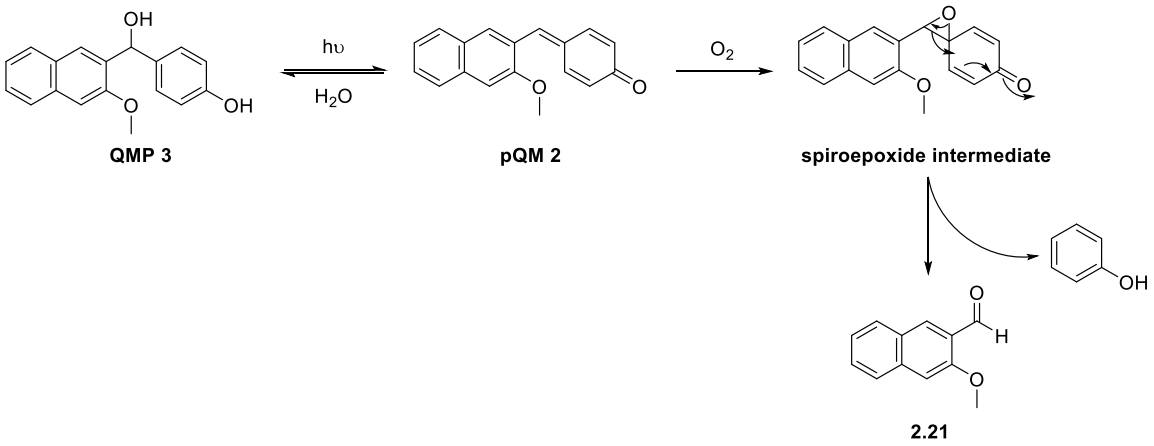

Scheme 2.17. Plausible mechanism for QMP 3 oxidation.

2.9 Conclusions

In summary, we reported the photochemistry of a novel quinone methide precursor system that photo-generates two types of conjugated quinone methides, o-NQM and p-QM. We found that the o-NQM is the predominant form based on the unique primary photo-product formation (Naphthoquinone) from conjugated oNQMs and kinetic studies. It is evident that oNQM 1 is the predominant form of QM in the competing QMP 1 system mainly because both **QMP 1** and **QMP 2** generate primary photoproducts or derivatives of 1,2-nahthoquinone and **QMP 3** does not generate such species.

o-NQMs (**oNQM 1** and **oNQM 2**) are short-lived, whereas **pQM 3** is relatively long-lived (40-50 ms vs. 1 s). The reactivity **oNQM 1** is higher than that of **pQM 1** with the same nucleophile (~4000 fold higher when the nucleophile is thiol/cysteamine and ~400 fold higher when the nucleophile is azide). Additionally, the rate constant values of **QMP 1** are closer to that of **parent oNQMP**: 2,3-naphthoquinone-3-methide precursor (Table 2.6). Thus, based on the rate constant values it is evident that **oNQM 1** is the predominant form of QM in the competing **QMP 1** system. The only deviation for **oNQM 1** and the parent oNQM is the rate constants for the IEDDA with EVE which is due to the steric and electronics of **QMP 1** compared to the parent oNQMP.

This study remarks on the first reported conjugated o-NQM and we confirm that o-NQMs are prone to oxidation leading to the formation of Naphthoquinone. The formation of irreversible naphthoquinone methide product is fluorescent making **QMP 2** a photoactivatable fluorophore. Additionally, we took the benefit of long-lived, conjugated pQMs fluorescence behavior to develop a novel photoswitchable fluorophore.

Table 2.5. Second-order rate constants of QMPs with various quenching agents.

QM precursor	second-order rate constant $M^{-1}s^{-1}$		
	NaN_3	$HSCH_2CH_2NH_2$	EVE
Parent oNQMP	$(2.00\pm0.11)x10^4$	$(2.24\pm0.06)x10^5$	$(4.07\pm0.19)x10^4$
QMP 1	$(2.73\pm0.05) \times 10^3$	$(6.73\pm0.32) \times 10^4$	(1.49 ± 0.07)
QMP 3	(7.56 ± 0.05)	(16.45 ± 0.01)	~0

2.10 Experimental Section

2.10.1 General Information

All the chemicals were obtained from commercial sources and were used without further purification. Solvents, Tetrahydrofuran (THF), and dichloromethane (DCM) were purified using the M. Braun solvent purification system. Column chromatography was performed using 40-63 μm silica gel. All glassware was thoroughly cleaned, and oven-dried before use.

^1H and ^{13}C NMR spectra were recorded at 400 or 600 MHz at room temperature using residual solvent proton as a reference, and chemical shifts were reported in parts per million (ppm). COSY (^1H-^1H correlation spectroscopy), HSQC (heteronuclear single quantum correlation), HMBC (heteronuclear multiple bond correlation) spectra were collected using a 600 MHz NMR spectrometer. Abbreviations used in NMR data interpretation are as follows: $CDCl_3$ (deuterated chloroform), MeOD (deuterated methanol), DMSO (deuterated dimethyl sulfoxide), singlet (s), doublet (d), triplet (t),

multiplet (m), broad (br). High-resolution mass spectra were obtained using electron spray ionization and orbitrap mass analyzer.

2.10.2 Synthesis Procedures and Compound Characterization

Synthesis of methyl 3-methoxy-2-naphthoate, 2.19

Methyl 3-hydroxy-2-naphthoate (10.00 g, 50 mmol) and K_2CO_3 (34 g, 246 mmol) were mixed with acetone (120 mL). Me_2SO_4 (12 mL, 15.88 g, 126 mmol) was added dropwise, then the reaction mixture was refluxed for 12 hours. The reaction mixture was filtrated from salt, acetone was evaporated, and the residue was dissolved in CH_2Cl_2. The obtained solution was washed with water, brine, and dried over Na_2SO_4. The solvent was evaporated and product 2.19 was obtained as a yellow oil (10.48 g, 98 %). No purification was required. ^{1}H NMR (400 MHz, $CDCl_3$): δ 8.30 (s, 1H), 7.79 (d, J = 8.0 Hz, 1H), 7.71 (d, J = 8.4 Hz, 1H), 7.52-7.47 (m, 1H), 7.38 -7.33 (m, 1H), 7.18 (s, 1H), 3.97 (s, 3H), 3.95 (s, 3H). ^{13}C NMR (100 MHz, $CDCl_3$): δ 166.5, 155.3, 135.9, 132.6, 128.5, 128.3, 127.3, 126.3, 124.2, 121.5, 106.6, 55.8, 52.1. HRMS-ESI (m/z): [M+Na]+ calculated for $[C_{13}H_{12}O_3Na]$+: 239.0679, found: 239.0678

Synthesis of (3-methoxynaphthalen-2-yl)methanol, 2.20

Methyl 3-methoxy-2-naphthanoate, **1** (10.48 g, 48.5 mmol) was dissolved in anhydrous THF (500 mL), the solution was cooled to 0 ^{0}C, and $LiAlH_4$ (10.78 g, 291 mmol) was added in small portions. The reaction mixture was allowed to react for 2 hours at room temperature, then 0.1 M solution of HCl was added and the product was extracted with EtOAc, washed with water, brine, and dried over Na_2SO_4. The solvent was evaporated and product, **2.20** was obtained as white solid (8.89 g, 97%). No purification was required. ^{1}H NMR (400 MHz, $CDCl_3$): δ 7.77-7.72 (m, 3H), 7.46-7.7.42 (m, 1H), 7.38-7.33 (m, 1H),

7.12 (s, 1H), 4.82 (s, 2H), 3.96 (s, 3H). ^{13}C NMR (100 MHz, $CDCl_3$): δ 155.94, 134.13, 130.46, 128.67, 127.68, 127.58, 126.46, 126.35, 123.96, 105.19, 62.51, 55.40. HRMS-ESI (m/z): $[M+Na]^+$ calculated for $[C_{12}H_{12}O_2Na]^+$: 211.0730, found: 211.0727

Synthesis of 3-methoxy-2-naphthaldehyde, 2.21

PCC (18.9 g, 73 mmol) was slowly added to 0 °C solution of **2** (8.89 g, 47.3 mmol) and sodium acetate (6.05 g, 73 mmol) in CH_2Cl_2 (400 mL). When the addition was finished, the reaction mixture was left at room temperature overnight. The next day CH_2Cl_2 was evaporated, and the residue was purified via column chromatography (CH_2Cl_2/Hexanes, 1:1). Product **2.21** was obtained as yellow crystals (8.70 g, 99 %). ^{1}H NMR (400 MHz, $CDCl_3$): δ 10.57 (s, 1H), 8.35 (s, 1H), 7.87 (d, J = 8.0 Hz, 1H), 7.73 (d, J = 8.4 Hz, 1H), 7.54 (t, J = 6.92 Hz, 1H), 7.38 (t, J = 8.32 Hz, 1H), 7.18 (s, 1H), 4.01 (s, 3H). ^{13}C NMR (100 MHz, $CDCl_3$): δ 190.34, 157.62, 137.54, 130.03, 129.95, 129.24, 127.76, 126.62, 125.61, 124.66, 106.36, 55.65. HRMS-ESI (m/z): $[M+Na]^+$ calculated for $[C_{12}H_{10}O_2+Na]^+$: 209.0573, found: 209.570.

Synthesis of (3-methoxynaphthalen-2-yl)(4-methoxyphenyl)methanol, 2.22

4-Bromoanisole (2.442 g, 13 mmol) was dissolved in anhydrous diethyl ether (25 mL). The obtained solution was cooled to -78 ºC and n-BuLi (2.5 M in hexane, 4.80 mL, 12 mmol) was added dropwise. The mixture was allowed to react for 1 hour at -78 ºC, then compound **2.21** (1.962 g, 10.6 mmol) in THF (20 mL) was added dropwise. The mixture was allowed to reach room temperature and was left overnight. The next day water (40 mL) was added, the product was extracted with ethyl acetate, washed with water, brine, and dried over Na_2SO_4. Product **2.22** was isolated via column chromatography (EtOAc/Hexanes, 1:6) as pale-yellow crystals (2.24 g, 69 %). ^{1}H NMR (400 MHz, MeOD):

δ 8.00 (s, 1H), 7.68-7.77 (m, 2H), 7.34-7.38 (m, 1H), 7.27-7.30 (m, 3H), 7.12 (s, 1H), 6.78-6.80 (m, 2H), 6.16 (s, 1H), 3.74 (s, 3H), 3.65 (s, 3H). ^{13}C NMR (100 MHz, $CDCl_3$): δ 158.8, 155.4, 135.1, 133.8, 133.4, 128.6, 128.0, 127.9, 126.8, 126.3, 123.9, 113.6, 105.6, 72.3, 55.4, 55.2. HRMS-ESI (m/z): $[M+Na]^+$ calculated for $[C_{19}H_{18}O_3Na]^+$: 317.1154, found: 317.1149.

Synthesis of (3-methoxynaphthalen-2-yl)(4-methoxyphenyl)methanone, 2.23

Compound **2.22** (2.11 g, 6.9 mmol) was dissolved in CH_2Cl_2 (200 mL), activated MnO_2 (12.3 g, 142 mmol) was added to the solution. The mixture was stirred at room temperature for 12 hours, then the precipitate was filtered off. The solvent was evaporated. Product **2.23** was obtained as white crystals (2.08 g, 99 %). No purification was required. ^{1}H NMR (400 MHz,): δ 7.84 (d, J = 8.80 Hz, 2H), 7.78 (m, 3H), 7.50 (t, 1H), 7.38 (t, 1H), 7.22 (s, 1H), 6.90 (d, J = 8.84 Hz, 2H), 3.86 (s, 3H), 3.85 (s, 3H). ^{13}C NMR (100 MHz, $CDCl_3$): δ 194.70, 163.72, 155.00, 135.20, 132.44, 130.96, 130.69, 129.15, 128.30, 128.01, 127.54, 127.66, 126.66, 124.41, 113.58, 106.10, 55.67, 55.52. HRMS-ESI (m/z): $[M+H]^+$ calculated for $[C_{19}H_{16}O_3H]^+$: 293.1172, found: 293.1175.

Synthesis of (3-hydroxynaphthalen-2-yl)(4-hydroxyphenyl)methanone, 2.24

A solution of **2.23** (1 g, 3.4 mmol) in CH_2Cl_2 (100 mL) was cooled to –78 ^{0}C, then BBr_3 (9.6 g, 3.7 mL, 39.1 mmol) was added dropwise. The reaction mixture was allowed to reach room temperature overnight. The next day, water (40 mL) was added, and the obtained precipitate was filtered off. The solution was extracted with EtOAc, washed with water, brine and dried over Na_2SO_4. The product **2.24** was obtained as yellow crystals (0.89 g, 99 %). No purification was required. ^{1}H NMR (400 MHz, DMSO-d): 10.46 (s, 1H), 10.15 (s, 1H), 7.86 (d, J = 8.16 Hz, 1H), 7.84 (s, 1H), 7.76 (d, J = 8.72 Hz, 2H), 7.48 (t, J

= 7.04 Hz, 1H), 7.33 (t, J = 7.88 Hz, 1H), 7.26 (s, 1H), 6.87 (d, J = 8.72 Hz, 2H). ^{13}C NMR (100 MHz, DMSO-d): 194.96, 162.98, 153.24, 135.51, 132.74, 130.33, 129.36, 129.15, 128.74, 127.82, 127.44, 126.34, 123.96, 115.70, 110.09. HRMS-ESI (m/z): $[M+H]^+$ calculated for $[C_{17}H_{12}O_3H]^+$: 265.0859, found: 265.0860.

Synthesis of 3-(hydroxy(4-hydroxyphenyl)methyl)naphthalen-2-ol, QMP 1

The compound **2.24** (100 mg, 0.38 mmol) was dissolved in anhydrous THF (15 mL), the solution was cooled to 0 ºC, and $LiAlH_4$ (38 mg, 1 mmol) was added. The reaction mixture was allowed to react for 1 hour at room temperature, then 2 mL of concentrated HCl was added and the product was extracted with EtOAc, washed with water, brine, and dried over Na_2SO_4. The solvent was evaporated and **QMP 1** was obtained as yellow-orange crystals (98 mg, 99 %). No purification was required. ^{1}H NMR (400 MHz, MeOD): 7.79 (1H, s), 7.70 (1H, d, J = 8.0 Hz), 7.59 (2H, d, J = 8.0 Hz), 7.34-7.30 (1H, m), 7.24-7.21 (3H, m), 7.07 (1H, s), 6.74-6.71 (2H, m), 6.12 (1H, s), 4.63 (0.24H, s, br). ^{13}C NMR (100 MHz, MeOD): 157.6, 154.5, 136.0, 135.6, 134.6, 129.7, 129.5, 128.8, 127.1, 126.8, 126.7, 124.0, 116.0, 115.8, 110.1, 72.5. HRMS-ESI (m/z): $[M-H]^-$ calculated for $[C_{17}H_{14}O_3-H]^-$: 265.0870, found: 265.0867.

Synthesis of (3-hydroxynaphthalen-2-yl)(4-methoxyphenyl)methanone, 2.25

Compound **2.24** (0.1 g, 0.38 mmol) was dissolved in 7 mL of acetone, and K_2CO_3 (0.1 g, 0.75 mmol) followed by dimethyl sulfate (0.1 mL, 0.75 mmol) was added while stirring at room temperature for 2 hours. The reaction was quenched with water (5 mL) and extracted with ethyl acetate (20 mL*3) and washed with brine (5 mL). The solvent was evaporated. The residue was purified using column chromatography (eluent EtOAc: hexane 1:4) to obtain compound 7 as a yellow solid (65 mg, 0.23 mmol, 94% at 66%

conversion of **2.24**). ^{1}H NMR (400 MHz, $CDCl_3$): δ 10.98 (s, 1H) 8.10 (s, 1H), 7.73 (d, J = 8.72 Hz, 2H), 7.62-7.68 (m, 2H), 7.45 (t, J = 7.32 Hz, 1H), 7.29 (s, 1H), 7.24 (t, J = 7.52 Hz, 1H), 6.96 (d, J = 8.72 Hz, 2H), 3.85 (s, 3H). ^{13}C NMR (100 MHZ, $CDCl_3$): δ 200.00 163.27, 157.13, 137.60, 135.99, 132.28, 130.38, 129.51, 129.42, 126.69, 126.27, 123.99, 121.42, 113.79, 112.22, 55.58. HRMS-ESI (m/z): $[M+H]^+$ calculated for $[C_{18}H_{14}O_3H]^+$: 279.1016, found: 279.1015.

Synthesis of 3-(hydroxy(4-methoxyphenyl)methyl)naphthalen-2-ol, QMP 2

Compound **2.25** (60 mg, 0.14 mmol) was dissolved in 10 mL of THF and cooled to 0 ^{0}C. LAH pellets (20 mg, 0.43 mmol) was slowly added and stirred for 1 hour. Reaction was quenched by adding 0.1 M HCl, extracted to EtOAc. (20 mL*3) solvent was evaporated off and product was obtained as a yellow oil. (35 mg, 0.125 mmol, 90%). ^{1}H NMR (400 MHz, MeOD): δ 7.69 (s, 1H) 7.58 (d, J = 8.12 Hz, 1H), 7.47 (d, J = 8.16 Hz, 1H), 7.18-7.22 (m, 3H), 7.10 (m, 1H), 6.97 (s, 1H), 6.72 (d, J = 8.72 Hz, 2H), 6.05 (s, 1H), 3.61 (s, 3H). ^{13}C NMR (100 MHz, MeOD): δ 158.92, 153.07, 135.83, 134.19, 133.24, 128.85, 128.31, 128.05, 127.38, 125.28, 125.59, 113.03, 108.60, 70.83, 54.23. HRMS-ESI (m/z): $[M-H]^-$ calculated for $[C_{18}H_{16}O_3-H]^-$: 279.1027, found: 279.1026.

(4-bromophenoxy)(tert-butyl)dimethylsilane

(4-bromophenoxy)(tert-butyl)dimethylsilane was synthesized according to a slightly modified previously published procedure (Scheme 2.17).[84] Tert-Butyldimethylsilyl chloride, TBSCl (2.1 g, 14 mmol), imidazole (1.2 g, 18 mmol), and 4-bromophenol (2.1 g, 12 mmol) was added to DCM (24 mL) and the reaction was stirred at room temperature overnight. Next day, the reaction was quenched with water, extracted to EtOAc, washed with water, brine and dried over Na_2SO_4. Only one spot (product) was

observed on the TLC. So, column purification was not done. The product, 4-(hydroxy(3-methoxynaphthalen-2-yl)methyl)phenol was obtained as a colorless thick liquid (2 g, 60%). ^{1}H-NMR (400 MHz, $CDCl_3$): δ 0.27 (6H), 1.07 (9H), 6.78 (2H), 7.38 (2H). ^{13}C NMR (400 MHz, CDCl3): δ −4.3, 18.3, 113.8, 25.8, 122.1, 132.4, 155.0 ppm. ESI-MS (m/z): $[M+Na]^+$ calculated for $[C_{12}H_{19}BrOSi+Na]^+$: 309.0, found: 309.1.

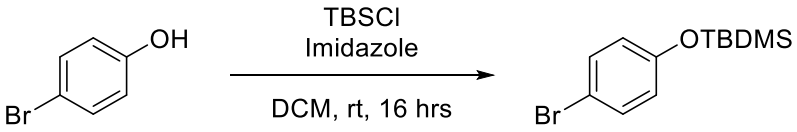

Scheme 2.17. Synthesis scheme for TBDMS protected 4-bromophenol.

Synthesis of 4-(hydroxy(3-methoxynaphthalen-2-yl)methyl)phenol, QMP 3

(4-bromophenoxy)(tert-butyl)dimethylsilane (2.0 g, 6.96 mmol) was dissolved in 30 ml of THF/Et_2O mixture (2:1) and cooled to -78 ^{0}C. 2.5 M n-BuLi in hexane (7.0 mL, 17.5 mmol) was added to the solution and stirred for one hour. Previously synthesized compound **3**, 3-methoxy-2-naphthaldehyde (0.624 g, 3.3 mmol) in 10 mL of THF/Et_2O (1:1) was added to the mixture dropwise and stirred overnight. Next day, the reaction was quenched with water, solvent was evaporated off and extracted using EtOAC. Formation of (4-((tert-butyldimethylsilyl)oxy)phenyl)(3-methoxynaphthalen-2-yl)methanol was not observed. **QMP 3** was isolated via column chromatography (EtOAC: hexane= 1:4 followed by EtOAC: hexane= 1:1). The TBDMS protecting group cleaved at this step. Therefore, an additional deprotecting step was not required. **QMP 3** was obtained as a yellow solid. (0.5 g, 36%). ^{1}H NMR (400 MHz, MeOD): δ 7.79 (s, 1H, 7.56-7.61 (m, 2H), 7.01-7.02 (m, 2H), 7.14 (t, J = 7.88 Hz, 1H), 7.22 (t, J = 7.56 Hz, 1H), 6.99 (s, 1H), 6.53 (d, J = 8.48 Hz, 2H), 5.93 (s, 1H), 3.68 (s, 3H). ^{13}C NMR (100 MHz, MeOD): δ 158.92, 153.07, 135.83, 134.19, 133.24, 128.85, 128.31, 128.05, 127.38, 125.70, 125.45, 125.28,

122.99, 113.03, 108.60, 70.83, 54.23. HRMS-ESI (m/z): $[M-H]^-$ calculated for $[C_{18}H_{16}O_3-H]^-$: 279.1027, found: 279.1024.

2.10.3 Quantum Yield Determination

The general procedure used for quantum yield determination will be described in this section following a sample calculation based on **QMP 3**. Quantum efficiencies (Φ_R) of QMPs were measured in aqueous acetonitrile (1:1) for the photochemical reaction of each QM trapping with 2-mercaptoethylamine hydrochloride. The actinometer, 4-nitoveratrole, or 3,4-dimethoxynitrobenzene with a known $\Phi = 0.116$ in aqueous KOH was used as the reference reaction (Scheme 2.13).

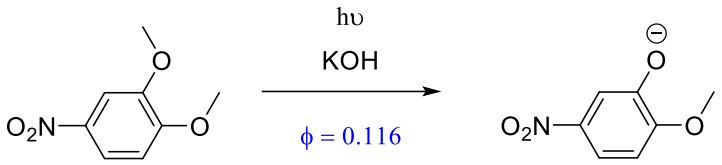

Scheme 2.11. 4-Nitroveratrole irradiation reaction.

The concentration of the actinometer and quinone methide precursor (QMP) was adjusted such that both species have the same absorbance at 300 nm in the UV spectrum. At this condition, the standard quantum yield equation (equation 2.1) can be simplified to equation 2.2. A solution of QMP with an excess of mercaptoethylamine hydrochloride is irradiated and the change in the QMP concentration was measured by HPLC. The chemical actinometer was irradiated under identical conditions as with the QMP and the change in the concentration was measured by the change in the absorbance at 450 nm, maximum absorbance of the product in reference reaction ($\delta = 3040\ M^{-1}\ cm^{-1}$).[85] Subsequently, the photochemical quantum yield of each QMP was calculated according to equation 2.2. Each measurement was carried out in triplicates and the average was taken.

$$\Phi_R = \frac{k_{Actinometer}(1-10^{-Abs\,(S)})}{k_S\,(1-10^{-Abs\,(A)})} \qquad \textbf{(Equation 2.1)}$$

$$\Phi_R = \frac{\Delta[QMP]\ x\ \Phi_{Actinometer}}{\Delta[Actinometer]} \qquad \textbf{(Equation 2.2)}$$

QMP 3 (0.3 mM) in aqueous acetonitrile (1:1) with 30 mM of 2-mercaptoethylamine (30 mM) in a 3 mL quartz cuvette was prepared. 0.0567 mM of 1,2-dimethoxy-4-nitrobenzene in 0.5 M KOH was used as the reference. Both QMP 3 and reference sample showed the same absorbance (0.4 a.u.) at 300 nm wavelength (Figure 2.9A). Both samples were irradiated using two 8 W 300 nm lamps for 20 seconds and HPLC chromatograms were collected before and after irradiation of **QMP 3** (Figure 2.9C). QMP 3 concentration change was determined based on the HPLC calibration curve (Figure 2.9B). Quantum yield calculation is shown in Table 2.6. QMP 3 retention time 7.8 minutes and thiol retention time 2.5 minutes.

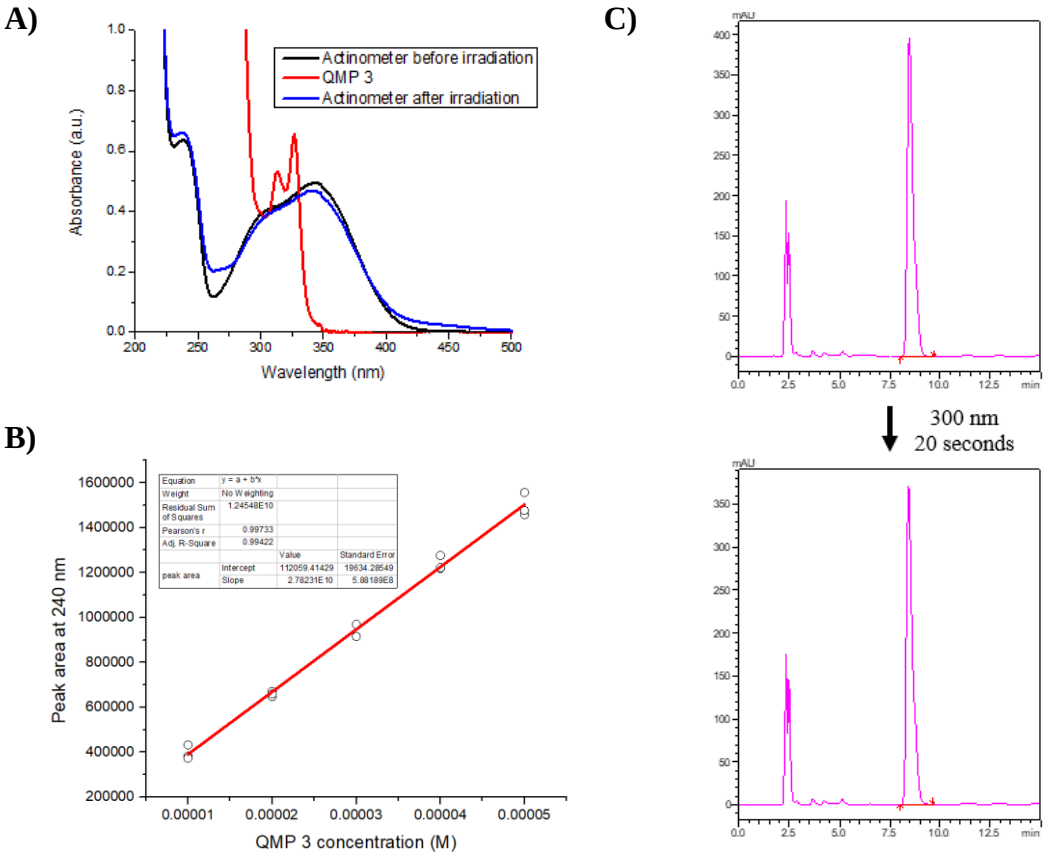

Figure 2.9. A) UV spectra of actinometer, QMP 3 before irradiation and actinometer after irradiation, B) QMP 3 HPLC calibration curve, C) HPLC chromatograms of QMP 3 before irradiation (top), and after irradiation (bottom).

Table 2.6. Experimental data and calculations of the actinometer and QMP 3.

	Trial 1	**Trial 2**	**Trial 3**
Actinometer			
Abs at 450 nm- 0 s	0.003192	0.0	0.0
Abs at 450 nm- 20 s	0.022883	0.021031	0.019295
ΔAbsorbance	0.019691	0.021031	0.019295
ΔConcentration	6.477E-6	6.92E-6	6.35E-6
QMP 3			
Peak area at 0 s	8460441	8475096	9135942
Peak area 20 s	8000351	8011723	8683775
ΔPeak area	460090	463373	452167
ΔConcentration	1.24E-5	1.25E-5	1.21E-5
QY	0.22	0.21	0.22

Standard error= Standard deviation/$(n)^{1/2}$ = 0.003

$$QY_{(QMP\ 3)} = (0.217 \pm 0.003)$$

2.10.4 Irradiation Experiments

All the photoreactions were conducted using a Rayonet photoreactor equipped with ten 8W 300 nm fluorescent lamps unless otherwise specified. A two-way light-quartz cuvette was used for all the irradiation experiments uncles otherwise stated. Stock solutions

were prepared using HPLC-grade acetonitrile. All the reactions were carried out in phosphate buffer prepared in aqueous acetonitrile (IS =0 .1 M, $[H_3PO_4]$ = 0.005 M, $[H_2PO_4^-]$ = 0.008 M, $[NaClO_4]$ = 0.07 M, BR= 0.6, calculated pH 7.00, final pH measured 7.04). Absorbance spectral changes of photolysates were recorded using Cary 5000 spectrophotometer. The qualitative product analysis of the photolysis mixture was carried out by reverse phase HPLC (high-performance liquid chromatography), and pre-known product peaks were identified based on the unique absorbance spectra and by LC-MS (Phenomenex, 5u, C-18, 4.6 x 250 mm column). The mass spectrometer used in LC-MS is Bruker, Impact II quadrupole-time of flight (Q-TOF). Preparative photolysis was performed, product/s were isolated and fully characterized for novel photoproducts.

2.10.4.1 Irradiation of QMPs in the absence of a quencher

This section elaborates the initial photoirradiation results of **QMP 1**, **QMP 2** and logical designing of experiments to identify the primary photoproduct formed from the irradiation of **QMP 1** and **QMP 2**. Short irradiation (≤10 minutes) of **QMP 1** in aqueous phosphate buffer solutions formed a new compound with maximum absorbance at 420 nm according to HPLC analysis (solvent system- methanol: water: acetonitrile 50%:49%:1%, observation wavelength 240 nm). Prolong irradiation (>70 minutes) resulted in the decomposition of both **QMP 1** and the new product, resulting in the formation of which eluted early and/or trapped in the column (Figure 2.10A). Irradiation of **QMP 2** under the same conditions as **QMP 1** and analysis by HPLC showed a similar observation as **QMP 1**. HPLC solvent system- methanol: water 60%:40%, observation wavelength 240 nm. Short irradiation (<2 minutes) of **QMP 2** formed a novel photoproduct with red-shifted absorbance (λ_{max} = 420 nm) and prolong irradiation (>40 minutes) caused decomposition

of both the starting material and novel photoproduct leading to unknown products (Figure 2.10B). Both primary photoproducts formed from **QMP 1** and **QMP 2** have the same chromophore due. Attempts to isolate the primary photoproduct of **QMP 1** was unsuccessful due to the poor stability, and low yield (~<1%) at high conversion (>90%). However, the primary photoproduct formed from **QMP 2** was stable compared to that of **QMP 1**. Hence, the primary photoproduct was isolated via preparative photolysis, and fully characterized by ^{1}H NMR, ^{13}C NMR, COSY (correlation spectroscopy), HSQC (Heteronuclear Single Quantum Correlation), HMBC (Heteronuclear Multiple Bond Correlation), and HR-MS. We found the structure of the primary photoproduct generated from **QMP 2** as 3-(hydroxy(4-methoxyphenyl)methyl)naphthalene-1,2-dione, **NPQ 2**. We concluded that **QMP 1** also produces the respective naphthoquinone derivative, **NPQ 1** as both primary photoproducts have similar absorbance spectra. The unique maximum absorbance values were further confirmed in comparison to commercially purchased 1,2-naphthoquinone as well.

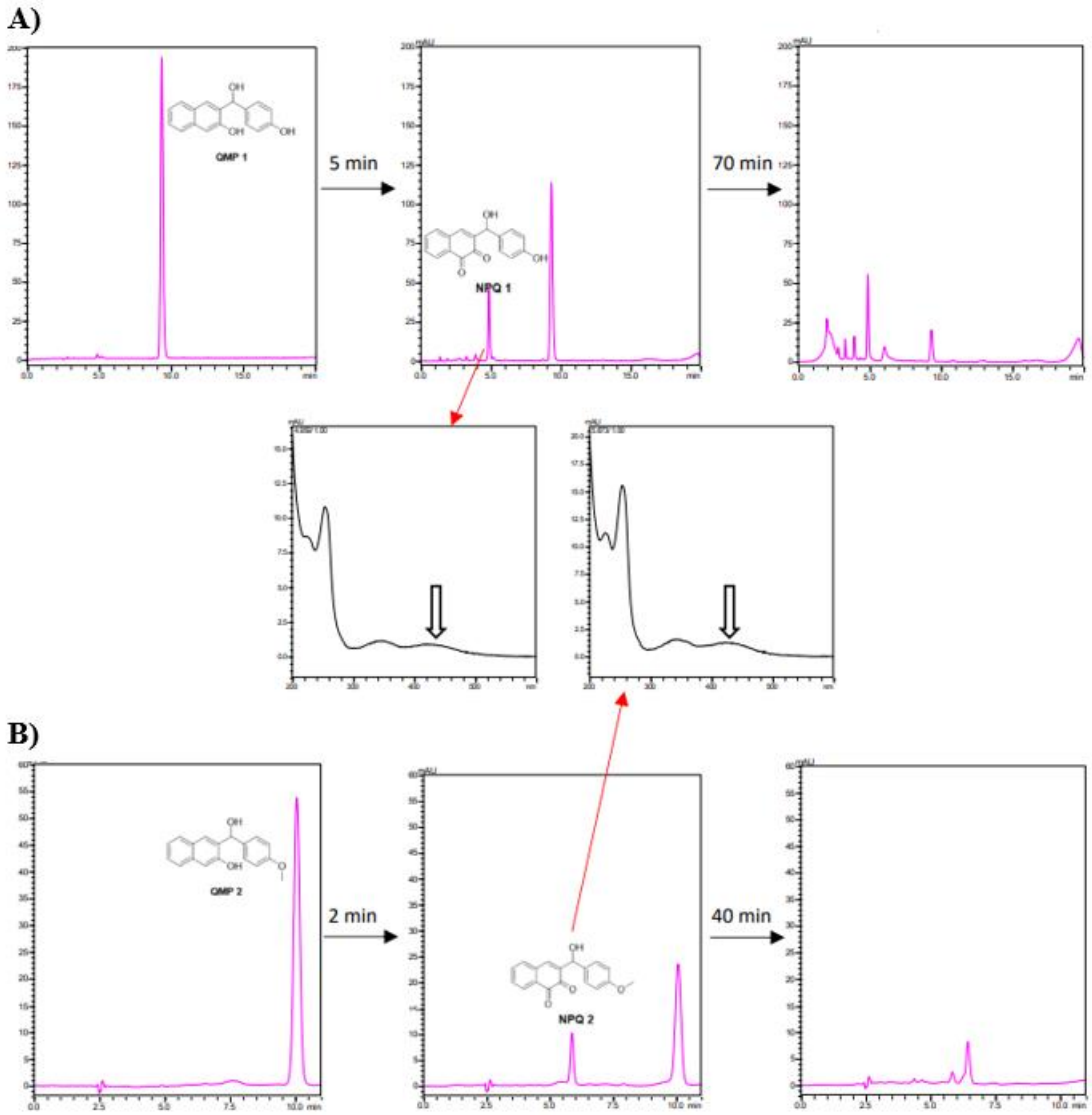

Figure 2.10. HPLC chromatograms and UV spectra of primary photoproducts for A) QMP 1 and B) QMP 2 photolysate with irradiation time.

Irradiation of **QMP 3** for <10 minutes in aqueous phosphate buffer solution without a quencher did not show formation of any new product or no decomposition of the starting material according to our HPLC analysis (HPLC solvent system- methanol: water 60%:40%, observation wavelength: 240 nm). However, prolong irradiation (>3 hours) showed formation of a new compound, and decomposition of **QMP 3** (Figure 2.11).

Isolation of the new product by preparative photolysis confirmed the structure to be 3-methoxy-2-naphthaldehyde, **2.1**.

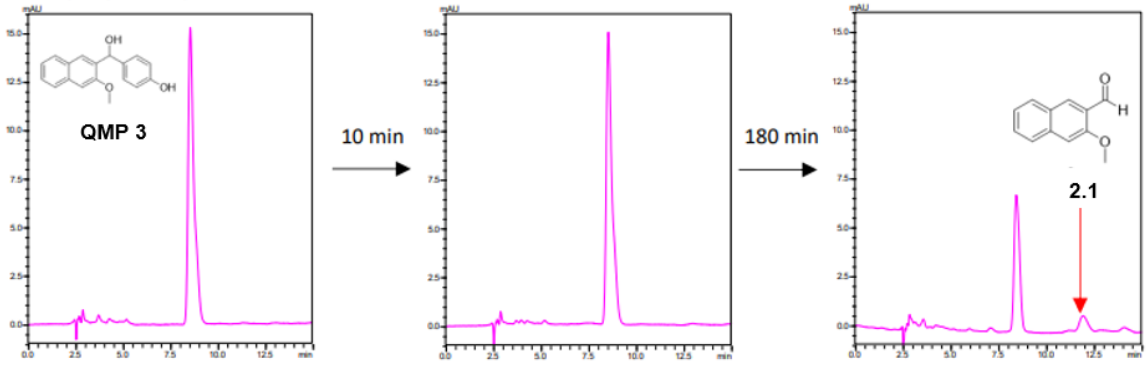

Figure 2.11. HPLC chromatograms of QMP 3 photolysate with irradiation time.

2.10.4.2 Irradiation of QMPs in the absence of a quencher

QMPs in methanol were irradiated using 300 nm lamps and the photolysate was tested by HPLC and LC-MS after each irradiation. HPLC and LC solvent system- methanol 60%: water 40% (0-11 minutes) followed by gradient reaching methanol 100% (11-25 minutes), Observation wavelength 240 nm. Percentage conversion of starting material was calculated from HPLC peak area, and the product peaks were confirmed by LC-MS. **QMP 1** photomethanolysis was conducted jointly with a former lab member Dr. Mariia Sutton.[85] Irradiation of **QMP 2** in methanol ($2.5x10^{-5}$ M) resulted forming methylated adduct, **2.10**. **QMP 2** retention time 10.1 minutes, and compound **2.10** retention time 18.8 minutes (Figure 2.12A). **QMP 3** in methanol ($6x10^{-5}$ M) showed the formation of methylated adduct, **2.15** upon irradiation. **QMP 3** retention time 7.8 minutes, and compound **2.15** retention time 18.8 minutes (Figure 2.12B).

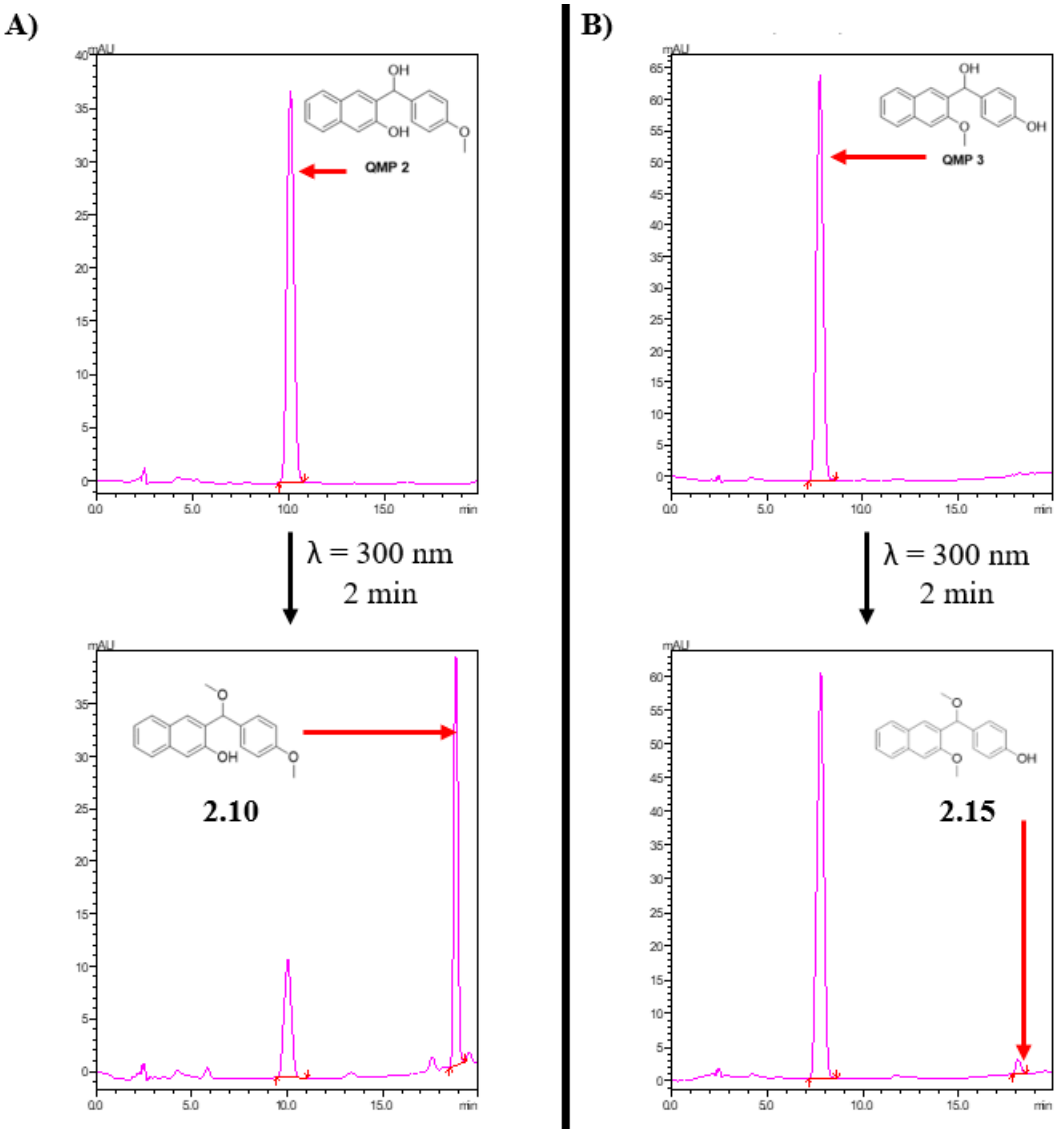

Figure 2.12 HPLC chromatograms before and after irradiation of A) QMP 2. B) QMP 3.

2.10.4.3 Photosynthesis of, 3-(hydroxy(4-methoxyphenyl)methyl)naphthalene-1,2-dione, NPQ 2

1 mM stock solution of **QMP 2** in acetonitrile was prepared (60 mg, 0.214 mmol). 60 μM **QMP 2** solution in DI water was prepared using the above stock solution. (90 ml from the above stock solution in 1500 ml DI water) This solution was irradiated in a rayonet photoreactor equipped with ten, 8 W, 300 nm UV lamps for 10 minutes while stirring

manually using a glass rod in between 2 minutes intervals of irradiation. Compounds were extracted to ethyl acetate and purified using column chromatography (EtOAc: hexane 1:4). **NPQ 2** was isolated as a red-orange crystalline solid. (4 mg, 6%). ^{1}H NMR (600 MHz, MeOD): δ 7.98-7.99 (m, 1H), 7.68-7.71 (m, 2H), 7.49-7.53 (m, 2H), 7.38-7.39 (m, 2H), 6.88-6.90 (m, 2H), 5.73 (s, 1H), 3.77 (s, 3H). ^{13}C NMR (151 MHz, MeOD): δ 181.28, 180.50, 160.90, 143.64, 141.34, 137.30, 136.64, 135.63, 132.01, 131.63, 131.52, 130.59, 129.51, 114.89, 70.32, 55.84, 49.15. HRMS -ESI (m/z): $[M-H]^-$ calculated for $[C_{18}H_{14}O_4-H]^-$: 293.0819, found: 293.0813 and calculated for $[C_{18}H_{16}O_4-H]^-$: 295.0976, found: 295.0968. HRMS -ESI (m/z): $[M+H]^+$ calculated for $[C_{18}H_{14}O_4+H]^+$: 317.0784, found: 317.0779. Absorbance spectra of NPQ 2 resembles that of 1,2-napthoquinone (Figure 2.13). Both compounds have maximum absorbance at 420 nm.

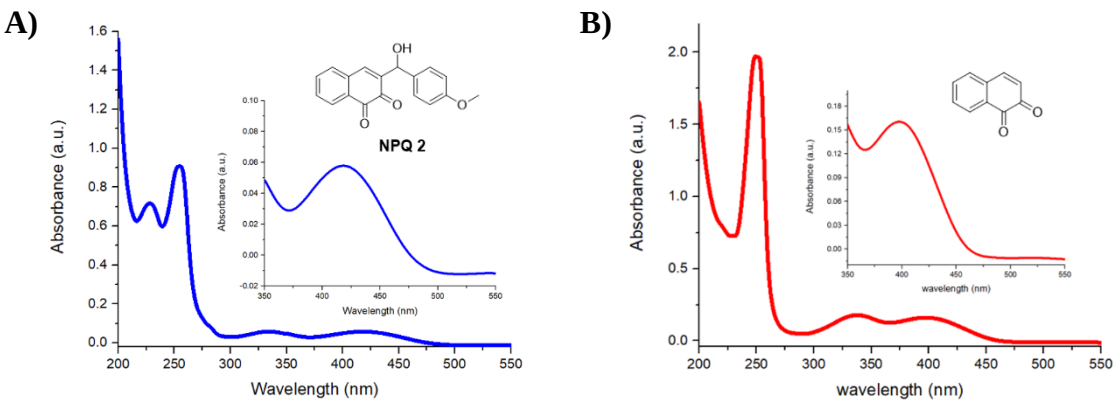

Figure 2.13. Absorbance spectra of A) NPQ 2, B) 1,2-Naphthoquinone.

The detailed assignment of proton (blue) and carbon (red) to the NPQ 2 structure based on HMBC spectrum is shown in Figure 2.14.

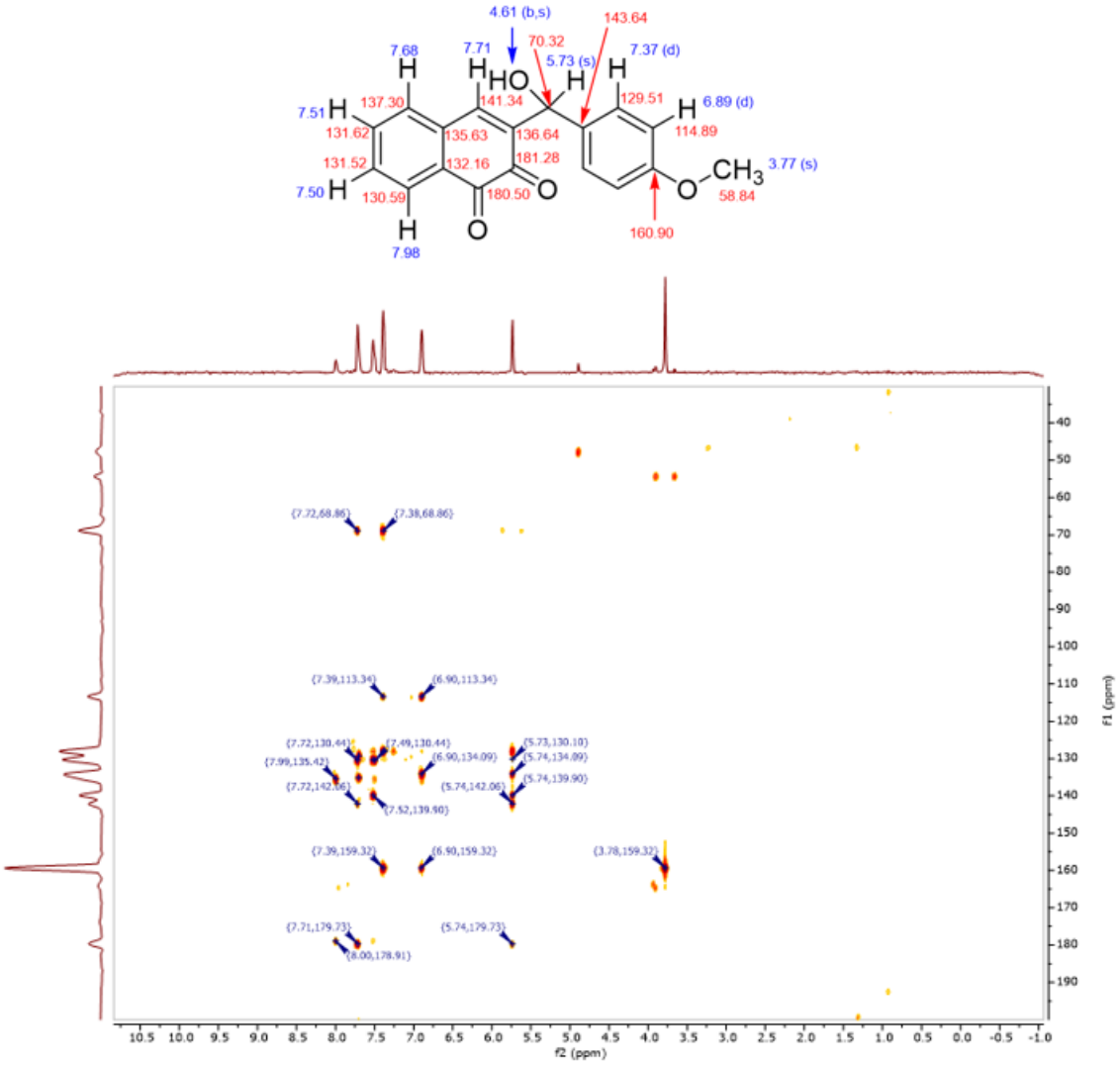

Figure 2.14. Proton and carbon NMR peak assignments and HMBC spectra of NPQ 2.

An interesting observation of NPQ 2 was noted in the HRMS spectra in the negative mode. We found peaks for both naphthoquinone derivative and the respective reduced form, 3-(hydroxy(4-methoxyphenyl) methyl)naphthalene-1,2-diol (Figure 2.15). Since the NPQ 2 product was unknown in our research work, we speculated the possibility of forming both isomers during QMP 2 irradiation. However, according to literature, reduction of pure naphthoquinone to dihydroxy naphthalene is a common behavior due to the electron discharge in the negative mode ESI-MS (Scheme 2.11).[86, 87] Additionally, two

different species were not observed in HRMS positive mode (Figure 2.16). Thus, it confirms the unknown product formed is pure naphthoquinone isomer and not the reduced form or a mixture of both.

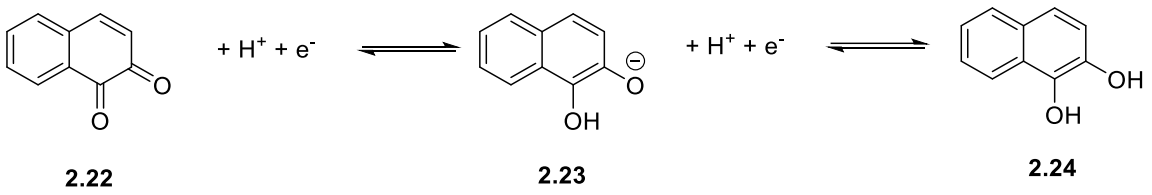

2.22 **2.23** **2.24**

Scheme 2.12. Stepwise reduction of 1,2-naphthoquinone to 1,2-dihydroxynaphthalene.

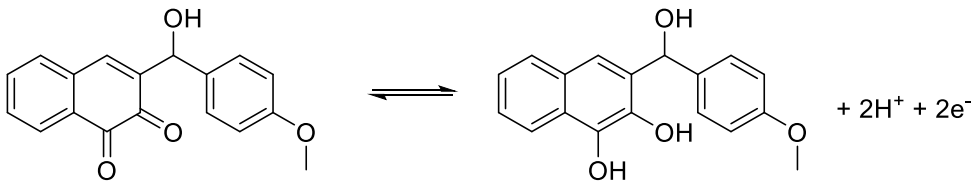

NPQ 2 **2.25**

Scheme 2.13. Reduction of NPQ 2 to 2.25.

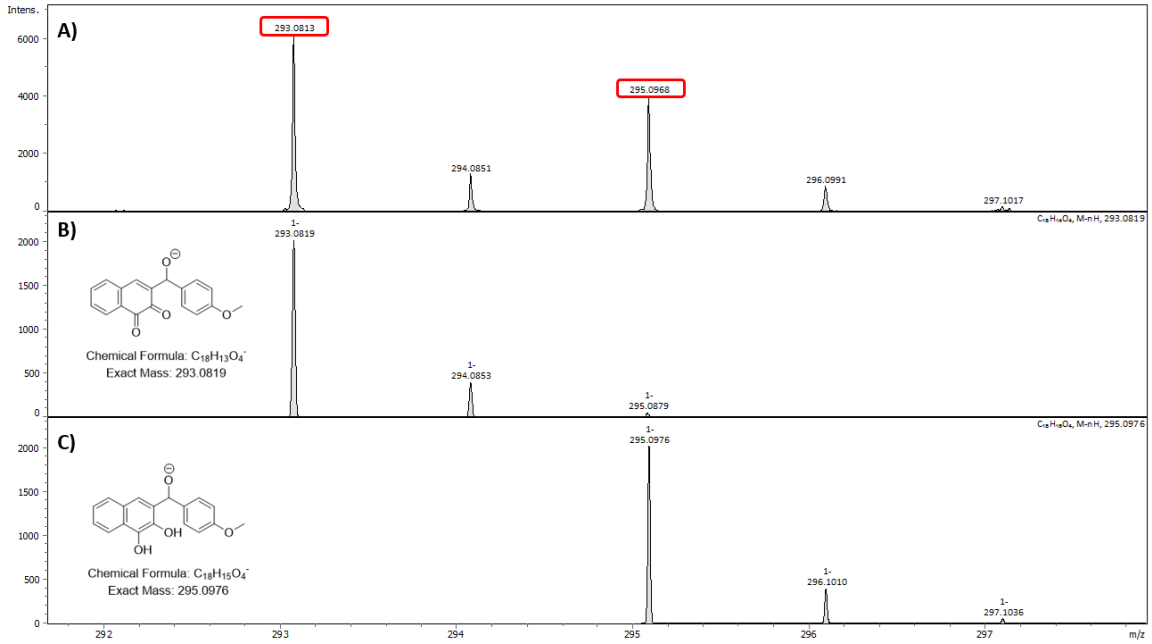

Figure 2.15. A) Experimental negative mode HR-MS spectrum, B) Theoretical simulation NPQ 2, C) Theoretical simulation for 2.25.

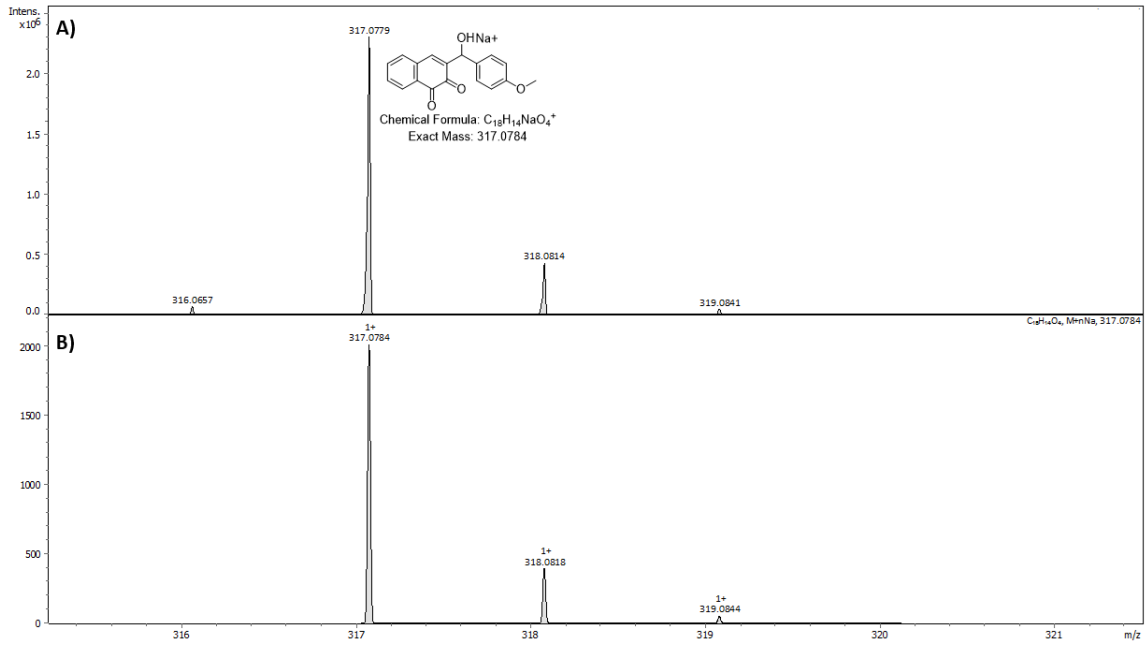

Figure 2.16. A) Experimental positive mode HR-MS spectrum, B) Theoretical simulation of NPQ 2.

2.10.5 Kinetic Studies

Quenching kinetics was studied using laser flash photolysis (LFP), fiber modified Cary 60, and a LED modified Cary 60 spectrophotometer for in situ irradiation and follow kinetics depending on the half-lifetime of each QM. A four-way light/fluorescence quartz cuvette (45x12.5x12.5 mm) was used for kinetic studies. LFP studies were carried out using a nanosecond kinetic spectrophotometer equipped with a pulsed Nd:YAG laser, 266 nm as the excitation source, and in non-pulsed mode. Kinetics with a long half-lifetime (>5 minutes) was studied using a temperature-controlled Shimadzu UV-2600 spectrophotometer. QMP 1 pseudo first-order rate constants taken in triplicate at varying quencher concentrations can be found in Table A.1, A.2 and A.3. QMP 3 pseudo first-order rate constants measured three-times at varying quencher concentrations are shown in Table A.4, Table A.5, and Table A.6.

CHAPTER 3

TOWARDS UV LIGHT INDUCED DEPOLYMERIZATION: INCORPORATION OF PHOTOLABILE LINKER INTO POLYETHYLENE TEREPHTHALATE PLASTIC BACKBONE

3.1 Introduction

Polyethylene terephthalate (PET), a semi-crystalline, thermoplastic polymer made of terephthalic and ethylene glycol repeating units. PET forms an excellent physical barrier for gases such as oxygen and carbon dioxide.[88] Therefore, PET is an excellent material for beverage bottles, food containers to preserve food quality. Additionally, PET has been used in fibers/fabrics, packing films, recording tapes, resins, and so on. PET is the fourth most-produced plastic in the world and the current global supply of PET is more than twenty million tons.[89,90]

3.1.1 PET Synthesis

PET is industrially synthesized via three different methods (Scheme 3.1).[91,92] First production method of PET is a polyesterification process between terephthalic acid (TPA) and ethylene glycol (EG). The second method is a (poly)transesterification reaction between dimethyl terephthalte and EG to generate PET. In the third method, bishydroxyethylene terephthalate (BHET) is subjected to polycondensation. All three methods require high temperature, pressure and a catalyst. In general, metal oxides, alkoxides and acetates are used. The metals used are calcium, magnesium, zinc, titanium, antimony, aluminum, and tin. Antimony based catalysts (Sb) such as Sb_2O_3,

$Sb(CH_3COO)_3$, and $Sb_2(OC_2H4O)_3$ are the most common catalyst used in all the PET synthesis methods.[93,94] However, more attention is focused on less toxic tin (Sn) catalysts now a days.[95]

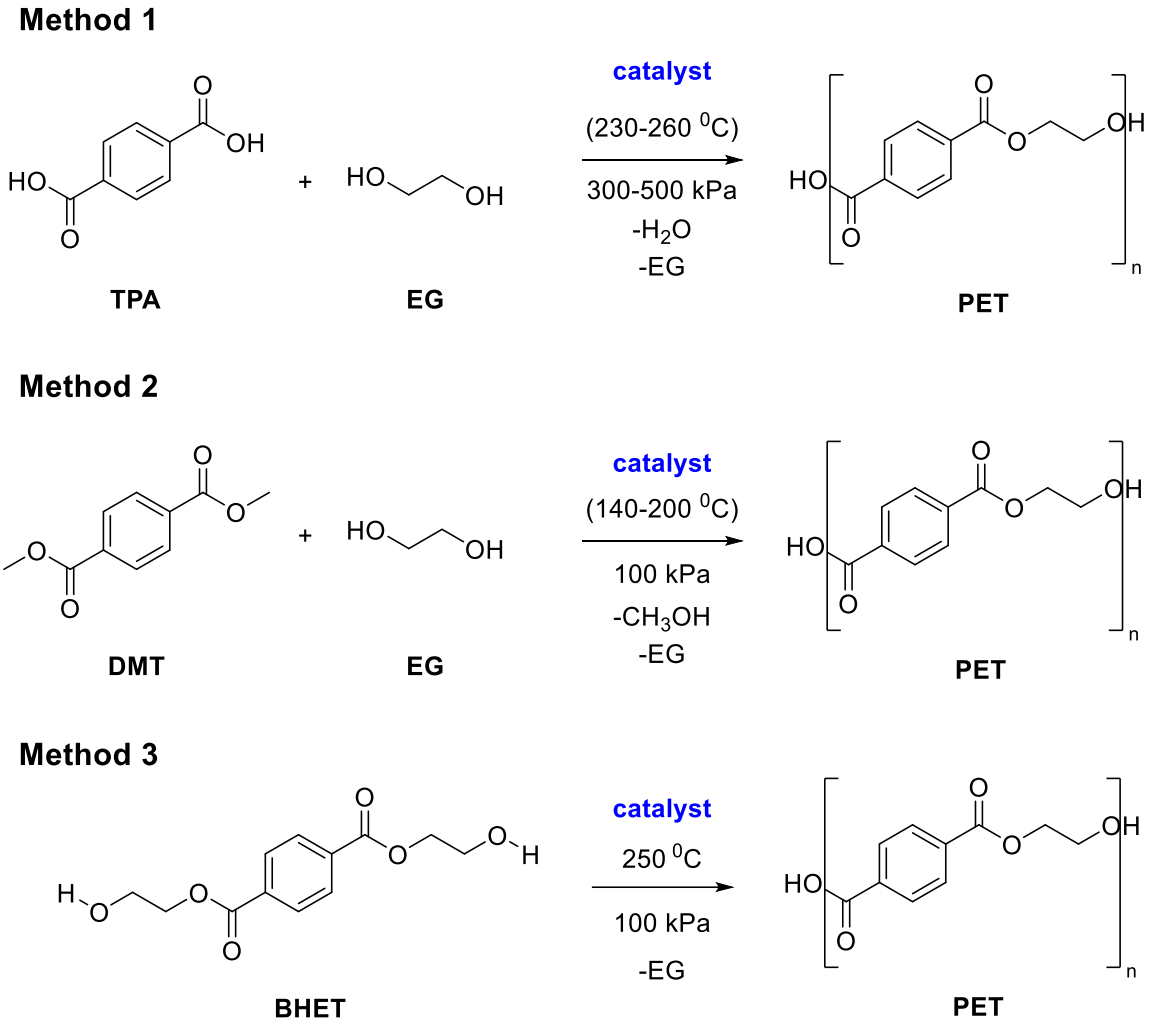

Scheme 3.1. PET industrial synthesis methods.

3.1.2 PET Pollution, Lifetime and Alternatives to PET

PET has integrated seamlessly into society and our way of life due to the advantages, including light weight, low cost, good mechanical and thermal qualities, and ease of processing. The majority of PET bottles are improperly disposed in to the environment and it causes a negative impact as PET is not a biodegradable polymer. Dorin and co-workers

experimentally evaluated the PET degradation lifetime in oceans of tropical regions by conducting PET degradation in marine water samples collected from the Black Sea and Atlantic Ocean. PET complete degradation requires 72 years total and 50% PET conversion occurs in 4.5 years.[96] Chamen and co-workers measured the rate of specific PET surface area degradation and reported only 0.1-10 μm PET degrades per years in both marine and land.[97] Accumulation of PET bottles in nature, especially in marine environment is now a severe threat to marine creatures.

Throughout the past few decades, a number of recycling methods have been started, including. Alternatively, material chemists are now being concentrating on developing novel polymers that would naturally degrade as substitutes for PET.[98] One of the approach is to use bio-based monomers to save petroleum resources and to improve biodegradation.[99,100] For example, polyethylene 2,5-furandicarboxylate (PEF) is made from lignocellulosic biomass, furan dicarboxylic acid (FDCA) and ethylene glycol utilizing conventional melt polymerization with antimony glycolate as the catalyst (Scheme 3.2).[101] Austin et al. studied the enzymatic hydrolysis of PEF and reported efficient biodegradation of PEF compared to PET.[102]

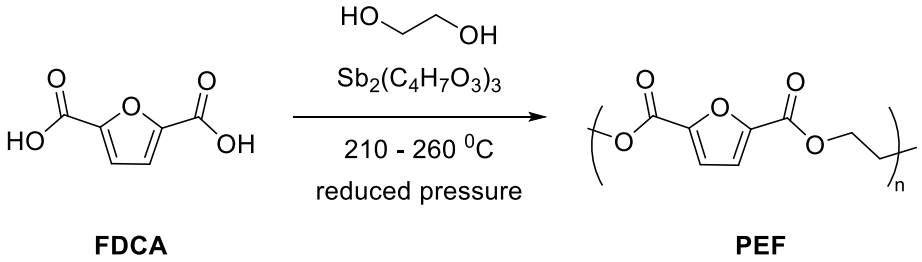

FDCA **PEF**

Scheme 3.2. Synthesis of PEF from FDCA.

Another example of bio-based polyesters are polymers of phloretic acid where the monomers are derived from lignin biomass.[103] Authors have used Sb_2O_3 as the catalyst and

4-methoxyphenol (MEHQ) was used as an inhibitor to avoid oxygen radical pathways in the polymerization (Scheme 3.3). Polymerization was carried out in a 3-neck round bottom flask with an overhead stirrer, heating mantle with a temperature probe and short-path vacuum distillation equipment. First, the monomer/s is melted at low temperature, 140 ^{0}C while stirring and once the monomer is melted, the reaction temperature is raised to 200 ^{0}C over the course of 6 hours. After that, vacuum (<0.1 kPa) is applied for 30 minutes while stirring and the mixture is reacted for an additional 1 hour at 200 0C. The reported polymers have high molecular weight (40-90 kg/mol) and high yields.

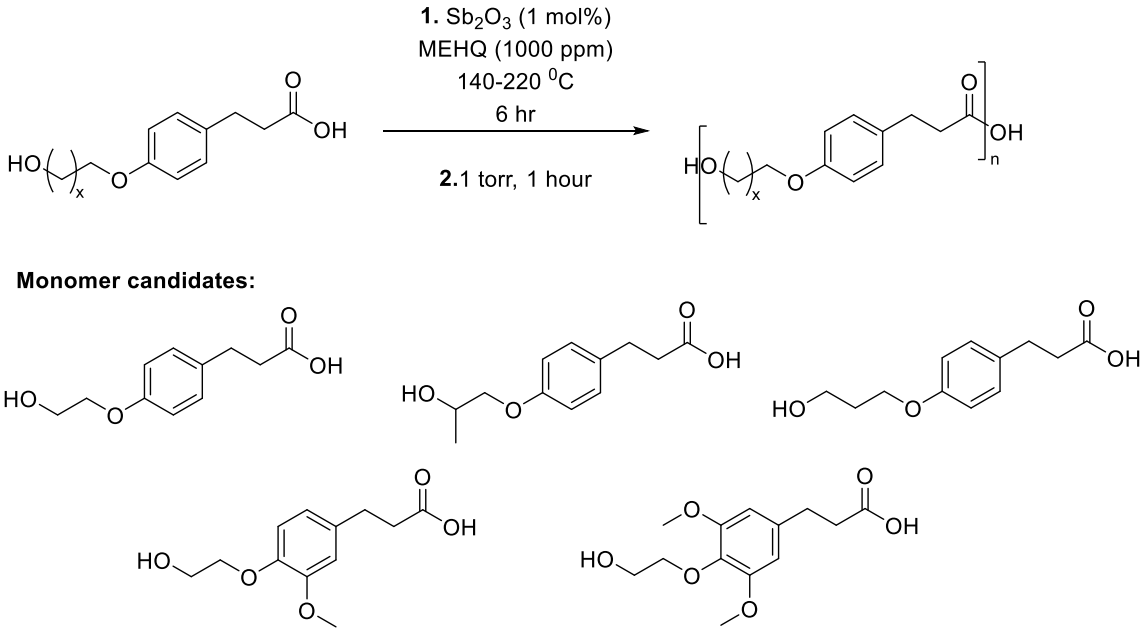

Scheme 3.3. Synthesis of polymers of phloretic acid derivatives.

Even though PEF and phloretic acid derived from biomass, a number of drawbacks prevent them from competing with conventional synthetic plastics or being used as perfect biomaterials. These disadvantages are poor mechanical strength, vulnerability to thermal damage and incompatibility with traditional thermal processing methods. Additionally, PEF does not undergo biodegradation in marine environments where the majority of the

plastic bottles are disposed and accumulated in the marine environment. Therefore, a novel analog of PET that has similar properties as conventional PET and that would degrade in the marine environment condition is highly necessary.[104] One of the great natural resources at the marine environment is sunlight. Our goal is to gain the benefit of sunlight which is plentiful on earth/ocean for the natural degradation of PET. Choices of photolabile protecting groups (PPG) to design a biodegradable/photodegradable will be described in the next section.

3.2 Photolabile Linkers for Polymer Synthesis

Photolabile protecting groups (PPG) allow for the spatial and temporal control of substrate release,[26] as well as are environmentally friendly and appealing in the context of greener chemistry as it allows the release of specific molecule simply by irradiation, without using any reagents.[27] Requirements of photolabile protecting groups (PPGs) include, strong absorption at wavelength above 300 nm, clean photoreaction n with high quantum yield, soluble in the targeted media, stability, sensitive detection and the byproducts should not absorb any light at the wavelength of irradiation.[28,] Photolabile linkers are widely used in solid phase organic synthesis, biological screening experiments, polymer, and material science.[29,30]

There are various PPGs reported in the literature since 1970s and are used in polymer applications such as block copolymers, thin films, hydrogels, and micelles.[105,106] For example o-nitro benzyl, arylmethyl groups, hydroxyaryl photocage, aryl carbonyl methyl derivatives, and coumarin-4-ylmethyl PPGs.[107] The most researched photocages for polymer design are o-nitro benzyl derivatives, however they lack the ability to decage quickly.[108] Additionally, the product, o-nitroso benzaldehyde formed upon photocleavage

is highly toxic and can be a life-threatening to the marine animals if a polymer is made using o-NB derivatives as a solution to PET pollution (Scheme 3.4A). Arylmethyl PPGs undergo photocleavage via homolysis or heterolysis depending on the substituents in the aryl ring (Scheme 3.4B). Hydroxybenzyl or hydroxy naphthyl PPGs undergo photolysis via quinone methide formation (Scheme 3.4C). Photochemical and photophysical properties of aromatic ketones are well understood and various phenacyl groups are used as PPGs for carboxylic acids, alcohols, phosphates, sulfonates, and amines. Phenacyl compounds form acetophenone, dihydroindenone, benzoic acid derivatives or benzofurans depending on the substituents in the starting phenacyl group. Furthermore, leaving group attachment in the ortho position of the benzophenone via an ethylene linker is also possible that leads to the formation of vinylphenylethanone (Scheme 3.4D). The mechanism of each arylcarbonylmethyl group derivative is different even though they are classified in the same group. Lastly, coumarin based PPGs are also used in designing hydrogel (Schem 3.4E).

Photoactivation step of most of the PPGs produces products that cannot be re-used in the synthesis of the PPG again. For example, ortho nitrobenzyl PPGs produces ortho nitroso benzaldehyde (Scheme 3.4A). The product, ortho nitroso benzaldehyde cannot be used to regenerate ortho nitro bezyl PPG.[109] On the other hand, orthohydroxybenzyl PPGs form o-(hydroxymethyl)phenol derivatives in aqueous medium which can simply be etherified to get ortho hydrobenzyl PPG again (Scheme 3.4C). The ability to re-use products is an especially important feature when designing a recyclable polymer. because it not only allows to degrade the polymer faster in nature or industry, but also allows to repolymerize to save monomer from petroleum sources. Therefore, we have selected ortho hydroxybenzyl PPGs for the design of photodegradable analog of PET polymer.

A) Photochemistry of o-Nitrobenzyl PPGs

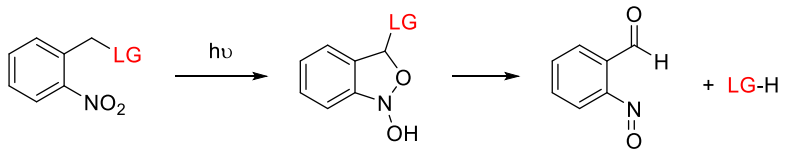

B) Photocleavage Mechanism of Arylmethyl PPGs

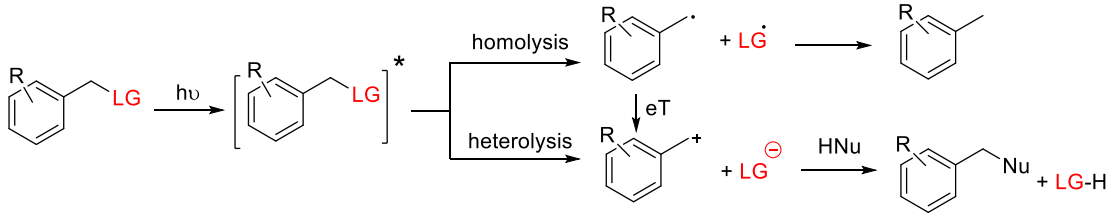

C) Substrate Release from o-Hydroxybenzyl/naphthyl Cage via Quinone Methide Formation

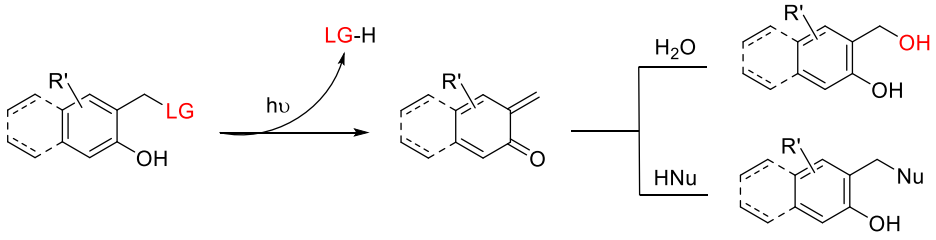

D) Aryl Carbonylmethyl Derivatives as PPGs

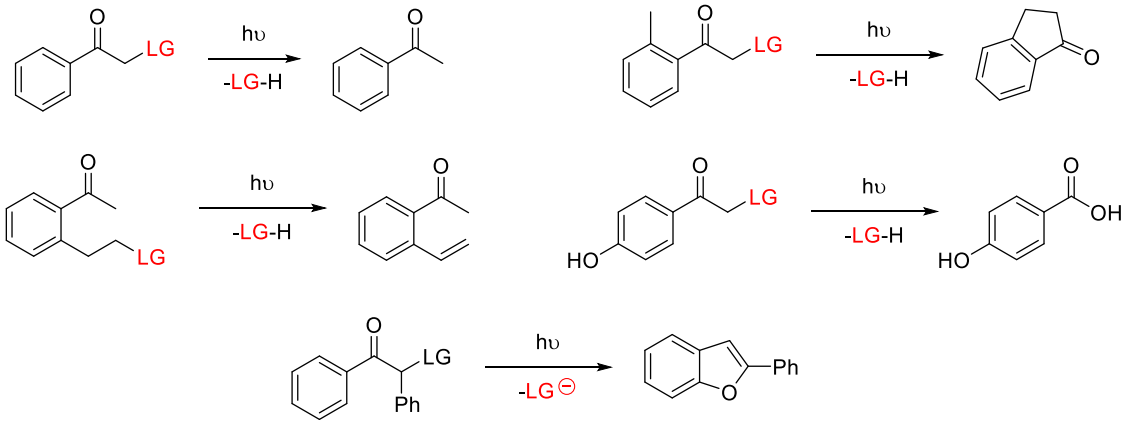

E) Coumarin-4-ylmethyl PPGs

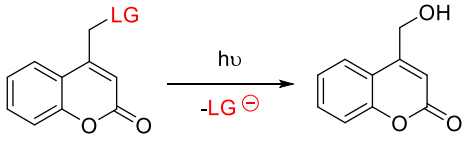

Scheme 3.4. Examples of the most common PPGs.

3.3 Importance of QMP Photolabile Linkers and Novel Polymer Design

o-hydroxybenzyl based PPGs[110] and their naphthyl analogues have been widely studied by our research group. Quantitative release of an alcohol from o-hydroxybenzyl/naphthyl ether and the formation of oQM derivative has been shown[5,31] (Scheme 3.5). In the presence of water, QM undergoes rapid hydration to form the parent diol. This diol can be converted back into the o-(hydroxy benzyl) ether by reacting it with the alcohol again in the presence of suitable conditions such as heat, acid catalyst or even light.[4,5] Thus, unlike the other PPGs that produces irreversible products, photochemical reversibility feature of oQMP and oNQMP is an excellent feature for the development of a polymer that can depolymerize-and-repolymerize back in the development of a recyclable polymer. The reversibility of quinone methide reaction has established an excellent basis for polymer disassembly to the benefit of numerous processes in material science.

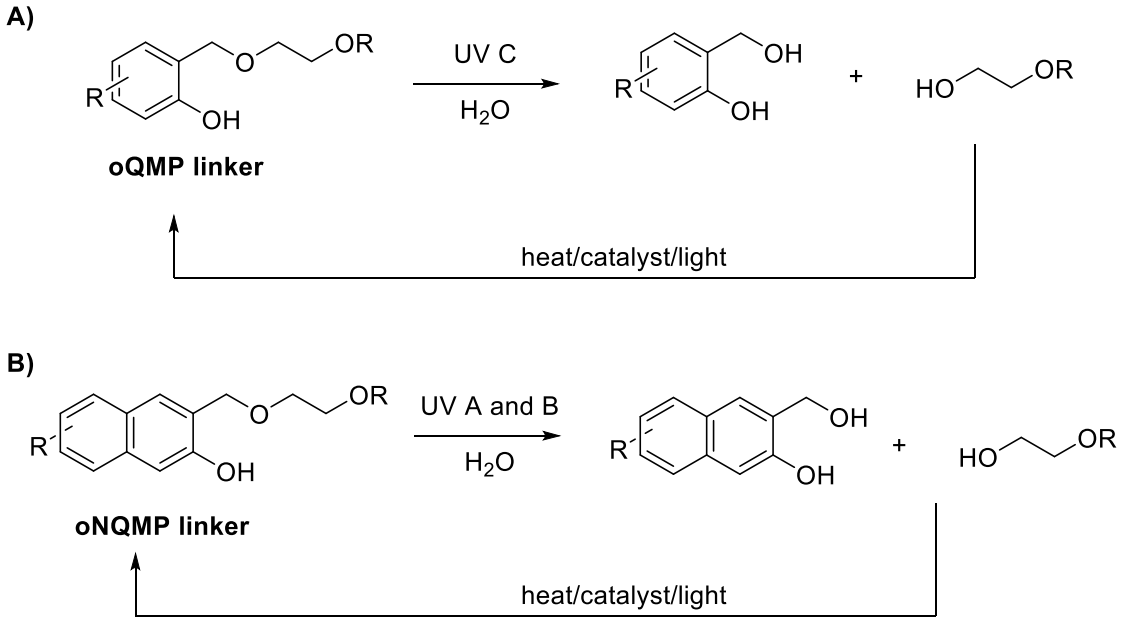

Scheme 3.5. Photolabile linkers based on A) oQMP and B) oNQMP.

The UV composition of solar radiation comprises approximately 95% of UV A and 5% of UVB. All the UVC and most of the UVB radiation does not reach the earth's surface due to the protection from the ozone layer. oQMP linkers cleave under UVC (100-280 nm) light and oNQMP linkers undergo photolysis using UVB (280-315 nm) and UVA (315-400 nm). Therefore, oNQMP is most suitable when designing a bio-/photodegradable polymer as UV A in the oceans are plenty. However, since we want to explore to feasibility of incorporation of any quinone methide precursors to PET polymer backbone, both oQMP monomers and oNQMP linkers/monomers were considered in our study.

The monomers need to be bifunctional in order to synthesize a linear condensation polymer as PET. Furthermore, the modification should not decrease the photo reactivity of the photolabile oNQMP or oQMP linker units. Our research group have demonstrated that derivatives of 3-hydroxy-2-naphthalenemethanol based linkers are suitable for the design of various polymers of different purpose.[32] Additionally, our research group has reported that the parent oNQMP, 3- (hydroxymethyl)-2-naphthol (compound **1.17**) can be easily modified via a hydroxyl/phenol group the 8th position. The presence of a triethylene glycol, triethylene glycol ether, azide, amine or biotin does not affect the photo reactivity of the photolabile linker and not intramolecular side reaction (Scheme 3.6).[111]

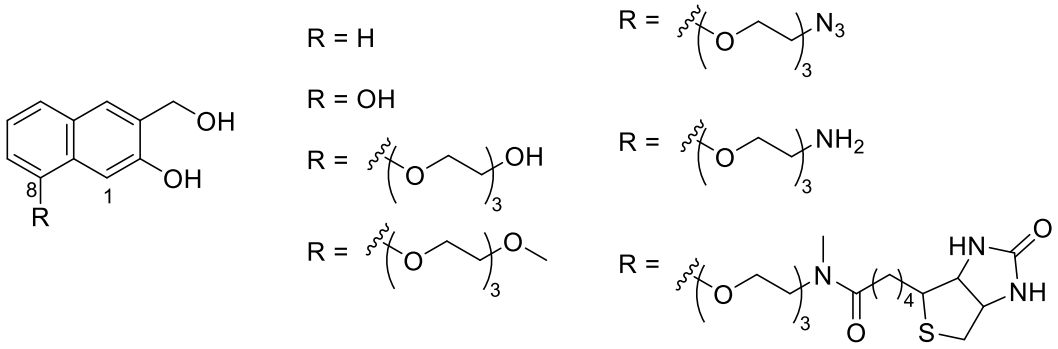

Scheme 3.6. Previously reported oNQMP linkers.

Based on our previous published results, we propose the simplest oNQMP monomer with an ethylene glycol unit attached to the 8' OH position. It should be noted that 8' phenolic group must be derivatized/functionalized with a linker for polymerization reaction monomers as the phenolic OH is not nucleophilic enough to undergo polycondensation. Additionally, we have designed a similar oQMP monomer analog. Schematic representation of oNQMP and oQMP monomers candidates are shown in Scheme 3.7.

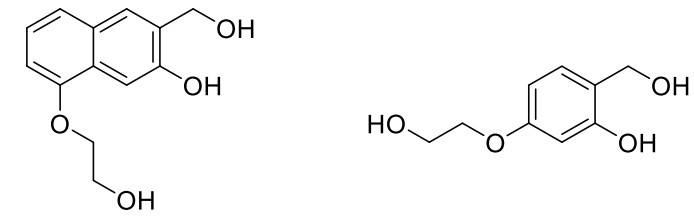

oNQMP monomer, 3.4 **oQMP monomer, 3.9**

Scheme 3.7. Structures of photodegradable oNQMP and oQMP monomer candidates.

We propose synthesis of a novel polymer using o-NQMP linkers that could be substituted for polyester based plastics and depolymerize upon irradiation with a suitable wavelength of light. Furthermore, we planned to study recycling of polymers using recovered monomers after photolysis. red circle: oNQMP/oQMP monomer, black rectangle: PET (BHET-EG) repeating units (Figure 3.1).

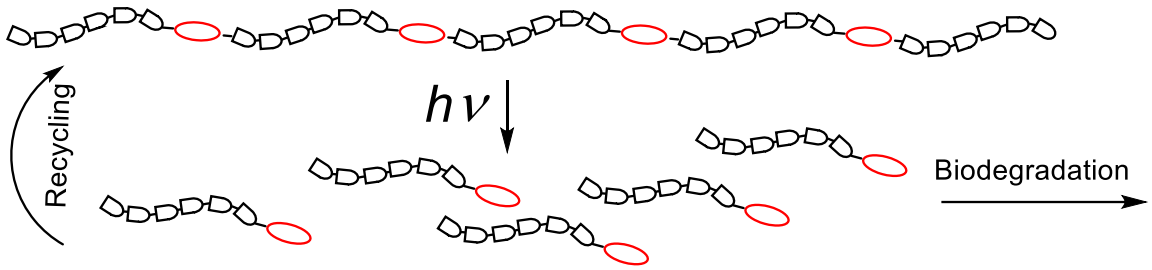

Figure 3.1. Design of photolabile polymer. Synthesis of oNQMP Monomers.

3.4 Synthesis of oNQMP Monomers

Synthesis of oNQMP monomer, **3.4** starts with commercially available acid, 3,5-dihydroxy-2-naphthoic acid. First, the carboxylic acid is esterified in the presence of methanol and sulfuric acid. After that, etherification was carried out using 2-bromoethanol and finally, reduction of the compound, **3.3** was carried out to obtain oNQMP monomer, **3.4** in 90% yield (Scheme 3.8). Etherification step was also conducted using synthesized monotosylated ethylene glycol, 2-hydroxyethyl 4-methylbenzenesulfonate instead of 2-bromoethanol as tosylates are better leaving groups than bromides.

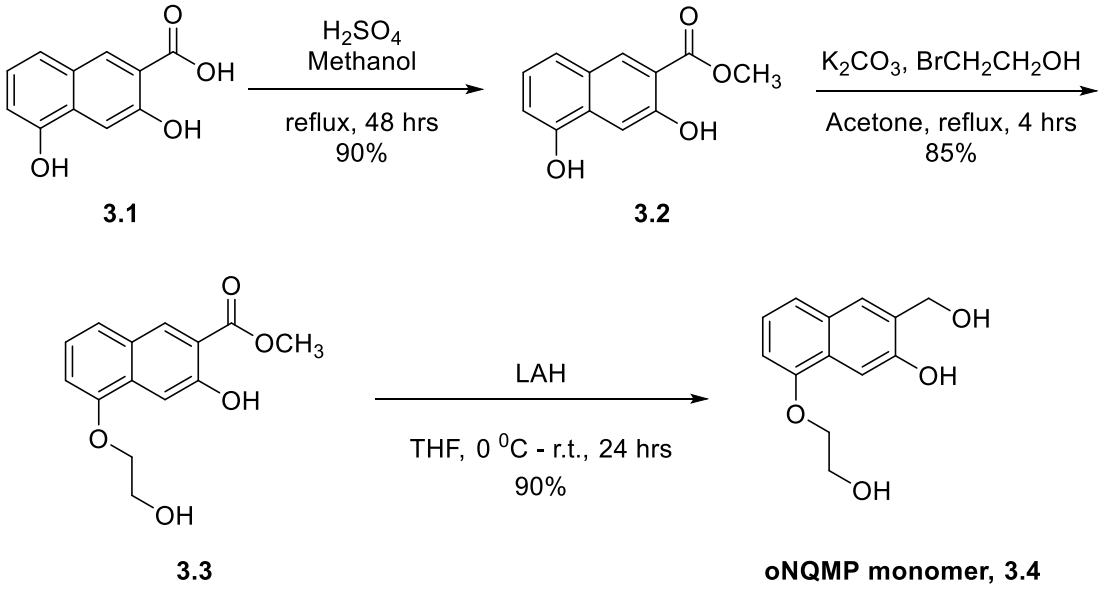

Scheme 3.8. Synthesis scheme for oNQMP monomer.

As it was mentioned in section 3.3, one of our goals in this research project is to monitor the photodegrdation of the oNQMP/PET copolymer. We wanted to get a preliminary understanding about how a similar photolabile linker would dissociate and its photochemical properties. We synthesized an oNQMP model linker to study the photochemical properties as studying the photochemical properties of a polymer could be too complex

3.5 oNQMP Linker Synthesis and Photochemistry

The oNQMP model linker, **3.5** was synthesized by heating oNQMP monomer in excess of ethylene glycol in the presence of a Lewis acid catalyst, p-toluene sulfonic acid: p-TSA (Scheme 3.9).

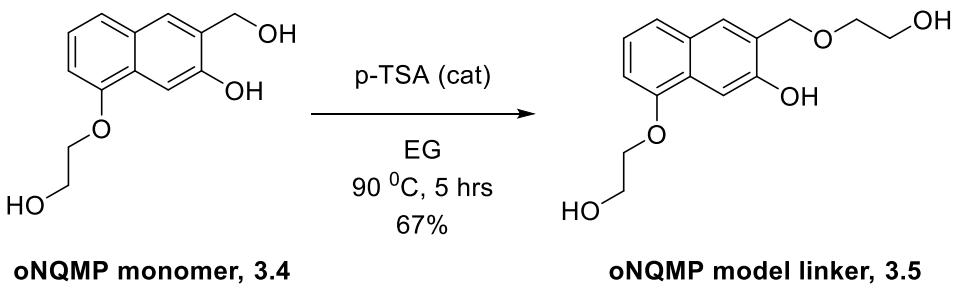

oNQMP monomer, 3.4 **oNQMP model linker, 3.5**

Scheme 3.9. Synthesis scheme for the oNQMP model linker.

UV-Visible spectrum of oNQMP model linker, **3.5** showed four main absorbance bands at 218 nm, 239 nm, 284 nm, and 330 nm which are identical to 6-(hydroxymethyl)naphthalene-1,7-diol (Figure 3.2A).[111] Quantum yield of the oNQMP model linker was experimentally calculated and found as (0.37±0.02). Quantum yield was experimentally measured using nitroveratryl as the actinometer and same procedure as described in the section 2.10.3 was followed.

Irradiation of the oNQMP model linker using 300 nm UV lamps in aqueous acetonitrile solution (1:1) did not show any changes at the 300 nm region. However, a decrease in the intensity of 218 and 239 nm bands were noted. No new peaks/bands formation was observed upon irradiation (Figure 3.2B). In aqueous solution, oNQMP model linker undergoes photodissociation to form oNQMP monomer. Since, both oNQMP monomer and linker has same chromophore, observations of UV spectral changes are not sufficient and photolysates were further analyzed by HPLC (Section 3.5.1).

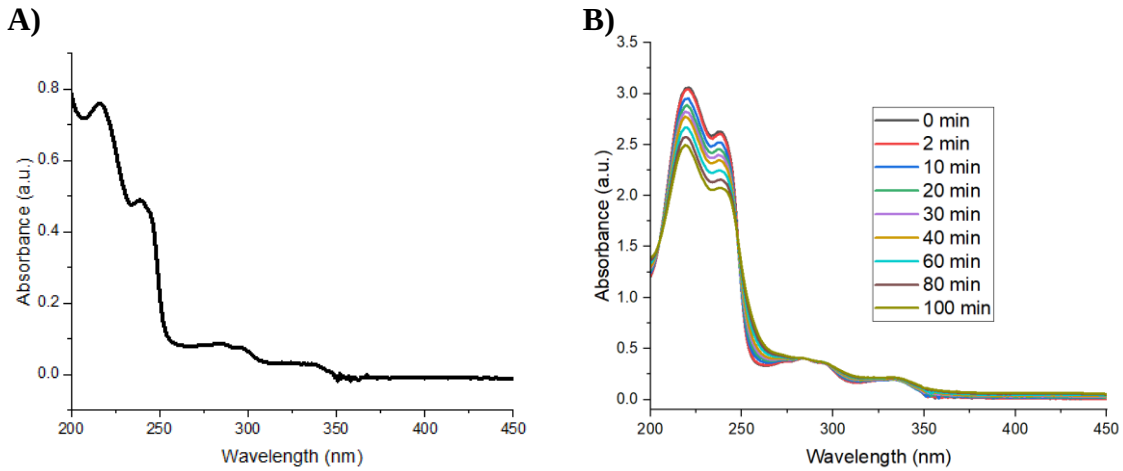

Figure 3.2. Absorbance spectra of A) 3.5, B) 3.5 photolysate upon irradiation.

3.5.1 Stability of oNQMP model linker in solution under ambient light

A solution of oNQMP linker in water and methanol was separately prepared and left in a water bath at room temperature. The composition of the mixture was monitored by HPLC by taking an aliquot from each sample. No changes in the peak area were observed in both solutions over the course of ten days indicating oNQMP linker is stable under ambient light conditions.

3.5.2 Aqueous photolysis of oNQMP linker

Irradiation of a sample of oNQMP linker in water resulted in the formation of only the oNQMP monomer according to HPLC which confirms the oNQM formation and release of EG (Scheme 3.10). Irradiation experiments were performed in quartz cuvette and irradiated using mini-rayonet 300 nm, 8 lamps. oNQMP model linker retention time 10.5 minutes and oNQMP monomer retention time 7.1 minutes. oNQMP linker concentration and oNQMP monomer concentration after each irradiation was determined based on HPLC calibration curves for both (Section 3.10.5). HPLC chromatograms before and after irradiation showed clean conversion of oNQMP linker to oNQMP monomer (Figure 3.3 and B). However, at 80% conversion of oNQMP, only 40% of **3.4** yield was obtained in 7

minutes of irradiation (Figure 3.4). The low yield at high conversion could be due to the decomposition of the product oNQMP monomer, **3.4** as it also can absorb 300 nm light. It was observed that the degradation of oNQMP monomer occurs at prolong irradiation.

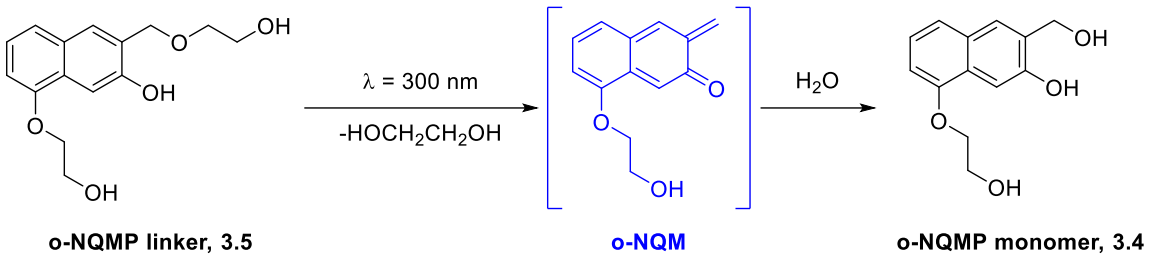

Scheme 3.10. Aqueous photolysis of oNQMP linker to oNQMP monomer via oNQM.

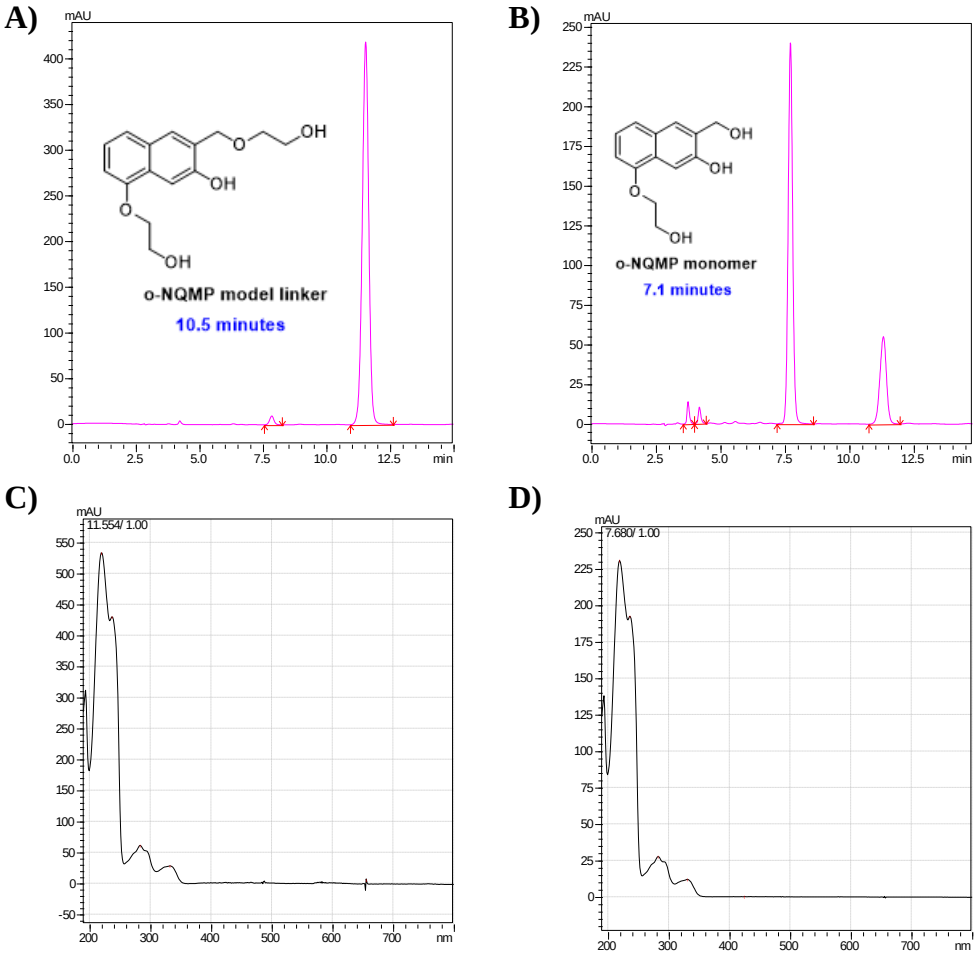

Figure 3.3. HPLC chromatogram of 3.5 in aqueous solution A) before irradiation, B) 5 minutes after irradiation. UV spectra of C) 3.5, D) 3.4.

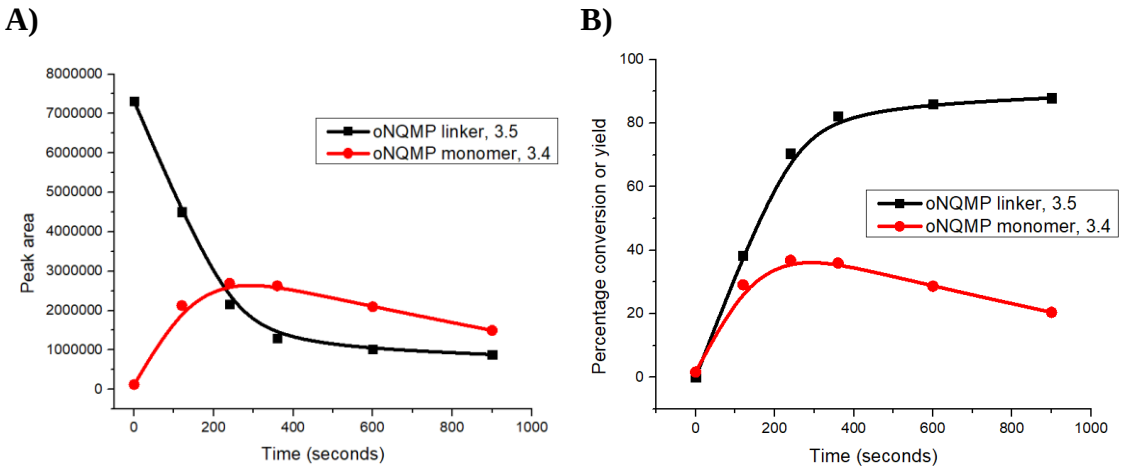

Figure 3.4. A) HPLC peak area changes with irradiation time for 3.5 and 3.4, B) 3.5 percentage conversion and 3.4 yield with irradiation time.

3.5.3 Photomethanolysis of oNQMP linker

Irradiation of a sample of oNQMP linker, **3.5** in methanol resulted in the formation of only the **3.6** which confirms the oNQM formation and release of EG (Scheme 3.11). oNQMP linker elutes at 10.0 minutes and **3.6** at 16.8 minutes. Photolysate oNQMP methanolic solution composition was followed by HPLC with irradiation time. After 5 minutes of irradiation the main product was **3.6** along with some other minor products (Figure 3.5A and B). oNQMP linker concentration and **3.6** concentration after each irradiation was determined based on HPLC calibration curves for both (Section 3.10.5). At 20% conversion of oNQMP linker, only 10% of **3.6** was observed (Figure 3.6B). This may be because of the internal filter effect where both starting material and product has the same chromophore and competes for light.

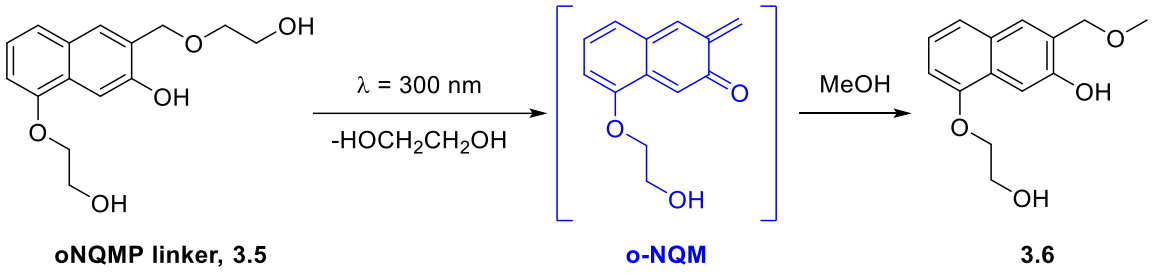

Scheme 3.11. oNQMP linker conversion to 3.6.

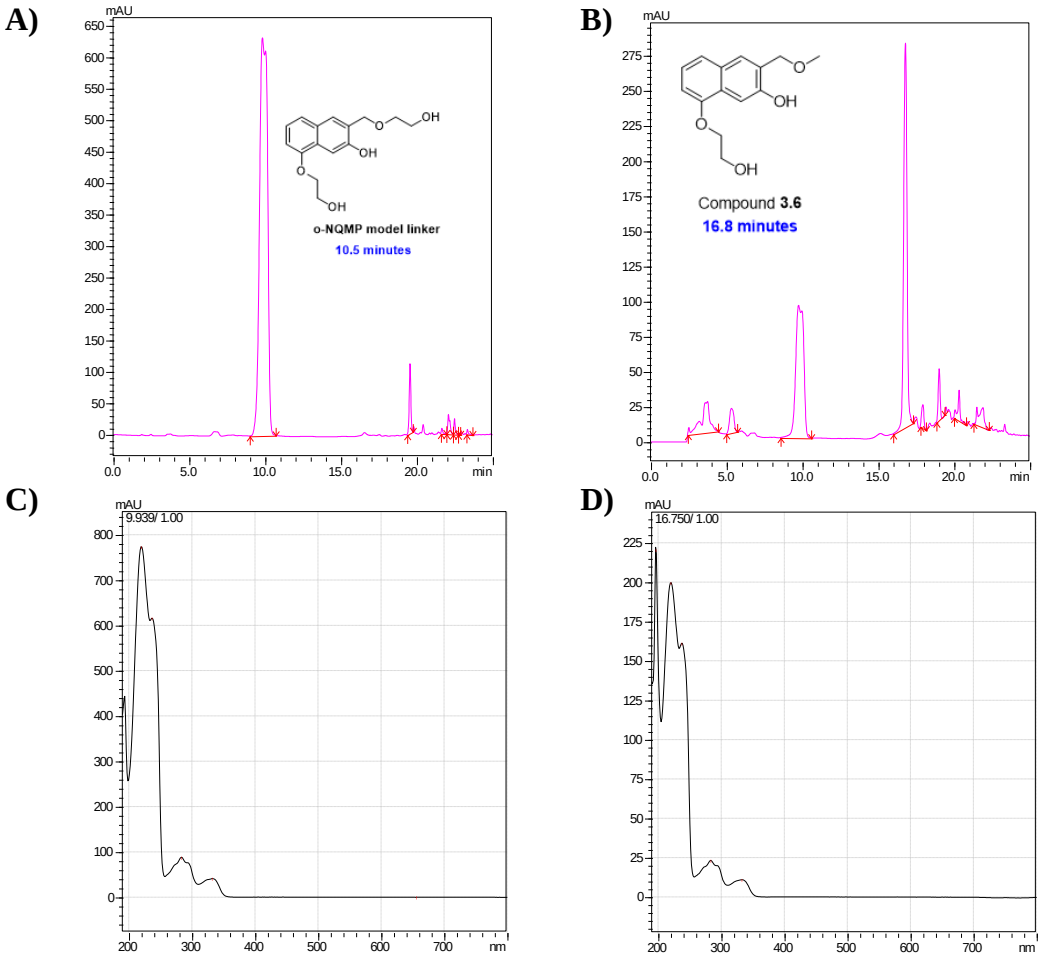

Figure 3.5. HPLC chromatogram of oNQMP linker in methanol A) before irradiation, B) 10 minutes after of irradiation. UV spectra of C) oNQMP linker, D) 3.6.

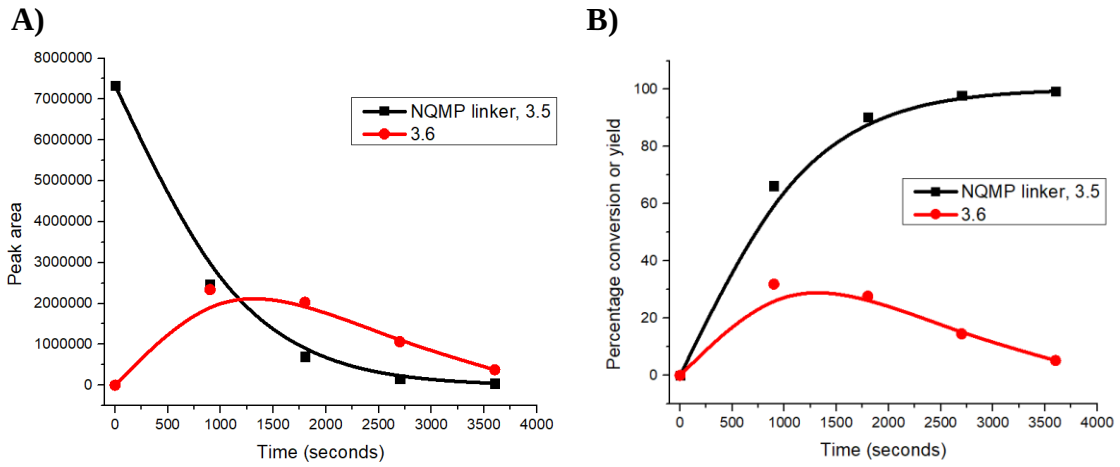

Figure 3.6. A) HPLC peak area changes with irradiation time for 3.5 in methanol B) 3.5 percentage conversion and 3.6 yield with irradiation time.

oNQMP linker cleavage is faster in aqueous solution than in methanolic solution (80% vs 20% conversion after 5 minutes of irradiation) which is due to the fact oNQM formation is restricted via excited state proton transfer (ESPT) in organic/methanolic solution. After the preliminary studies with oNQMP linker, we moved on to the synthesis of oNQMP monomer-PET copolymer.

3.6 oNQMP Monomer and BHET Copolymerization

Our goal is to incorporate a minimum amount of oNQMP or oQMP monomer (3% - 20%) to conventional PET monomers (BHET and/or EG) in the polymer synthesis and study polymer properties, stability, and photodegrdation to obtain monomers. Theoretically, it is expected to form oligomers of PET (BHET-EG repeating unit), as well as oNQMP self-oligomer units and oNQMP attachment to BHET or EG units (Scheme 3.12 reaction with dashed arrow). The condensation byproduct will be ethylene glycol and water. We attempted polymerization by melting oNQMP solid and in solvent, and results will be described in this section.

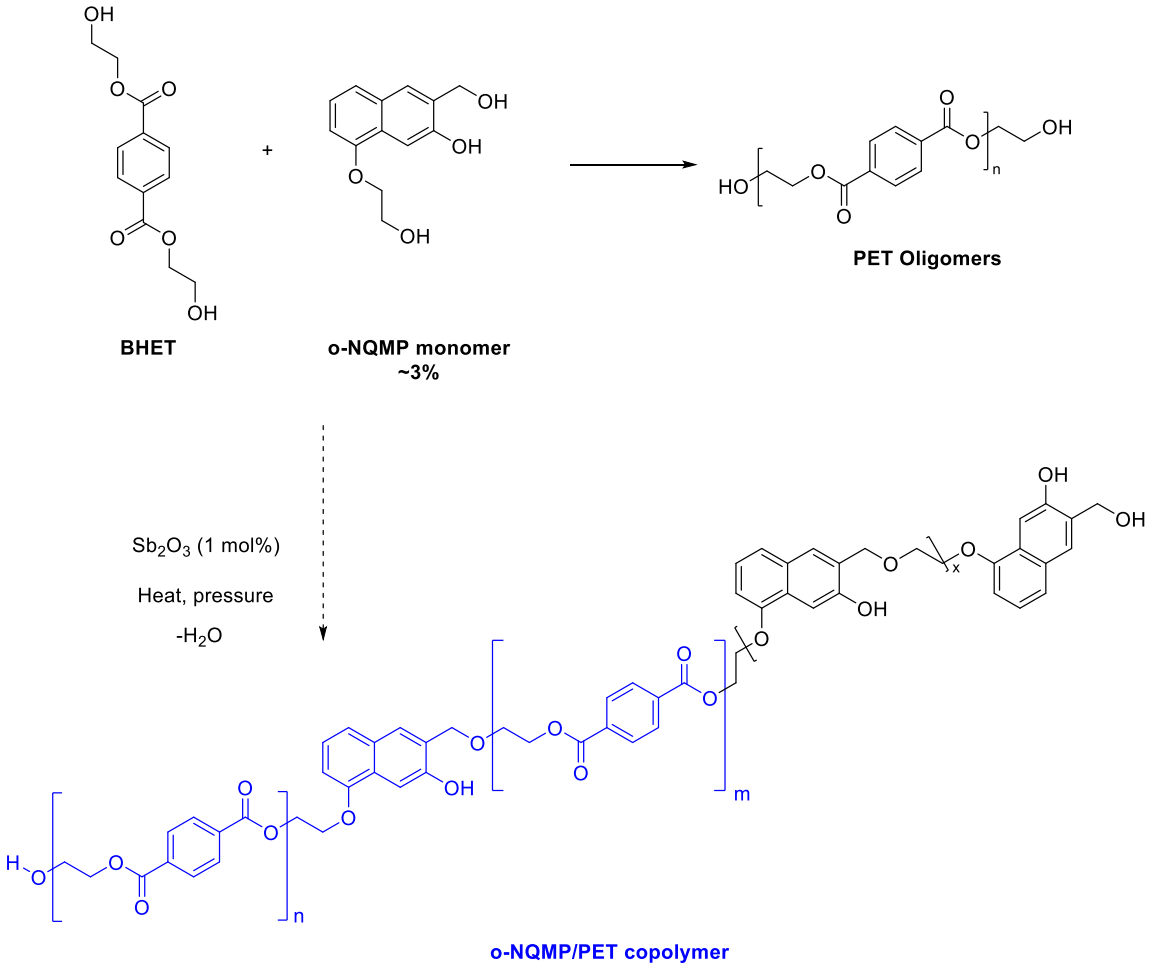

Scheme 3.12. oNQMP monomer, BHET and EG copolymerization reaction.

3.6.1 Melt Copolymerization

BHET (0.5 g, 1.97 mmol) with oNQMP monomer (0.014 g, 0.06 mmol) and Sb_2O_3 at 160 ^{0}C were heated for 12 hours while stirring and the slurry was dissolved in dimethyl sulfoxide and analyzed by HPLC. We only observed the formation of oligomers of PET according to HPLC and HR-MS results (Scheme 3.12 reaction with full arrow). BHET, BHET dimer, and BHET trimer elutes at 5.41, 20.01, and 23.17 minutes, respectively. oNQMP monomer elutes at 10.2 minutes which is barely visible on HPLC as only 3% was used compared to BHET initial moles (Figure 3.8).

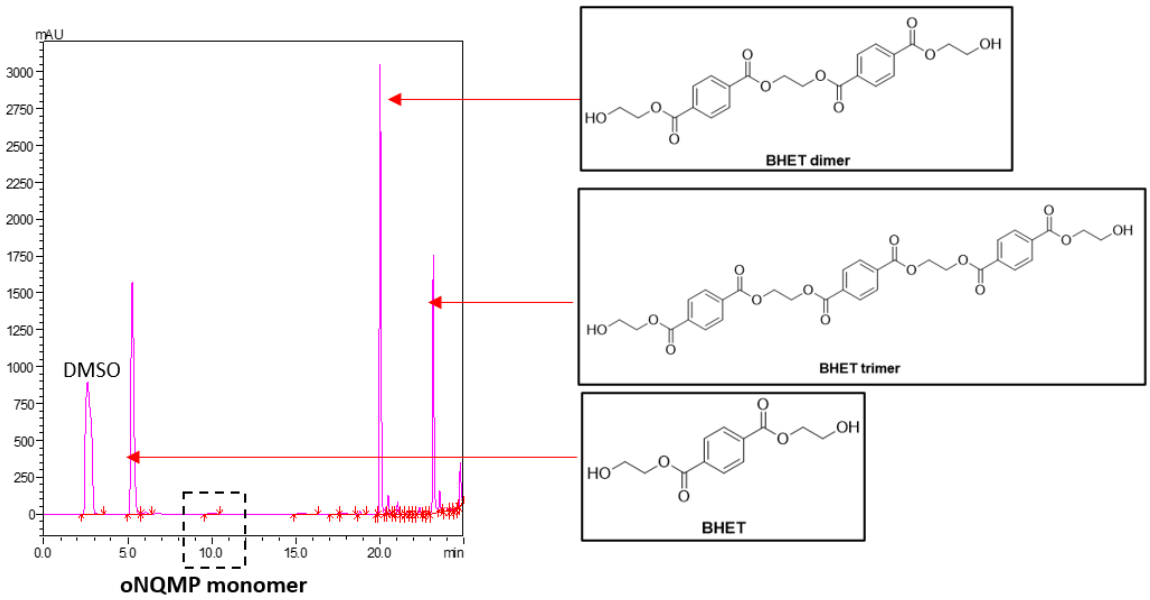

Figure 3.7. HPLC chromatogram of BHET and oNQMP melt polymerization.

3.6.2 BHET-oNQMP Monomer Copolymerization in Solvent

BHET (50 mg, 0.2 mmol) and oNQMP monomer (10 mg, 0.04 mmol) was dissolved in benzene (20 mL) and heated under argon at 100 ^{0}C, overnight. Next day solvent was evaporated off and sample was characterized by ESI-MS. Results showed a distribution of

masses. However, did not match with any of the expected oligomer masses. (Figure B.1. and Figure B.2.).

3.7 oNQMP Self-polymerization

We then investigated if oNQMP monomer, **3.4** undergo formation of oNQM under thermal conditions and undergo any self-polymerization in pure oNQMP only without adding any BHET or EG (Scheme 3.13). We have conducted the reaction in melt-state and in various organic solvents, which will be described in this section.

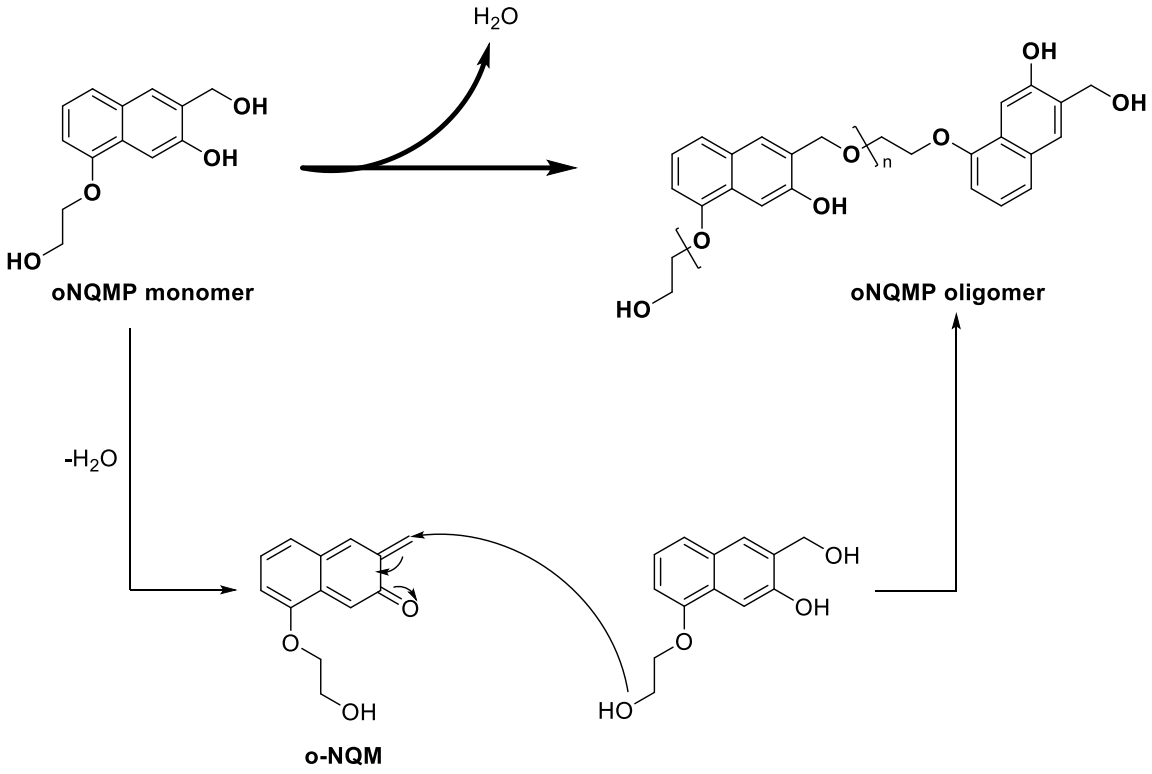

Scheme 3.13. oNQMP self-oligomerization reaction.

3.7.1 oNQMP Monomer Melt Polymerization

Thermal stability studies of oNQMP monomer using thermogravimetric analysis (TGA) show a sharp decrease in mass (~10%) around 130 ^{0}C that corresponds to the elimination of water and probably oNQM formation. Another gradual mass loss (~25%)

was observed around 350-400 ^{0}C. Further heating beyond 450 ^{0}C caused decomposition of the remaining solid (Figure 3.8A). Differential Scanning Colorimetry (DSC) results did not show any peak in the range of -60 ^{0}C to 130 ^{0}C which indicates melting does not occur below 130 ^{0}C (Figure 3.8B). The melting point of oNQMP monomer is ~170 ^{0}C.

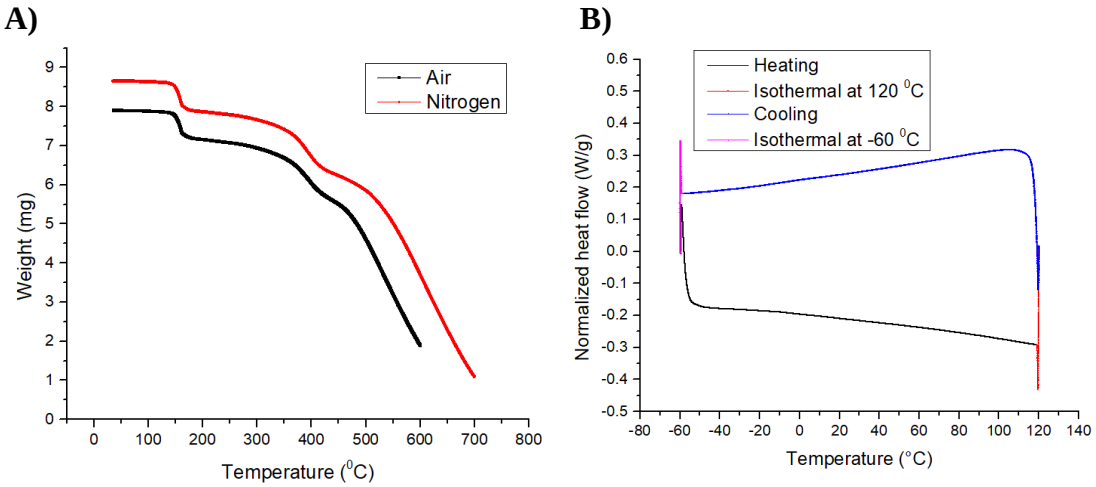

Figure 3.8. oNQMP monomer A) TGA curved in air and nitrogen, B) DSC curve.

We also tried to identify the products formed upon heating a solid sample of oNQMP. A pure sample oNQMP monomer solid was placed in a round bottom flask and heated at a constant temperature and the composition was monitored by taking the crude residue, dissolved in methanol, and analyzed by HPLC, ESI-MS, HR-MS or MALDI-TOF. Heating of oNQMP monomer at temperatures below 100 ^{0}C for 6 hours did not form any new products; only the monomer was recovered back. oNQMP melt polymerization at temperatures above 130 ^{0}C showed formation of a mixture of products according to HPLC, HR-MS analysis (Figure B.3, B.4 and B.5). Newly formed products did not match with any of the predicted self-oligomerization substances. Instead, a complicated mixture with a low molecular weight (<600 g/mol) which indicates possibly a different reaction mechanism other than thermal quinone methide generation and self-nucleophilic addition reaction

which is to be further investigated. Additionally, oNQMP monomer was heated in the presence of a catalyst (p-TSA or Sb_2O_3) and the formation of same unknown products were observed, yet the formation of self-oligomers were not observed.

Condensation polymerization of BHET to form PET requires a temperature above 200 ^{0}C. Our thermal analysis studies of both oNQMP monomer and oNQMP linker show initial mass loss around 160 ^{0}C in both air and nitrogen and unknown product formation other than self-oligomers. Therefore. We attempted oNQMP in solution polymerization over melt polymerization to obtain high molecular weight oligomer/polymer. Next section describes our attempts to study oNQMP thermal behavior in various solvents.

3.7.2 oNQMP Polymerization in Solvent

3.7.2.1 Solvent: Benzene and toluene

Our first solvents of choice were benzene and toluene. These solvents create an azeotropic mixture with the condensation polymerization byproduct, water and has a density less than water. Therefore, advantages of both benzene and toluene are that it allows removal of water from the reaction mixture and according to the Le-Chatelier principle, removal of water favors the forward equilibrium towards polymerization. Dean-Stark trap was used for quantitative analysis of water removal. However, only pure monomer was obtained after refluxing the solution overnight with and without a catalyst.

3.7.2.2 Solvent: Tetrahydrofuran (THF)

oNQMP monomer (10 mg, 0.043 mmol) was dissolved in THF (10 mL), and a pinch of pTSA (catalyst) was added and refluxed for 4 hours. After that THF was evaporated off and solid was analyzed by ESI-MS. oNQMP monomer, oNQMP dimer and other unknown products were observed along with other products (Figure B.6 and B.7).

3.7.2.3 Solvent: Ethylene glycol

Heating a solution of oNQMP monomer in excess of ethylene glycol at 160 ^{0}C resulted only in the formation of the oNQMP linker and no other byproducts or polymers were observed (Scheme 3.14). Even though self-polymerization was not observed, the result confirms that oNQMP monomer is stable at or below 160 ^{0}C and thermal decomposition does not occur in nucleophilic solvents such as ethylene glycol.

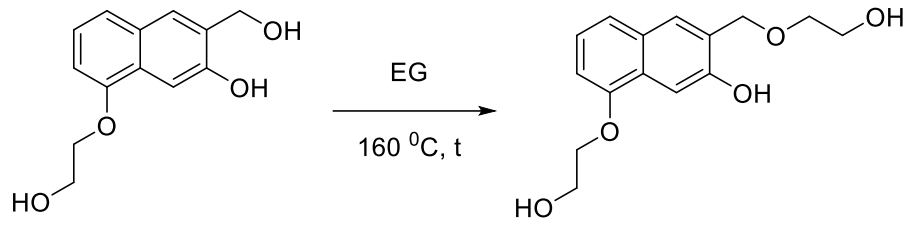

oNQMP monomer, 3.4 **oNQMP model linker, 3.5**

Scheme 3.14. oNQMP monomer conversion to oNQMP linker in excess EG under heat.

oNQMP monomer (7 mg, 0.03 mol) was heated at 160 ^{0}C in excess of EG (10 mL) and a diluted sample of the mixture was tested by HPLC with time. HPLC chromatograms collected at four time points are shown in Figure 3.9. oNQMP monomer retention time 6.9 minutes and oNQMP linker retention time is 10.2 minutes.

HPLC peak area change for both oNQMP monomer and the oNQMP linker is shownin Figure 3.10A. Stoichiometric conversion of oNQMP monomer-to-oNQMP linker was observed until 10 hours of heating. After that, oNQMP linker formation was not observed or decomposition of the oNQMP linker was observed even when oNQMP monomer reached 100% conversion (Figure 3.10B). Thus, prolonged heating causes decomposition of both the oNQMP monomer and linker.

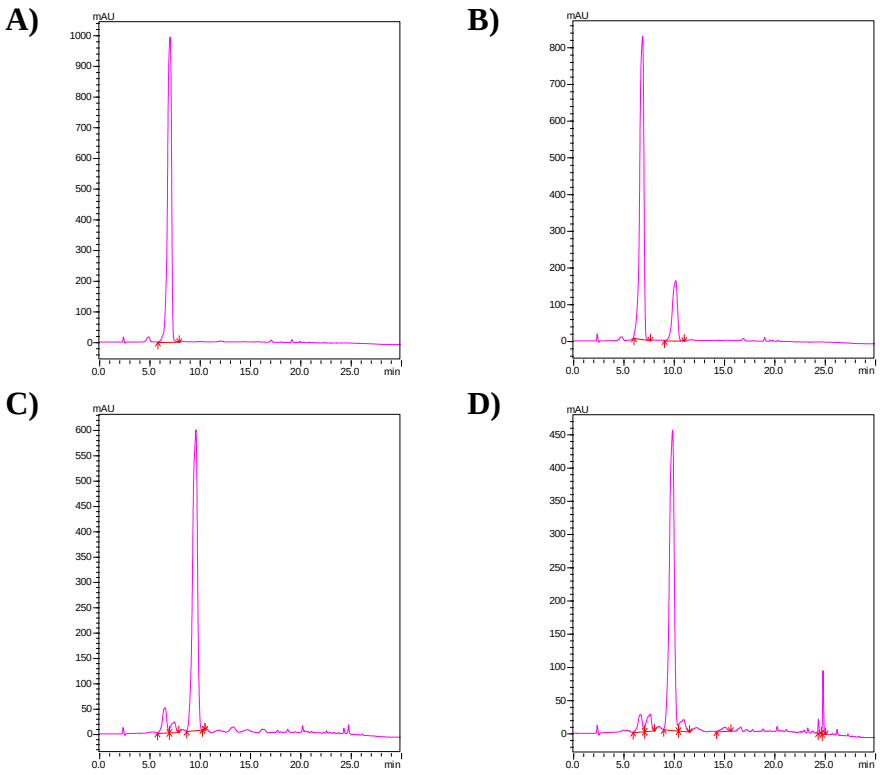

Figure 3.9. HPLC chromatograms collected at various time points of 3.4 excess EG under heat A) 0 hours, B) 2 hours, C) 9 hours, D) 78 hours.

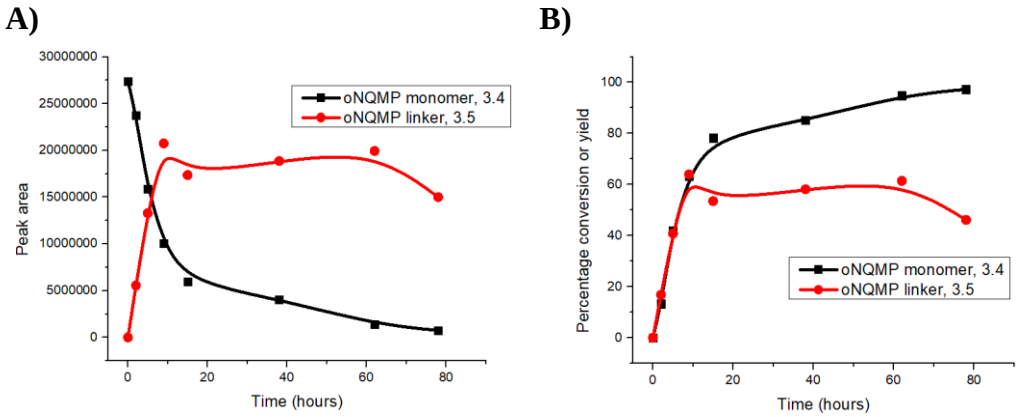

Figure 3.10. A) HPLC peak area change, B) Plot of 3.4 percentage conversion and 3.5 percentage yield with time.

3.7.2.4 Solvent: Diglyme

Prompted by the observations of oNQMP monomer heating in ethylene glycol, we explored a protected glycolic solvent, diglyme for oNQMP solution polymerization.

oNQMP monomer (10 mg, 0.04 mmol) was dissolved in diglyme (15 mL) and heated at 160 ^{0}C for 10 hours. HR-MS of the mixture in both positive (Figure 3.11A) and negative (Figure 3.11B) mode did not show the presence of any oNQMP monomer indicating complete conversion of the starting material. Additionally, HR-MS positive mode represents a typical polymer distribution pattern with 14 or 16 g/mol mass repeating unit/difference between two adjacent peaks (Figure 3.11A). However, all the mass values were less than the calculated molecular weight of a dimer which means decomposition of monomers.

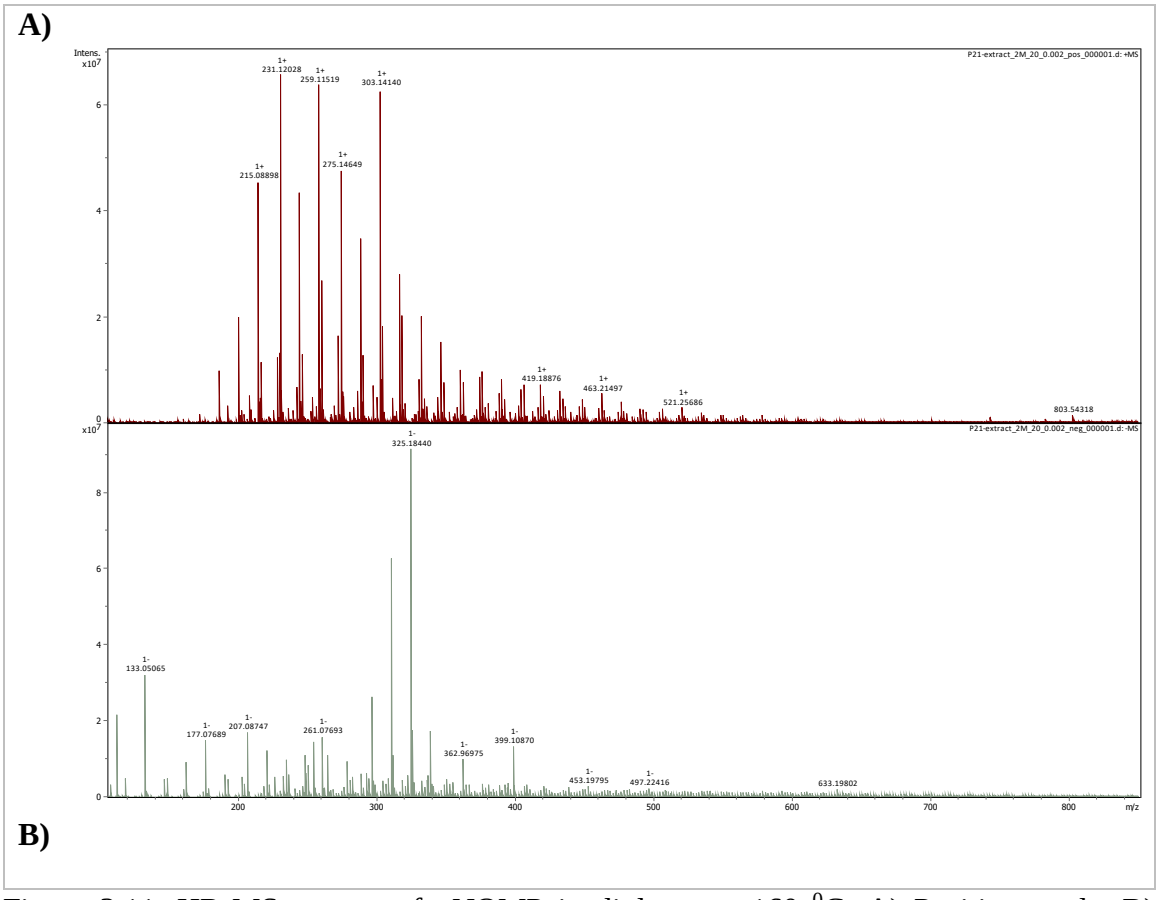

Figure 3.11. HR-MS spectra of oNQMP in diglyme at 160 ^{0}C; A) Positive mode, B) negative mode.

All the solid and solution state copolymerization and self-polymerization conditions attempted at various temperatures and pressures resulted in the formation of unknown compounds. It is evident that oNQMP does not thermally degrade in solution based on our experiments of oNQMP heating in ethylene glycol. Therefore, we strongly believe that oNQMP self and co-polymerization is possible where more optimization experiments need to be carried out. For example, one improvement is to use concentrated solutions and test the effect of polymerization. In general polymerization requires at least 300 mmol (50-70 g of oNQMP monomer). All the above conditions were carried out under dilute or using minimal amount of oNQMP monomer (<0.1 mmol) as the purpose was to test oNQMP monomer stability and optimize conditions. Furthermore, we are explored the oQMP monomers to achieve our purpose of designing photodegradable polymer.

3.8 Synthesis oQMP Monomers

Two methods were proposed and attempted in the synthesis of oQMP monomers.

3.8.1 Method 1

The synthesis of oQMP monomer can be carried out in two steps starting from the commercially available methyl 2,4-dihydroxybenzoate (Scheme 3.15). First, the starting ester is etherified with 2-bromoethanol to get **3.8** in 85% yield. Second, LAH reduction of **3.8** to get the oQMP monomer, **3.9**. However, the yield of oQMP monomer was very low (<5%) due to its high-water solubility, loss of product, oQMP monomer during the quenching step of the reduction reaction and purification was noted. Attempts were made to improve the yield of oQMP monomer by saturating the water layer with sodium chloride and lyophilization. However, obtaining pure oQMP monomer with high yield was not possible.

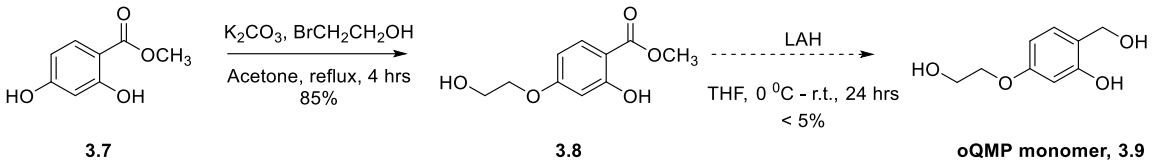

Scheme 3.15. oQMP monomer synthesis approach 1.

A second synthesis path was attempted to avoid the drawbacks in method 1 by using tert-butyl dimethyl silyl (TBDMS) protection of the glycol unit and form compound **3.11** instead of **3.8**. The reduction product of **3.11** is **3.12** and **3.12** is expected to be less water soluble and will not dissolve in aqueous solution.

3.8.2 Method 2

Synthesis of oQMP via method 2 is a three-step process (Scheme 3.16). It again starts with methyl 2,4-dihydroxybenzoate and etherified using pre-synthesized TBDMS protected 2-bromoethanol to get **3.11** followed by the LAH reduction and deprotection using TBAF in THF. Etherification step was successful with 80% yield of the **3.11**. However, the yield at LAH reduction step was low and the amount recovered was not sufficient to conduct deprotection. It is possible that the deprotection of TBDMS has occurred under reduction condition as it was noted in **QMP 3** synthesis (Section 2.2). oQMP monomer may have formed during the second step.

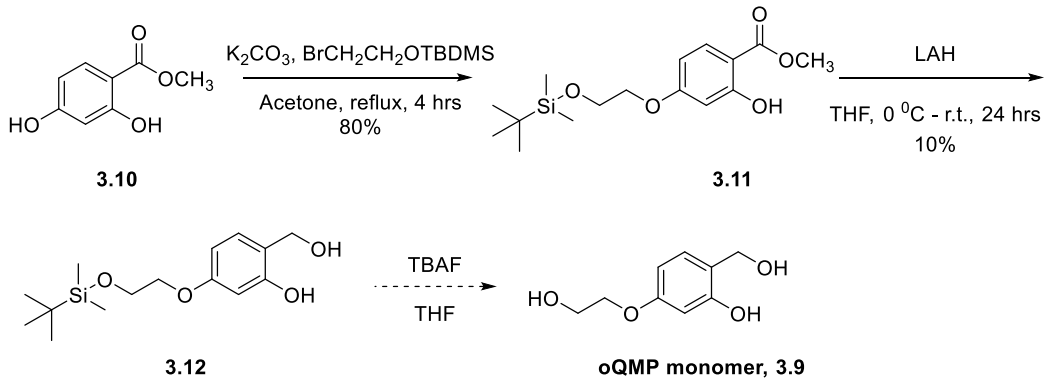

Scheme 3.16. oQMP monomer synthesis approach 2.

Removal of TBDMS protecting group during LAH reduction step have been reported in the literature.[112] Therefore, approach 2 also needs to be modified to get oQMP monomer in a good yield for polymerization.

3.9 Conclusions and Future Directions

Herein, we report our attempts to synthesize a novel photodegradable analog of PET as a solution to improperly disposed of plastic bottles in oceans. Irradiation experiments of the oNQMP linker have given the hope that the copolymer of oNQMP-PET can be degraded by light. However, co-polymer synthesis conditions need to be optimized to obtain a polymer with properties similar to PET. PET is generally synthesized via melt-polymerization where BHET is melted at (~120 ^{0}C), allowing to form oligomers and then raising the temperature up to 250 ^{0}C to get high molecular weight PET. Conventional melt-polymerization is not suitable for oNQMP monomer, **3.4** as the monomers decompose (at 130 ^{0}C) before melting (170 ^{0}C). Polymerization in THF under temperatures below 60 ^{0}C in the presence of a Lewis acid catalyst seems the best based on the results from self-polymerization in solvent (Section 3.7.2.2).

oNQMP monomer, **3.4** upon heating in solvent forms oNQM, and reacts with the hydroxyl group at the 8th position of another oNQMP monomer leading to self-oligomers. It is better to avoid self-oligomerization in co-polymerization to get a clean alternating polymer chain. Therefore, we plan to synthesize dimers such as **3.13** in the future to obtain a sequence defined oligomer.

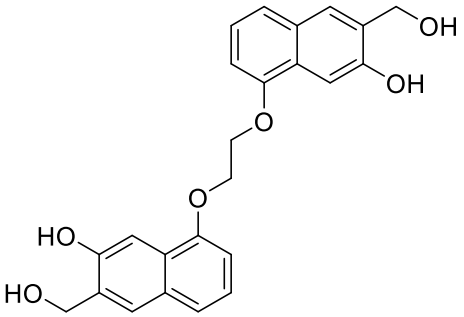

3.13

Scheme 3.17. Structures of alternative oNQMP monomers.

Alternatively, linkers at the 7th position of the ortho-hydroxynaphthyl group (compound **3.14**) are interesting structures to explore in the synthesis of photodegradable polymer. The advantage of **3.14** over the oNQMP monomer **3.4** is that **3.14** allows to generate a linear polymer chain geometrically similar to PET polymer.

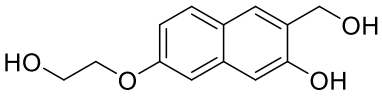

3.14

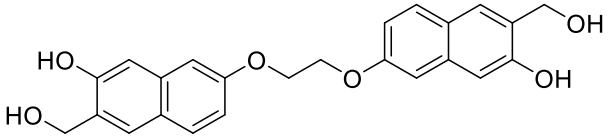

3.15

Scheme 3.18. Alternative oNQMP monomers and dimer structures.

Photoirradiation of oNQMP linker in an aqueous solution experiment shows a low yield of oNQMP monomer at high conversion (Section 3.5.1 and 3.5.2). The low yield may be because the oNQMP linker, **3.5** and oNQMP monomer, **3.4** have the same chromophore and compete for light. Therefore, an alternative oNQMP structure with efficient photocleavage is required. Our research group has designed 2,5-dihydroxybenzyl or naphthyl to solve this problem. The dihydroxy benzyl/naphthyl derivatives form oQMs upon irradiation and undergo tautomerization to generate 2-methyl-1,4-benzoquinone

derivatives (Scheme 3.19). This feature is called safety catch or reductive arming and has a high quantum yield (0.2-0.5) compared to oNQMPs (0.2-0.3).[113,114]

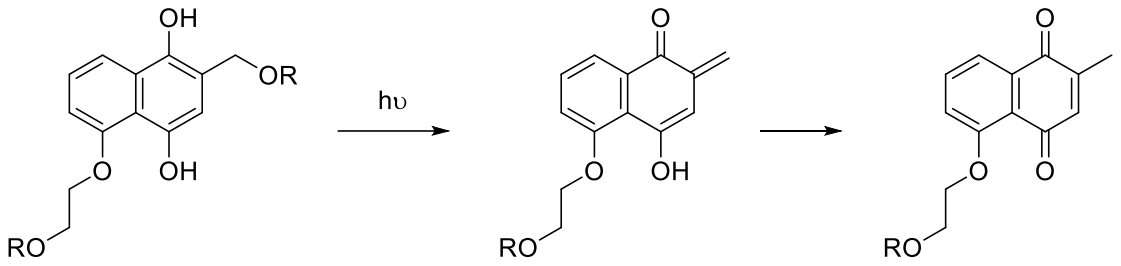

3.16 **3.17** **3.18**

Scheme 3.19. Alternative oNQMP photo linkers that produce quinone products.

oQMP monomers proposed in this study are highly water soluble, and synthesis of oQMP monomers is challenging. Alternative oQMP structures that are expected to have low water solubility compared to the oQMP monomer are shown in Scheme 3.20. oQMP dimer, **3.19** or sterically hindered oQMP, **3.20** can be other exciting options.

As mentioned in section 3.2, Scheme 3.4B, Aryl ethers are also excellent reversible PPGs. Photocleavage of aryl ethers occurs via homolysis or heterolysis. In the 1990s, Zimmerman and co-workers proposed that C-O bond heterolysis is facilitated over homolysis when ortho and meta substituents are present in the leaving group functionality.[115–117] This is proposed as a meta-effect, and various research groups have demonstrated efficient photocleavage of these systems.[118,119] Therefore, having meta methoxy groups (compound **3.21**) will help to reduce the water solubility of monomers and may provide efficient photocleavage as well.

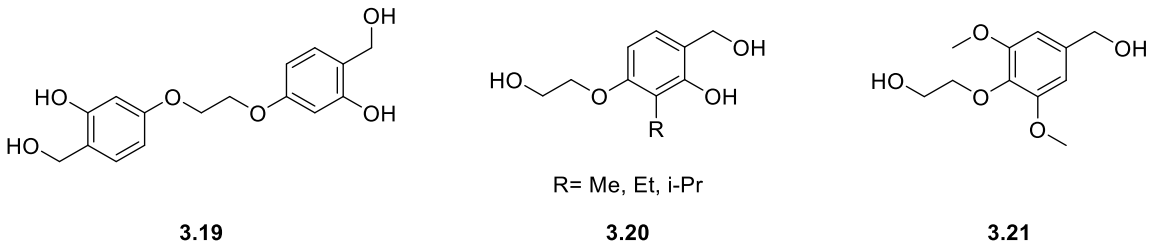

3.19 **3.20** **3.21**

Scheme 3.20. Alternative photo linkers based on hydroxy benzyl groups.

3.10 Experimental Section

3.10.1 General Information

Solvents, THF, DCM and acetone were purified using a solvent purification system prior to use and all the other commercially purchased reagents were used without further purification. Silica gel powder was used for all the column chromatography. All the NMR spectra were recorded in a 400 MHz Bruker instrument and the chemical shifts were referenced to the deuterated solvents used in each experiment. Deuterated solvents used are chloroform, methanol and dimethyl sulfoxide. Electrospray ionization mass spectrometry, high resolution mass spectrometry was used in small molecule and monomer analysis. Matrix-assisted laser desorption spectroscopy (MALDI-MS) was used to analyze polymer reaction mixtures. 2,5-dihydroxybenzoic acid (DHB) was used as the matrix compound in MALDI analysis. Shimadzu HPLC was used and HPLC grade solvents/methanol, and water was used. HPLC grade water was pre-filtered prior to the use and 0.1% trifluoroacetic acid (TFA) was used in the water mobile phase. A single HPLC solvent system was used for all the experiments unless otherwise noted. HPLC solvent system is methanol: water 45%:55% (0-11 minutes), gradient reaching methanol 100% (11-25 minutes), finally isocratic elution at methanol 100% (25-30 minutes); observation wavelength 240 nm.

TGA and DSC analysis were conducted using a Metler Toledo instrument. GPC analyses were conducted using a Shimadzu GPC instrument. All the photoreactions were conducted in quartz cuvette and irradiated using mini-rayonet 300 nm, 8 lamps, 4 W each unless otherwise noted. Absorbance spectra were collected using a Cary300 spectrophotometer. Melting point was taken using MPA160 & MPA161 Melting Point Apparatus

3.10.2 Synthesis Procedures and Compound Characteristics

Synthesis of methyl 3,5-dihydroxy-2-naphthoate, 3.2

3,5-dihydroxy-2-naphthoic acid (10 g, 48.9 mmol) was dissolved in 400 mL of methanol and conc. H_2SO_4 (10 mL) was added dropwise at room temperature. The reaction mixture was refluxed for 2 days. After 2 days, the reaction was quenched by pouring in ice-water mixture. It was filtered and dried under vacuum to obtain methyl 3,5-dihydroxy-2-naphthoate as a yellow color solid. (10.53 g, 99%). ^{1}H NMR (400 MHz, $CDCl_3$) δ 10.37 (s, 1H) 8.39 (s, 1H), 7.56 (s, 1H), 7.34 (d, J = 8 Hz, 1H), 7.09 (t, 1H), 6.78 (d, J = 8 Hz, 1H), 3.96 (s, 3H).

Synthesis methyl 3-hydroxy-5-(2-hydroxyethoxy)-2-naphthoate, 3.3

Potassium carbonate (1.13 g, 8.17 mmol) was added to a solution of methyl 3,5-dihydroxy-2-naphthoate (0.9 g, 4.1 mmol) in acetone (10 mL), followed by a dropwise addition of 2-bromoethanol (300 μL, 4.1 mmol); and reaction mixture was refluxed for 4 hours. After 4 hours, solvent was removed under rotary evaporator, the residue re-dissolved in ether (50 mL), washed with brine (20 mL), dried over anhydrous magnesium sulfate, and the solvent was removed under reduced pressure. The product was purified by column chromatography using 1:2 ethyl acetate in hexanes, and then 1:1 to give methyl 3-hydroxy-

5-(2-hydroxyethoxy)-2-naphthoate. (0.3 g, 62% yield based on 45% conversion of starting material). ^{1}H NMR (400 MHz, $CDCl_3$) δ 10.45 (s, 1H), 8.47 (s, 1H), 7.74 (s, 1H), 7.42-7.44 (d, J = 8 Hz, 1H), 7.24 (t, J = 7.8 Hz, 1H), 6.86-6.88 (d, J = 7.6 Hz, 1H), 4.26 (t, J = 4.2 Hz, 2H), 4.12 (t, J = 4.4 Hz, 2H), 4.05 (s, 3H). HRMS-ESI (m/z) $[M+H]^+$ calculated for $[C_{14}H_{14}O_5+H]^+$: 263.0914, found: 263.0915.

Alternatively, the same reaction procedure was carried out with 2-hydroxyethyl 4-methylbenzenesulfonate (3 g, 13.74 mmol), instead of 2-bromoethanol and obtained the same yield of methyl 3-hydroxy-5-(2-hydroxyethoxy)-2-naphthoate. The synthesis of 2-hydroxyethyl 4-methylbenzenesulfonate is described below.

Synthesis of 2-hydroxyethyl 4-methylbenzenesulfonate

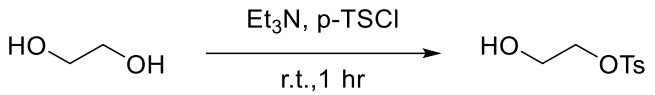

2-hydroxyethyl 4-methylbenzenesulfonate was synthesized based on a previously published procedure.[120] p-TsCl (10.0 g, 0.052 mol) was added to ethylene glycol (180 mL, 3.23 mol) while stirring at room temperature. Et_3N (7.24 ml, 0.052 mmol) was then added dropwise in the course of 5 minutes. After 1 hour, the reaction mixture was transferred to a separate funnel with water (400 mL), $CHCl_3$ (400 mL). After shaking, the organic phase was separated, and the H_2O phase was extracted with another 200 mL of $CHCl_3$. Organic extracts were merged, dried with anhydrous Na_2SO_4 and evaporated in vacuum. The product was obtained as a colorless viscous liquid (5 g, 52%). ^{1}H NMR (400 MHz, $CDCl_3$) δ 7.78-7.80 (d, 2H), 7.33-7.35 (d, 2H), 4.11 (t, 2H), 3.76 (t, 2H), 2.38 (s, 3H). HRMS-ESI (m/z); $[M+H]^+$ calculated for $[C_9H_{12}O_4S+H]^+$: 217.0529, found: 217.0529.

Synthesis of 8-(2-hydroxyethoxy)-3-(hydroxymethyl)naphthalen-2-ol, 3.4

Methyl 3-hydroxy-5-(2-hydroxyethoxy)-2-naphthoate (1.5 g, 6 mmol) was dissolved in THF (150 mL) and cooled to 0 ^{0}C. Pieces of LAH pellets (0.5 g, 13 mmol) was added and stirred overnight at room temperature. Next day, the reaction was quenched with aqueous HCl, THF was evaporated off, and product was extracted to ethyl acetate, washed with water and brine. 8-(2-hydroxyethoxy)-3-(hydroxymethyl)naphthalen-2-ol was purified by ethyl acetate: hexane 1:1 followed by 100% ethyl acetate. The product was obtained as a brown-yellow solid. (1.2 g, 90%). ^{1}H NMR (400 MHz, MeOD) δ 7.59 (s, 1H), 7.42 (s, 1H), 7.20-7.18 (d, 1H), 7.01 (t, 1H), 6.67-6.65 (d, 1H), 4.66 (s, 2H), 4.05 (t, 2H), 3.87 (t, 2H). ^{13}C NMR (400 MHz, MeOD) δ 153.29, 152.86, 130.35, 129.45, 126.23, 125.91, 122.46, 119.87, 104.54, 103.20, 69.32, 60.53, 59.91. HRMS-ESI (m/z) $[M-H]^-$ calculated for $[C_{13}H_{14}O_5-H]^-$: 233.0808, found: 233.0809. ESI-MS for $[C_{13}H_{14}O_4-H]^-$ 233.1; found 233.1. Melting point (168.5±0.5) ^{0}C.

Synthesis of 8-(2-hydroxyethoxy)-3-((2-hydroxyethoxy)methyl)naphthalen-2-ol, 3.5

8-(2-hydroxyethoxy)-3-(hydroxymethyl)naphthalen-2-ol (0.02 g, 0.085 mmol) was dissolved in ethylene glycol (2 mL, 35.8 mmol) and catalytic amount of p-TSA was added (less than 0.0001 g). Reaction mixture was stirred at 90 ^{0}C for 5 hours. After 5 hours, the reaction was quenched with solid NH_4Cl and then with water and extracted using ethyl acetate. Both product and starting material was observed. The product was purified by column chromatography; 5% methanol in DCM and obtained a brown-yellow solid. (0.016 g, 67%). ^{1}H NMR (400 MHz, MeOD); δ 7.77 (s, 1H), 7.60 (s, 1H), 7.34 (d, 1H), 7.17 (t, 1H), 6.81 (d, 1H), 4.75 (s, 2H), 4.19 (t, 2H), 4.02 (t, 2H), 3.77 (t, 2H), 3.70 (t, 2H). ^{13}C NMR (400 MHz, MeOD) δ 153.31, 153.00, 129.35, 127.46, 127.31, 126.49, 122.59,

119.91, 104.69, 103.52, 71.72, 69.33, 68.57, 60.89, 60.51, 47.84. HRMS-ESI (m/z) $[M-H]^-$ calculated for $[C_{15}H_{18}O_5-H]^-$: 277.1081, found: 277.1082.

Synthesis of methyl 2-hydroxy-4-(2-hydroxyethoxy)benzoate, 3.8

Methyl 2,4-dihydroxybenzoate (3 g, 17.84 mmol) and K_2CO_3 (4.9 g, 35.68 mmol) was dissolved in 300 mL of acetone and refluxed at 72 ^{0}C for 1 hour. After 1 hour, $BrCH_2CH_2OH$ (1.2 ml, 17.84 mmol) was added dropwise. Next day, the reaction mixture was filtered and concentrated using the rotary evaporator. Starting material and the product was isolated via column chromatography. Eluent system: First, hexane: EtOAc = 4:1. Second, hexane: EtOAc = 2:1. Product was isolated as a white solid (1.73 g, 86% yield for 46% conversion of starting material). ^{1}H NMR (400 MHz, $CDCl_3$); δ 10.98 (s, 1H), 7.74-7.76 (d, 1H), 6.45-6.48 (m, 2H), 4.53 (s, 1H), 4.11 (t, 2H), 3.98 (t, 2H), 3.92 (s, 3H). ^{13}C NMR (400 MHz, $CDCl_3$) δ 170.36, 164.55, 163.69, 131.36, 107.74, 105.83, 101.35, 69.37, 61.19, 52.05. HRMS-ESI (m/z) $[M+H]^+$ calculated for $[C_{10}H_{12}O_5+H]^+$: 213.0757, found: 213.0760.

Synthesis of 5-(2-hydroxyethoxy)-2-(hydroxymethyl)phenol, oQMP monomer, 3.9

Slurry of LAH (0.14 g, 3.77 mmol) was dissolved in THF (10 mL) and cooled to 0 ^{0}C. A solution of methyl 2-hydroxy-4-(2-hydroxyethoxy)benzoate (0.2 g, 0.94 mmol in 5 mL of THF) was added dropwise. The mixture was stirred at room temperature for 3 hours. Then, refluxed for 1 hour. Reaction was quenched with HCl and extracted to EtOAC. Solvent was evaporated and various methods were employed for purification to obtain the product in several trials. Purification methods attempted are column chromatography, recrystallization using methanol, lyophilization. However, clean product of oQMP monomer was not obtained.

Synthesis of (2-bromoethoxy)(tert-butyl)dimethylsilane

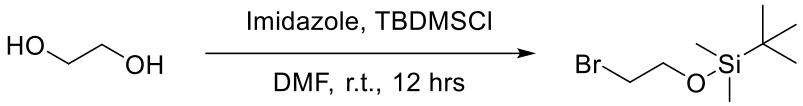

(2-bromoethoxy)(tert-butyl)dimethylsilane was synthesized according to a previously published procedure.[121] 2-bromoethanol (10 mL, 141 mmol) was added imidazole (12.5 g, 184 mmol) and tert-butyldimethylsilyl chloride (21.1 g, 140 mmol) mixture in anhydrous DMF (25 mL). The reaction was stirred at room temperature for 12 hours. After 12 hours, reaction was quenched with water and diethyl ether were added. The aqueous phase was extracted twice with diethyl ether. The extracted organic phase was washed with water and brine. The solution was dried with sodium sulfate. Evaporation of the solvent yielded 90% of the product as a colorless liquid. ^{1}H NMR (400 MHz, $CDCl_3$); δ 3.80 (t, 2H), 3.30 (t, 2H), 0.82 (s, 9H), 0.00 (s, 6H).

Synthesis of methyl 4-(2-((tert-butyldimethylsilyl)oxy)ethoxy)-2-hydroxybenzoate, 3.10

Methyl 2,4-dihydroxy benzoate (0.5 g, 2.97 mmol) was dissolved in acetone (50 mL) and potassium carbonate (1 g, 5 mmol) was added. Reaction mixture was stirred for 1 hour. (2-bromoethoxy)(tert-butyl)dimethylsilane (1 g, 5.94 mmol) was added dropwise and refluxed for 24 hours. Next day, white solid was filtered off and solvent was evaporated. Both product and starting material spot was observed on TLC. Product was purified via column chromatography. Hexane: EtOAc = 4:1. The product was isolated as a colorless liquid (0.6 g, 80%). ^{1}H NMR (400 MHz, $CDCl_3$); δ 7.80-7.82 (d, 1H), 6.50-6.57 (m, 2H), 4.11-4.29 (m, 4H), 3.85 (s, 3H), 0.21 (s, 6H), 0.00 (s, 9H).

Synthesis of 5-(2-((tert-butyldimethylsilyl)oxy)ethoxy)-2-(hydroxymethyl)phenol, 3.11

4-(2-((tert-butyldimethylsilyl)oxy)ethoxy)-2-hydroxybenzoate (0.7 g, 2.1 mmol) was dissolved in THF (2 mL) and cooled to 0 ^{0}C. LAH powder (0.16 g, 4.2 mmol) was added slowly. Reaction was stirred from 0 ^{0}C to room temperature. After that, the reaction was quenched with HCl and extracted with EtOAc. Product was washed with water and brine. The product was obtained as colorless liquid (64 mg, 10%). ^{1}H NMR (400 MHz, MeOD); δ 6.80-7.00 (d, 1H), 6.10-6.29 (m, 2H), 4.30 (s, 1H), 3.88 (m, 4H), 3.23 (s, 2H), 0.81 (s, 9H), 0.00 (s, 6H).

oNQMP methyl linker synthesis and characterization, 3.6

A methanolic solution of oNQMP monomer in methanol (0.5 mM) was irradiated using 300 nm lamps and photolysate was analyzed by LC-MS. HRMS (m/z) of oNQMP methyl linker: $[M-H]^-$ calculated for $[C_{14}H_{16}O_4-H]^-$: 247.0976, found: 247.0975.

3.10.3 Photophysical Properties of oNQMP Linker

3.10.3.1 Extinction coefficient determination

A series of oNQMP linker solutions in aqueous acetonitrile (1:10) at the given concentrations were prepared: 0.03, 0.04, 0.05, 0.06, 0.07, 0.08, 0.09 and 0.1 mM. Absorbance spectra of each solution was taken (Figure 3.12A) and the molar extinction coefficients at each maximum absorbance was determined based on the Beer-Lambert Law from a plot between absorbance vs concentration (Figure 3.12B, C, D, and E). Logarithm of molar extinction coefficient at 218, 239, 284 and 330 nm are 4.05, 3.98, 3.2, and 2.8 respectively.

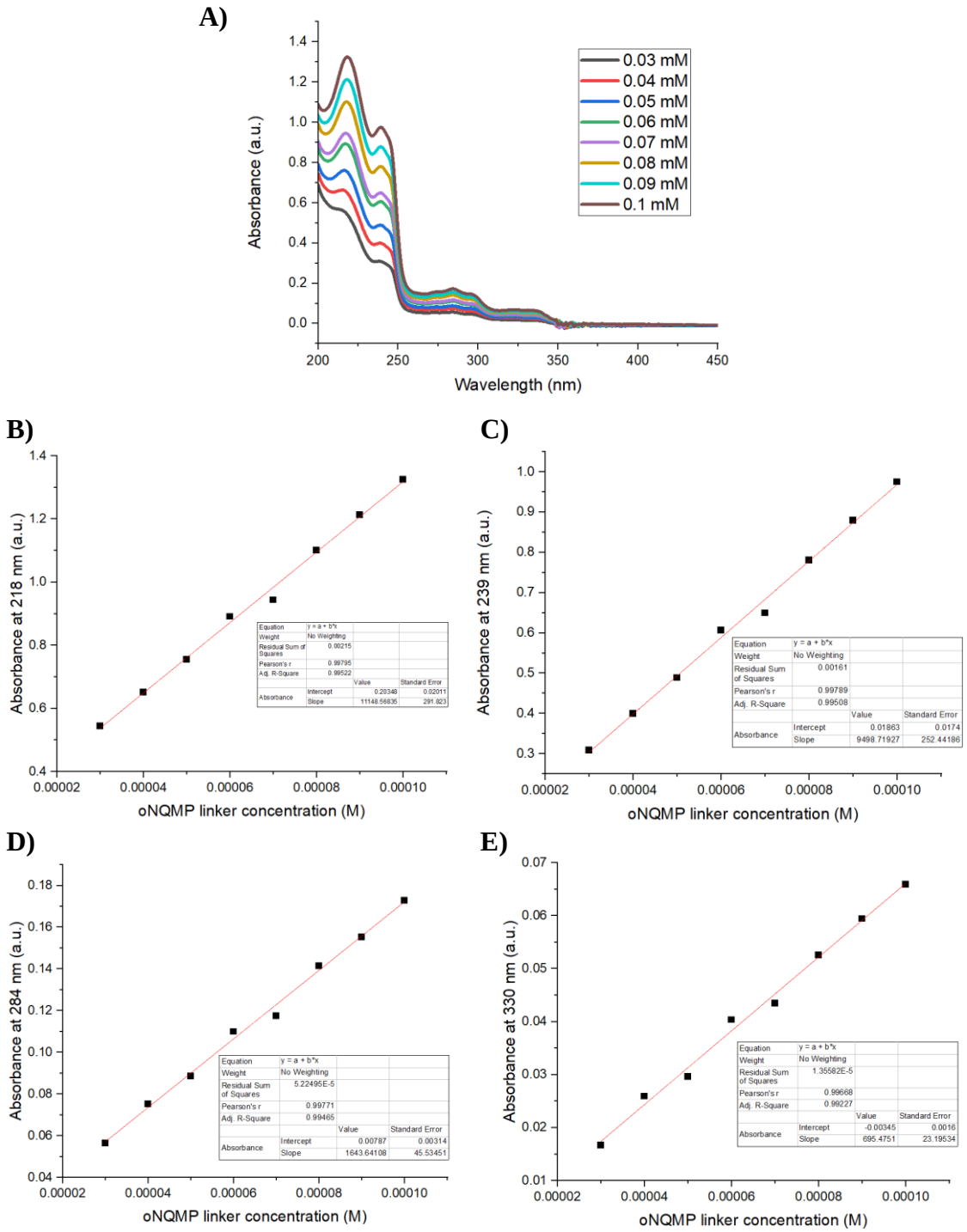

Figure 3.12. A) Absorbance spectra of oNQMP concentration series. Plot of absorbance vs oNQMP linker concentration at B) 218 nm, C) 239 nm, C) 284 nm, and E) 330 nm.

3.10.4 HPLC calibration curves for NQMP monomer and linker

Calibration curve data for oNQMP monomer and oNQMP linker are presented in this section. HPLC solvent system is methanol: water (45%:55%) for 0 to 11 minutes, then gradient reaching 100% methanol from 11 to 25 minutes and finally isocratic elution at 100% methanol from 25-30 minutes; observation wavelength 240 nm. HPLC chromatogram of oNQMP monomer in methanol (10 μm): retention time 7.0 minutes and the calibration curve is shown in Figure 3.14.

Table 3.1. HPLC peak area of known concentrations of oNQMP monomer.

[oNQMP monomer] (M)	**Trial 1**	**Trial 2**	**Trial 3**
1.7E-5	2088011	1988225	2020431
3E-5	3121620	3101450	3111630
5E-5	4769510	4673058	4595286
8.3E-5	8054116	8295043	8212445
1E-4	9152494	9294630	9227951

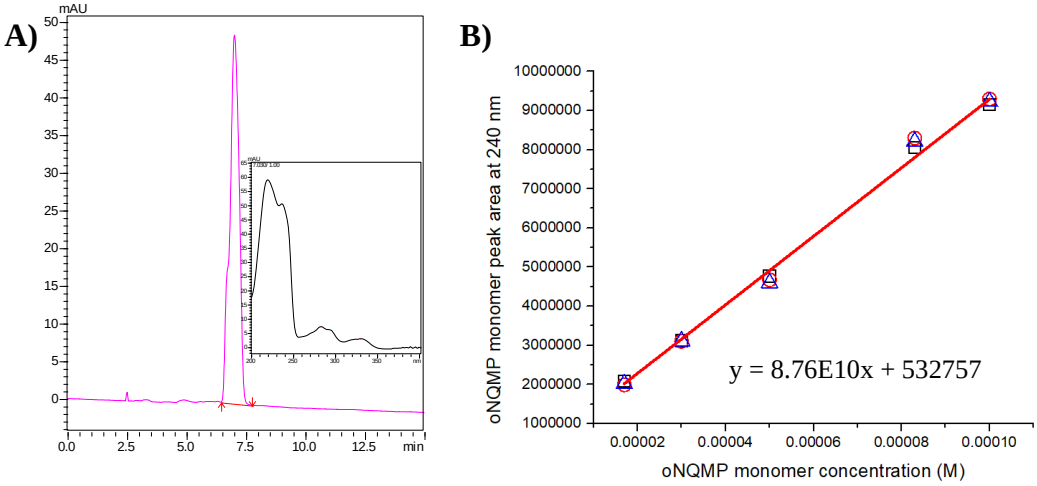

Figure 3.13. A) HPLC chromatogram, B) HPLC calibration curve of oNQMP monomer.

Table 3.2. HPLC peak area for oNQMP linker known concentrations.

[oNQMP linker] (M)	**Trial 1**	**Trial 2**	**Trial 3**
1.33E-5	1320760	1310460	1310790
6.65E-5	6083224	6103215	6083223
8E-5	7310144	7330144	7334555
9.31E-5	8509144	8508864	8519345

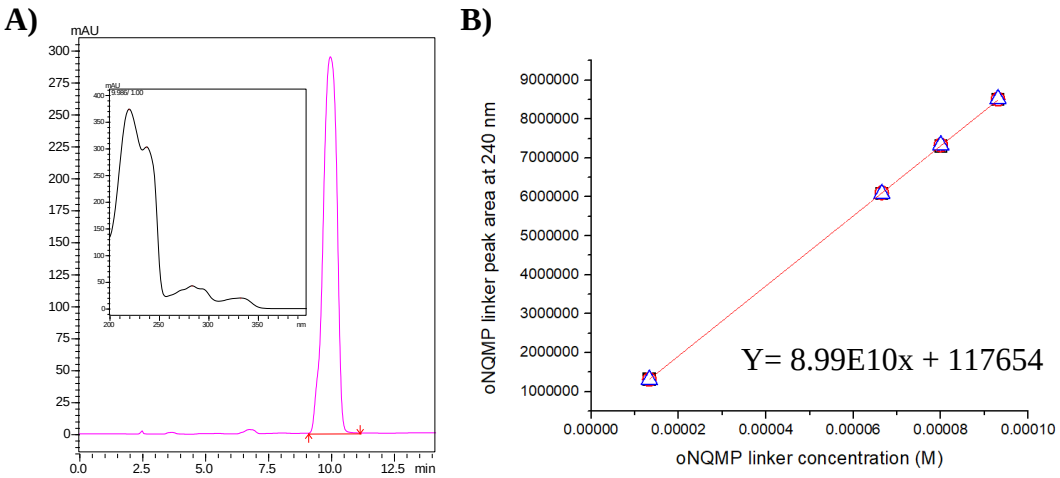

Figure 3.14. A) HPLC chromatogram, UV spectrum (insert), B) HPLC calibration curve of oNQMP linker, 3.5.

CHAPTER 4

MECHANISM OF THIOL-CATALYZED HYDROLYSIS OF P-NITROPHENYL ACETATE ESTER: TOWARDS THE DEVELOPMENT OF A NOVEL CATALYST FOR POLYESTER RECYCLING

4.1 Introduction

Polyethylene terephthalate is a recyclable polymer. Two main conventional recycling pathways are used in the industry; mechanical and chemical recycling of PET.[69] A recent green approach for PET recycling uses microbes such as bacteria or enzymes to degrade PET.[122] These three recycling methods, their pros and cons, will be described in this section.

4.1.1 Mechanical Recycling of PET

Mechanical recycling is a process that involves washing PET to remove dirt and other contaminants, grinding, crushing, extrusion by heat, and reprocessing into new PET products such as carpets and fleece vests.[123]

4.1.2 Chemical Recycling of PET

Chemical recycling of PET is a sustainable method that uses chemicals to depolymerize PET polymer into monomers.[124] Commonly used chemical methods involve the reaction of PET with nucleophiles. Chemical recycling methods can be classified into five categories. They are hydrolysis,[125] methanolysis, glycolysis, ammonolysis, and aminolysis when the nucleophile is water, methanol, ethylene glycol, ammonia, and amines, respectively (Scheme 4.1). Products of hydrolysis, methanolysis, glycolysis,

ammonolysis, and aminolysis are terephthalic acid (TPA), dimethyl terephthalate (DMT), bis hydroxyethyl terephthalate (BHET), terephthalate (TPA), and diamides of terephthalic acid, respectively.

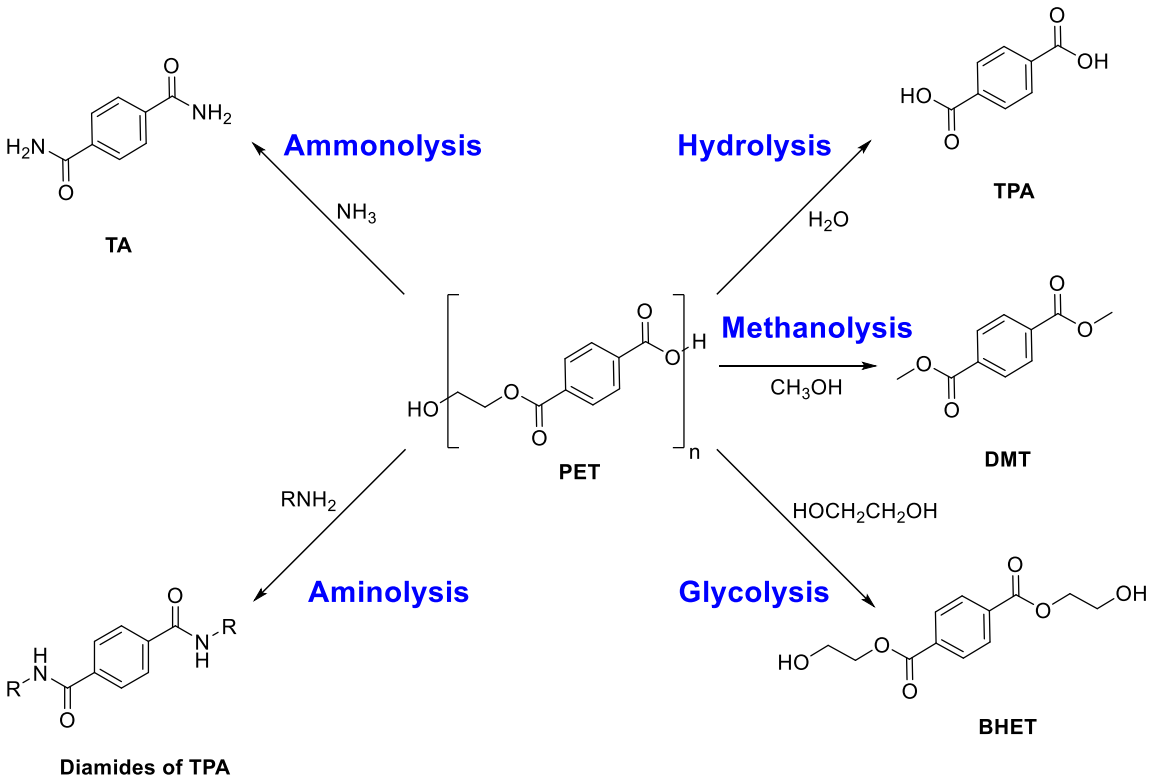

Scheme 4.1. PET chemical recycling methods.

The main advantage of chemical recycling is that it produces monomers that can be used to re-synthesize PET again. It saves monomers from petroleum fuel sources and contributes to a sustainable, circular economy. PET synthesis requires TPA, or DMT, BHET (Section 3.1.1). Products of ammonolysis and aminolysis, TPA and diamides of terephthalic acid cannot be utilized back in the PET synthesis. Therefore, ammonolysis and aminolysis are called ‘dead-end depolymerization for PET’ as they do not support PET circular economy and are less common in the industry. On the other hand, all the products of hydrolysis, glycolysis, and methanolysis produce useful sustainability monomers.

4.1.3 Enzymes or Microbes aided Recycling of PET

Enzymes produced by certain microbes are capable of hydrolyzing PET into TPA and ethylene glycol (EG).[126] The most common example is *Ideonella sakaiensis*, a bacterium that produces PETase and MHETase enzymes.[127] PETase converts PET into BHET, monohydroxyethyl terephthalate (MHET), and TPA. MHETase enzyme facilitates the conversion of MHET to TPA and EG.[102] These two enzymes have the capability to degrade high crystalline PET as well. However, the process is very slow, and recently genetically modified microbes or protein engineering have taken much attention to improving the green PET degradation process. PETcutinases from engineered leaf-branch compost cutinase were reported as an efficient PET degrading enzyme.[128] PET cutinase produces BHET, MHET and TPA similar to PETase.

4.1.4 Challenges in PET Recycling

Each of the recycling methods described above has its advantages and disadvantages. Mechanical recycling leads to low-commodity value plastics such as carpets. It is not popular in the PET recycling industry. It cannot produce food-grade PET again. Chemical recycling, on the other hand, has taken the attraction industrially as it can recover monomers and reuse them to make food-grade, quality plastic. Enzymatic degradation of PET also leads to the generation of monomers. However, the process is slow and provides low yields of monomers. The recent use of genetically modified mutants for the generation of efficient PET depolymerase is under argument as it can be a potential threat to other organisms and a concern for environmental safety.[129]

Apart from the inherent drawbacks of the current recycling methods, one of the main obstacles to recycling plastics is contamination from traces of other plastic materials

such as polyethylene, and additives, etc. Only single type plastics can be recycled in the current chemical recycling approaches. Another barrier to PET recycling is the low cost of virgin monomers from fossil fuels compared to the total cost for chemical recycling. This is mainly because chemical recycling is a slow process at room temperature and atmospheric pressure conditions. Hence, it often requires an expensive catalyst, elevated temperature, and pressure conditions, and requires equipment that could withstand harsh conditions. Even though chemical recycling facilitates a circular economy, it is neglected by the industry for the above reasons.[130] Therefore, we attempted to develop a novel, inexpensive catalyst that can be utilized in both hydrolysis and solvolysis under mild conditions. This chapter will describe the thiol catalysts of choice as a novel catalyst and their use in PET hydrolysis. The foundation for our research work came from a recent study on organocatalytic amine catalysts.

4.2 Motivation Towards the Study – Organocatalytic Amine Catalysts

Researchers from International Business Machines (IBM) Corporation have recently patented the utilization amines as an effective catalyst for glycolysis. They have screened a range of amine organocatalysts with varying acidity constants (pK_a) on PET glycolysis reaction.[131,132] The organocatalysts screened are 1,5-diazabicyclo-[4,3,0]-non-5-ene (DBN), 4-(N,N-dimethylamino)pyridine (DMAP), 1,4-diazabicyclo-[2,2,2]-octane (DABCO), N-methylimidazole (NMI), N,N-dimethylaniline (DMA), 1,5,7-triazabicyclo-[4,4,0]-dodecene (TBD), and 1,8-diazabicyclo[5,4,0]undec-7-ene (DBU). They only observed the conversion of PET to BHET under glycolysis conditions and were highly efficient compared to other metal catalysts used in PET glycolysis (Scheme 4.2).[133] The researchers have reported the degradation time required for complete conversion of PET

and also the oligomer percentage with respect to the total (oligomer+BHET) content. The lowest degradation time and low oligomer content was noted when the catalyst was DBU, TBD, or DBN (Table 4.1). Furthermore, researchers have proposed the reaction mechanism is facilitated via hydrogen bonding between the catalyst and EG.[134]

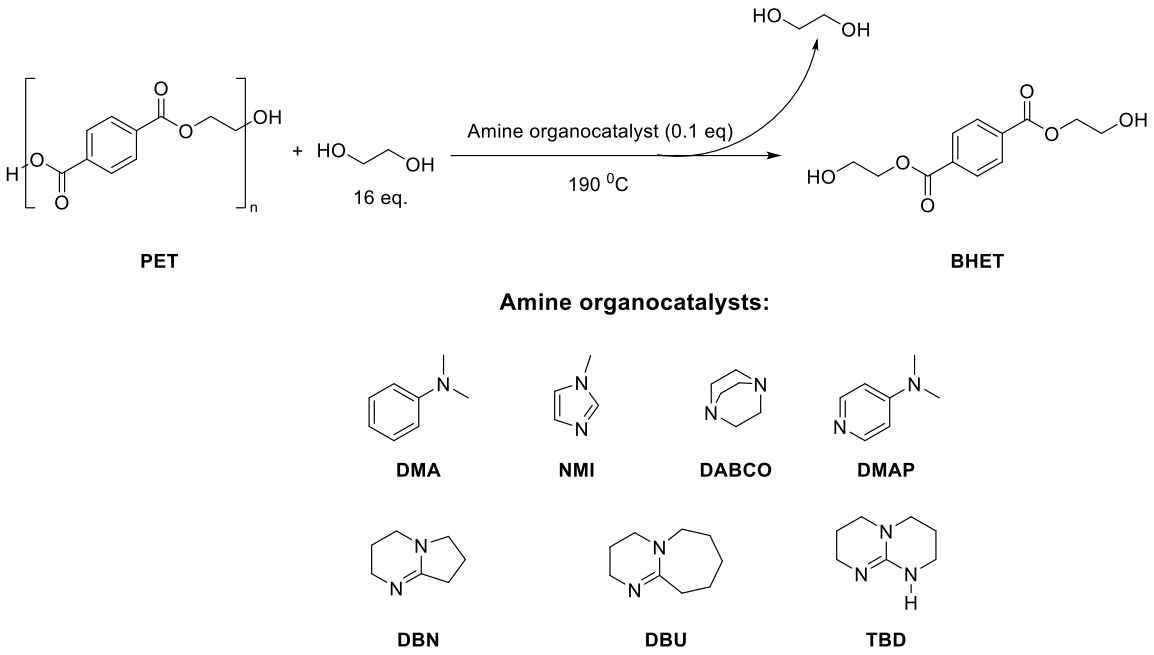

Scheme 4.2. PET glycolysis in the presence of organocatalytic amines.

Even though TBD, DBU and DBN shows excellent results for PET depolymerization within a short time, these catalysts are expensive, and removal of catalyst is not possible. Catalyst accumulation is toxic upon re-polymerization and not ideal for food-grade PET. Same researchers in 2013, developed the depolymerization method employing volatile amines. The amines used are triethylamine (TEA) and tetramethyl ethylenediamine (TMEDA). The main reason for choice of TEA and TMEDA is their low boiling point compared to TBD, DBU or DBN. Boiling points of TEA and TMEDA are 88 ^{0}C, 121 ^{0}C, respectively, whereas for DBN, DBU and TBD are 233 ^{0}C, 261 ^{0}C, 263 ^{0}C, respectively. Upon completion of the PET depolymerization, the solution is evaporated and distilled off

to recover the catalysts TEA or TMEDA. Then, the solution is filtered, decolored and further purified using Amberlyst to get pure BHET, and EG is re-used for depolymerization. The protocol was patented as 'Volcat' technology as it uses volatile amines and process is capable of recovering catalyst after depolymerization.[135] Other research groups also have demonstrated amines such as cyanamide, melamine, and even urea as efficient PET glycolysis catalysts after IBM's innovation.[136, 137]

Table 4.1. PET depolymerization results for various amine organocatalysts.

Catalyst	**$pK_{a(water)}$**	**$pK_{a(acetonitrile)}$**	**Degradation time minutes**	**Oligomer %**
None	-	-	2400	9.4
DMA	5.07	11.43	2755	7.6
NMI	7.4	N/A	300	7.4
DABCO	8.2	N/A	120	6.9
DMAP	9.7	17.95	100	6.4
DBN	11.0	N/A	7	1.5
DBU	11.9	24.34	6.5	1.1
TBD	N/A	26.03	8	5.1

In our perspective, some critical factors of amine catalysts still need to be addressed or neglected by the researchers even though these catalysts are widely reported in the literature. The mechanism for amine catalyst depolymerization was proposed only based on DBU which is a bulky base and less nucleophilic. According to Fukushima and co-workers' computation studies of transesterification of methyl benzoate in ethylene glycol

and DBU, is facilitated via hydrogen bonding between sp2 hybridized nitrogen and solvent. This hydrogen bond increases the nucleophilicity of the ethylene glycol oxygen group. Furthermore, hydrogen bonding between solvent, ethylene glycol and carbonyl oxygen also reported that increases the electrophilicity of the carbonyl carbon (Scheme 4.3).[134] However, mechanism when the catalyst is nucleophilic TEA or TMEDA was not reported. It is possible that TEA and TMEDA amines to facilitate ester dissociation and form salts which would inactivate the catalyst during the reaction and cannot be recovered (Scheme 4.4).[138] Additionally, the yields of BHET was not reported, instead only BHET: oligomer ratio was reported.

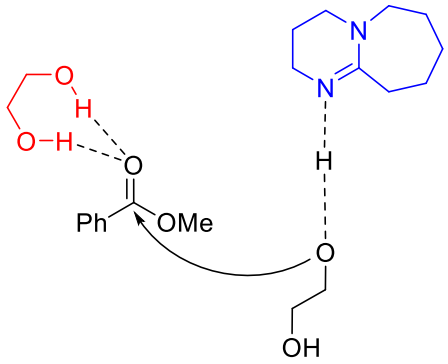

Scheme 4.3. Reported mechanism for amine catalyzed transesterification.

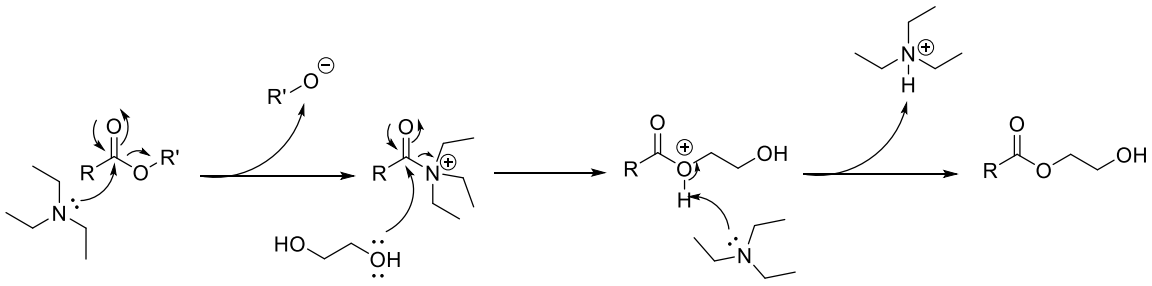

Scheme 4.4. Nucleophilic acyl substitution of amines.

Nevertheless, prompted by the results from IBM researchers, we explored the feasibility of using thiols as catalysts for the depolymerization or transesterification

because thiolates are good nucleophile as well as better leaving groups. Therefore, we screened various thiols to find a suitable catalyst in PET depolymerization.

4.3 Experiment Design and Goals

The first goal of our research work was to find the best thiol catalyst for ester cleavage or hydrolysis. To the best of our search, thiol-catalyzed hydrolysis of PET or any esters has not been done industrially or in laboratories. Also, while thiol-thioester exchange has been widely studied, literature data on the hydrolysis of esters with thiol catalysts are limited. P-Nitrophenyl acetate (p-NPA) is the most used substrate to detect the catalytic activity of esterases in biological systems, and the reaction is easy to follow by UV spectroscopy due to the formation of strongly absorbing product, p-nitro phenolate (p-NP) at 400 nm (Figure 4.1).[139]

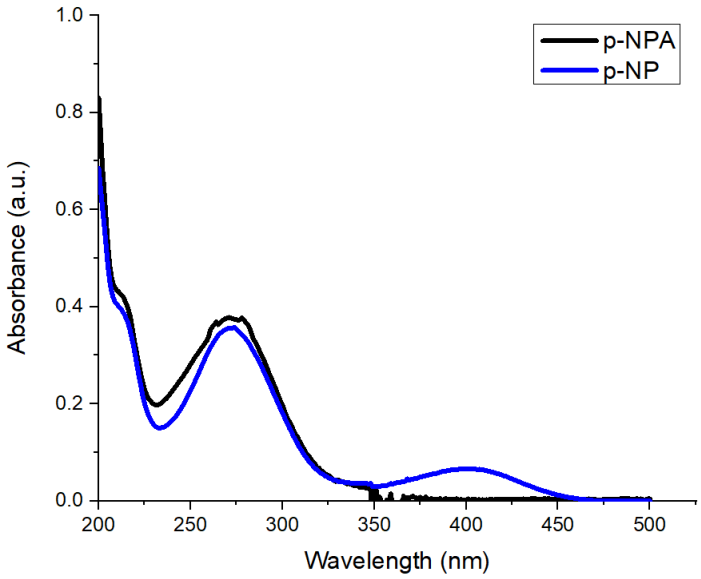

Figure 4.1. Absorbance spectra of p-NPA and p-NP.

Thiol catalysis on p-NPA hydrolysis to p-NPA was studied by Whitaker, Bender, and many other research groups in the 1960s.[140, 141] However, all the experiments were carried out at neutral pH because their goal was to model enzymes in biological systems.

It is well known that thiols can exist in thiol or thiolate form depending on the pH of the medium, and thiolate is more reactive/nucleophilic compared to the protonated form. The reactivity of thiol can vary widely depending on the pK_a of thiol. In 1964 Strauch and coworkers studied the kinetics for the hydrolysis of p-NPA reaction at various pHs with different thiols.[142] But, the relationship between pK_a of thiols and pH is unclear and has not been reported. Therefore, we conducted an initial kinetic study using p-NPA as the model ester with various thiols. The two goals of this study were to find the relationship between pK_a values of each thiol vs. the efficiency of catalysis at different pHs and the most efficient thiol catalyst for ester hydrolysis (Scheme 4.5).

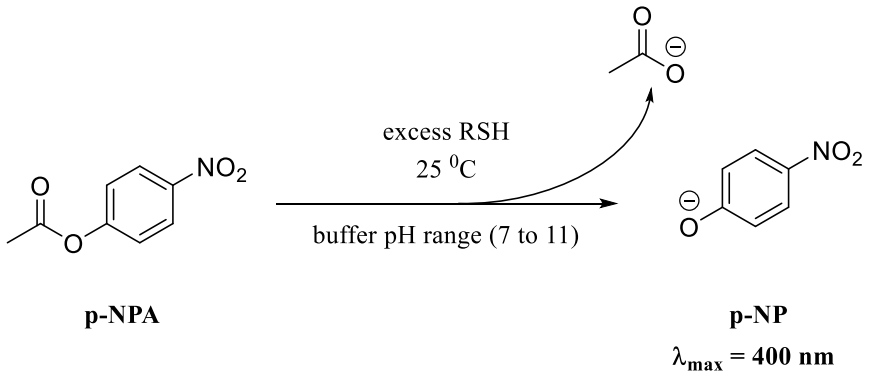

Scheme 4.5. Hydrolysis of p-NPA to p-NP.

We then used thiols with the highest catalytic efficiency to investigate thiol catalysis on the simplest oligomer of PET, Bis(hydroxyethyl) terephthalate, BHET (Scheme 4.6).

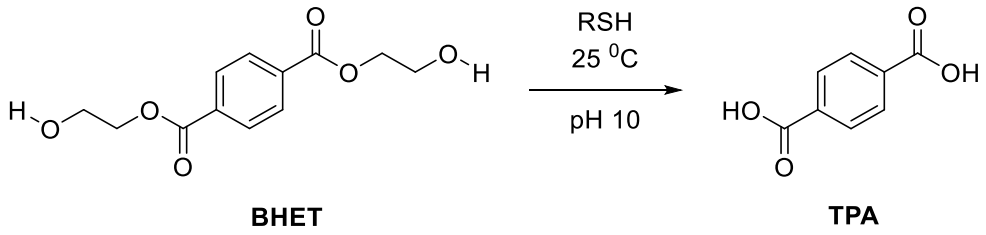

Scheme 4.6. BHET hydrolysis catalyzed by thiols.

4.4 Thiol Catalyst Candidates

The choice of thiol was based on the pK_a values. In general, a thiol with a lower pK_a value corresponds to weaker nucleophilicity and has a lower S-H bond dissociation energy. Another factor considered in selecting thiol candidates is the odor of the thiol. Thiols smell strongly, like rotten eggs or garlic. Thiols with short carbon chain length have a strong odor compared to the longer carbon chain in the alkanethiol series. For example, ethanethiol has a strong odor and dodacanethiol is odorless.[143] It is ideal to use simple, low molecular weight thiols for our study as the main goal is to utilize them polymer depolymerization, bulky, long chain thiols can cause steric issues. Since simple thiols have a strong odor, we decided to use thiols with other functional groups that have no or less odor. For example, instead of ethanethiol, 2-mercaptoethanol was selected that as odorless and it has both SH and OH functionalities.

Thiols with different acidity constants varying from pK_a 6 to 9 were selected taking into consideration of their odorless nature as well.[144,145] The selected thiols were thiophenol (TP), 4-mercaptobenzoic acid (4-MBA), 2,2,2-trifluoroethane thiol (TFET), cysteine, cysteamine, 2-mercaptoethanol (2-ME), thiocholine (TC), diethylaminoethanethiol (DEAET), and 3-mercaptopropionic acid (3-MPA). The thiol structure and their pK_a values taken from literature are shown in Table 4.1.[146, 147]

Table 4.2. Selected thiol candidates and their pK_a values.

Thiol	Abbreviation	Structure	pK_a (RSH)
Thiophenol	TP	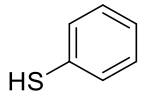	6.61
4-Mercaptobenzoic acid	4-MBA	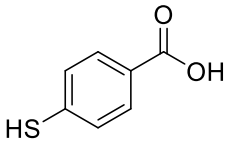	6.8
2, 2, 2-Trifluoroethane thiol	TFET	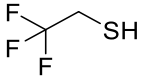	7.3
Cysteamine/2-Aminoethanethiol	AET	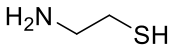	8.19
2-(Diethylamino)ethanethiol	DEAET	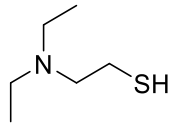	7.7
Cysteine	N/A	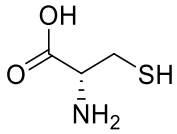	8.55
2-Mercaptoethanol	2-ME	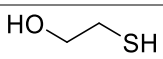	9.61
3-Mercaptopropionic acid	3-MPA	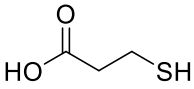	10.27
Thiocholine	TC	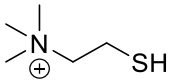	7.7

4.5 Determination of Catalytic Coefficient of thiols at varying pH

4.5.1. Kinetic Experiments

The catalytic coefficient or k_{cat} in catalyzed reactions is a constant that relates to the reaction rate constant to catalyst concentration.[148] Hydrolysis of p-NPA to p-NP was used to determine k_{cat} values of thiols at each pH. At a given pH, p-NPA hydrolysis was studied by monitoring the absorbance increase at 400 nm using a UV spectrophotometer, which indicates the formation of the product p-NP. Pseudo first-order kinetics conditions was used where p-NPA concentration is 0.005 mM and series varying excess thiol concentration, 0, 0.2, 0.3, 0.4, and 0.5 mM. A plot of thiol concentration vs. observed rate constant is used, and the slope of the plot represents k_{cat} the at the specific pH. The experiment was repeated in aqueous buffer solutions with a pH range from 7 to 11. After that, a plot of pH vs k_{cat} was constructed. An example of kinetic traces taken with varying cysteamine concentrations at pH 11 is shown in Figure 4.2A below by, taking cysteamine as a catalyst at pH 11.

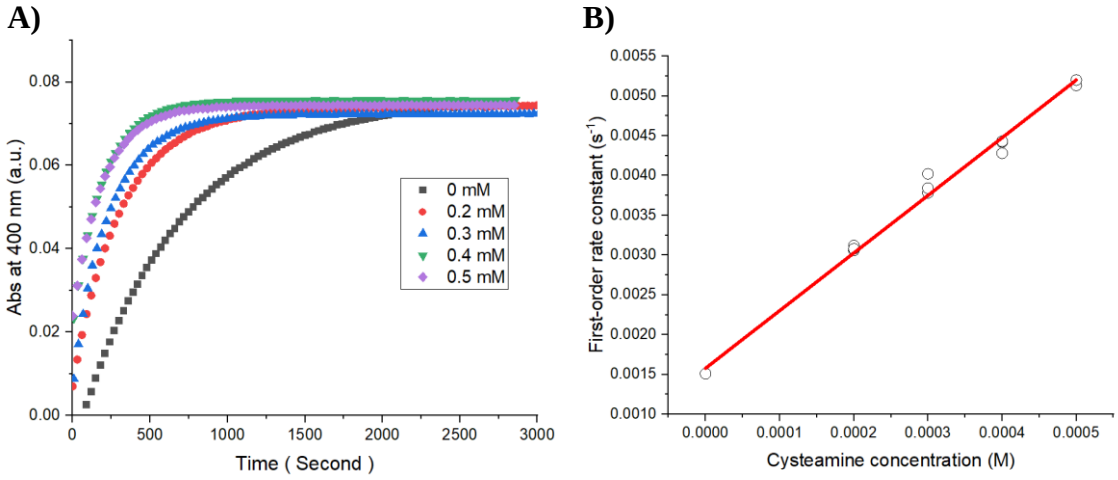

Figure 4.2. A) p-NPA (0.005 mM) hydrolysis kinetics at various excess cysteamine concentrations, pH 11, B) Catalytic coefficient plot of cysteamine at pH 11.

4.5.2. Results, pH vs. Catalytic Coefficient Plot

TP and 4-MBA were found unsuitable for the p-NPA hydrolysis as disulfide formation competed with ester hydrolysis (*Vide infra*, see section 4.8). All the other thiols demonstrated increasing k_{cat} upon increasing pH (Table 4.3 and Figure 4.3). This is because the thiolate percentage is increasing compared to thiol when increasing the pH and nucleophilicity of thiolates is higher than thiols. Thiol's nucleophilicity is constrained, and sulfhydryl mostly exists in protonated RSH form when the pH of the aqueous buffer solution is lower than the thiol pK_a. Thiol is then deprotonated once the pH rises and transforms into high-nucleophilic thiolate.

Table 4.3. Catalytic coefficients of thiol candidates at different pHs.

Thiol	**pK_a**	**k_{cat}**				
	(RSH)	**pH = 7**	**pH= 8**	**pH= 9**	**pH= 10**	**pH= 11**
TFET	7.3	0.022±0.001	0.56±0.05	0.56±0.06	0.58±0.02	N/A
Cysteamine	8.19	0.18±0.03	1.73±0.09	3.9±0.1	4.9±0.2	7.6±0.4
DEAET	7.7	0.78±0.03	2.6±0.1	4.1±0.2	4.03±0.23	8.9±0.8
Cysteine	8.55	0.15±0.01	1.23±0.02	3.1±0.2	4.3±0.1	8.1±0.4
2-ME	9.61	0.021±0.006	0.03±0.01	2.1±0.1	4.03±0.05	4.09±0.07
3-MPA	10.27	0.05±0.01	0.14±0.02	0.71±0.05	3.8±0.1	3.9±0.5
TC	7.7	0.19±0.01	1.22±0.05	1.80±0.04	2.5±0.1	4.1±0.3

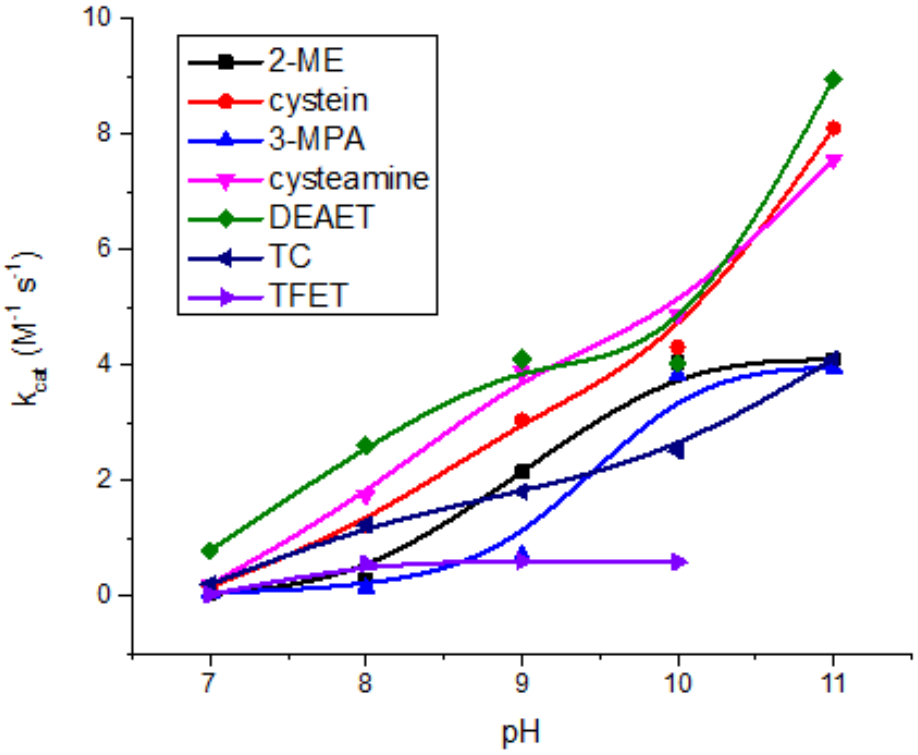

Figure 4.3. pH vs. catalytic coefficient (k_{cat}) plot for various thiols.

The k_{cat} of 2-ME, TFET, and 3-MPA showed an expected sigmoidal dependence with pH, which agrees on rate-limiting thiolate attack on ester carbonyl (Scheme 4.7).

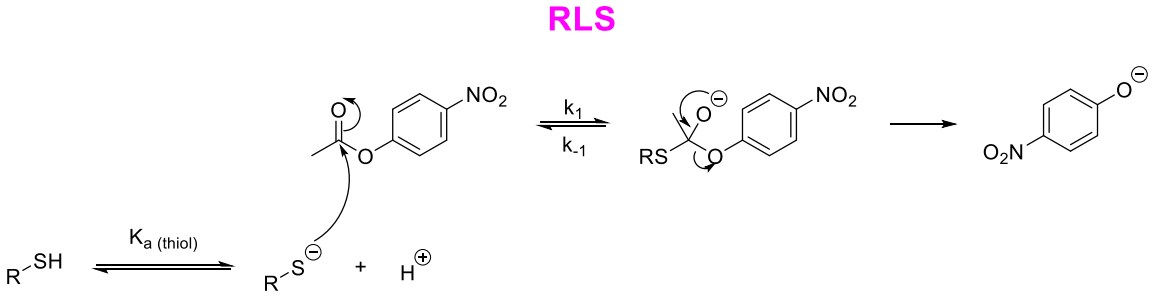

Scheme 4.7. Thiol-catalyzed ester p-NPA hydrolysis mechanism.

Cysteine, cysteamine, DEAET, and thiocholine did not reach a plateau in pH vs. k_{cat} plots suggesting a more complex mechanism rather than conventional nucleophilic acyl substitution or due to the participation of other functional groups in the ester hydrolysis.[149]

Cysteine has carboxylate and amine functionality in addition to thiol/thiolate. pH vs. k_{cat} plot of cysteine should reach a plateau after the thiol pK_a if thiol is the only active nucleophile. However, it is likely that beyond pH 10, the cysteine ammonium group gets deprotonated, which could also facilitate ester hydrolysis (Scheme 4.8A). A similar effect is expected in cysteamine and DEAET (Scheme 4.8B and 4.8C).

A) Cysteine

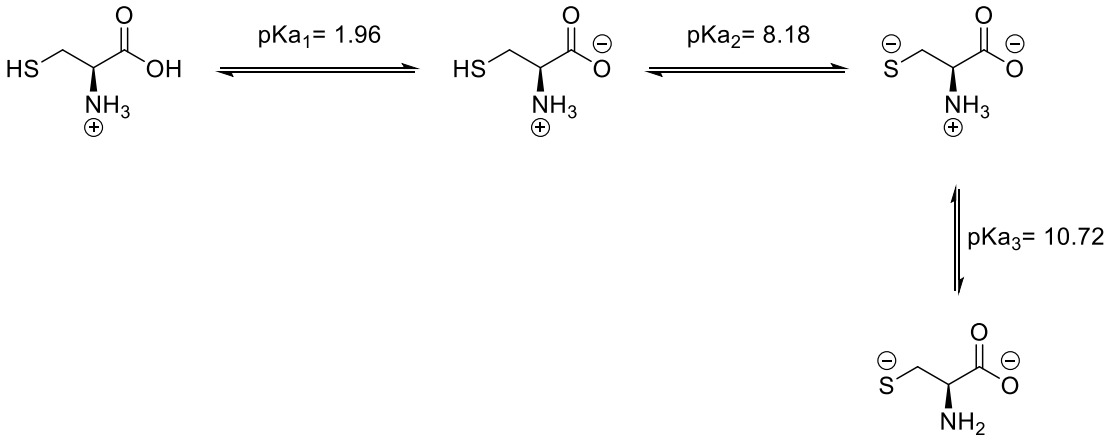

B) Cysteamine

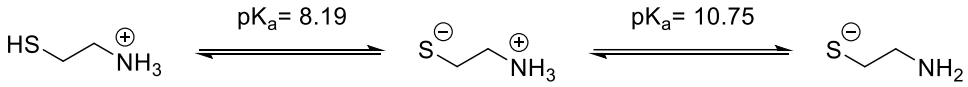

C) DEAET

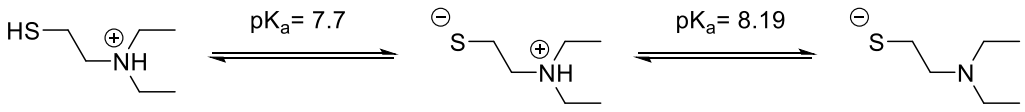

Scheme 4.8. Multi-functional nature of A) cysteine, B) cysteamine, C) DEAET.

TC is the trimethylammonium analog of cysteamine and does not possess amine nucleophile functionality. The only active functional group at all pHs is thiol/thiolate. However, TC also showed increasing catalytic activity upon increasing pH similar to multifunctional thiols. More experiments need to be carried out to explain this deviation as TC is expected to produce a sigmoidal curve.

After finding the relationship between pH, and k_{cat} of thiols, we investigated the thiol-catalyzed hydrolysis kinetics of BHET, the simplest oligomer of PET.

4.6 Thiol-catalyzed BHET Hydrolysis Kinetics

pH 10 buffer was chosen to conduct BHET hydrolysis. The choice of thiol was from the pH vs. k_{cat} plot. 2-ME showed the highest k_{cat} among the three thiols (TFET, 2-ME, 3-MPA) that showed a sigmoidal shape in the pH vs. k_{cat} plot. Therefore, 2-ME was selected to screen BHET hydrolysis efficiency (Scheme 4.9).

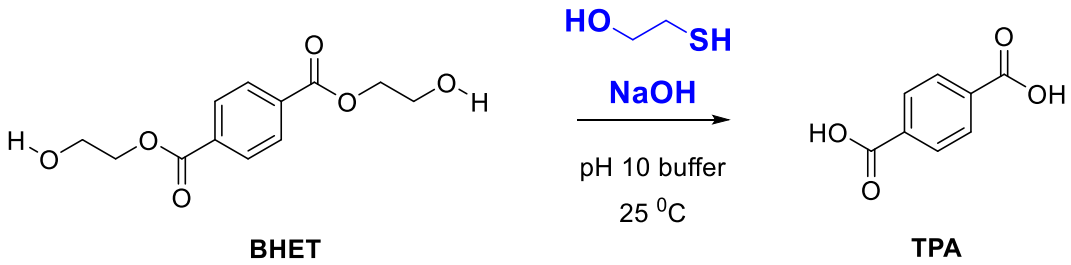

Scheme 4.9. BHET hydrolysis reaction scheme with selected thiols.

BHET hydrolysis kinetics was followed in pH 10 buffer with thiolate (2-ME) catalyst by HPLC. HPLC chromatograms were collected starting from mixing of the solutions until complete disappearance of BHET was observed, and HPLC chromatograms were collected 15-minute intervals. BHET (0.006 mM) was used, and the hydrolysis was monitored using a series of excess 2-ME concentrations, 0.067, 0.15, 0.3, and 0.45 mM. Thiolate stock solutions were used to avoid buffer neutralization. HPLC solvent system: pre-mixed methanol 30%: water 70% with 0.2% TFA. The Chromatograms observation wavelength is 254 nm. BHET, MHET, and TPA retention times were 19.6, 16.5, and 14.2 minutes, respectively. Formation of any thioester species was not observed (Scheme 4.12). According to the HPLC chromatograms, BHET hydrolysis is a stepwise process with two

steps. The first step is the conversion of BHET to mono hydroxy ethyl terephthalic acid (MHET). The second step is the hydrolysis of MHET to TPA (Figure 4.4).

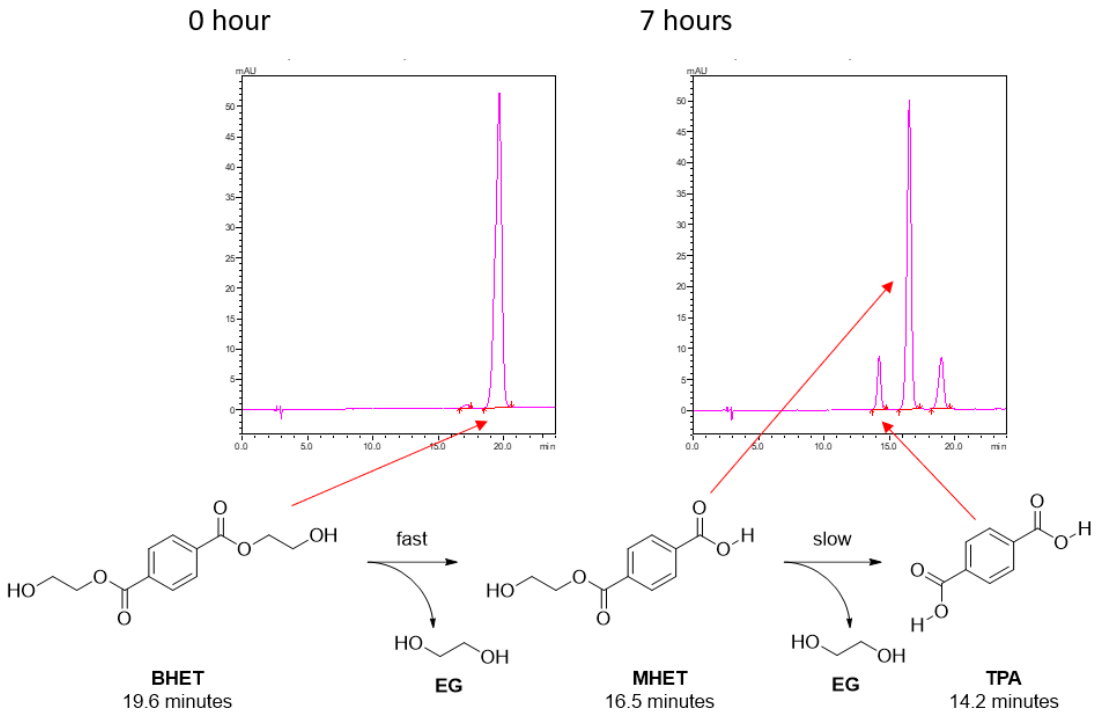

Figure 4.4. HPLC chromatograms at two time points (0, 7 hours) for BHET (0.006 mM) hydrolysis in the presence 2-ME (0.067 mM) in pH 10 buffer.

BHET to MHET reaction rate constant is faster than the BHET to TPA conversion (Figure 4.5A). BHET to MHET conversion was calculated, and it was (0.13±0.02) M^{-1} s^{-1} when BHET (0.006 mM) was reacted with 2-ME (0.067 mM) in pH 10 (Figure 4.5B). The conversion of MHET to TPA was estimated based on the zeroth-order approximation, as the complete formation of TPA was not observed during the 11 hours of kinetic study time. THE TPA formation rate constant (0.039±0.005) M^{-1} s^{-1} under the same condition (Figure 4.5C) is four times lower than the first step.

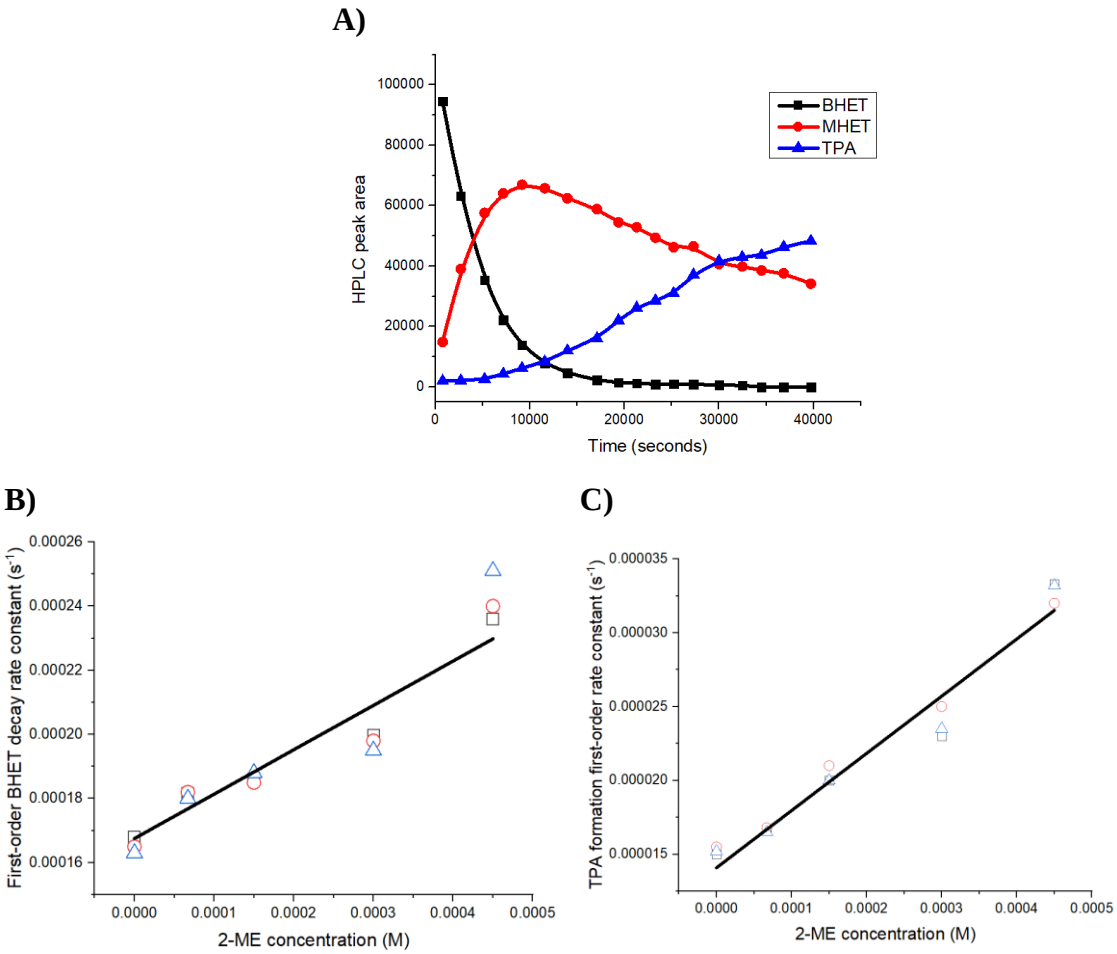

Figure 4.5. A) HPLC peak area change for BHET, MHET, and TPA during the hydrolysis of BHET (0.006 mM) in the presence of 2-ME (0.067 mM) in pH 10 buffer, B) plot of 2-ME concentration vs. BHET pseudo-first-order rate constant, C) 2-ME concentration vs. TPA pseudo-first-order formation rate constant.

4.7 BHET Solvolysis/Methanolysis using 'Thiol-Thiolate mixture' as Catalyst

As mentioned in the introduction, hydrolysis and solvolysis are suitable for PET depolymerization as they produce valuable monomers that can be used in the re-synthesis of PET. Therefore, we extended our study to explore thiol catalysis in methanolysis reactions. We have selected 2-ME as the thiol catalyst and monitored the BHET methanolysis kinetics by HPLC. Interestingly, we observed that methanolysis produces DMT as the main product, and the formation of TPA was not observed, at least during the period in which the reaction was followed (Scheme 4.10).

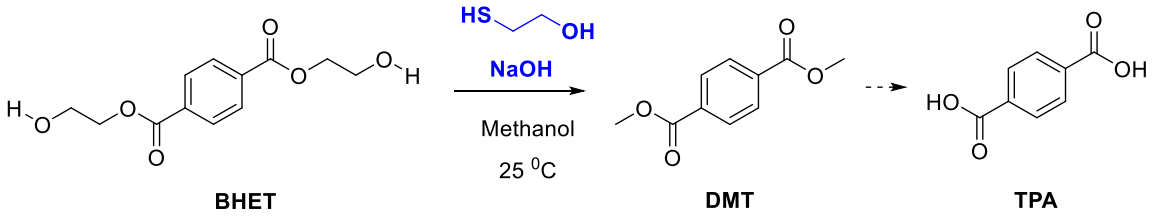

Scheme 4.10. BHET methanolysis reaction in the presence of 2-mercaptoethanol.

The second-orde rate constant for BHET methanolysis in the presence of excess 2-ME is (0.34±0.06) M^{-1} s^{-1} (Figure 4.5).

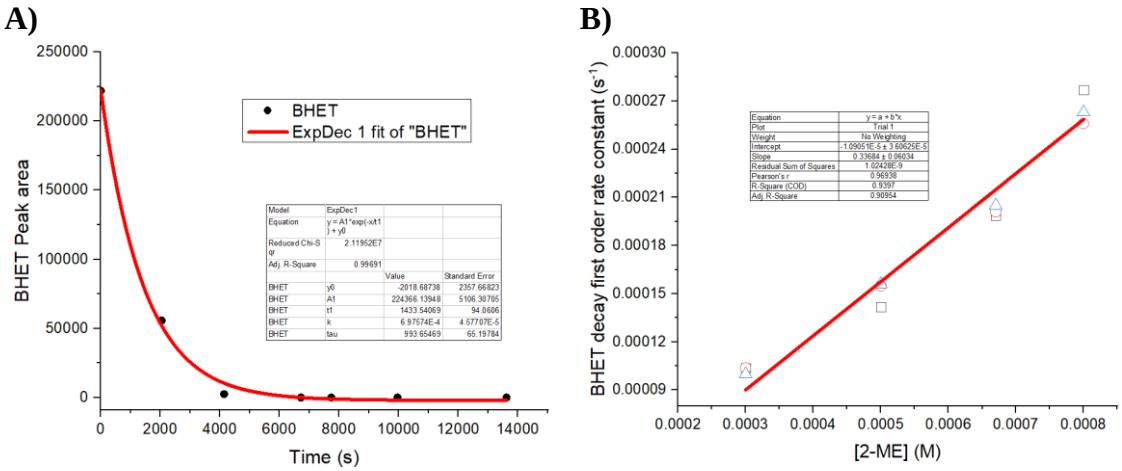

Figure 4.5. A) BHET decay plot for BHET initial concentration 0.013 mM, 2-ME 0.8 mM, NaOH 0.8 mM in methanol (3 mL), B) Second-order rate constant plot of BHET decay vs. 2-ME excess concentration.

Another interesting observation from the above reaction is that formation of thioesters was not observed. Hence, we carried out a control experiment where we studied BHET alkaline methanolysis without thiol (Chapter 5, Section 5.2). Promisingly, we confirmed that NaOH in solvent (methanol or ethylene glycol) itself acts as a catalyst and conducted a series of PET depolymerization/solvolysis method development which will be described in Chapter 5.

4.8 Thiol Dimerization Rate Constant Determination

One of the potential challenges associated with thiol oxidation to form disulfide bonds and leading to thiol-dimers (Scheme 4.11).

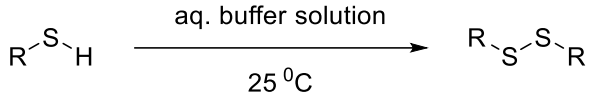

Scheme 4.11. Thiol dimerization reaction.

Thiol oxidation is pH dependent, and disulfide formation is faster at high pH when thiolates are predominant in the reaction mixture compared to thiol, S-H form. However, the mechanism of disulfide formation in aqueous buffer conditions and the reason for fast disulfide formation at high pH is still unclear and lacks evidence from literature reports to the best of our search. Additionally, Dimerization was very fast for aromatic thiols, TP, and 4-MBA were unsuitable for p-NPA hydrolysis compared to alkanethiols such as 2-ME. The reaction rate constants for disulfide formation in TP, 4-MBA were measured in pH 5 buffer and 2-ME in pH 9 buffer. The rate constant for disulfide formation from 2-ME at

pH 9 is still lower than that for 4-MBA and TP in pH 5 aqueous buffer (Table 4.4). This means TP, and 4-MBA may approximately dimerize at a rate of 10^{-1} s^{-1} or even faster at pH 9 as disulfide formation is pH dependent and making aromatic thiols not suitable as a catalyst for ester hydrolysis or PET depolymerization. The relationship between disulfide formation vs. pH or pKa of all thiols was not studied in this research work as it is beyond the scope of our research aims.

Table 4.4. Thiol dimerization rate at a specific pH.

Thiol	**pH of the medium**	**Thiol dimerization rate constant s^{-1}**
TP	5	~$1x10^{-4}$
4-MBA	5	~$4\ x10^{-5}$
2-ME	9	~$5\ x10^{-6}$

4.9 Conclusions and Future Directions

Herein, we reported the effective use of thiols as catalysts in ester studies which is not reported before to the best of our knowledge. All the alkane thiols, TFET, cysteine, cysteamine, 2-ME, 3-MPA, DEAET, and TC showed an increase in k_{cat} with increasing pH. TFET, 2-ME, and 3-MPA showed sigmoidal type curve reaching a plateau beyond pH 9 in in pH vs k_{cat} plot indicating rate limiting step as the thiolate attack from the nucleophile. Cysteine, cysteamine, and DEAET did not reach the saturation of the k_{cat} at higher pH, suggesting the participation of amine groups in the hydrolysis of p-NPA. These three thiols have similar k_{cat} values at pH 10 (4-5 M^{-1} s^{-1}). Additionally, comparison of catalytic activity of TC and cysteamine allowed for the evaluation of the effect of amine functionality on the

reactivity. Furthermore, cysteine and cysteamine having high k_{cat} is advantageous as they are also environmentally benign catalysts and not toxic to the environment. Further investigation on cysteine, cysteamine and DEAET is required to get a detailed understanding about the mechanism. Among all the catalysts, 2-ME was the most appropriate for studying BHET hydrolysis kinetics, as 2-ME is a monofunctional, thiol catalyst with the highest catalytic activity among the three thiol (2-ME, 3-MPA, and TFET) that showed sigmoidal curve.

BHET hydrolysis to TPA occurred via two steps: BHET to MHET hydrolysis followed by MHET to TPA hydrolysis. Respective thioester intermediates, 1, and 2 that could result from the nucleophilic attack from thiol, were not observed (Scheme 4.12). This indicates a faster hydrolysis of thioester intermediates or a different mechanism other than conventional nucleophilic catalysis.

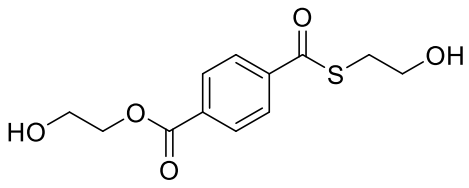

Intermediate 1

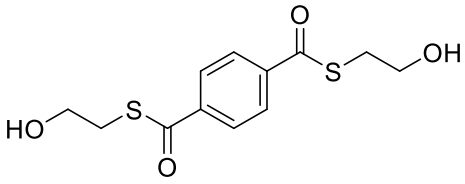

Intermediate 2

Scheme 4.12. Structures of BHET thio-esters of 2-ME.

Reaction kinetics of BHET hydrolysis to TPA is slower than p-NPA hydrolysis to p-NPA (~4 M^{-1} s^{-1} vs >0.1 M^{-1} s^{-1}). This was expected as the carbonyl group of BHET is highly stabilized by the electron delocalization with the aromatic ring system and it has two similar carbonyl groups to hydrolyze compared to p-NPA. Additionally, p-NPA hydrolysis produces a stable p-NP anion which also may be the driving force for the reaction, whereas BHET hydrolysis produces 2-hydroxyethan-1-olate anion which is

relatively less stable compared to p-NP. We also investigated the benefit of 2-ME as a catalyst in BHET methanolysis. Interestingly, methanolysis is faster than BHET hydrolysis (0.13 vs 0.34 M^{-1} s^{-1}). Furthermore, BHET methanolysis is a stepwise process where transesterification to DMT occurs prior to the formation of TPA.

Thiol oxidation to form disulfide bonds leading to thiol-dimers could be a challenging situation to address to avoid reduction in the catalytic activity. However, among the thiols screened, only aromatic thiols, TP and 4-MBA showed rapid disulfide formation compared to alkane thiols and the latter has high k_{cat} as well making them still suitable catalysts. Additionally, thiol-dimer formation can be easily avoided by using disulfide reducing agents such as dithiothreitol (DTT), tris (2-carboxyethyl) phosphine hydrochloride (TCEP), and mercaptoethanol (2-ME).[150]

4.10 Experimental Section

4.10.1 General Information

BHET, TPA, DMT, p-NPA and p-NPA were commercially purchased and used without purification. All the thiols were commercially purchased except thiocholine, and all the thiols were stored in a refrigerator (-14 ^{0}C) to avoid degradation/dimerization. Buffer solutions were freshly prepared using DI water and commercially purchased conjugate acid/base. Calculations for all the buffer solutions were done using acidity constants taken from literature sources. All the solvents were used without further purification, HPLC grade methanol and water was used to run HPLC analysis.

UV/Visible spectra and kinetic traces were monitored using Shimadzu-UV 2600 spectrometer with a multicell compartment (capacity of 6 cells) and a temperature control. All the kinetic reactions were carried out at 25 ^{0}C and the temperature was controlled using

a Thermoscientific circulating water bath. 400 MHz instrument was used for both proton and carbon NMR analysis. Shimadzu HPLC was used and HPLC grade solvents/methanol, and water was used. Kinetics of p-NPA was followed in quartz cuvettes. The total volume of the reaction mixture was adjusted to 3 mL. Kinetics at each thiol concentration was carried out in triplicates.

4.10.2 Thiocholine Synthesis

Thiocholine was synthesized by slightly modifying a previously reported procedure.[151]

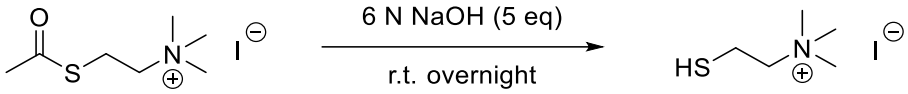

Acetylthicholine iodide (0.16 g, 0.55 mmol) was added to 0.1 N NaOH (1 mL, 1 mmol) and sparged with argon. An additional 6 N NaOH (0.16 ml, 0.96 mmol, 1.7 eq) was added to increase the pH. 6 N NaOH solution was prepared by dissolving NaOH pellets (0.24 g, 6 mmol) in 1 mL of DI water. The reaction was left to stir overnight. Next day, the reaction was cooled in an ice bath and quenched by careful addition of conc. HCl (0.16 mL) under argon. Acetic Acid (boiling point 118 ^{0}C) and water were removed by rotary evaporator (water bath temperature 60 ^{0}C, pressure 100 mbar), leaving a white solid. The compound was further dried under oil pump overnight. (0.13 g, ~99% yield). ^{1}H NMR (400 MHz, DMSO): δ 3.54-3.58 (m, 2H), 3.16 (s, 9H) 2.87-2.97 (m, 3H). ^{13}C NMR (100 MHz, DMSO): δ 67.42, 52.80, 17.14. HRMS-ESI (m/z) $[M+H]^{+}$ calculated for $[C_5H_{14}ONS]^{+}$: 120.08415, found: 120.08418.

4.10.3 Buffer Calculation and Preparation Recipe

Acetic acid/acetate buffer, Hydroxylamine hydrochloride, Monosodium phosphate, Tris hydrochloride was used as the conjugate acid in the preparation pH 5, 6, 7 and 8 buffers respectively. Sodium bicarbonate was used to prepare pH 9 and 10 buffers. pH 11 buffer

was made using triethylamine hydrochloride. The pK_a values of each conjugate acid, acid dissociation quotient, Q_{HA}, buffer ratio, conjugate acid and conjugate base concentrations are shown in Table 4.5. pK_a and Q_{HA} values are taken from literature.[152–157] Ionic strength of all the buffer solutions were maintained at 0.1 M.

Table 4.5. Buffer preparation calculations.

Buffer pH (Calc.)	**Buffer**	**pK_a**	**Q_{HA}**	**Buffer ratio**	**[HA] (M)**	**[A^-] (M)**
5.00	CH_3COOH/ CH_3COO^-	4.76	$2.719x10^{-5}$	0.368	0.0538	0.1462
6.00	$[NH_3OH]^+Cl^-$/ $[NH_2OH]$	5.95	$1.081x10^{-6}$	0.925	0.048	0.052
7.00	$[H_2PO_4]^-$/ $[HPO_4]^{2-}$	7.20	$1.659x10^{-7}$	0.603	0.0167	0.0277
8.00	$[NH_2C(CH_2OH)_3]^+Cl^-$ /$NH_2C(CH_2OH)_3$	8.07	$8.204x10^{-9}$	1.22	0.076	0.062
9.00	$[HCO_3]^-/[CO_3]^{2-}$	10.33	$1.21x10^{-10}$	9.94	0.077	0.0077
10.00				0.994	0.025	0.025
11.00	$(CH_3CH_2)_3NH^+$/ $(CH_3CH_2)_3NH$	10.87	$1.3x10^{-11}$	0.769	0.0043	0.0056

4.10.3 Kinetic Study of Thiol Dimerization

HPLC was used to study the dimerization of thiols, TP, 4-MBA and 2-ME which will be discussed in detail in this section.

4.10.3.1 TP

TP (0.3 mM) in pH 5 acetic acid buffer was prepared and the stability was monitored at 25 ^{0}C to study the kinetics of TP conversion to 1,2-diphenyldisulfane, DPDS (Scheme 4.13).

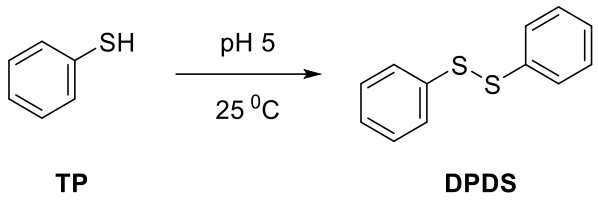

Scheme 4.13. TP conversion tp DPDS.

Gradient HPLC solvent system was used. Methanol: water 35%: 65% (0 to 7 minutes), and gradient reaching methanol 100% from 7 to 20 minutes. All the chromatograms were observed at 254 nm. TP and DPDS retention time are 6.1 and 18.3 minutes, respectively (Figure 4.6).

HPLC peak area of TP was converted to a plot of time vs TP concentration using a standard of TP. TP decomposition rate constant ~$2x10^{-8}$ M^{-1} s^{-1} (Figure 4.7). First-order rate constant assuming zeroth-order approximation is ~$1x10^{-4}$ s^{-1}.

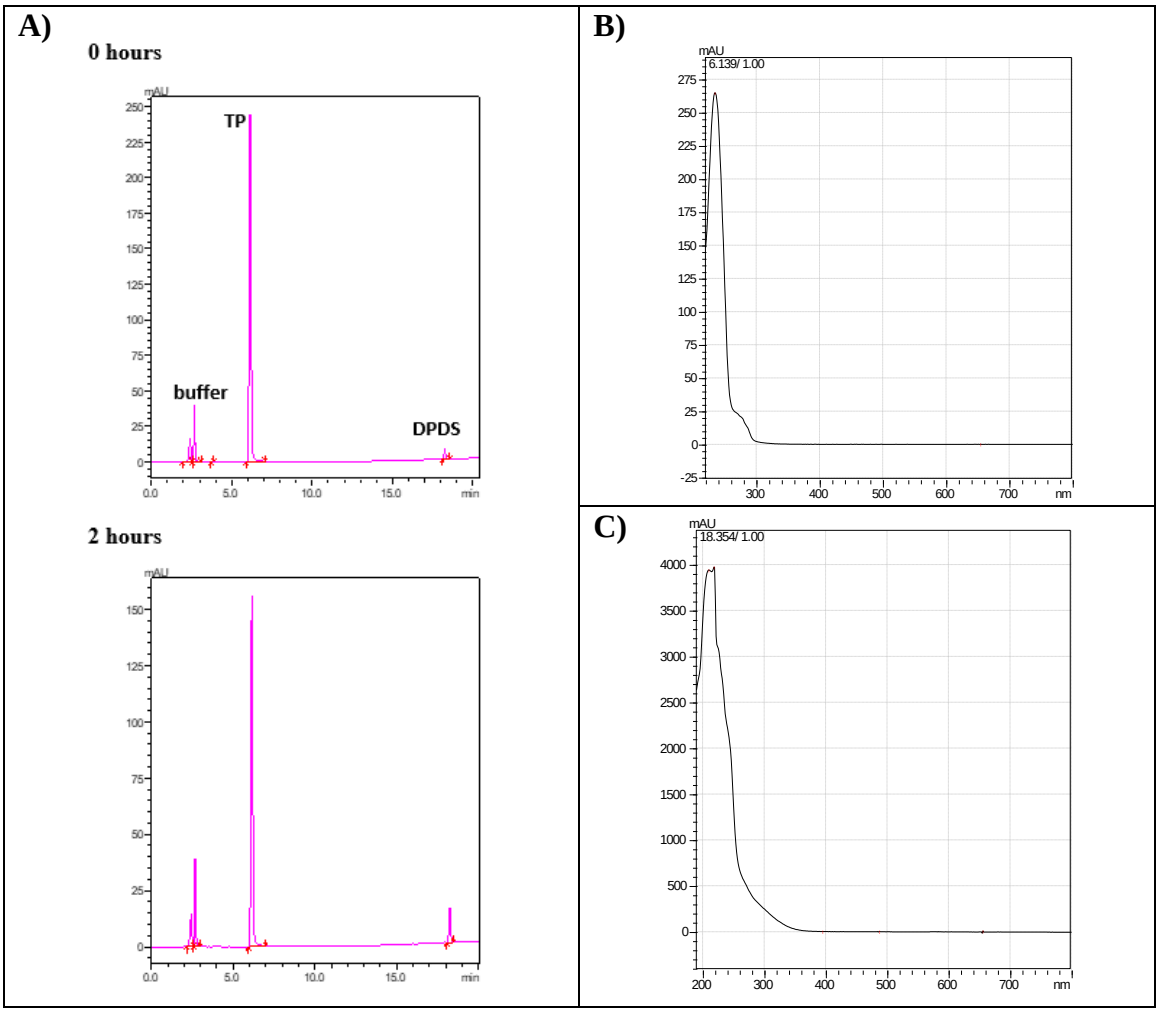

Figure 4.6. A) HPLC chromatograms of TP in pH 5 buffer with time (0 and 4 hours), B) absorbance spectrum of TP, C) absorbance spectrum of DPDS.

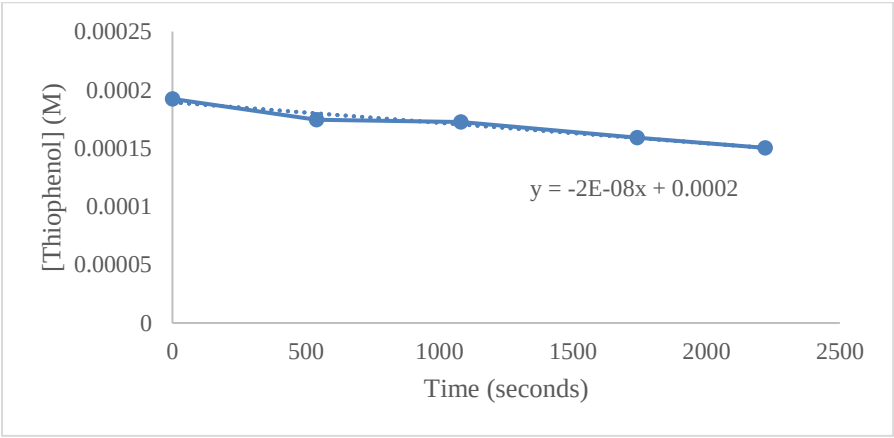

Figure 4.7. Plot of time vs TP concentration change.

4.10.3.2 4-MBA

4-MBA (0.3 mM) in pH 5 acetic acid buffer was prepared and the stability was monitored at 25 ^{0}C to study the kinetics of 4-MBA conversion to 4,4'-disulfanediyldibenzoic acid, DSDBA (Scheme 4.14).

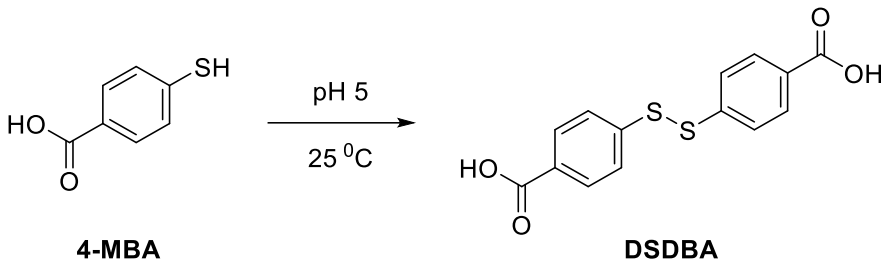

Scheme 4.14. 4-MBA conversion to DSDBA.

HPLC solvent system is methanol is water 50%: 50% and all chromatograms were observed at 272 nm. 4-MBA retention time is 8.5 minutes. DSDBA was not observed in this HPLC method. However, formation of DSDBA was confirmed by mass analysis. An aliquot of 4-MBA in pH 5 was taken every one-hour time interval and analyzed by HPLC. HPLC chromatogram shows a decrease in the peak intensity of 4-MBA indicating decomposition (Figure 4.8).

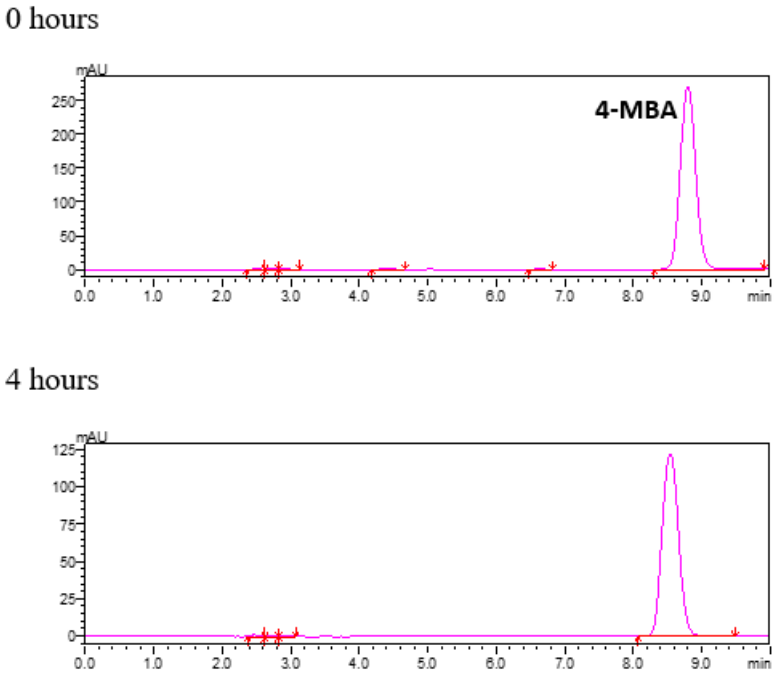

Figure 4.8. HPLC chromatograms of4-MBA in pH 5 buffer with time (0 and 4 hours).

HPLC peak area of 4-MBA was converted to a plot of time vs 4-MBA concentration using a standard of 4-MBA. 4-MBA decomposition rate constant ~1.92x10^{-8} M^{-1} s^{-1} (Figure 4.9A and B). First-order rate constant assuming zeroth-order approximation is ~4x10^{-5} s^{-1}.

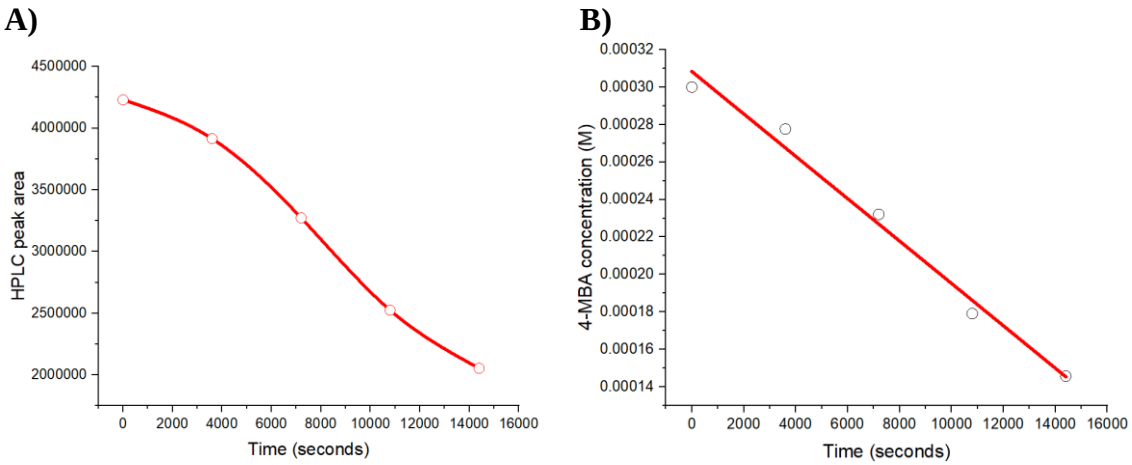

Figure 4.9. A) HPLC peak area changes for 4-MBA with time, B) plot of time vs 4-MBA concentration change.

4.10.3.3 2-ME

2-ME (3.6 mM) in pH 9.01 bicarbonate buffer was prepared and the stability was monitored at 25 ^{0}C to study the kinetics of 2-ME conversion to 2,2'-disulfanediylbis(ethan-1-ol), DTDE (Scheme 4.15).

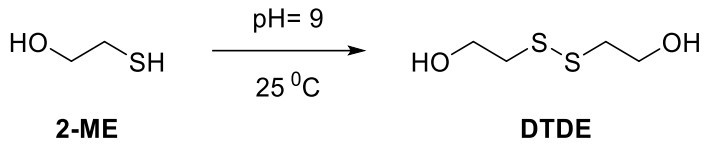

Scheme 4.15. 2-ME conversion to DTDE.

HPLC solvent system is methanol is water 5%:95% and all chromatograms were observed at 245 nm. 2-ME and DTDE retention time is 4.9 and 17.2 minutes respectively. HPLC chromatograms collected with time by taking an aliquot from 2-ME in pH10 buffer is shown in Figure 4.10A and 2-ME, DTDE absorbance spectra in Figure 4.10B and C, respectively.

HPLC peak area of DTDE was converted to a plot of time vs DTDE concentration using a standard of DTDE. Disulfide formation rate constant ~1.92x10^{-8} M^{-1} s^{-1} (Figure 4.11A and B). First-order rate constant assuming zeroth-order approximation is ~5x10^{-6} s^{-1}.

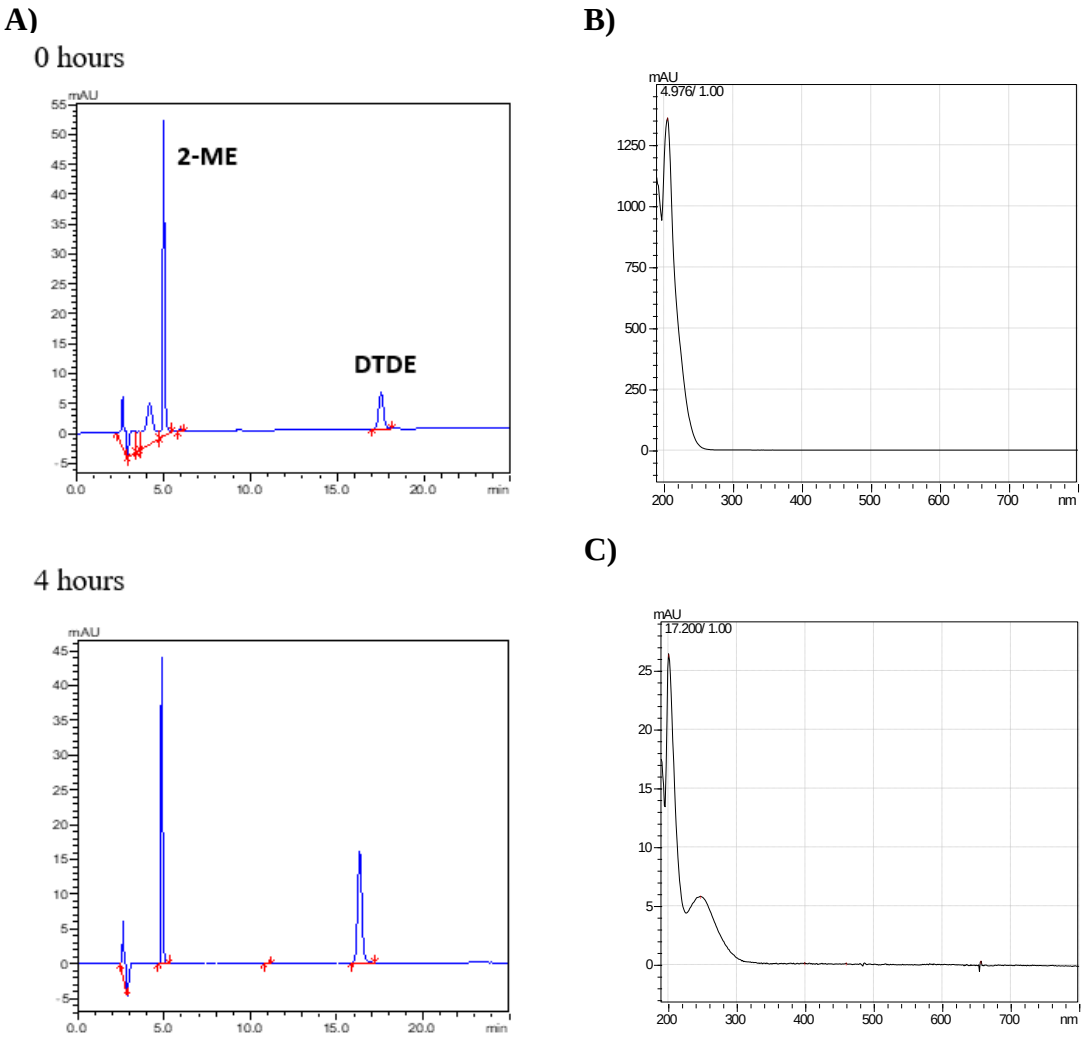

Figure 4.10. A) HPLC chromatograms of 2-ME in pH 9 buffer with time (0 and 4 hours), B) absorbance spectrum of 2-ME, C) absorbance spectrum of DTDE.

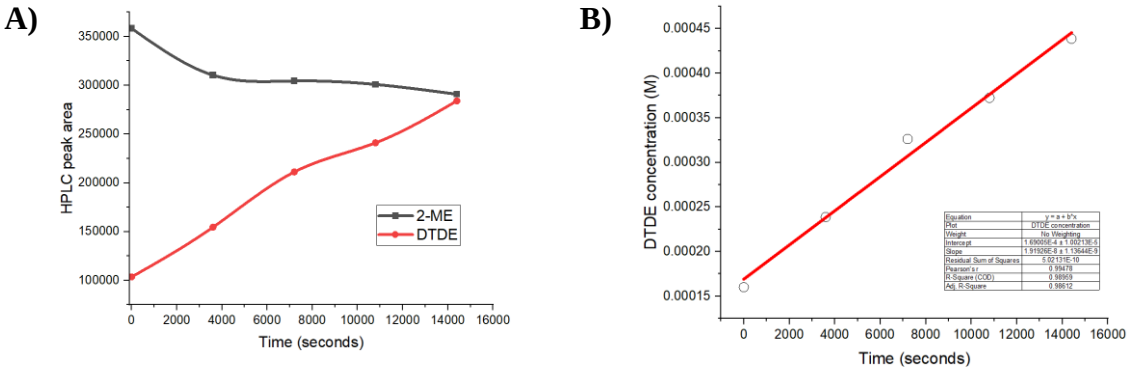

Figure 4.11. A) HPLC peak area changes for 2-ME and DTDE with time, B) plot of time vs DTDE concentration change.

CHAPTER 5

KINETICS OF BASE-CATALYZED ESTER TRANSESTERIFICATION AND HYDROLYSIS: TOWARDS A MILD METHOD FOR POLYETHYLENE TEREPHTHALATE ALKALINE SOLVOLYSIS

5.1 Introduction

Polyethylene terephthalate (PET) chemical recycling is an excellent option to recover monomers and reuse them to minimize PET plastic pollution to the environment. As mentioned in Section 4.1, PET solvolysis is the most preferred recycling method due to mild conditions, fast reaction, and the possibility of continuous production. The two PET solvolysis methods are glycolysis and methanolysis, producing bishydroxyethylene terephthalate (BHET) and dimethyl terephthalate (DMT), respectively. PET glycolysis is preferred over methanolysis due to its direct applicability of the monomer, BHET, as a feedstock in the PET synthesis process (Section 3.1, Scheme 3.1-Step 2). Nevertheless, both solvolysis processes require harsh conditions, such as temperatures above the solvents' boiling point and pressure above atmospheric conditions due to the semi-crystalline nature of PET.[92,135] Therefore, the choice of catalyst is crucial to conduct PET solvolysis under mild conditions while achieving fast rates and high monomer production yields. The characteristics of the best catalyst/s for an economical operation are readily available or easy to synthesize, inexpensive, able to use in multiple cycles/recyclable, and high thermal and mechanical stability under depolymerization conditions.

The catalysts used for the PET glycolysis process are organometallic species such as salts of Zinc, Magnesium, Sodium, Titanium, or even Niobium,[158] deep-eutectic solvents, and ionic liquids. Metal-based catalysts are commonly used due to their high reactivity and stability under high temperature/pressure processing conditions. However, organometallic catalysts cause heavy metal pollution and introduce additional environmental impact. PET methanolysis catalysts are metal salts such as lead or zinc acetates,[159],[160] metal oxides, for example, sodium silicate and aluminum isopropoxide,[161,162] metal hydroxides,[163], and ionic liquids.[164] Both processes are essentially a transesterification process where the ester group in the oligomers is replaced by ethylene glycol or methyl unit. Transesterification is commonly used in producing biodiesel/methyl esters from natural resources (Scheme 5.1). Triglycerides are converted to methyl esters in the presence of a base catalyst, either sodium hydroxide NaOH or potassium hydroxide (KOH).[165]

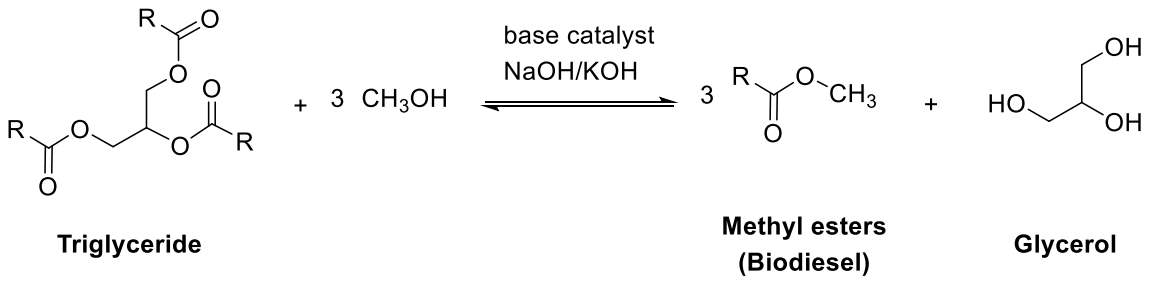

Scheme 5.1. Transesterification of Triglycerides.

Therefore, metal hydroxides such as NaOH or KOH are inexpensive catalysts for PET glycolysis and methanolysis. Although the concept transesterification using alkaline conditions seems a viable option to depolymerize PET, few literature reports have been published about PET alkaline glycolysis or methanolysis. Additionally, the products formed from alkaline glycolysis or methanolysis are unclear, whether it is the transesterified products, BHET/DMT or TPA. Yamada and co-workers reported PET

conversion to terephthalic acid (TPA) in a 1:2 ratio of PET: NaOH (Scheme 5.2A).[166] Sanda and peers studied PET depolymerization in an alkaline alcoholic solution using either methanol, ethanol, or butanol using PET: NaOH 1:3 ratio. The authors claimed a stepwise process where PET first converted to dialkyl terephthalates such as DMT, diethyl terephthalate (DET), and dibutyl terephthalate (DBT) when the solvent is methanol, ethanol, and butanol, respectively. Then, the transformation of dialkyl terephthalates to TPA in the second step (Scheme 5.2B).[163,167] However, proper experimental evidence for the step-wise transformation is lacking. PET methanolysis using KOH in a microwave reactor has been reported. The product was TPA at high temperatures and DMT at low temperatures when PET: KOH molar ratio was 1: 5.[168,169] Solid state depolymerization via ball milling that converts PET to TPA in NaOH- hydroxide attack on carbonyl was also reported.[170]

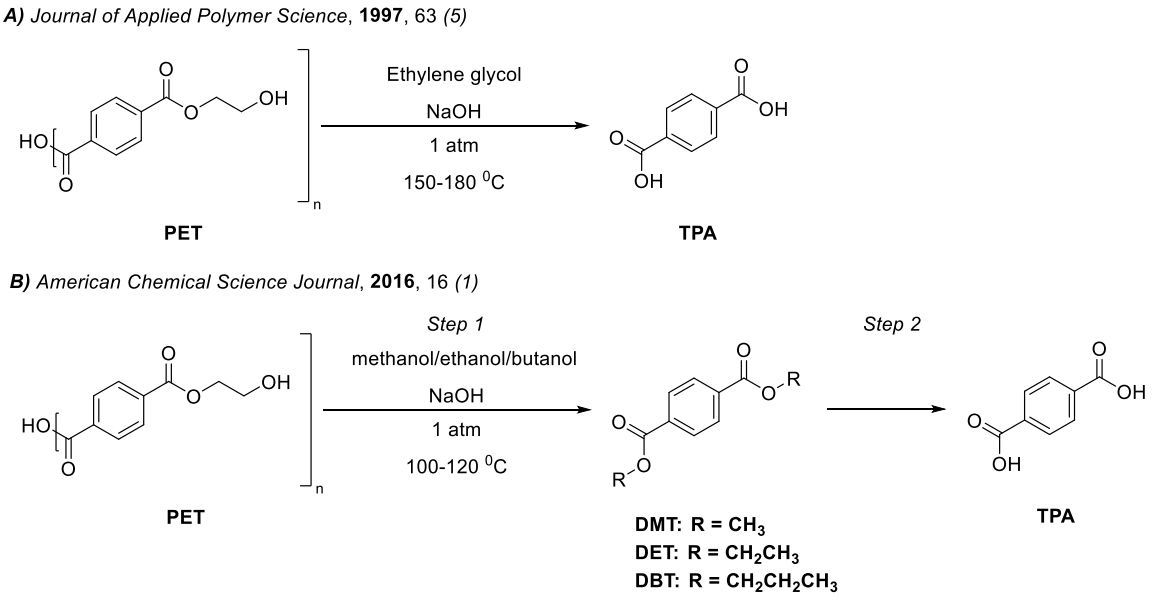

Scheme 5.2. PET alkaline solvolysis.

Even though at least a handful of research on alkaline solvolysis is available, and most of the papers claim the product to be TPA, the mechanism of TPA formation is not

mentioned. Additionally, none of the research is carried out with catalytic amounts of NaOH or KOH relative to PET, and the complete evaluation of the effect of catalyst/NaOH concentration, temperature, and reaction time is not studied.

The present study aims to investigate the products formed in PET alkaline solvolysis and elucidate a plausible mechanism. A preliminary kinetic study to determine the reaction rate constants of transesterification and acid formation was carried out using BHET, the simplest PET oligomer. Herein, we report the rate constants for BHET transesterification and acid formation in an alkaline methanol solution (Section 5.2). The reaction products formed under varying conditions, PET load, NaOH concentration, and temperature in glycolysis and methanolysis will also be described. Furthermore, optimization of PET glycolysis and methanolysis conditions to obtain pure transesterified products, BHET or DMT for glycolysis and methanolysis will be described.

5.2 BHET Transesterification and Acid Formation Kinetics in Alkaline Methanol

The simplest oligomer of PET, BHET, was chosen to study the rates of transesterification vs. acid formation in alkaline methanol. Interestingly, we observed that transesterification of BHET to DMT occurs first, followed by acid formation of DMT to TPA. The transformation of BHET to DMT is a two-step process where the conversion of BHET to hydroxyethyl methyl terephthalate (HEMT) occurs first, followed by the transition of HEMT to DMT. The translation of DMT to TPA also occurs via two steps. First, DMT is converted into monomethyl terephthalic acid (MMT), and second, MMT is converted to TPA (Scheme 5.3).

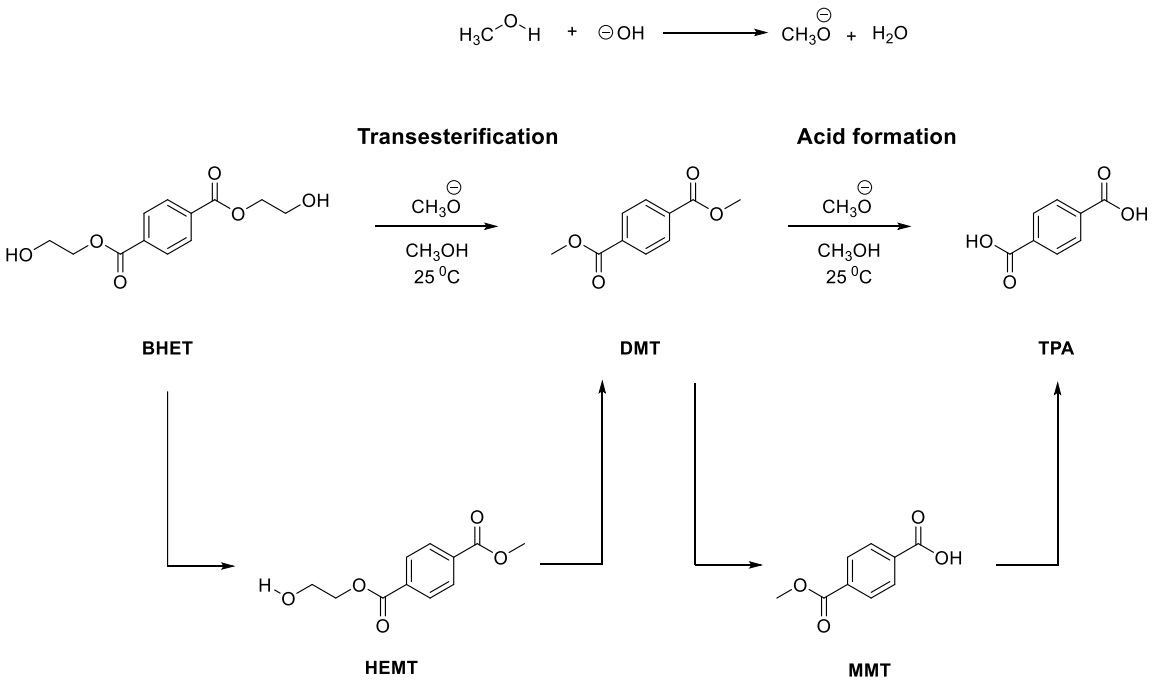

Scheme 5.3. Transesterification followed by acid formation of BHET.

The kinetics of BHET (1.56 mM), and NaOH (0.01 M) in methanol (3 mL) was studied at room temperature, 25 ^{0}C. The reaction progress of BHET in alkaline methanol with time was monitored by HPLC (Figure 5.1). Retention times of the species are BHET

12.2 minutes, HEMT 18.6 minutes, DMT 21.7 minutes, MMT 19.1 minutes, and TPA 10.6 minutes. BHET is fully dissociated within 10 minutes of the reaction (compare the peak at 12.2 minutes in 0 minutes and 10 minutes plot in Figure 5.1). Complete formation of DMT at 21.7 minutes was noted 60 minutes after the reaction (Figure 5.1C). Formation of TPA was also observed at 60 minutes. Transesterification was plotted only 0-10 minutes as the reaction was complete within thatime limit, and acid formation was followed by 60 minutes and beyond up to 30 hours.

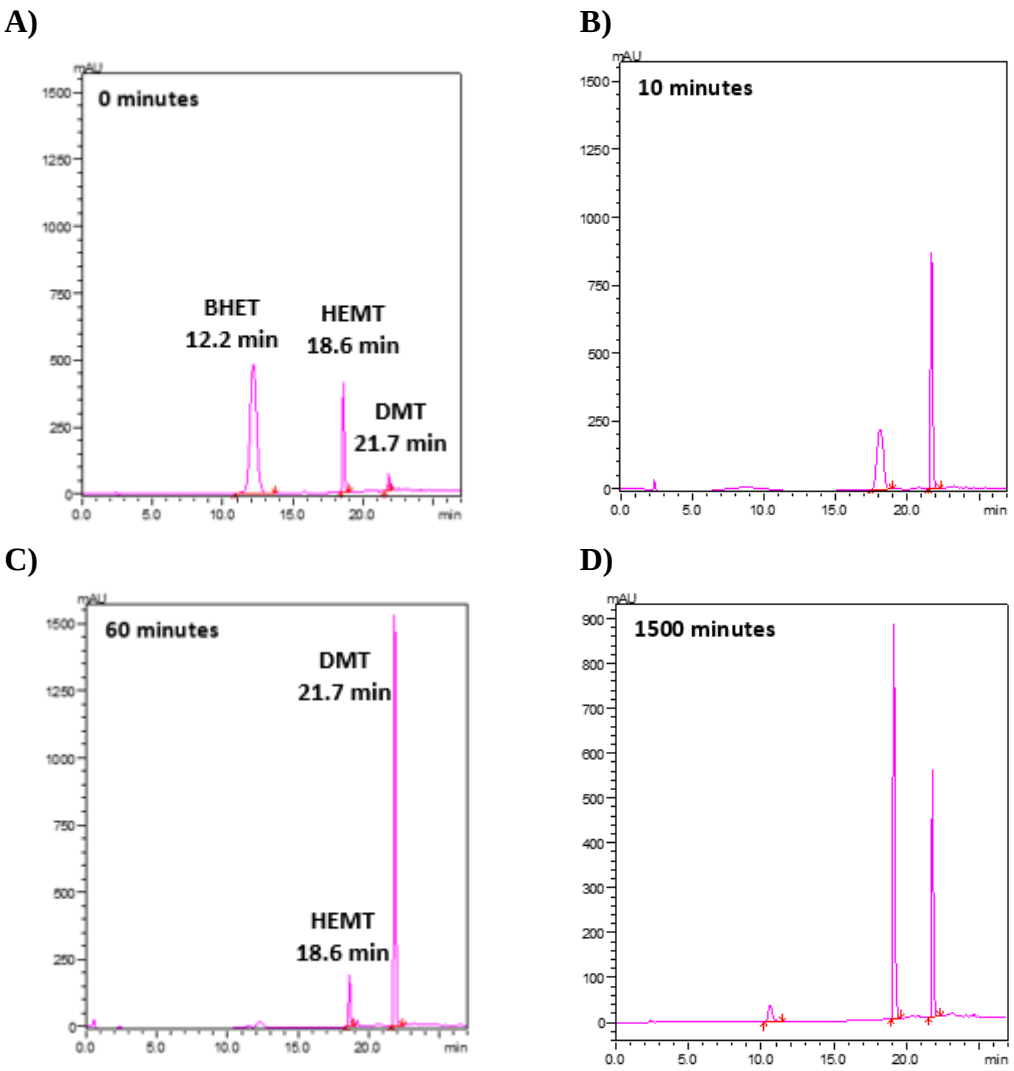

Figure 5.1. HPLC traces BHET alkaline methanolysis with time; A) 0 minutes, B) 10 minutes, C) 60 minutes, D) 1500 minutes.

HPLC peak area vs. time for the change in peak area for transesterification and acid formation species are shown in Figures 5.2A and 5.2B, respectively.

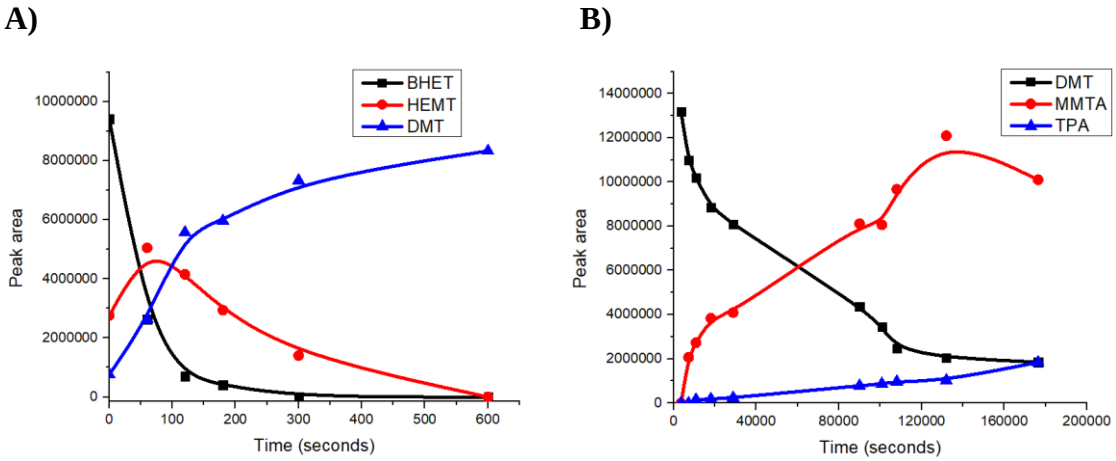

Figure 5.2. Peak area vs. time plots: A) BHET to DMT, B) DMT to TPA conversion.

The Kinetics of all four steps in the process was calculated. The reaction rate constant of BHET to HEMT conversion was determined by the BHET decay plot. The reaction rate constant for HEMT to DMT conversion was calculated from a plot of DMT formation/growth with time. HEMT or MMT formation/decomposition was not used in the kinetic rate constant analysis as both species are pseudo-steady state species. That means species were consumed in the next step, soon after formation. Proper first-order kinetic decay or growth was not observed for these species. Instead, an initial growth followed by consumption was observed.

BHET decay kinetics and DMT formation in transesterification correspond well into a single exponential fit. The rate of BHET decay and DMT formation is to ~$2x10^{-2}$ s^{-1} and ~$7x10^{-3}$ $s^{-1,}$ respectively (Figure 5.3A and B). In the acid formation step, DMT decay to MMT conversion fits well with single exponential kinetics. The rate of DMT decay is ~$2x10^{-5}$ s^{-1} (Figure 5.4A). However, the rate of formation of TPA from MMT is prolonged, and zeroth-order approximation was used to determine the rate constant. The TPA

formation occurs at ~7.5x10^{-10} M^{-1} s^{-1}, corresponding to ~7x10^{-7} s$^{-1,}$ assuming complete conversion of BHET to TPA (Figure 5.4B).

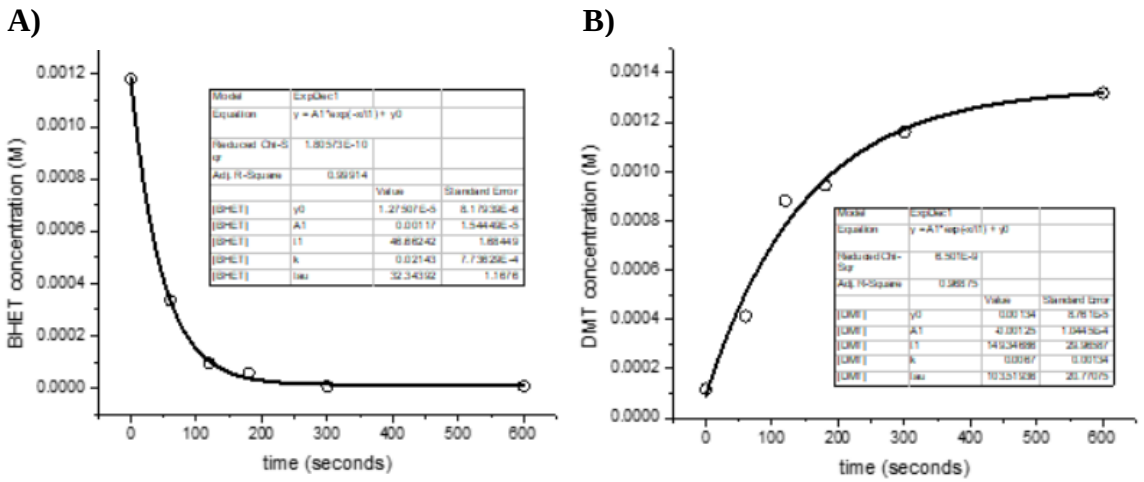

Figure 5.3. Transesterification kinetics; A) BHET decay, B) DMT formation plot.

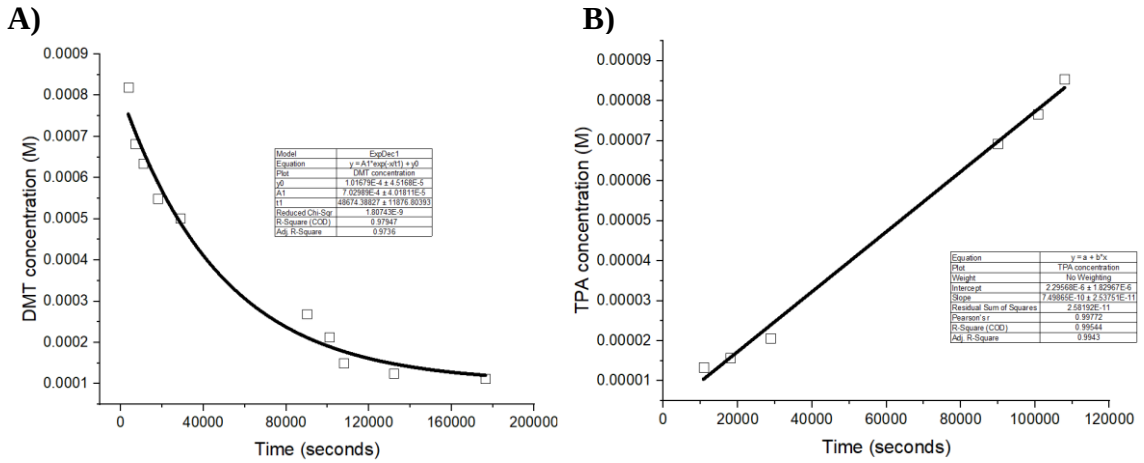

Figure 5.4. Acid formation kinetics; A) DMT decay, B) TPA formation.

BHET decay to HEMT rate is ten-times higher than DMT formation from HEMT. On the other hand, DMT decay to MMT is a hundred-fold higher compared to TPA formation from MMT. Considering the two slow steps in each process (HEMT to DMT and MMT to TPA), the transesterification is ~10^{4} times higher than acid formation when BHET: NaOH ratio is 1:6, and NaOH concentration is 0.01 M.

Transesterification rates at two different NaOH concentrations (0.005 M and 0.01 M) were measured, and the results are shown in table 4.1. This is because reaction rates are dependent on NaOH concentration, and the same is expected for acid formation.

Table 5.1. BHET transesterification rates at different NaOH concentrations.

[NaOH] (M)	**BHET decay rate s^{-1}**	**DMT formation rate s^{-1}**
0.005	$(4.2\pm0.6)\ x10^{-3}$	$(9.5\pm1.6)\ x10^{-4}$
0.01	$(2.1\pm0.1)\ x10^{-2}$	$(6.7\pm1.3)\ x10^{-3}$

BHET (1.56 mM) in methanol (3 mL) at 25 ^{0}C.

5.3 Investigation of PET Depolymerization

The main goal of this project is to identify the products formed in PET alkaline solvolysis (glycolysis and methanolysis). HPLC with a UV detector is the traditional method used to detect the release of monomers in PET depolymerization. depolymerization.[128,171–173] Thus, the analysis of the products of PET alkaline solvolysis was carried out by HPLC. The formation of simplest diesters, BHET, and MMT during the reaction process was confirmed using authentic compounds as standards. Intermediates formed during solvolysis, i.e., MHET and MMT, were tentatively identified based on the relative polarity/retention time difference. However, these compounds are beyond the scope of the investigation. The yields of BHET, DMT, and TPA were determined using a calibration curve prepared with commercial standards (Section 5.10.5). PET depolymerization at conditions was followed to the point of complete conversion to ultimate monomeric product. Calculating both the PET conversion and the yield of the monomer is essential in this study to ensure that all PET is converted to monomers only.

PET or any other polymer depolymerization occurs via the initial scission of long chains to give shorter oligomers (Scheme 5.4). HPLC often does not detect all the oligomer species. Thus, PET conversion was calculated using UV spectroscopy. The oligomers of PET, diesters, monoesters, as well as TPA, have the same chromophore with λ_{max} ~ 240-260 nm.[174] Molar extinction coefficient of DMT was determined and the value was used to calculate the PET concentration in solution. Since PET is not soluble in MeOH or EG, this value represents the total amount products produced by PET solvolysis. (Vide infra; experimental section 5.10.3). Alternatively, the solvolysis can be quenched by adding acid and the mass of unreacted PET measured by filtration and drying the solid fraction.

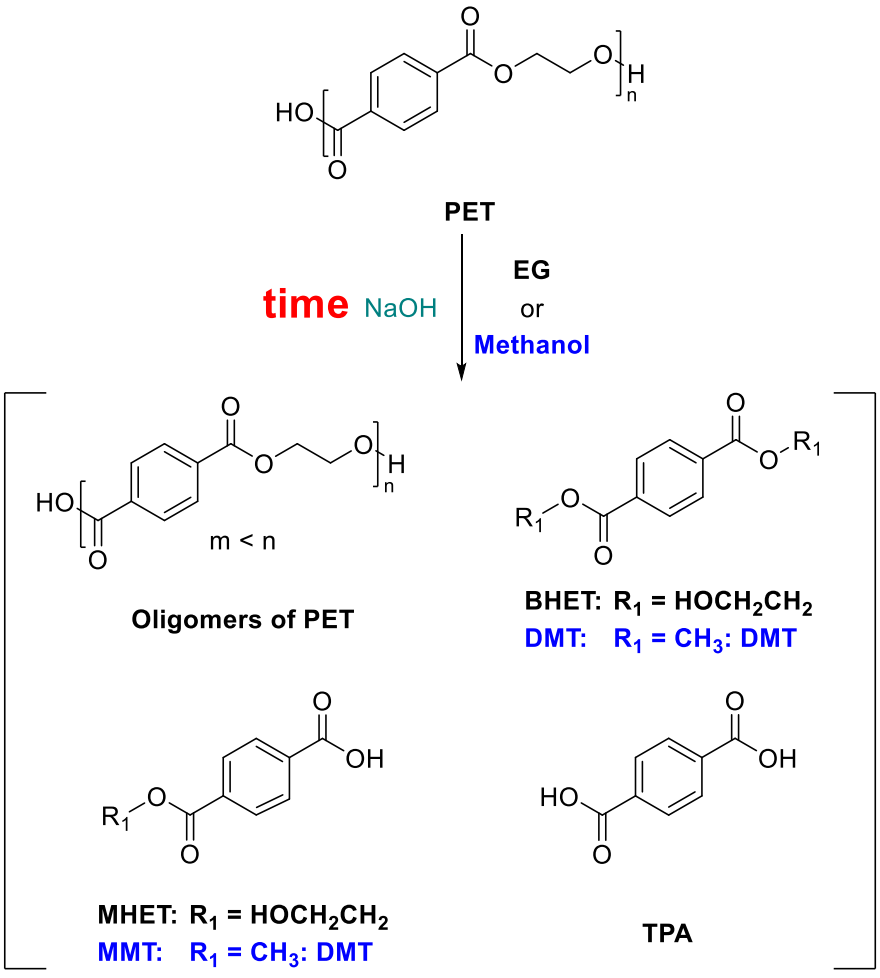

Scheme 5.4. PET depolymerization products; glycolysis (black) and methanolysis (blue).

5.4 PET Alkaline Glycolysis: Product Identification

We have explored the effect of the NaOH concentration, EG volume, and temperature on PET glycolysis. Representative results are shown in Table 5.2. PET glycolysis is slow at room temperature, requiring heating to 100 ^{0}C or above to obtain reasonable rates. Thus, under concentrations of PET and NaOH in EG produce almost complete conversion at 120 ^{0}C, while no consumption of PET has been observed at 25 ^{0}C (entries 6 and 7, Table 5.2). Another important factor controlling the outcome of glycolysis is the molar ratio of NaOH to PEG. is formed when NaOH is used in molar amount lower than PET (entries 1-3, Table 5.2). When more than two eq. of NaOH is used only TPA is produced (entries 4 and 6, Table 5.2)..

The conversion of PET to TPA requires two fold excess of NaOH (entries 5 and 6) as it is consumed in the process. When lower equivalents of NaOH are used, the reaction stops after complete consumption of the base (entries 1-4). Interestingly, all the entry 1-4 conditions showed high or equal BHET/MHET percentage compared to the hydrolysis product TPA which still confirms transesterification in polymers. Nevertheless, the sole formation of only BHET was not observed even when the NaOH was used in the catalytic amount (entries 1 and 2).

As was mentioned in the introduction, our goal is to develop PET alkaline glycolysis conditions to get 100% of a single monomer, not a mixture of monomers. The monomer mixtures are not favorable for production of polymers or the use in other applications. Therefore, we focused our reaction optimization studies on solvolysis using excess of NaOH over PET (entries 5-7) to achieve a quantitative yield of TPA under mild conditions

(Section 5.5). Additionally, we have tried to produce pure BHET using catalytic amounts by modifying conditions shown in entries 1-3, which will be described in section 5.6.

Table 5.2. Outcomes of selected PET alkaline glycolysis conditions.

Entry	PET: NaOH: EG molar ratio	[NaOH] M	Temp ^{0}C	Time hours	PET conversion %	% yield		
						BHET	MHET	TPA
1	1: 0.08: 14	0.1	160	10	<10	5	5	<0.1
2	1: 0.15: 14	0.2	160	72	~70	50	10	<1
3	1: 0.8: 14	1	160	8	100	30	30	30
4	1: 1: 14	1.25	120	8	100	25	20	40
5	1: 1: 180	0.1	120	8	50	0	0	40
6	1: 10: 180	1	120	8	100	0	0	99
7	1: 10: 180	1	25	24	0	0	0	0

Entry 1-4: PET 1 g (5 mmol), EG 4 mL (0.07 mol). **Entry 5-7**: PET 1 g (5 mmol), EG 50 mL (0.9 mol).

The use of catalytic amount of NaOH in PET alkaline glycolysis produces monomer mixtures, and use of excess NaOH results formation of BHET or BHET/MHET/TPA mixtures at the beginning and then, longer reaction time, converting BHET/MHET to 100% TPA and 100% conversion of PET.

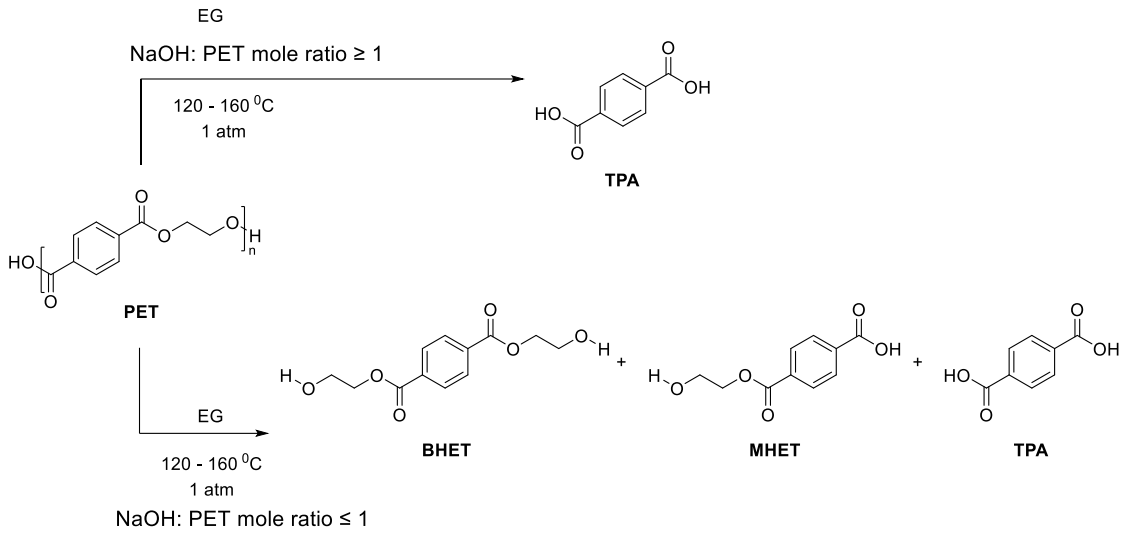

Scheme 5.5. Summary of PET alkaline glycolysis outcome.

5.5 PET Alkaline Glycolysis to TPA: Optimization of Conditions

The effect of NaOH concentration and temperature on the kinetics of TPA formation were tested using stoichiometric excess of NaOH over EG.

5.5.1 Kinetics of PET glycolysis

PET (50 mg, 0.26 mmol) in EG (50 mL, 55.5 g, 0.9 mol) was depolymerized at 100 ^{0}C using varying NaOH concentrations: 0, 0.1, 1, and 2 M. The yield of TPA and PET conversion was determined after 2 h. An exponential increase in the PET conversion was observed with increased NaOH concentration, reaching 100% at [NaOH]= 2 M (Figure 5.5).

5.5.2 Effect of NaOH concentration on solvolysis rate

PET (50 mg, 0.26 mmol) in EG (50 mL, 55.5 g, 0.9 mol) was depolymerized at 100 ^{0}C using varying NaOH concentrations: 0, 0.1, 1, and 2 M. The yield of TPA and PET conversion was determined after 2 h. An exponential increase in the PET conversion was observed with increased NaOH concentration, reaching 100% at [NaOH]= 2 M (Figure 5.6).

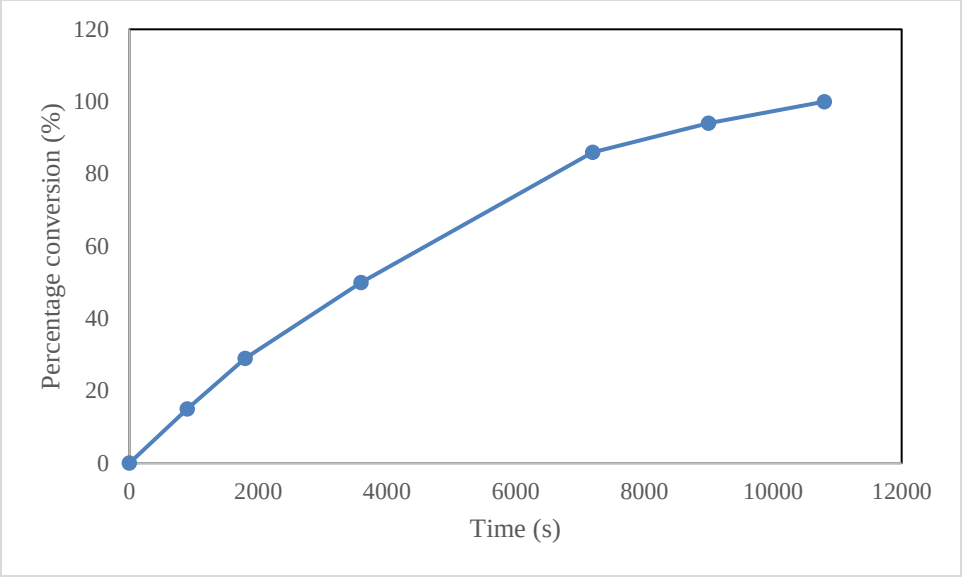

Figure 5.5. PET percentage conversion with reaction time.

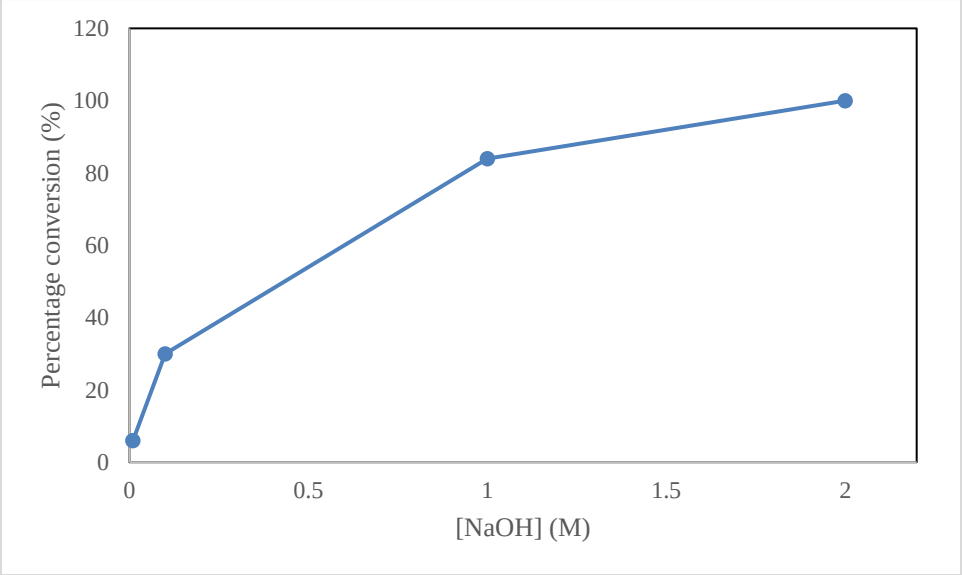

Figure 5.6. PET percentage conversion with increasing NaOH concentration.

5.5.3 Effect of temperature

PET (50 mg, 0.26 mmol) in EG (50 mL, 55.5 g, 0.9 mol) was depolymerized using NaOH (2 g, 0.05 mol) at different temperatures: 25, 60, 100, and 160 ^{0}C. The yield of TPA and PET conversion was determined after 15 min (Figure 5.7). Complete conversion was

observed at 160 ^{0}C. Therefore, temperature is the most significant factor affecting high yield of TPA in PET alkaline glycolysis.

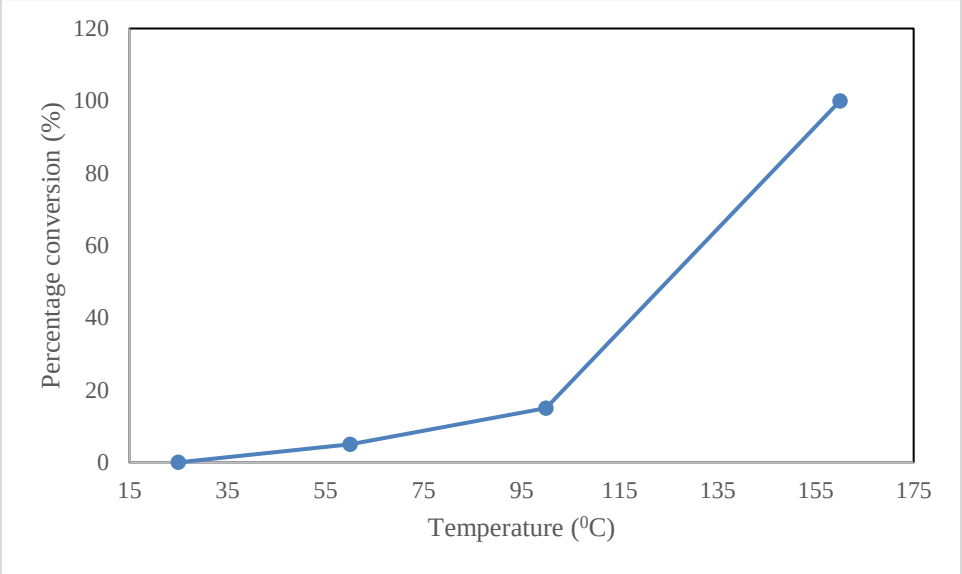

Figure 5.7. PET percentage conversion at different temperatures.

The most suitable conditions to get pure TPA in high yield (100%) in a short time is summarized in Table 5.3. All three sets of conditions are mild compared to conventional PET alkaline hydrolysis that requires high NaOH concentration (6 M), 100 ^{0}C processing temperature. In addition, yield of TPA only reaches 90%.[175] An added advantage of PET alkaline solvolysis is that the product, disodium terephthalate salt (Na_2TPA), is insoluble in EG. This allows for easy separation of the product and for recycling of the solvent. On the other hand, in alkaline hydrolysis the entire solution needs to be acidified to convert Na_2TPA to TPA. This can be a loss of alkaline aqueous batch and cannot be re-used.

Table 5.3. Time required to achieve complete conversion of PET to TPA.

PET: NaOH: EG mole ratio	[NaOH] M	Temperature ^{0}C	Time hours
1: 200: 3500	1	100	3
1: 400: 3500	2	100	2
1: 200: 3500	1	160	0.25

5.6 PET Alkaline Glycolysis Ethylene Glycol-Hexafluoro Isopropanol Mixture

PET is insoluble in EG. Thus, the experiments described in section 5.4 and 5.5 occurs at solid/liquid interface. Heterogenous reaction conditions may have been the reason to observe acid formation compared to transesterification in some conditions in section 5.5.

A cosolvent-assisted reaction medium was used in various research studies to increase the rate of PET glycolysis.[176] For example, PET glycolysis in mixtures of ethylene glycol and aromatic solvents such as aniline, nitrobenzene, 1-methyl-2-pyrrolidinone (NMP), or p-xylene have been reported go generate BHET in high yield.[177, 178] Dimethyl sulfoxide (DMSO) in glycolysis,[179] ethereal solvents such as dioxane, tetrahydrofuran, or dimethoxy ethane in methanolysis[166] and halogenated solvents have also been reported. Therefore, one option to obtain 100% pure monomer (BHET) in high yield efficiently is to dissolve PET in a suitable solvent, and conduct depolymerization in co-solvent mixtures of EG. The only solvents that can dissolve PET at room temperature (25 ^{0}C) are trifluoroacetic acid (TFA) and 1,1,1,1,1-hexafluoroisopropanol (HFIP) DMSO dissolves PET at high temperatures (>190 ^{0}C).[180] A co-solvent system of HFIP-EG was attempted to

maximize and predominate the transesterification reaction in PET depolymerization reaction instead of acid formation in the presence of NaOH as the catalyst.

PET (10 mg, 0.056 mmol) was dissolved in HFIP (2 mL), and EG (2 mL). Two different NaOH concentrations were used to depolymerization, 0.75 M and 0.2 M.

NaOH concentration of NaOH gave BHET and MHET mixture starting from the beginning leading to pure TPA in 3 hours (Figure 5.8). On the other hand, low NaOH concentration of 0.2 M, gave pure BHET 50% yield in 2 hours. However, a mixture of monomers was observed upon prolong stirring indicating incomplete conversion. Solution depolymerization helps to control the reaction more towards transesterification than hydrolysis (Table 5.2, entry 5 vs. Figure 5.9).

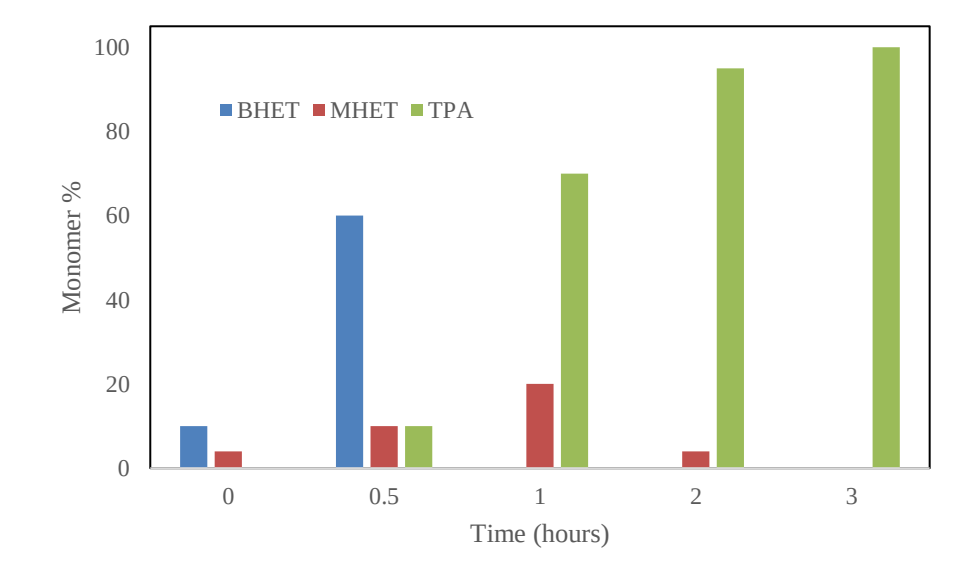

Figure 5.8. PET glycolysis products in EG-HFIP co-solvent, PET: NaOH 1: 45.

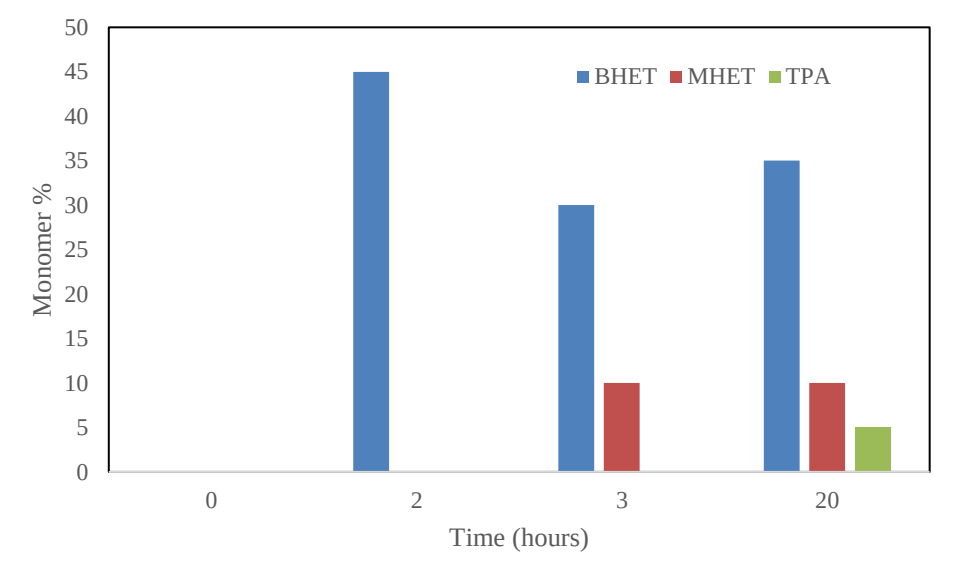

Figure 5.9. PET glycolysis products in EG-HFIP co-solvent, PET: NaOH 1: 3.

5.7 PET Alkaline Methanolysis: Product Identification and Optimization

Both single solvent and solvent mixtures were used to study PET alkaline methanolysis based on the learning from PET glycolysis where heterogeneous solutions are slow or uncontrolled, produces multiple monomers.

5.7.1 PET Methanolysis in Single Solvent

PET methanolysis is slow at room temperature, under low NaOH concentration, 0.01 M (Table 5.4, entry 1). However, at high concentration of NaOH (1M and 2 M), PET was fully converted to TPA even at room temperature (Table 5.4, entry 2 and 3). Increasing the temperature to 60 ^{0}C, increases the PET conversion as it was expected (Table 5.4, entry 1 vs. entry 4). However, DMT, MMTA, TPA all species were formed at the beginning and then transformation of DMT to MMTA and then to TPA was observed upon stirring longer (Table 5.4, entry 4 and 5). Catalytic amount of NaOH also showed similar observations as entry 4 and 5 or non-reactive when the NaOH moles is lower than PET.

Table 5.4. Outcomes of selected PET alkaline methanolysis conditions.

Entry	PET: NaOH: MeOH molar ratio	[NaOH] M	Temp ^{0}C	Time hours	PET conversion %	% yield		
						DMT	MMT	TPA
1	1: 2: 5000	0.01	25	48	1	<1	0	0
2	1: 200: 5000	1	25	23	100	0	<1	97
3	1: 400: 5000	2	25	12	100	<1	<1	99
4	1: 2: 5000	0.01	60	20	60	0	40	10
5	1: 1: 5000	0.005	60	20	40	0	12	5

PET 0.05 g (0.26 mmol, EG 50 mL (55.5 g, 0.9 mol)

PET alkaline methanolysis produces pure TPA under high NaOH concentration solutions even at room temperature. However, depolymerization under stoichiometric quantities of PET: NaOH produces mixtures of monomers, DMT, MMTA, TPA even at refluxing conditions, 60 ^{0}C.

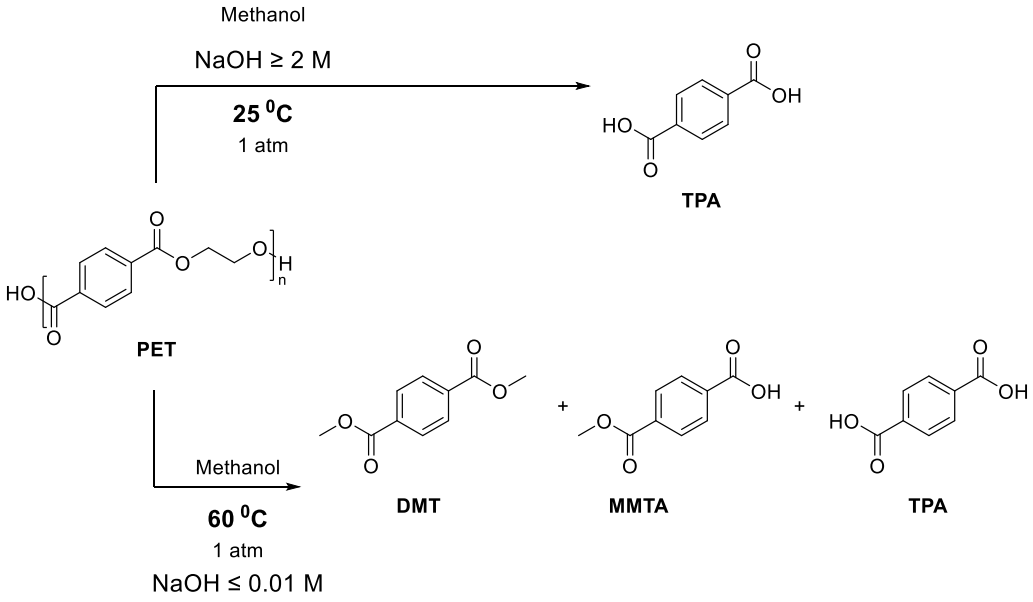

Scheme 5.6. Summary of PET alkaline methanolysis outcome.

5.7.2 PET Alkaline Methanolysis in Co-solvents

Ethereal solvents such as dioxane, tetrahydrofuran, or dimethoxy ethane and halogenated solvents in methanol have been reported to give high yield of DMT in the presence of metal catalysts.[166] DMSO was selected to use as a co-solvent in PET methanoolysis as a positive effect from DMSO for depolymerization was reported before even though PET is insoluble in DMSO at temperatures below 190 ^{0}C.[135] We attempted alkaline methanolysis using two solvent ratios of DMSO: methanol; 1:4 and 1:1. The lowest NaOH concentration from Table 5.4 was chosen for comparison purpose. PET (0.05 g, 0.26 mmol) in DMSO: methanol mixture (50 mL) in NaOH (0.02 g, 0.5 mmol) was used. An aliquot of the reaction mixture was taken at different time intervals, filtered to remove any solid before HPLC analysis. Both MMTA and TPA are insoluble in pure methanol or DMSO: methanol mixtures. Therefore, MMTA or TPA was not observed to determine the yield with time by HPLC. DMT yields for both co-solvent ratios, DMSO: methanol 1:1 and 1:4. Both co-solvent ratios showed increase in DMT yield followed by a gradual decrease due to the conversion to MMTA and TPA.

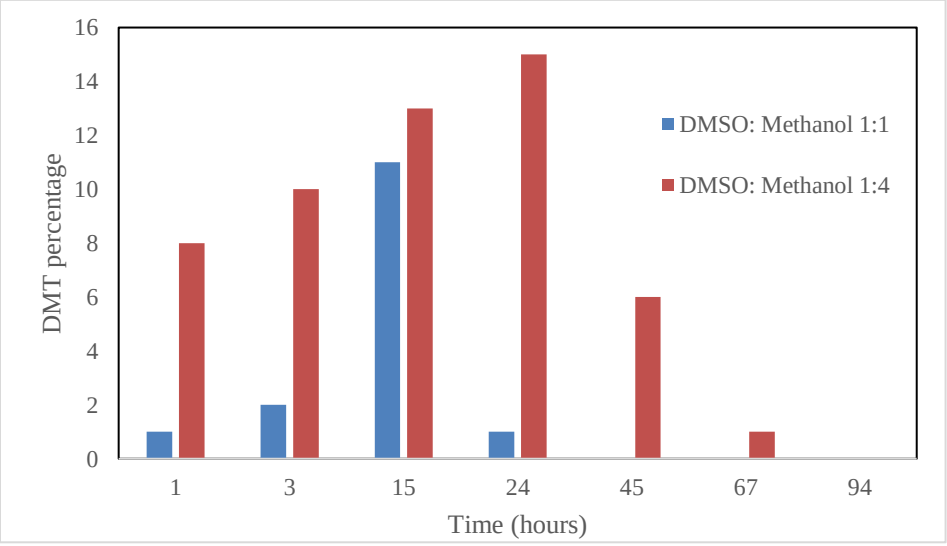

Figure 5.10. DMT yield from PET alkaline methanolysis in varying DMSO: methanol.

5.8 Mechanism of Transesterification and Acid Formation

The mechanism of transesterification is well known and occurs via nucleophilic attack from deprotonated solvent which is the rate limiting step. The catalyst, methoxide, is regenerated in the process. An example of transesterification is shown in Scheme 5.7 by taking transformation of BHET to HEMT in alkaline methanol.

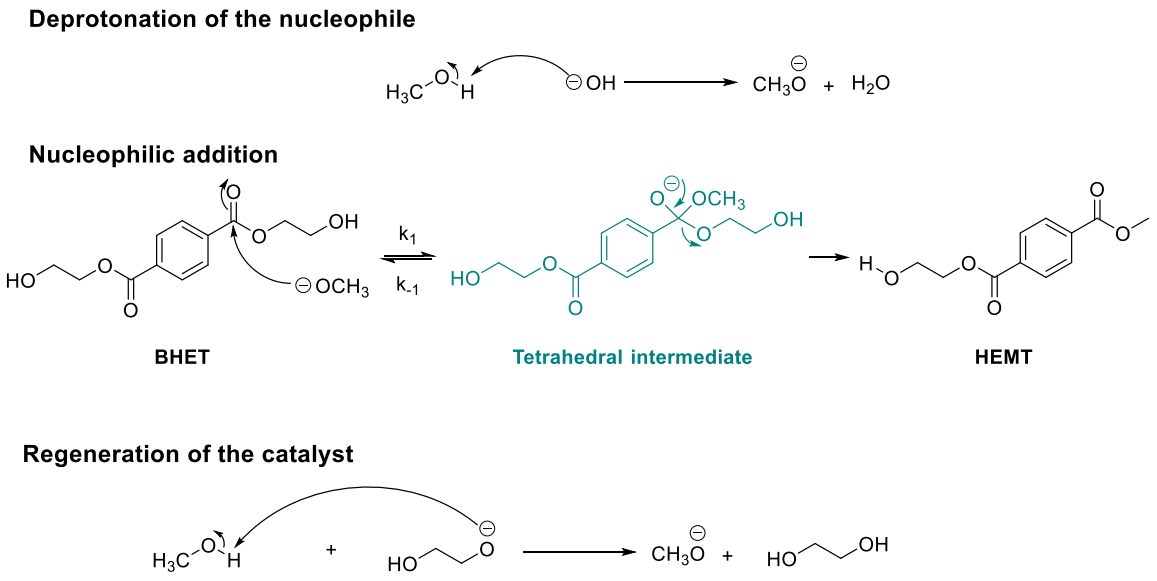

Scheme 5.7. Transesterification via nucleophilic acyl substitution mechanism.

The most common mechanism for acid formation is via hydrolysis pathway (Scheme 5.8-Mechanism 1). The catalyst, sodium hydroxide, is not regenerated in the reaction mechanism. Furthermore, the mechanism could consume another equivalent of hydroxide to form the anion of HEMT in basic medium. Therefore, acid formation halts the transesterification process of a monomer/polymer. However, in alkaline solvents/methanol, the active nucleophile is methoxide, and no hydroxides are available. In order to better understand the mechanism of acid formation under basic conditions, we studied the products of BHET in alkaline ethylene glycol solution (Section 5.10.6). Formation of MHET, and TPA from alkaline BHET was observed by HPLC. Additionally,

we confirmed the formation of diethylene glycol (DEG) by GC-MS analysis. Therefore, the acid formation mechanism is the nucleophilic S_N2 attack of deprotonated solvent to the alkyl group next to the ester hydroxyl (Scheme 5.8-Mechanism 2) or a direct displacement mechanism. Catalyst/methoxide is not regenerated in the direct displacement mechanism similar to mechanism 1/conventional hydrolysis.

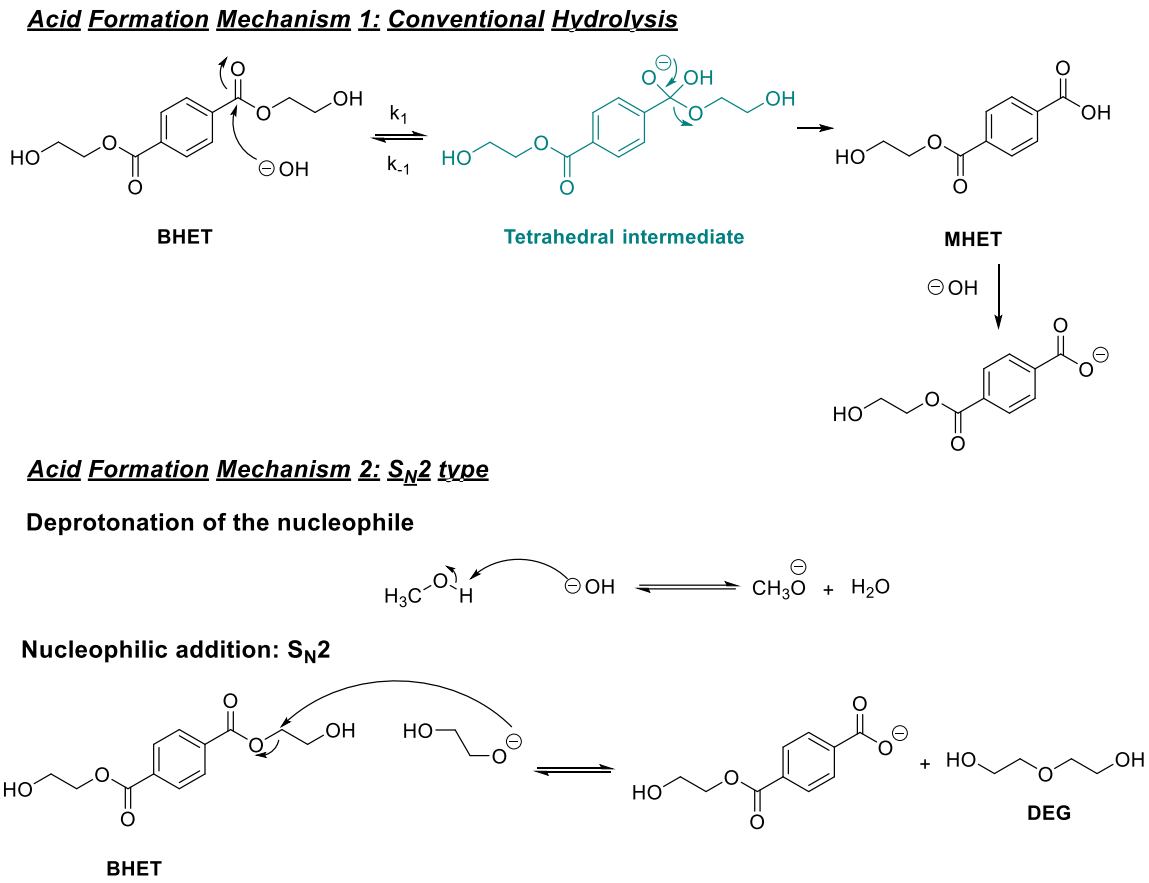

Scheme 5.8. Mechanisms of acid formation in alkaline solvolysis.

5.9 Discussion and Conclusion

Transesterification of small molecules is faster compared to succeeding acid formation step (10,000-fold). Transesterification is a nucleophilic acyl substitution reaction that occurs via S_N1 nucleophilic acyl substitution by alkoxide ions. The detection od DEG in a reaction mixture of BHET in alkaline ethylene glycol confirms that TPA formation from an ester in an alkaline solvent proceeds via S_N2 pathway direct displacement pathway. The latter mechanism is further proved by doing the reactions in a medium where there is no hydroxide ions from a base and only alkoxide ions. BHET in NaH and ethylene glycol instead alkaline ethylene glycol. The formation of TPA was still observed in the solution of NaH in ethylene glycol where there are only alkoxide ions and no hydroxide ions. (Section 5.10.6). Transesterification regenerates the alkoxide catalyst. However, consumes the alkoxide catalyst during the acid formation step, halting the transesterification process.

The kinetics of transesterification and acid formation of a polymer is different compared to small molecules. Polymer transesterification is slow due to its crystalline nature. It is still a stepwise process as observed with BHET conversion to DMT followed by TPA formation in methanolysis. We developed a spherical model to explain the PET depolymerization kinetics in alkaline ethylene glycol solution assuming PET as a sphere (Figure 5.11). At first, only the outer surface of PET polymer reacts with alkoxide forming BHET or small oligomers leaving the core unreacted. As soon as the transesterified product, BHET is released to the medium, it converts to MHET or TPA as the alkoxide attack to a small molecule is easier than onto a polymer. Eventually, forms 100% TPA when PET is also fully consumed. Above explanation is the rational when NaOH molar ratio is higher than PET. However, when the NaOH molar ratio is lower than PET, a

mixture of monomers BHET, MHET, and TPA along with unreacted PET was observed due to the fact that alkoxide are consumed in the acid formation steps leaving no catalyst in the medium to form transesterified products or depolymerize the unreacted PET polymer.

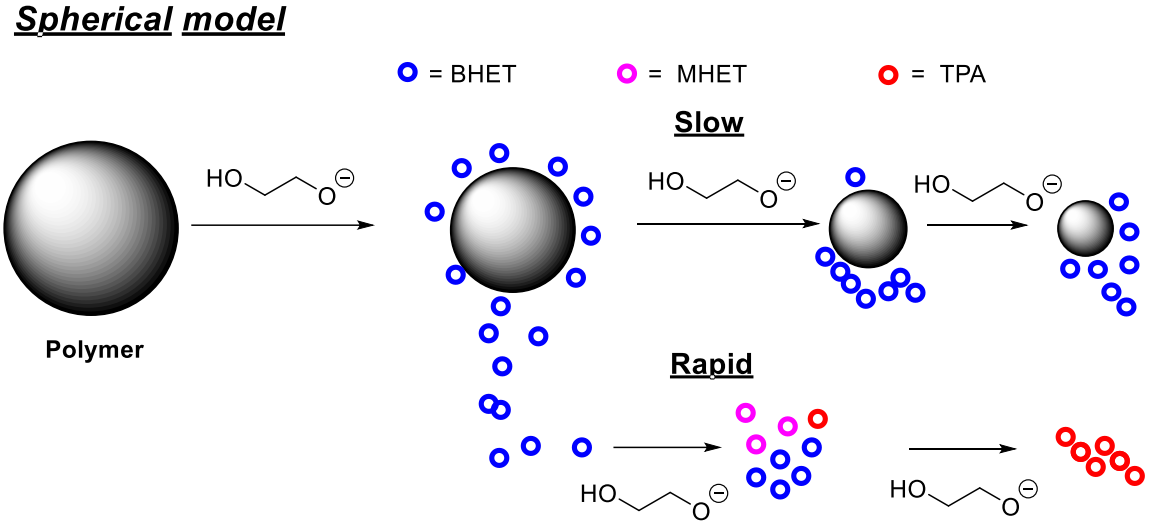

Figure 5.11. Proposed spherical model to explain PET alkaline depolymerization kinetics.

Herein we report conditions that fully convert PET to TPA. The reaction system is simple; no water and no extra reagent other than NaOH and EG or methanol are used. The conditions are milder than conventional alkaline hydrolysis and completes faster (2 M vs >16 M NaOH). Conventional aqueous hydrolysis is often neglected by the industries due to water pollution by the release of highly acidic or alkaline waste to natural wetlands. However, in alkaline solvolysis, alkaline solvent can be re-used to depolymerize another batch of PET which is an added advantage.

Another goal of the project was to find conditions that stop PET depolymerization at the simplest diester, BHET for glycolysis and DMT for methanolysis. The use of co-

solvents, HFIP and DMSO helped to maximize BHET or DMT monomers instead of TPA. However, complete conversion of PET to pure BHET or DMT was still not possible.

5.10 Experimental Section

5.10.1 General Information

PET flakes were obtained as described in section 5.11.2. Both glycolysis and methanolysis reactions were carried out in a temperature-controlled silicon oil bath and refluxing if necessary. All the solvents, methanol, ethylene glycol, HFIP and all the chemicals were used as received and no purification was carried out unless otherwise stated. ESI-MS and Shimadzu GC-MS was used for mass analysis of the samples. Cary 5000 UV spectrophotometer was used to collect absorbance spectra. Shimadzu HPLC was used and HPLC grade solvents/methanol, and water was used. HPLC grade water was pre-filtered prior to the use and 0.1% trifluoroacetic acid (TFA) was used in the water mobile phase. Both glycolysis and methanolysis was followed using the same HPLC solvent system unless otherwise noted. The HPLC solvent system is methanol: water 33%: 67% (0 to 11 minutes), then the mobile phase was changed from methanol 33% to 100% within 11 to 25 minutes, finally, 100% methanol for 5 more minutes 25 to 30 minutes; observation wavelength 254 nm.

5.10.2 Conversion of PET bottles to PET flakes

A food grade plastic bottle was taken, label, adhesive was removed, and washed with water. After fully drying the bottle under air, the bottle was cut into pieces (of ~ 6 inches) except the lid and capping portion. The pieces were blended in a high-speed multifunctional blender. The particle size was further reduced using a cryogenic grinder to get PET flakes with <3 mm size.

5.10.3 Absorbance Spectra of DMT

A stock solution of DMT in methanol (0.1 mM) was prepared. A concentration series of DMT in methanol was prepared from the above stock solution: 10, 25, 50, 70, 80, and 100 μM. UV absorbance spectra of each concentration was recorded in 3 mL quartz cuvette. Three main absorbance bands at 240, 286 and 296 nm were observed (Figure 5.12). Each concentration in the dilution series was prepared in triplicate and the absorbance spectra were collected. The molar extinction coefficient at each maximum absorbance was calculated by plotting the absorbance value vs. concentration (Figure 5.12A, 4B, and C). The logarithm of molar extinction coefficient values at 240, 286, and 296 nm are 4.28, 3.18, and 3.06, respectively.

A) **B)**

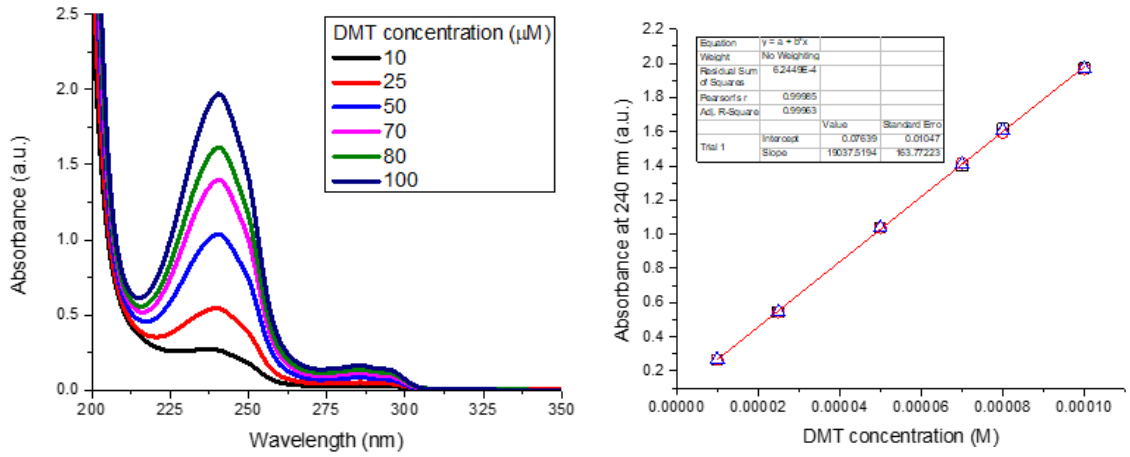

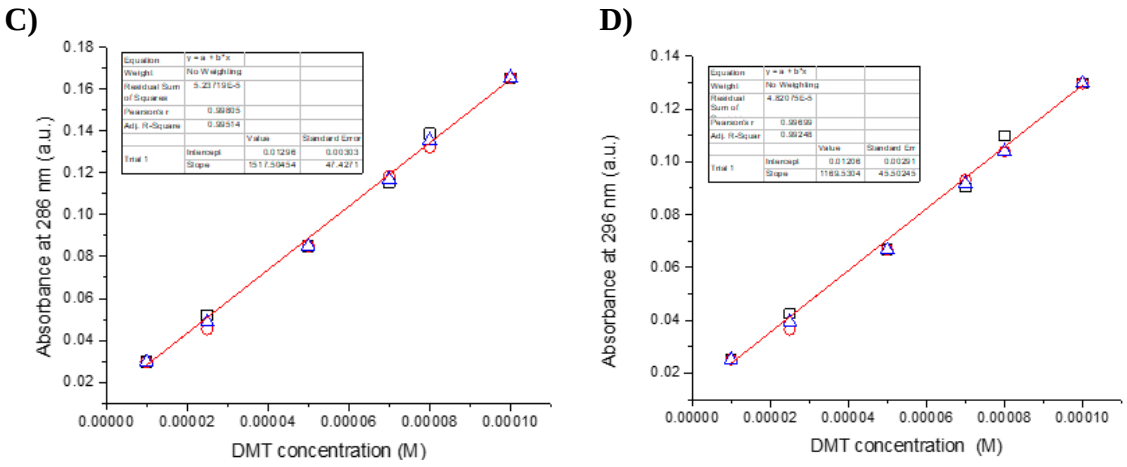

Figure 5.12. A) Absorbance spectra of various concentrations of DMT in methanol. Plot DMT concentration vs. absorbance at B) 240 nm C) 286 D) 296 nm.

5.10.4 HPLC Calibration Curves: BHET, DMT, and TPA

Shimadzu 20A HPLC instrument (serial no. 55475) with SPD-M20A Diode Array Detector (DAD) and (5 µm, 4.6, 250 mm) kinetex C-18 column was used. All the HPLC analysis were carried out at 25 ^{0}C. Methanol and 0.1% trifluoroacetic acid (TFA) in water gradient system was used to separate the monomers at 1 mL/min flow rate. Methanol 33% was used from t=0 to t=11 minutes, then the mobile phase was changed from methanol 33% to 100% within t=11 to t=25 minutes, finally, 100% methanol for 5 more minutes: t=25 to t=30 minutes. All three monomers, TPA, BHET and DMT were analyzed at 254 nm wavelength and detected at 9.5 (Table 5.5, Figure 5.13), 11.1 (Table 5.6, Figure 5.14), and 24.5 minutes (Table 5.7, Figure 5.15) respectively.

Table 5.5. TPA standards concentration vs. HPLC peak area for three trials.

[TPA]	**HPLC peak area at 9.5 minutes**		
(M)	**Trial 1**	**Trial 2**	**Trial 3**

9.60E-04	10938792	10911052	10664659
6.40E-04	7322791	7327426	7377903
4.90E-04	5289005	5454715	5416035
3.20E-04	3460662	3286594	3310712
9.60E-05	137982	1278515	1228216

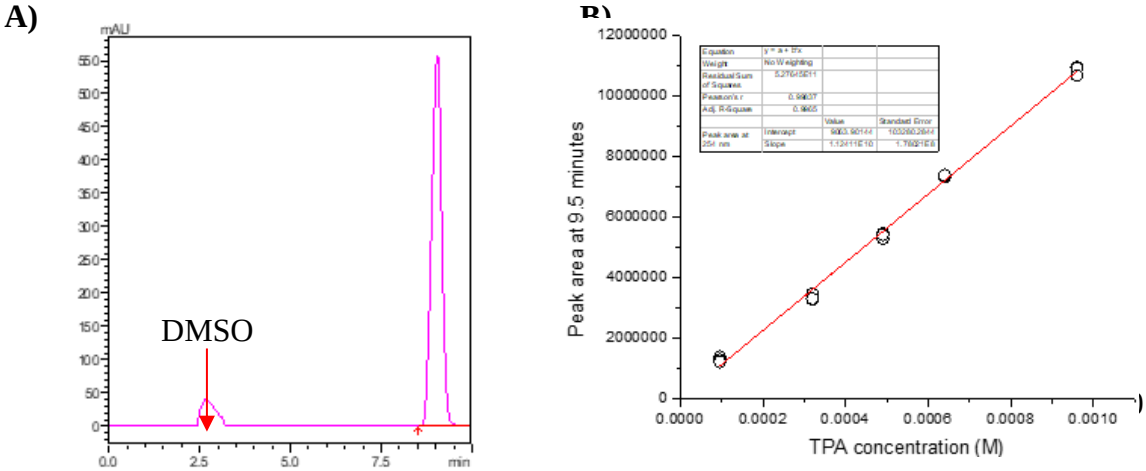

Figure 5.13. Reference HPLC chromatogram of 0.96 mM TPA, B) HPLC calibration curve for TPA.

Table 5.6. BHET standards concentration vs. HPLC peak area for three trials.

[BHET]	**HPLC peak area at 11.1 minutes**		
(M)	**Trial 1**	**Trial 2**	**Trial 3**
1.53E-04	2303833	2440490	2430363
3.10E-04	4925654	4894433	4727520
4.99E-04	8327096	8304357	8159799
6.14E-04	9893251	9728717	9724867

7.67E-04	12523672	12234049	12000725

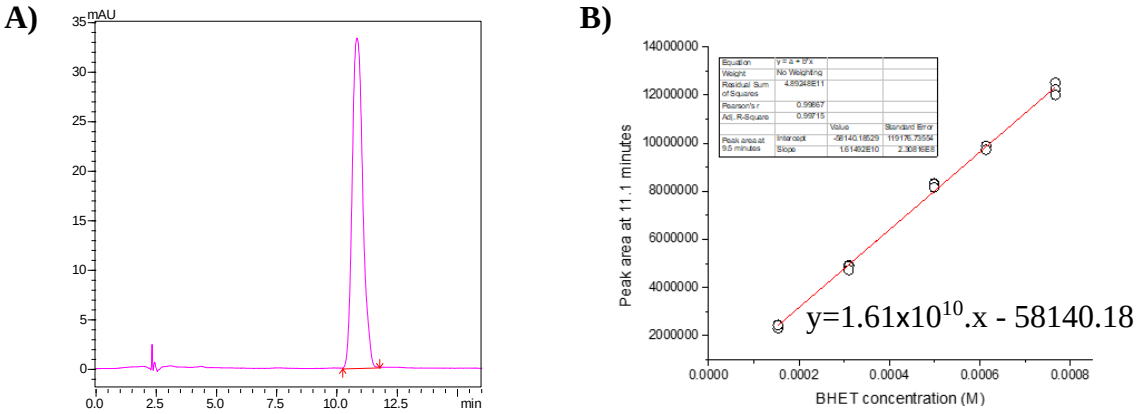

Figure 5.14. Reference HPLC chromatogram of 0.024 mM BHET, B) HPLC calibration curve for BHET.

Table 5.7. DMT standards concentration vs. HPLC peak area for three trials.

[DMT]	**HPLC peak area at 24 minutes**		
(M)	**Trial 1**	**Trial 2**	**Trial 3**
2.30E-04	2885670	2909423	2909168
1.70E-04	2184213	2197823	2197329
1.00E-04	1255762	1285135	1286580
5.00E-05	670736	657306	657057
1.25E-05	163005	164970	165237

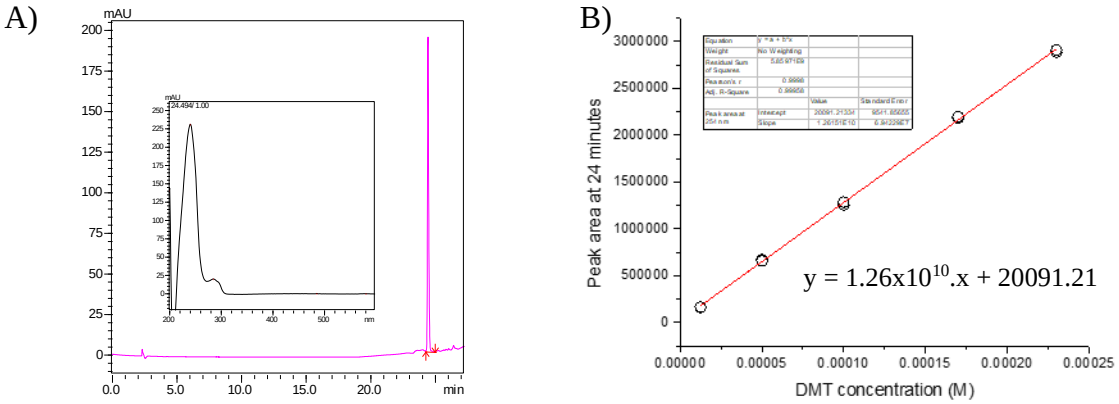

Figure 5.15. A) Reference HPLC chromatogram of 0.1 mM DMT and the UV spectra (insert), B) HPLC calibration curve for DMT.

5.10.5 Quantitative Analysis of PET Depolymerization

Percentage Conversion of PET was determined by UV spectrometer. Absorbance spectra of PET is featureless. However, the monomers formed has a defined absorbance spectra and resembles the absorbance spectra of DMT (Figure 5.16 and Figure 5.12A). The percentage conversion was determined according to the equation below. The initial concentration of PET was determined by taking the molar mass of a PET repeating unit, 192 g/mol. The concentration of the depolymerization mixture at a given time was determined from the molar extinction coefficient of DMT at 240 nm.

$$\%\ \text{conversion of PET} = \frac{\text{Amount of PET reacted (g)}}{\text{Initial mass of PET (g)}}$$

$$= \frac{Concentration\ of\ total\ monomer\ products\ formed\ (M)}{Initial\ concentration\ of\ PET\ (M)}$$

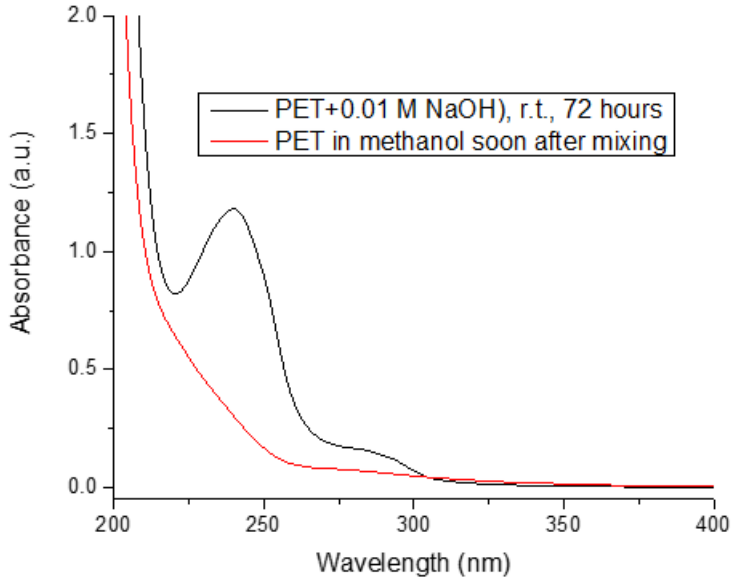

Figure 5.16. Absorbance spectra of PET and PET alkaline methanolic depolymerization solution.

5.10.6 BHET Stability Ethylene Glycol

5.10.6.1 Stability in NaOH

Attempts were taken to determine a condition at which BHET is not converted MHET or TPA at least for a short duration in varying alkaline conditions. If successful, the conditions could be used in PET depolymerization. First a kinetic study using BHET (3.4 mM), NaOH (0.01 M), EG (3 mL) was carried out. HPLC traces of reaction progress with time showed that BHET forms MHET and TPA in alkaline ethylene glycol (Figure 5.17A, Scheme 5.9).

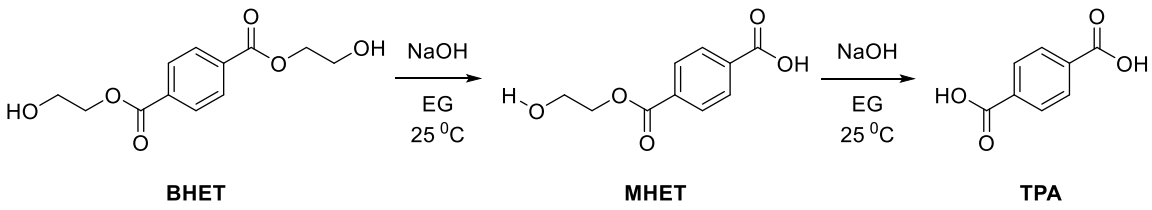

Scheme 5.9. BHET stepwise transformation to TPA.

BHET decay fits well into a single-exponential decay with rate constant 0.0013 s^{-1} MHET formation showed an increase at the beginning reaching a plateau. The plot was fit into a single-exponential decay and showed rate constants 0.0019 s^{-1}. Both BHET decay and MHET formation having the same rate indicates that BHET to MHET is a single step. TPA formation rate is very slow and estimated based on zero-order approximation, 2.5x10^{-5} s^{-1}.

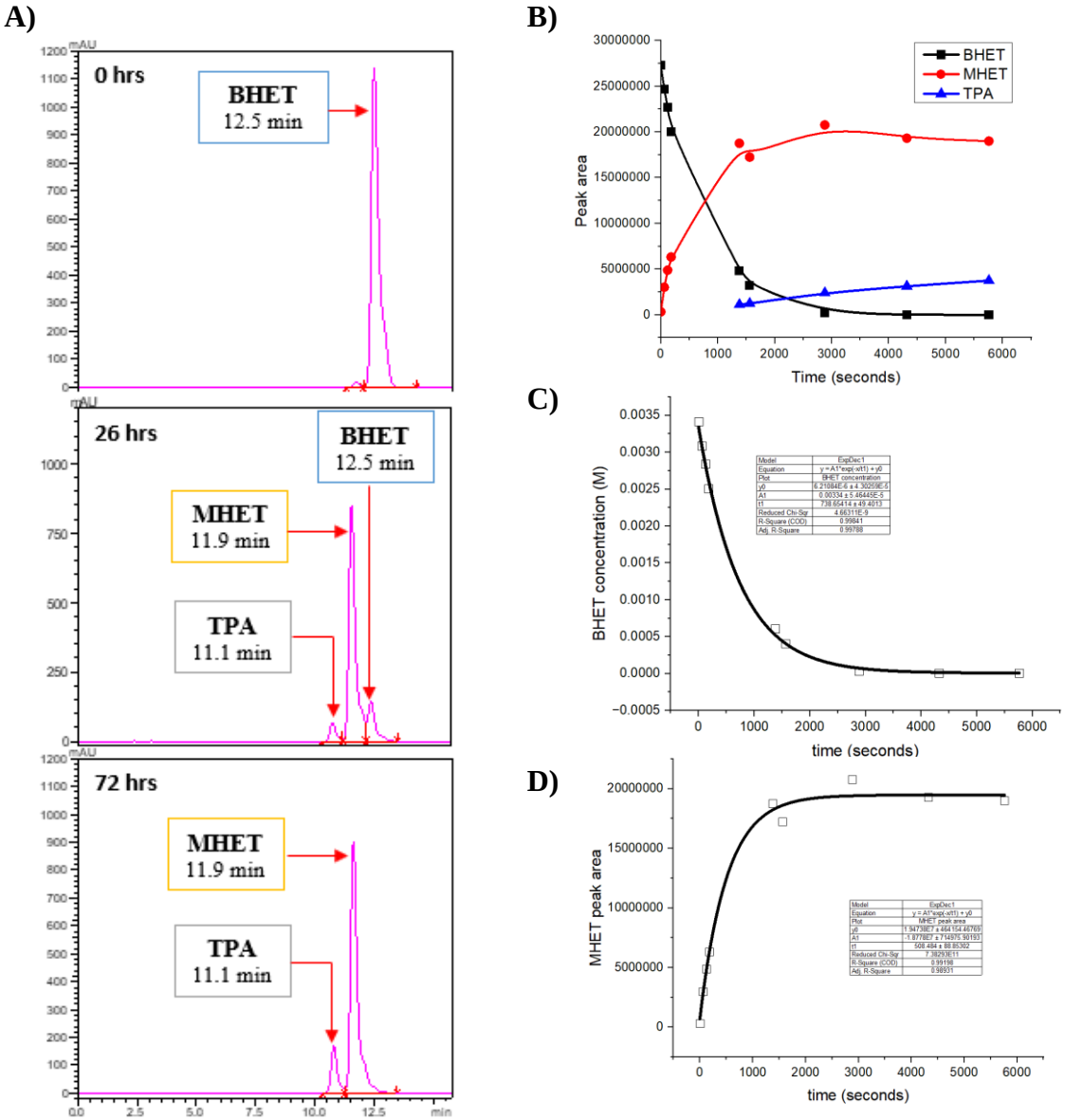

Figure 5.17. A) HPLC traces of BHET in alkaline EG with time, B) HPLC peak area vs. time for BHET, MHET, and TPA, C) BHET decay kinetic trace, D) MHET formation kinetic trace.

The composition of BHET in varying alkaline conditions was also tested. High concentration of NaOH converted BHET to TPA instantaneously and low concentrations results in a mixture of BHET, MHET, and TPA (Table 5.8). Therefore, an alkaline condition where BHET stays in its original form does not exist.

Table 5.8. BHET conversion to TPA in EG under varying NaOH concentrations.

BHET: NaOH: EG mole ratio	**Temp ^{0}C**	**Time hours**	**BHET %**	**MHET %**	**TPA %**
1: 10: 179	120	1.5	0	0	100
1: 20: 1795	120	0.25	0	0	100
1: 5: 1795	120	3	0	0	100
1:3:5300	25	72	0	90	5
1: 0.8: 14	120	0.2	40	30	10
1: 0.8: 14	160				
1: 0.15: 14	160				

5.10.6.2 Stability in NaH

Attempts were taken to determine the products formed when BHET is in NaH. This was to understand if the S_N2 type acid formation mechanism is viable. BHET in two different NaH concentrations showed TPA formation and results are similar to that of

BHET in NaOH (Table 5.9). Results confirm that the only mechanism that could occur when BHET is in NaH is S_N2 direct displacement for the acid formation.

Table 5.9. BHET conversion to TPA in EG under varying NaH concentrations.

BHET: NaH: EG mole ratio	Time hours	BHET %	MHET %	TPA %
1: 10: 179	1	0	0	100
1: 0.8: 14	0.25	45	30	10

5.10.7 DMT Stability in Methanol

Attempts were taken to determine a condition at which DMT is not converted MMT or TPA at least for a short duration in varying alkaline conditions (Table 5.10). If successful, the conditions could be used in PET depolymerization. Similar to BHET in alkaline ethylene glycol, such conditions were not observed.

Table 5.10. DMT conversion to TPA in MeOH under varying NaOH concentrations.

DMT: NaOH mole ratio	[NaOH] M	Time hours	DMT %	MMTA %	TPA %
1: 5	0.05	72	68	13	0
1: 10	0.1	0.5	0	100	0
1: 20	0.2	72	11	74	11
1: 200	2	2	0	45	50

5.10.8 Product Characterization from BHET in Alkaline EG

By-product analysis of BHET in alkaline ethylene glycol was carried out by gas chromatography-mass spectrometry (GC-MS) to determine the acid formation mechanism. BHET (1.3 g, 5.1 mmol) in NaOH (0.16 g, 4 mmol) in EG (4 mL) was stirred at 160 ^{0}C. After 1.5 hours an aliquot was analyzed by GC-MS. GC parameters are start temperature 40 ^{0}C and hold for 2 minutes, then ramp to 200 ^{0}C at a rate of 20 ^{0}C/minute; injection temperature 270 ^{0}C, split injection mode, 1 mL/minute column flow, and total flow 20 mL/minute. EG elutes around 3.2-4.5 minutes, has a broader peak, shows the molecular ion m/z 62 in 30% intensity. DEG elutes at 6.7 minutes, and shows (2-hydroxyethoxy)methylium cation with exact mass 75 in 25% intensity. DEG molecular ion (106 g/mol) was not observed in GC-MS analysis (Figure 5.18A, B and C). An aliquot taken from BHET alkaline ethylene glycol shows a peak at 7 minutes that corresponds to the mass of DEG (Figure 5.18D). EG showed broader and split peaks around 4-6.5 in the sample and it is not any other compound.

A)

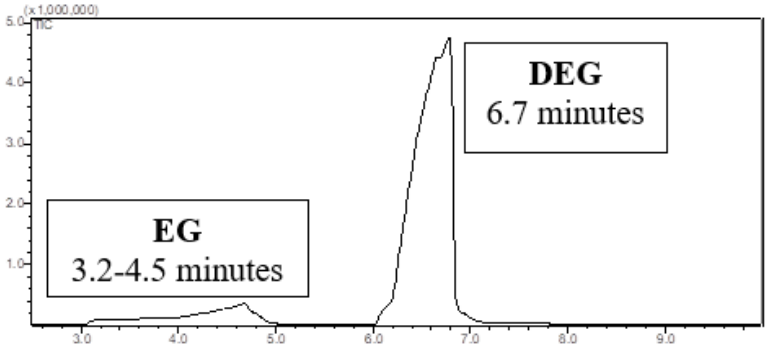

B)

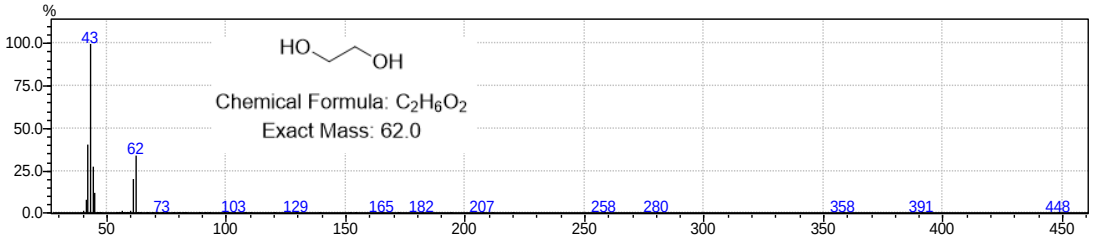

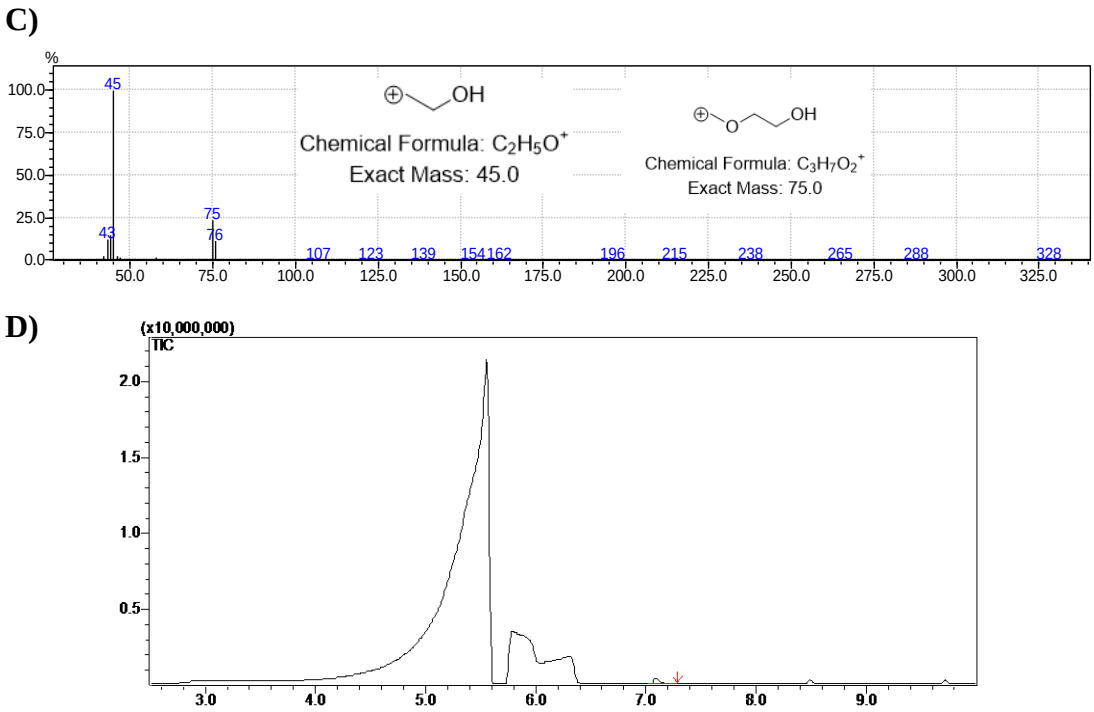

Figure 5.18. A) GC-MS reference chromatogram of EG (0.1 M)+ DEG (0.2 M) B) Reference mass spectrum of EG, C) Reference mass spectrum of DEG, D) GC chrmatogram of BHET in alkaline EG.

REFERENCES

(1) Rokita, S. E. *Wiley Series of Reactive Intermediates in Chemistry and Biology*; John Wiley & Sons, Inc.: Hoboken, New Jersey, 2009. https://doi.org/10.1002/9780470452882.

(2) Singh, M. S.; Nagaraju, A.; Anand, N.; Chowdhury, S. Ortho-Quinone Methide (o-QM): A Highly Reactive, Ephemeral and Versatile Intermediate in Organic Synthesis. *RSC Adv.* **2014**, *4* (99), 55924–55959. https://doi.org/10.1039/c4ra11444b.

(3) Wang, J. Y.; Hao, W. J.; Tu, S. J.; Jiang, B. Recent Developments in 1,6-Addition Reactions of: Para-Quinone Methides (p-QMs). *Org. Chem. Front.* **2020**, *7* (13), 1743–1778. https://doi.org/10.1039/d0qo00387e.

(4) Lima, C. G. S.; Pauli, F. P.; Costa, D. C. S.; de Souza, A. S.; Forezi, L. S. M.; Ferreira, V. F.; de Carvalho da Silva, F. Para-Quinone Methides as Acceptors in 1,6-Nucleophilic Conjugate Addition Reactions for the Synthesis of Structurally Diverse Molecules. *European J. Org. Chem.* **2020**, *2020* (18), 2650–2692. https://doi.org/10.1002/ejoc.201901796.

(5) Bai, W.; David, J. G.; Feng, Z.; Weaver, M. G.; Wu, K.; Pettus, T. R. R. The Domestication of Ortho -Quinone Methides. **2014**.

(6) Fries, K.; Kann, K. I. Ueber Die Einwirkung von Brom Und von Chlor Auf Phenole: Substitutionsproducte, Pseudobromide Und Pseudochloride. Ueber o-Pseudohalogenide Und o-Methylenchinone Aus o-Oxymesitylalkohol. *Liebigs*

Ann. Chem. **1907**, *3*, 335–353. https://doi.org/10.1002/jlac.19073530305.

(7) Toteva, M. M.; Richard, J. P. *The Generation and Reactions of Quinone Methides*; Elsevier Inc., 2011; Vol. 45. https://doi.org/10.1016/B978-0-12-386047-7.00002-3.

(8) Basaric, N.; Mlinaric-Majerski, K.; Kralj, M. Quinone Methides: Photochemical Generation and Its Application in Biomedicine. *Curr. Org. Chem.* **2014**, *18* (1), 3–18. https://doi.org/10.2174/1385272818011401211223330.

(9) Diao, L.; Yang, C.; Wan, P. Quinone Methide Intermediates from the Photolysis of Hydroxybenzyl Alcohols in Aqueous Solution. *J. Am. Chem. Soc.* **1995**, *117* (19), 5369–5370. https://doi.org/10.1021/ja00124a024.

(10) Chiang, Y.; Kresge, A. J.; Zhu, Y. Flash Photolytic Generation and Study of P-Quinone Methide in Aqueous Solution. An Estimate of Rate and Equilibrium Constants for Heterolysis of the Carbon-Bromine Bond in p-Hydroxybenzyl Bromide. *J. Am. Chem. Soc.* **2002**, *124* (22), 6349–6356. https://doi.org/10.1021/ja020020w.

(11) Willis, N. J.; Bray, C. D. Ortho-Quinone Methides in Natural Product Synthesis. *Chem. - A Eur. J.* **2012**, *18* (30), 9160–9173. https://doi.org/10.1002/chem.201200619.

(12) Water, R. W. Van De; Pettus, T. R. R. O -Quinone Methides : Intermediates Underdeveloped and Underutilized in Organic Synthesis. **2002**, *58* (612), 5367–5405.

(13) Byrne, S. R.; Rokita, S. E. Unraveling Reversible DNA Cross-Links with a Biological Machine. *Chem. Res. Toxicol.* **2020**, *33* (11), 2903–2913.

https://doi.org/10.1021/acs.chemrestox.0c00413.

(14) Hutchinson, M. A.; Deeyaa, B. D.; Byrne, S. R.; Williams, S. J.; Rokita, S. E. Directing Quinone Methide-Dependent Alkylation and Cross-Linking of Nucleic Acids with Quaternary Amines. *Bioconjug. Chem.* **2020**, *31* (5), 1486–1496. https://doi.org/10.1021/acs.bioconjchem.0c00166.

(15) Toteva, M. M.; Richard, J. P. *The Generation and Reactions of Quinone Methides*; Elsevier Inc., 2011; Vol. 45. https://doi.org/10.1016/B978-0-12-386047-7.00002-3.

(16) Wojciechowski, K.; Dolatowska, K. Generation of Ortho-Quinone Methides upon Thermal Extrusion of Sulfur Dioxide from Benzosultones. *Tetrahedron* **2005**, *61* (35), 8419–8422. https://doi.org/10.1016/j.tet.2005.06.087.

(17) Spence, J. T. J.; George, J. H. Biomimetic Total Synthesis of Ent-Penilactone A and Penilactone B. *Org. Lett.* **2013**, *15* (15), 3891–3893. https://doi.org/10.1021/ol4017832.

(18) George, J. H.; Baldwin, J. E.; Adlington, R. M. Enantiospecific, Biosynthetically Inspired Formal Total Synthesis of (+)-Liphagal. **2010**, No. 3. https://doi.org/10.1021/ol100756z.

(19) Shaikh, A.; Cobb, A. J. A.; Varvounis, G. Mild and Rapid Method for the Generation of Ortho - (Naphtho) Quinone Methide Intermediates. **2012**, 2–5.

(20) Jones, R. M.; Selenski, C.; Pettus, T. R. R. Rapid Syntheses of Benzopyrans from o -OBOC Salicylaldehydes and Salicyl Alcohols : A Three-Component Reaction. **2002**, No. 8, 6911–6915.

(21) Van de Water, R. W.; Pettus, T. R. R. O-Quinone Methides: Intermediates

Underdeveloped and Underutilized in Organic Synthesis. *Tetrahedron* **2002**, *58* (27), 5367–5405. https://doi.org/10.1016/S0040-4020(02)00496-9.

(22) Wan, P.; Brousmiche, D. W.; Chen, C. Z.; Cole, J.; Lukeman, M.; Xu, M. Quinone Methide Intermediates in Organic Photochemistry. *Pure Appl. Chem.* **2001**, *73* (3), 529–534.

(23) Diao, L.; Wan, P. Chemistry of Photogenerated α-Phenyl-Substituted o-, m-, and p-Quinone Methides from Phenol Derivatives in Aqueous Solution. *Can. J. Chem.* **2008**, *86* (2), 105–118. https://doi.org/10.1139/V07-125.

(24) Wan, P.; Barker, B.; Diao, L.; Fischer, M.; Shi, Y.; Yang, C. 1995 Merck Frosst Award Lecture Quinone Methides: Relevant Intermediates in Organic Chemistry. *Can. J. Chem.* **1996**, *74* (4), 465–475. https://doi.org/10.1139/v96-051.

(25) Nakatani, K.; Higashida, N.; Saito, I. Highly Efficient Photochemical Generation of O-Quinone Methide from Mannich Bases of Phenol Derivatives. *Tetrahedron Lett.* **1997**, *38* (28), 5005–5008. https://doi.org/10.1016/S0040-4039(97)01071-X.

(26) Modica, E.; Zanaletti, R.; Freccero, M.; Mella, M. Alkylation of Amino Acids and Glutathione in Water by O-Quinone Methide. Reactivity and Selectivity. *J. Org. Chem.* **2001**, *66* (1), 41–52. https://doi.org/10.1021/jo0006627.

(27) Padwa, A.; Dehm, D.; Oine, T.; Lee, G. A. Competitive Keto-Enolate Photochemistry in the 3-Phenylisocoumaranone System. *J. Am. Chem. Soc.* **1975**, *97* (7), 1837–1845. https://doi.org/10.1021/ja00840a040.

(28) Chan, A. W. K.; Gutsche, D. Photolysis of 2-Keto-2,3-Dihydrobenzofurans, o-Hydroxystyrenes, and 1 -(o-Hydroxyphenyl) -1,5-Hexadienes. *J. Org. Chem.* **1973**, *38* (11), 1993–2001. https://doi.org/10.1021/jo00951a006.

(29) Chiang, Y.; Kresge, A. J.; Zhu, Y. Flash Photolytic Generation and Study of 5-Methoxy-o-Quinone α-Phenylethide. *Photochem. Photobiol. Sci.* **2002**, *1* (1), 67–70. https://doi.org/10.1039/b107860g.

(30) Arumugam, S.; Popik, V. V. Photochemical Generation and the Reactivity of O-Naphthoquinone Methides in Aqueous Solutions. *J. Am. Chem. Soc.* **2009**, *131* (33), 11892–11899. https://doi.org/10.1021/ja9031924.

(31) Kulikov, A.; Arumugam, S.; Popik, V. V. Photolabile Protection of Alcohols, Phenols, and Carboxylic Acids with 3-Hydroxy-2-Naphthalenemethanol. *J. Org. Chem.* **2008**, *73* (19). https://doi.org/10.1021/jo801302m.

(32) Verga, D.; Nadai, M.; Doria, F.; Percivalle, C.; Di Antonio, M.; Palumbo, M.; Richter, S. N.; Freccero, M. Photogeneration and Reactivity of Naphthoquinone Methides as Purine Selective DNA Alkylating Agents. *J. Am. Chem. Soc.* **2010**, *132* (41), 14625–14637. https://doi.org/10.1021/ja1063857.

(33) Lukeman, M.; Veale, D.; Wan, P.; Munasinghe, V. R. N.; Corrie, J. E. T. Photogeneration of 1,5-Naphthoquinone Methides via Excited-State (Formal) Intramolecular Proton Transfer (ESIPT) and Photodehydration of 1-Naphthol Derivatives in Aqueous Solution. *Can. J. Chem.* **2004**, *82* (2), 240–253. https://doi.org/10.1139/v03-184.

(34) Škalamera, Đ.; Antol, I.; Mlinarić-Majerski, K.; Vančik, H.; Phillips, D. L.; Ma, J.; Basarić, N. Ultrafast Adiabatic Photodehydration of 2-Hydroxymethylphenol and the Formation of Quinone Methide. *Chem. - A Eur. J.* **2018**, *24* (37), 9426–9435. https://doi.org/10.1002/chem.201801543.

(35) Basaric, N.; Žabčić, I.; Mlinarić-Majerski, K.; Wan, P. Photochemical Formation

and Chemistry of Long-Lived Adamantylidene-Quinone Methides and 2-Adamantyl Cations. *J. Org. Chem.* **2010**, *75* (1), 102–116. https://doi.org/10.1021/jo902004n.

(36) Chiang, Y.; Kresge, A. J.; Zhu, Y. Kinetics and Mechanisms of Hydration of O-Quinone Methides in Aqueous Solution. *J. Am. Chem. Soc.* **2000**, *122* (40), 9854–9855. https://doi.org/10.1021/ja001557h.

(37) Chiang, Y.; Kresge, A. J.; Zhu, Y. Flash Photolytic Generation of Ortho-Quinone Methide in Aqueous Solution and Study of Its Chemistry in That Medium. *J. Am. Chem. Soc.* **2001**, *123* (33), 8089–8094. https://doi.org/10.1021/ja010826g.

(38) Chiang, Y.; Kresget, A. J.; Zhu, Y. Reactive Intermediates. Some Chemistry of Quinone Methides. *Pure Appl. Chem.* **2000**, *72* (12), 2299–2308. https://doi.org/10.1351/pac200072122299.

(39) Chang, J. A.; Kresge, A. J.; Zhan, H. Q.; Zhu, Y. Flash Photolytic Generation and Study of P-Quinone α-Phenylmethide and p-Quinone α,α-Diphenylmethide in Aqueous Solution. *J. Phys. Org. Chem.* **2004**, *17* (6-7 SPEC.ISS.), 579–585. https://doi.org/10.1002/poc.767.

(40) Weinert, E. E.; Dondi, R.; Colloredo-melz, S.; Frankenfield, K. N.; Mitchell, C. H.; Freccero, M.; Rokita, S. E. Substituents on Quinone Methides Strongly Modulate Formation and Stability of Their Nucleophilic Adducts. **2006**, *128* (36), 11940–11947. https://doi.org/https://doi.org/10.1021/ja062948k.

(41) Doria, F.; Lena, A.; Bargiggia, R.; Freccero, M. Conjugation, Substituent, and Solvent Effects on the Photogeneration of Quinone Methides. *J. Org. Chem.* **2016**, *81* (9), 3665–3673. https://doi.org/10.1021/acs.joc.6b00331.

(42) Zeng, Q.; Rokita, S. E. Tandem Quinone Methide Generation for Cross-Linking DNA. *J. Org. Chem.* **1996**, *61* (26), 9080–9081. https://doi.org/10.1021/jo961864z.

(43) Škalamera, D.; Bohne, C.; Landgraf, S.; Basarić, N. Photodeamination Reaction Mechanism in Aminomethyl P-Cresol Derivatives: Different Reactivity of Amines and Ammonium Salts. *J. Org. Chem.* **2015**, *80* (21), 10817–10828. https://doi.org/10.1021/acs.joc.5b01991.

(44) Lena, A.; Benassi, A.; Stasi, M.; Saint-Pierre, C.; Freccero, M.; Gasparutto, D.; Bombard, S.; Doria, F.; Verga, D. Photoactivatable V-Shaped Bifunctional Quinone Methide Precursors as a New Class of Selective G-Quadruplex Alkylating Agents. *Chem. - A Eur. J.* **2022**, *28* (35). https://doi.org/10.1002/chem.202200734.

(45) Veljković, J.; Uzelac, L.; Molčanov, K.; Mlinarić-Majerski, K.; Kralj, M.; Wan, P.; Basarić, N. Sterically Congested Adamantylnaphthalene Quinone Methides. *J. Org. Chem.* **2012**, *77* (10), 4596–4610. https://doi.org/10.1021/jo3002479.

(46) Sambol, M.; Ester, K.; Landgraf, S.; Mihaljević, B.; Cindrić, M.; Kralj, M.; Basarić, N. Competing Photochemical Reactions of Bis-Naphthols and Their Photoinduced Antiproliferative Activity. *Photochem. Photobiol. Sci.* **2019**, *18* (5), 1197–1211. https://doi.org/10.1039/c8pp00532j.

(47) Škalamera, D.; Mlinarić-Majerski, K.; Martin-Kleiner, I.; Kralj, M.; Wan, P.; Basarić, N. Near-Visible Light Generation of a Quinone Methide from 3-Hydroxymethyl-2-Anthrol. *J. Org. Chem.* **2014**, *79* (10), 4390–4397. https://doi.org/10.1021/jo500290y.

(48) Škalamera, D.; Mlinarić-Majerski, K.; Martin Kleiner, I.; Kralj, M.; Oake, J.; Wan, P.; Bohne, C.; Basarić, N. Photochemical Formation of Anthracene Quinone Methide Derivatives. *J. Org. Chem.* **2017**, *82* (12), 6006–6021. https://doi.org/10.1021/acs.joc.6b02735.

(49) Uzelac, L.; Skalamera, Đ.; Mlinari, K.; Basari, N. Selective Photocytotoxicity of Anthrols on Cancer Stem-like Cells : The Effect of Quinone Methides or Reactive Oxygen Species. *Eur. J. Med. Chem.* **2017**, *137*, 558–574. https://doi.org/10.1016/j.ejmech.2017.05.063.

(50) Richter, S. N.; Maggi, S.; Mels, S. C.; Palumbo, M.; Freccero, M. Binol Quinone Methides as Bisalkylating and DNA Cross-Linking Agents. *J. Am. Chem. Soc.* **2004**, *126* (43), 13973–13979. https://doi.org/10.1021/ja047655a.

(51) Matsumoto, J.; Ishizu, M.; Kawano, R. I.; Hesaka, D.; Shiragami, T.; Hayashi, Y.; Yamashita, T.; Yasuda, M. Generation of Quinone Methide from Aminomethyl(Hydroxy)Arenes Precursors in Aqueous Solution. *Tetrahedron* **2005**, *61* (24), 5735–5740. https://doi.org/10.1016/j.tet.2005.04.037.

(52) Sutton, M. V.; McKinley, M.; Kulasekharan, R.; Popik, V. V. Photo-Cleavable Analog of BAPTA for the Fast and Efficient Release of Ca2+. *Chem. Commun.* **2017**, *53* (41), 5598–5601. https://doi.org/10.1039/c7cc02056b.

(53) Arumugam, S.; Orski, S. V.; Locklin, J.; Popik, V. V. Photoreactive Polymer Brushes for High-Density Patterned Surface Derivatization Using a Diels-Alder Photoclick Reaction. *J. Am. Chem. Soc.* **2012**, *134* (1), 179–182. https://doi.org/10.1021/ja210350d.

(54) Arumugam, S.; Guo, J.; Mbua, N. E.; Friscourt, F.; Lin, N.; Nekongo, E.; Boons,

G. J.; Popik, V. V. Selective and Reversible Photochemical Derivatization of Cysteine Residues in Peptides and Proteins. *Chem. Sci.* **2014**, *5* (4), 1591–1598. https://doi.org/10.1039/c3sc51691a.

(55) Sambol, M.; Benčić, P.; Erben, A.; Matković, M.; Mihaljević, B.; Piantanida, I.; Kralj, M.; Basarić, N. Photochemical Reactivity of Naphthol-Naphthalimide Conjugates and Their Biological Activity. *Molecules* **2021**, *26* (11). https://doi.org/10.3390/molecules26113355.

(56) Sambol, M.; Košćak, M.; Uzelac, L.; Kralj, M.; Piantanida, I.; Basarić, N. Simultaneous Staining of Endoplasmic Reticulum and Lipid Droplets by Naphthol-Aminonaphthalimide Conjugates and Photoinduced Antiproliferative Effects. *Dye. Pigment.* **2022**, *206* (August). https://doi.org/10.1016/j.dyepig.2022.110651.

(57) Chozinski, T. J.; Gagnon, L. A.; Vaughan, J. C. Twinkle, Twinkle Little Star: Photoswitchable Fluorophores for Super-Resolution Imaging. *FEBS Lett.* **2014**, *588* (19), 3603–3612. https://doi.org/10.1016/j.febslet.2014.06.043.

(58) Raymo, F. M. Photoactivatable Synthetic Dyes for Fluorescence Imaging at the Nanoscale. *J. Phys. Chem. Lett.* **2012**, *3* (17), 2379–2385. https://doi.org/10.1021/jz301021e.

(59) Raymo, F. M. Photoactivatable Synthetic Fluorophores. *Phys. Chem. Chem. Phys.* **2013**, *15* (36), 14840–14850. https://doi.org/10.1039/c3cp51822a.

(60) Jia, S.; Sletten, E. M. Spatiotemporal Control of Biology: Synthetic Photochemistry Toolbox with Far-Red and Near-Infrared Light. *ACS Chem. Biol.* **2021**. https://doi.org/10.1021/acschembio.1c00518.

(61) Gaur, P.; Kucherak, O. A.; Ermakova, Y. G.; Shvadchak, V. V.; Yushchenko, D. A. Nitrobenzyl-Based Fluorescent Photocages for Spatial and Temporal Control of Signalling Lipids in Cells. *Chem. Commun.* **2019**, *55* (82), 12288–12291. https://doi.org/10.1039/c9cc05602e.

(62) Bojtár, M.; Kormos, A.; Kis-Petik, K.; Kellermayer, M.; Kele, P. Green-Light Activatable, Water-Soluble Red-Shifted Coumarin Photocages. *Org. Lett.* **2019**, *21* (23), 9410–9414. https://doi.org/10.1021/acs.orglett.9b03624.

(63) Nekongo, E. E.; Popik, V. V. Photoactivatable Fluorescein Derivatives Caged with a (3-Hydroxy-2- Naphthalenyl)Methyl Group. *J. Org. Chem.* **2014**, *79* (16), 7665–7671. https://doi.org/10.1021/jo501116g.

(64) Kwon, J.; Hwang, J.; Park, J.; Han, G. R.; Han, K. Y.; Kim, S. K. RESOLFT Nanoscopy with Photoswitchable Organic Fluorophores. *Sci. Rep.* **2015**, *5*, 1–8. https://doi.org/10.1038/srep17804.

(65) Roubinet, B.; Weber, M.; Shojaei, H.; Bates, M.; Bossi, M. L.; Belov, V. N.; Irie, M.; Hell, S. W. Fluorescent Photoswitchable Diarylethenes for Biolabeling and Single-Molecule Localization Microscopies with Optical Superresolution. *J. Am. Chem. Soc.* **2017**, *139* (19), 6611–6620. https://doi.org/10.1021/jacs.7b00274.

(66) Jambeck, J.; Geyer, R.; Wilcox, C.; Siegler, T. R.; Perryman, M.; Andrady, A.; Narayan, R.; Law, K. L. Marine Pollution. Plastic Waste Inputs from Land into the Ocean. *Mar. Pollut.* **2015**, *347* (6223), 768-.

(67) A. F. Sousa, C. Vilela, M. Matos, C. S. R. Freire, A. J. D. Silvestre, F. J. C. Polyethylene Terephthalate: Copolyesters, Composites, and Renewable Alternatives. In *Poly(Ethylene Terephthalate) Based Blends, Composites and*

Nanocomposites; 2015; pp 113–141. https://doi.org/https://doi.org/10.1016/B978-0-323-31306-3.00007-5.

(68) Lambert, S.; Wagner, M. Environmental Performance of Bio-Based and Biodegradable Plastics: The Road Ahead. *Chem. Soc. Rev.* **2017**, *46* (22), 6855–6871. https://doi.org/10.1039/c7cs00149e.

(69) George, N.; Kurian, T. Recent Developments in the Chemical Recycling of Postconsumer Poly(Ethylene Terephthalate) Waste. *Ind. Eng. Chem. Res.* **2014**, *53* (37), 14185–14198. https://doi.org/10.1021/ie501995m.

(70) Ghosal, K.; Nayak, C. Recent Advances in Chemical Recycling of Polyethylene Terephthalate Waste into Value Added Products for Sustainable Coating Solutions – Hope vs . Hype . *Mater. Adv.* **2022**, *3* (4), 1974–1992. https://doi.org/10.1039/d1ma01112j.

(71) Alexander H. Tullo. Plastic Has a Problem; Is Chemistry the Solution? *C&EN Glob. Enterp.* **2019**, *97* (39), 29–34. https://doi.org/10.1021/cen-09739-cover.

(72) Yang, Y.; Lowry, M.; Xu, X.; Escobedo, J. O.; Sibrian-Vazquez, M.; Wong, L.; Schowalter, C. M.; Jensen, T. J.; Fronczek, F. R.; Warner, I. M.; Strongin, R. M. Seminaphthofluorones Are a Family of Water-Soluble, Low Molecular Weight, NIR-Emitting Fluorophores. *Proc. Natl. Acad. Sci. U. S. A.* **2008**, *105* (26), 8829–8834. https://doi.org/10.1073/pnas.0710341105.

(73) Brémond, É.; Alberto, M. E.; Russo, N.; Ricci, G.; Ciofini, I.; Adamo, C. Photophysical Properties of NIR-Emitting Fluorescence Probes: Insights from TD-DFT. *Phys. Chem. Chem. Phys.* **2013**, *15* (25), 10019–10027. https://doi.org/10.1039/c3cp43784a.

(74) Forest, K.; Wan, P.; Preston, C. M. Catechin and Hydroxybenzhydrols as Models for the Environmental Photochemistry of Tannins and Lignins. *Photochem. Photobiol. Sci.* **2004**, *3* (5), 463–472. https://doi.org/10.1039/b402241f.

(75) Kuhn, H. J.; Braslavsky, S. E.; Schmidt, R. Chemical Actinometry (IUPAC Technical Report). *Pure Appl. Chem.* **2004**, *76* (12), 2105–2146. https://doi.org/10.1351/pac200476122105.

(76) Osyanin, V. A.; Lukashenko, A. V.; Osipov, D. V. Cycloaddition Reactions of O-Quinone Methides with Polarized Olefins. *Russ. Chem. Rev.* **2021**, *90* (3), 324–373. https://doi.org/10.1070/rcr4971.

(77) Yang, B.; Gao, S. Recent Advances in the Application of Diels-Alder Reactions Involving o-Quinodimethanes, Aza-o-Quinone Methides and o-Quinone Methides in Natural Product Total Synthesis. *Chem. Soc. Rev.* **2018**, *47* (21), 7926–7953. https://doi.org/10.1039/c8cs00274f.

(78) Oelgemo, Michael; Mattay, Jochen; Gorner, H. Direct Photooxidation and Xanthene-Sensitized Oxidation of Naphthols : Quantum Yields. *J. Phys. Chem. A 2011* **2011**, *115*, 280–285. https://doi.org/10.1021/jp108832x.

(79) Brahmia, O.; Richard, C. Photochemical Transformation of 1-Naphthol in Aerated Aqueous Solution. *Photochem. Photobiol. Sci.* **2005**, *4*, 454–458. https://doi.org/10.1039/B504309C.

(80) Reddy, A. R.; Bendikov, M. Diels – Alder Reaction of Acenes with Singlet and Triplet Oxygen – Theoretical Study of Two-State Reactivity {. *Chem. Commun.* **2006**, 1179–1181. https://doi.org/10.1039/b513597d.

(81) Shvydkiv, O.; Limburg, C.; Nolan, K.; Oelgemo, M. Synthesis of Juglone (5-

Hydroxy-1 , 4-Naphthoquinone) in a Falling Film Microreactor. *J. Flow Chem.* **2012**, *2*, 52–55. https://doi.org/10.1556/jfchem.2012.00022.

(82) Murtinho, D.; Pineiro, M.; Pereira, M. M.; António, M.; Gonsalves, A. R.; Arnaut, L. G.; Miguel, G.; Burrows, H. D. Novel Porphyrins and a Chlorin as e Ffi Cient Singlet Oxygen Photosensitizers for Photooxidation of Naphthols or Phenols to Quinones. *J. Chem. Soc., Perkin Trans. 2*, **2000**, *2*, 2441–2447. https://doi.org/10.1039/b006583h.

(83) Uyanik, M.; Nishioka, K.; Kondo, R.; Ishihara, K. Chemoselective Oxidative Generation of Ortho-Quinone Methides and Tandem Transformations. *Nat. Chem.* **2020**, *12* (4), 353–362. https://doi.org/10.1038/s41557-020-0433-4.

(84) Mills, L. R.; Graham, J. M.; Patel, P.; Rousseaux, S. A. L. Ni-Catalyzed Reductive Cyanation of Aryl Halides and Phenol Derivatives via Transnitrilation. *J. Am. Chem. Soc.* **2019**, *141* (49), 19257–19262. https://doi.org/10.1021/jacs.9b11208.

(85) SUTTON, M. V. Quinone Methides: Multifunctional Tools for Chemical Biology and Material Science, 2019.

(86) Pei, J.; Hsu, C. C.; Wang, Y.; Yu, K. Corona Discharge-Induced Reduction of Quinones in Negative Electrospray Ionization Mass Spectrometry. *RSC Adv.* **2017**, *7* (69), 43540–43545. https://doi.org/10.1039/c7ra08523k.

(87) Fieser, M. The Reduction Potentials of Various Naphthoquinones. *J. Am. Chem. Soc.* **1935**, *57* (3), 491–494. https://doi.org/10.1021/ja01306a031.

(88) Olam, M. *PET : PRODUCTION , PROPERTIES AND APPLICATIONS*; Wythers, M. C., Ed.; nova science publishers: New York, 2022.

(89) Bråte, I. L.; Halsband, C.; Allan, I.; Thomas, K. V. *Report Made for the*

Norwegian Environment Agency : Microplastics in Marine Environments : Occurrence, Distribution and Effects; 2014.

(90) Jiang, Y.; Loos, K. Enzymatic Synthesis of Biobased Polyesters and Polyamides. *Polymers (Basel).* **2016**, *8* (7). https://doi.org/10.3390/polym8070243.

(91) R. J. Young and P. A. Lovell. *Introduction to Polymers*, Second edi.; 1981.

(92) Awaja, F.; Pavel, D. Recycling of PET. *Eur. Polym. J.* **2005**, *41* (7), 1453–1477. https://doi.org/10.1016/j.eurpolymj.2005.02.005.

(93) Kim, E. S.; Oh, H. J.; Kim, H. J.; Kim, C. G.; Park, S. Y.; Jeong, Y. G.; Hahm, W. G. Effect of Polycondensation Catalyst on Fiber Structure Development in High-Speed Melt Spinning of Poly (Ethylene Terephthalate). *Polymers (Basel).* **2019**, *11* (12). https://doi.org/10.3390/polym11121931.

(94) Pang, K.; Kotek, R.; Tonelli, A. Review of Conventional and Novel Polymerization Processes for Polyesters. *Prog. Polym. Sci.* **2006**, *31* (11), 1009–1037. https://doi.org/10.1016/j.progpolymsci.2006.08.008.

(95) Švec, P.; Hubená, P.; Růžičková, Z.; Holubová, J.; Pouzar, M.; Merna, J.; Růžička, A. Poly(Ethylene Terephthalate) Synthesis Catalysed by Chelated Sn, Zn and Mg Complexes. *Appl. Organomet. Chem.* **2016**, *30* (1), 20–25. https://doi.org/10.1002/aoc.3393.

(96) Stanica-Ezeanu, D.; Matei, D. Natural Depolymerization of Waste Poly(Ethylene Terephthalate) by Neutral Hydrolysis in Marine Water. *Sci. Rep.* **2021**, *11* (1), 1–7. https://doi.org/10.1038/s41598-021-83659-2.

(97) Chamas, A.; Moon, H.; Zheng, J.; Qiu, Y.; Tabassum, T.; Jang, J. H.; Abu-Omar, M.; Scott, S. L.; Suh, S. Degradation Rates of Plastics in the Environment. *ACS*

Sustain. Chem. Eng. **2020**, *8* (9), 3494–3511. https://doi.org/10.1021/acssuschemeng.9b06635.

(98) Koshti, R.; Mehta, L.; Samarth, N. Biological Recycling of Polyethylene Terephthalate: A Mini-Review. *J. Polym. Environ.* **2018**, *26* (8), 3520–3529. https://doi.org/10.1007/s10924-018-1214-7.

(99) Taniguchi, I.; Yoshida, S.; Hiraga, K.; Miyamoto, K.; Kimura, Y.; Oda, K. Biodegradation of PET: Current Status and Application Aspects. *ACS Catal.* **2019**, *9* (5), 4089–4105. https://doi.org/10.1021/acscatal.8b05171.

(100) Wu, X.; Galkin, M. V.; Stern, T.; Sun, Z.; Barta, K. Fully Lignocellulose-Based PET Analogues for the Circular Economy. *Nat. Commun.* **2022**, *13* (1), 1–12. https://doi.org/10.1038/s41467-022-30735-4.

(101) Kucherov, F. A.; Romashov, L. V.; Galkin, K. I.; Ananikov, V. P. Chemical Transformations of Biomass-Derived C6-Furanic Platform Chemicals for Sustainable Energy Research, Materials Science, and Synthetic Building Blocks. *ACS Sustain. Chem. Eng.* **2018**, *6* (7), 8064–8092. https://doi.org/10.1021/acssuschemeng.8b00971.

(102) Austin, H. P.; Allen, M. D.; Donohoe, B. S.; Rorrer, N. A.; Kearns, F. L.; Silveira, R. L.; Pollard, B. C.; Dominick, G.; Duman, R.; Omari, K. El; Mykhaylyk, V.; Wagner, A.; Michener, W. E.; Amore, A.; Skaf, M. S.; Crowley, M. F.; Thorne, A. W.; Johnson, C. W.; Lee Woodcock, H.; McGeehan, J. E.; Beckham, G. T. Characterization and Engineering of a Plastic-Degrading Aromatic Polyesterase. *Proc. Natl. Acad. Sci. U. S. A.* **2018**, *115* (19), E4350–E4357. https://doi.org/10.1073/pnas.1718804115.

(103) Winfield, D.; Ring, J.; Horn, J.; White, E. M.; Locklin, J. Semi-Aromatic Biobased Polyesters Derived from Lignin and Cyclic Carbonates. *Green Chem.* **2021**, *23* (23), 9658–9668. https://doi.org/10.1039/d1gc03135j.

(104) Subramaniyan, S.; Najjarzadeh, N.; Vanga, S. R.; Liguori, A.; Syrén, P. O.; Hakkarainen, M. Designed for Circularity: Chemically Recyclable and Enzymatically Degradable Biorenewable Schiff Base Polyester-Imines. *ACS Sustain. Chem. Eng.* **2022**. https://doi.org/10.1021/acssuschemeng.2c06935.

(105) Wang, P. Photolabile Protecting Groups : Structure and Reactivity. *Asian J. Org. Chem.* **2013**, *2*, 452–464. https://doi.org/10.1002/ajoc.201200197.

(106) Dunkel, P. Photoremovable Protecting Groups. *Encyclopedia* **2022**, *2*, 1225–1236.

(107) Kla, P.; Bochet, C. G.; Givens, R.; Rubina, M.; Popik, V.; Kostikov, A.; Wirz, J. Photoremovable Protecting Groups in Chemistry and Biology : Reaction Mechanisms and Efficacy. *Chem. Rev.* **2013**, *113*, 119–191.

(108) Zhao, H.; Sterner, E. S.; Coughlin, E. B.; Theato, P. O -Nitrobenzyl Alcohol Derivatives : Opportunities in Polymer and Materials Science. *Macromolecules* **2012**, *45*, 1723–1736. https://doi.org/dx.doi.org/10.1021/ma201924h.

(109) Romano, A.; Roppolo, I.; Rossegger, E.; Schlögl, S.; Sangermano, M. Recent Trends in Applying Ortho-Nitrobenzyl Esters for the Design of Photo-Responsive Polymer Networks. *Materials (Basel).* **2020**, *13* (12), 1–26. https://doi.org/10.3390/ma13122777.

(110) Arumugam, S.; Popik, V. V. Dual Reactivity of Hydroxy- and Methoxy-Substituted o-Quinone Methides in Aqueous Solutions: Hydration versus Tautomerization. *J. Org. Chem.* **2010**, *75* (21), 7338–7346.

https://doi.org/10.1021/jo101613t.

(111) Arumugam, S.; Popik, V. V. Light-Induced Hetero-Diels-Alder Cycloaddition: A Facile and Selective Photoclick Reaction. *J. Am. Chem. Soc.* **2011**, *133* (14), 5573–5579. https://doi.org/10.1021/ja200356f.

(112) Crouch, R, D. Selective Deprotection of Silyl Ethers. *Tetrahedron*. 2013, pp 2383–2417.

(113) Kostikov, A. P.; Popik, V. V. 2,5-Dihydroxybenzyl and (1,4-Dihydroxy-2-Naphthyl)Methyl, Novel Reductively Armed Photocages for the Hydroxyl Moiety. *J. Org. Chem.* **2007**, *72* (24), 9190–9194. https://doi.org/10.1021/jo701426j.

(114) Kostikov, A. P.; Malashikhina, N.; Popik, V. V. Caging of Carbonyl Compounds as Photolabile (2 , 5-Dihydroxyphenyl) Ethylene Glycol Acetals. *J. Org. Chem.* **2009**, *74*, 1802–1804. https://doi.org/10.1021/jo802612f.

(115) Zimmerman, H. E. The Meta Effect in Organic Photochemistry: Mechanistic and Exploratory Organic Photochemistry. *J. Am. Chem. Soc.* **1995**, *117* (35), 8988–8991. https://doi.org/10.1021/ja00140a014.

(116) Zimmerman, H. E. Meta-Ortho Effect in Organic Photochemistry: Mechanistic and Exploratory Organic Photochemistry. *J. Phys. Chem. A* **1998**, *102* (28), 5616–5621. https://doi.org/10.1021/jp9803182.

(117) Rieke, R. D.; Rich, W. E. Mechanistic Organic Photochemistry: Solvolytic Photochemical Reactions. *J. Am. Chem. Soc.* **1970**, *92* (25), 7349–7353. https://doi.org/10.1021/ja00728a018.

(118) Ding, X.; Wang, P. Photochemical Cleavage of Benzylic C-O Bond Facilitated by an Ortho or Meta Amino Group. *J. Org. Chem.* **2017**, *82* (14), 7309–7316.

https://doi.org/10.1021/acs.joc.7b00927.

(119) Škalamera, D.; Blažek Bregović, V.; Antol, I.; Bohne, C.; Basarić, N. Hydroxymethylaniline Photocages for Carboxylic Acids and Alcohols. *J. Org. Chem.* **2017**, *82* (23), 12554–12568. https://doi.org/10.1021/acs.joc.7b02314.

(120) Popr, M.; Hybelbauerová, S.; Jindřich, J. A Complete Series of 6-Deoxy-Monosubstituted Tetraalkylammonium Derivatives of α-, β-, and γ-Cyclodextrin with 1, 2, and 3 Permanent Positive Charges. *Beilstein J. Org. Chem.* **2014**, *10*, 1390–1396. https://doi.org/10.3762/bjoc.10.142.

(121) Borbas, K. E.; Mroz, P.; Hamblin, M. R.; Lindsey, J. S. Bioconjugatable Porphyrins Bearing a Compact Swallowtail Motif for Water Solubility. *Bioconjug. Chem.* **2006**, *17* (3), 638–653. https://doi.org/10.1021/bc050337w.

(122) Kim, H. T.; Kim, J. K.; Cha, H. G.; Kang, M. J.; Lee, H. S.; Khang, T. U.; Yun, E. J.; Lee, D. H.; Song, B. K.; Park, S. J.; Joo, J. C.; Kim, K. H. Biological Valorization of Poly(Ethylene Terephthalate) Monomers for Upcycling Waste PET. *ACS Sustain. Chem. Eng.* **2019**, *7* (24), 19396–19406. https://doi.org/10.1021/acssuschemeng.9b03908.

(123) Benyathiar, P.; Kumar, P.; Carpenter, G.; Brace, J.; Mishra, D. Polyethylene Terephthalate (PET) Bottle-to-Bottle Recycling for the Beverage Industry: A Review. *Polymers (Basel).* **2022**, *14* (12), 2366.

(124) Uekert, T.; Singh, A.; DesVeaux, J. S.; Ghosh, T.; Bhatt, A.; Yadav, G.; Afzal, S.; Walzberg, J.; Knauer, K. M.; Nicholson, S. R.; Beckham, G. T.; Carpenter, A. C. Technical, Economic, and Environmental Comparison of Closed-Loop Recycling Technologies for Common Plastics. *ACS Sustain. Chem. Eng.* **2022**.

https://doi.org/10.1021/acssuschemeng.2c05497.

(125) Biermann, L.; Brepohl, E.; Eichert, C.; Paschetag, M.; Watts, M.; Scholl, S. Development of a Continuous PET Depolymerization Process as a Basis for a Back-to-Monomer Recycling Method. *Green Process. Synth.* **2021**, *10* (1), 361–373. https://doi.org/10.1515/gps-2021-0036.

(126) Thiyagarajan, S.; Maaskant-Reilink, E.; Ewing, T. A.; Julsing, M. K.; Van Haveren, J. Back-to-Monomer Recycling of Polycondensation Polymers: Opportunities for Chemicals and Enzymes. *RSC Adv.* **2022**, *12* (2), 947–970. https://doi.org/10.1039/d1ra08217e.

(127) Yang, Y.; Yang, J.; Jiang, L. A Bacterium That Degrades and Assimilates Poly(Ethylene Terephthalate). *Science (80-.).* **2016**, *353* (6301), 759. https://doi.org/10.1126/science.aaf8305.

(128) Tournier, V.; Topham, C. M.; Gilles, A.; David, B.; Folgoas, C.; Moya-Leclair, E.; Kamionka, E.; Desrousseaux, M. L.; Texier, H.; Gavalda, S.; Cot, M.; Guémard, E.; Dalibey, M.; Nomme, J.; Cioci, G.; Barbe, S.; Chateau, M.; André, I.; Duquesne, S.; Marty, A. An Engineered PET Depolymerase to Break down and Recycle Plastic Bottles. *Nature* **2020**, *580* (7802), 216–219. https://doi.org/10.1038/s41586-020-2149-4.

(129) Urbanek, A. K.; Kosiorowska, K. E.; Mirończuk, A. M. Current Knowledge on Polyethylene Terephthalate Degradation by Genetically Modified Microorganisms. *Front. Bioeng. Biotechnol.* **2021**, *9* (November), 1–15. https://doi.org/10.3389/fbioe.2021.771133.

(130) Smith, R. L.; Takkellapati, S.; Riegerix, R. C. Recycling of Plastics in the United

States: Plastic Material Flows and Polyethylene Terephthalate (PET) Recycling Processes. *ACS Sustain. Chem. Eng.* **2022**, *10* (6), 2084–2096. https://doi.org/10.1021/acssuschemeng.1c06845.

(131) Fukushima, K.; Coady, D. J.; Jones, G. O.; Almegren, H. A.; Alabdulrahman, A. M.; Alsewailem, F. D.; Horn, H. W.; Rice, J. E.; Hedrick, J. L. Unexpected Efficiency of Cyclic Amidine Catalysts in Depolymerizing Poly(Ethylene Terephthalate). *J. Polym. Sci. Part A Polym. Chem.* **2013**, *51* (7), 1606–1611. https://doi.org/10.1002/pola.26530.

(132) Fukushima, K.; Lecuyer, J. M.; Wei, D. S.; Horn, H. W.; Jones, G. O.; Al-Megren, H. A.; Alabdulrahman, A. M.; Alsewailem, F. D.; McNeil, M. A.; Rice, J. E.; Hedrick, J. L. Advanced Chemical Recycling of Poly(Ethylene Terephthalate) through Organocatalytic Aminolysis. *Polym. Chem.* **2013**, *4* (5), 1610–1616. https://doi.org/10.1039/c2py20793a.

(133) Matsumura, S.; Hlil, A. R.; Lepiller, C.; Gaudet, J.; Guay, D.; Shi, Z.; Holdcroft, S.; Hay, A. S. Organocatalytic Depolymerization of Poly(Ethylene Terephthalate). *J. Polym. Sci. Part A Polym. Chem.* **2008**, *46* (April), 7207–7224. https://doi.org/10.1002/pola.

(134) Horn, H. W.; Jones, G. O.; Wei, D. S.; Fukushima, K.; Lecuyer, J. M.; Coady, D. J.; Hedrick, J. L.; Rice, J. E. Mechanisms of Organocatalytic Amidation and Trans-Esterification of Aromatic Esters as a Model for the Depolymerization of Poly(Ethylene) Terephthalate. *J. Phys. Chem. A* **2012**, *116* (51), 12389–12398. https://doi.org/10.1021/jp304212y.

(135) Allen, Robert David, Bajjuri, Krishna Mohan, Breyta, Gregory, Hedrick James

Lupton, Larson, C. E. Methods and Materials for Depolymerizing Polyesters. WO 2015/056377 Al, 2015.

(136) Wang, Z.; Jin, Y.; Wang, Y.; Tang, Z.; Wang, S.; Xiao, G.; Su, H. Cyanamide as a Highly Efficient Organocatalyst for the Glycolysis Recycling of PET. *ACS Sustain. Chem. Eng.* **2022**, *10* (24), 7965–7973. https://doi.org/10.1021/acssuschemeng.2c01235.

(137) Wang, Q.; Yao, X.; Tang, S.; Lu, X.; Zhang, X.; Zhang, S. Urea as an Efficient and Reusable Catalyst for the Glycolysis of Poly(Ethylene Terephthalate) Wastes and the Role of Hydrogen Bond in This Process. *Green Chem.* **2012**, *14* (9), 2559–2566. https://doi.org/10.1039/c2gc35696a.

(138) Ammer, J.; Baidya, M.; Kobayashi, S.; Mayr, H. Nucleophilic Reactivities of Tertiary Alkylamines. *J. Phys. Org. Chem.* **2010**, *23* (11), 1029–1035. https://doi.org/10.1002/poc.1707.

(139) Meyer, A. G.; Dai, L.; Chen, Q.; Easton, C. J.; Xia, L. Selective Adsorption of Nitro-Substituted Aromatics and Accelerated Hydrolysis of 4-Nitrophenyl Acetate on Carbon Surfaces. *New J. Chem.* **2001**, *25* (7), 887–889. https://doi.org/10.1039/b101963p.

(140) Whitaker, J. R. The Reaction of P-Nitrophenyl Acetate with Thiols. *J. Am. Chem. Soc.* **1962**, *84* (10), 1900–1904. https://doi.org/10.1021/ja01599a071.

(141) Schonbaum, G. R.; Bender, M. L. The Hydrolysis of P-Nitrophenyl Acetate Catalyzed by o-Mercaptobenzoic Acid. *J. Am. Chem. Soc.* **1960**, *82* (8), 1900–1904. https://doi.org/10.1021/ja01493a017.

(142) Ogilvie, J. W.; Tildon, J. T.; Strauch, B. S. A Kinetic Study of the Reaction of

Thiols with P-Nitrophenyl Acetale. *Biochemistry* **1964**, *3* (6), 754–758. https://doi.org/10.1021/bi00894a003.

(143) Node, M.; Kumar, K.; Nishide, K.; Ohsugi, S. I.; Miyamoto, T. Odorless Substitutes for Foul-Smelling Thiols: Syntheses and Applications. *Tetrahedron Lett.* **2001**, *42* (52), 9207–9210. https://doi.org/10.1016/S0040-4039(01)02024-X.

(144) Ilke Ugur, A. M. et. al. Rationalization of the PKa Values of Alcohols and Thiols Using Atomic Charge Descriptors and Its Application to the Prediction of Amino Acid PKa's. *J. Chem. Inf. Model. 2014*, **2014**, *54*, 2200–2213.

(145) Thapa, B.; Schlegel, H. B. Density Functional Theory Calculation of PKa's of Thiols in Aqueous Solution Using Explicit Water Molecules and the Polarizable Continuum Model. *J. Phys. Chem. A* **2016**, *120* (28), 5726–5735. https://doi.org/10.1021/acs.jpca.6b05040.

(146) Maria, B. P. De; Fini, A.; Hall, F. M. Thermodynamic Acid Dissociation Constants of Aromatic Thiols. *J. Chem. Soc., Perkin Trans. 2*, **1973**, 1971–1973. https://doi.org/DOI https://doi.org/10.1039/P29730001969.

(147) Moss, R. A.; Bizzigotti, G. O.; Huang, C. W. Nucleophilic Esterolytic and Displacement Reactions of a Micellar Thiocholine Surfactant. *J. Am. Chem. Soc.* **1980**, *102* (2), 754–762. https://doi.org/10.1021/ja00522a053.

(148) Fraga, E. R.; Schifino, J.; Gomez, I. Determination of Catalytic Coefficient for a First-Order Reaction an Undergraduate Physical Chemistry Experiment. *J. Chem. Educ.* **1975**, *52* (11), 749. https://doi.org/10.1021/ed052p749.

(149) Sardi, F.; Manta, B.; Portillo-Ledesma, S.; Knoops, B.; Comini, M. A.; Ferrer-Sueta, G. Determination of Acidity and Nucleophilicity in Thiols by Reaction with

Monobromobimane and Fluorescence Detection. *Anal. Biochem.* **2013**, *435* (1), 74–82. https://doi.org/10.1016/j.ab.2012.12.017.

(150) Mthembu, S. N.; Sharma, A.; Albericio, F. Breaking a Couple: Disulfide Reducing Agents. *ChemBioChem* **2020**, *21*, 1947–1954. https://doi.org/10.1002/cbic.202000092.

(151) Suich, D. J, Zuckermann, R. N. Fluorogenic Dyes.

(152) Silvester, K. S. P. & L. F. Thermodynamics of Electrolytes. VI. Weak Electrolytes Including H3PO4. *J. Solution Chem.* **1976**, *5*, 269–278. https://doi.org/https://doi.org/10.1007/BF00645465.

(153) A. K. Grzybowski. The Standard Potential of the Calomel Electrode and Its Application in Accurate Physicoehemical Measurements. I. The Standard Potential. *J. Phys. Chem.* **1958**, *62* (4), 550–555.

(154) Jr., H. S. H. and S. R. S. The Ionization Constant of HCO3- from 0 to 50°. *J. Am. Chem. Soc.* **1941**, *63* (6), 1706–1709. https://doi.org/https://doi.org/10.1021/ja01851a058.

(155) Lumme, Paavo; Lahermo, Pertti; Tummavuori, J. Thermodynamics of the Ionization of Hydroxylamine and Nitrous Acid in Water. *Acta Chem. Scand.* **1965**, *19*, 2175–2188. https://doi.org/10.3891/acta.chem.scand.19-2175.

(156) Grzybowski, A. K.; Weston, A. The Acid Dissociation Constant of the Protonated Form of Tri(Hydroxymethyl)Methylamine. *J. Chem. Soc.*, **1963**, 792–796. https://doi.org/https://doi.org/10.1039/JR9630000792.

(157) J. E. Ablard, D. S. McKinney, and J. C. W. The Conductance , Dissociation Constant and Heat of Dissociation of Triethylamine. *J. Am. Chem. Soc.* **1940**, *62*

(8), 2181–2183. https://doi.org/https://doi.org/10.1021/ja01865a075.

(158) Shirazimoghaddam, S.; Amin, I.; Faria Albanese, J. A.; Shiju, N. R. Chemical Recycling of Used PET by Glycolysis Using Niobia-Based Catalysts. *ACS Eng. Au* **2023**. https://doi.org/10.1021/acsengineeringau.2c00029.

(159) Yoshioka, T.; Motoki, T.; Okuwaki, A. Kinetics of Hydrolysis of Poly(Ethylene Terephthalate) Powder in Sulfuric Acid by a Modified Shrinking-Core Model. *Ind. Eng. Chem. Res.* **2001**, *40* (1), 75–79. https://doi.org/10.1021/ie000592u.

(160) Mishra, S.; Goje, A. S. Kinetic and Thermodynamic Study of Methanolysis of Poly(Ethylene Terephthalate) Waste Powder. *Polym. Int.* **2003**, *52* (3), 337–342. https://doi.org/10.1002/pi.1147.

(161) Du, J. T.; Sun, Q.; Zeng, X. F.; Wang, D.; Wang, J. X.; Chen, J. F. ZnO Nanodispersion as Pseudohomogeneous Catalyst for Alcoholysis of Polyethylene Terephthalate. *Chem. Eng. Sci.* **2020**, *220*, 115642. https://doi.org/10.1016/j.ces.2020.115642.

(162) Kurokawa, H.; Ohshima, M. A.; Sugiyama, K.; Miura, H. Methanolysis of Polyethylene Terephthalate (PET) in the Presence of Aluminium Tiisopropoxide Catalyst to Form Dimethyl Terephthalate and Ethylene Glycol. *Polym. Degrad. Stab.* **2003**, *79* (3), 529–533. https://doi.org/10.1016/S0141-3910(02)00370-1.

(163) Sanda, O.; Taiwo, E.; Osinkolu, G. Alkaline Solvolysis of Poly(Ethylene Terephthalate) in Butan–1–Ol Media: Kinetics and Optimization Studies. *Br. J. Appl. Sci. Technol.* **2017**, *21* (5), 1–12. https://doi.org/10.9734/bjast/2017/32597.

(164) Liu, S.; Wang, Z.; Li, L.; Yu, S.; Xie, C.; Liu, F. Butanol Alcoholysis Reaction of Polyethylene Terephthalate Using Acidic Ionic Liquid as Catalyst. *J. Appl. Polym.*

Sci. **2013**, *130* (3), 1840–1844. https://doi.org/10.1002/app.39246.

(165) Hayyan, a; Alam, M. Z.; Mirghani, M E S., Kabbashi, N A., Hakimi, N I N M., Siran, Y M., Tahiruddin, S. Production of Biodiesel from Sludge Palm Oil by Esterification Process. *Energy power Eng.* **2010**, *4* (1), 11–17.

(166) Oku, A.; Hu, L. C.; Yamada, E. Alkali Decomposition of Poly(Ethylene Terephthalate) with Sodium Hydroxide in Nonaqueous Ethylene Glycol: A Study on Recycling of Terephthalic Acid and Ethylene Glycol. *J. Appl. Polym. Sci.* **1997**, *63* (5), 595–601. https://doi.org/10.1002/(SICI)1097-4628(19970131)63:5<595::AID-APP7>3.0.CO;2-P.

(167) Sanda, O., Taiwo, E. A. et al. A Study of the Alkaline Solvolysis of Postconsumer Polyethylene Terephthalate A Study of the Alkaline Solvolysis of Postconsumer Polyethylene Terephthalate in Primary C 1 – C 3 Aliphatic Alcohols. *Am. Chem. Sci. J.* **2016**, *16* (1), 1–14. https://doi.org/10.9734/ACSJ/2016/27697.

(168) Rubio Arias, J. J.; Thielemans, W. Instantaneous Hydrolysis of PET Bottles: An Efficient Pathway for the Chemical Recycling of Condensation Polymers. *Green Chem.* **2021**, *23* (24), 9945–9956. https://doi.org/10.1039/d1gc02896k.

(169) Javed, S.; Fisse, J.; Vogt, D. Optimization and Kinetic Evaluation for Glycolytic Depolymerization of Post-Consumer PET Waste with Sodium Methoxide. *Polymers (Basel).* **2023**, *15* (3). https://doi.org/10.3390/polym15030687.

(170) Štrukil, V. Highly Efficient Solid-State Hydrolysis of Waste Polyethylene Terephthalate by Mechanochemical Milling and Vapor-Assisted Aging. *ChemSusChem* **2021**, *14* (1), 330–338. https://doi.org/10.1002/cssc.202002124.

(171) Yan, X. 2018_Pnas_Si_Spe. *Proc. Natl. Acad. Sci.* **2017**, 2017.

https://doi.org/10.1073/pnas.

(172) Joo, S.; Cho, I. J.; Seo, H.; Son, H. F.; Sagong, H. Y.; Shin, T. J.; Choi, S. Y.; Lee, S. Y.; Kim, K. J. Structural Insight into Molecular Mechanism of Poly(Ethylene Terephthalate) Degradation. *Nat. Commun.* **2018**, *9* (1). https://doi.org/10.1038/s41467-018-02881-1.

(173) Son, H. F.; Cho, I. J.; Joo, S.; Seo, H.; Sagong, H. Y.; Choi, S. Y.; Lee, S. Y.; Kim, K. J. Rational Protein Engineering of Thermo-Stable PETase from Ideonella Sakaiensis for Highly Efficient PET Degradation. *ACS Catal.* **2019**, *9* (4), 3519–3526. https://doi.org/10.1021/acscatal.9b00568.

(174) Zhong-Johnson, E. Z. L.; Voigt, C. A.; Sinskey, A. J. An Absorbance Method for Analysis of Enzymatic Degradation Kinetics of Poly(Ethylene Terephthalate) Films. *Sci. Rep.* **2021**, *11* (1), 1–9. https://doi.org/10.1038/s41598-020-79031-5.

(175) Kandasamy, S.; Subramaniyan, A.; Ramasamy, G.; Ahamed, A. R.; Manickam, N.; Dhandapani, B. Study of Alkaline Hydrolysis of Post Consumed Polyethylene Terephthalate Waste. *AIP Conf. Proc.* **2020**, *2240* (May). https://doi.org/10.1063/5.0011020.

(176) Essaddam A.; Essaddam F. Terephthalic Acid Ester Formation. US10252976B1, 2019.

(177) Liu, B.; Lu, X.; Ju, Z.; Sun, P.; Xin, J.; Yao, X.; Zhou, Q.; Zhang, S. Ultrafast Homogeneous Glycolysis of Waste Polyethylene Terephthalate via a Dissolution-Degradation Strategy. *Ind. Eng. Chem. Res.* **2018**, *57* (48), 16239–16245. https://doi.org/10.1021/acs.iecr.8b03854.

(178) Guclu, G.; Kasgoz, A.; Ozbudak, S.; Ozgumus, S.; Orbay, M. Glycolysis of Poly

(Ethylene Terephthalate) Wastes in Xylene. *J. Appl. Polym. Sci.* **1998**, *69* (12), 2311–2319. https://doi.org/10.1002/(SICI)1097-4628(19980919)69:12<2311::AID-APP2>3.0.CO;2-B.

(179) Sharma, V.; Parashar, P.; Srivastava, P.; Kumar, S.; Agarwal, D. D.; Richharia, N. Recycling of Waste PET-Bottles Using Dimethyl Sulfoxide and Hydrotalcite Catalyst. *J. Appl. Polym. Sci.* **2013**, *129* (3), 1513–1519. https://doi.org/10.1002/app.38829.

(180) Pulido, B. A.; Habboub, O. S.; Aristizabal, S. L.; Szekely, G.; Nunes, S. P. Recycled Poly(Ethylene Terephthalate) for High Temperature Solvent Resistant Membranes. *ACS Appl. Polym. Mater.* **2019**, *1* (9), 2379–2387. https://doi.org/10.1021/acsapm.9b00493.

APPENDICES

A Pseudo First-Order Rate Constants for Quenching Kinetics of QMPs

Table A.1. Decay of o-NQM 1 photogenerated from QMP 1 (0.033 mM) in dilute aqueous phosphate buffer (pH 7.04) containing various concentrations of 2-mercaptoethylamine hydrochloride (Thiol) at 25 ^{0}C.

[Thiol] M	**k_{Obs} s^{-1}**		
	Trial 1	**Trial 2**	**Trial 3**
0.005	141	132	133
0.00575	208	208	197
0.0075	334	326	334
0.0085	364	370	380
0.01	485	477	479

Table A.2. Decay of o-NQM 1 photogenerated from QMP 1 (0.033 mM) in dilute aqueous phosphate buffer (pH 7.04) containing various concentrations of sodium azide at 25 ^{0}C.

[Sodium azide] M	**k_{Obs} s^{-1}**		
	Trial 1	**Trial 2**	**Trial 3**
0.01	14.4	14.4	15.2

0.025	58.8	56.0	58.0
0.04	103	99.0	104
0.05	124	122	117
0.06	158	158	153
0.0675	170	168	174

Table A.3. Decay of o-NQM 1 photogenerated from QMP 1 (0.033 mM) in dilute aqueous phosphate buffer (pH 7.04) containing various concentrations of ethyl vinyl ether (EVE) at 25 ^{0}C.

[EVE] M	**k_{Obs} s^{-1}**		
	Trial 1	**Trial 2**	**Trial 3**
0.01	0.051	0.05	0.056
0.025	0.059	0.063	0.061
0.03	0.092	0.082	0.080
0.05	0.115	0.109	115
0.0725	0.138	0.135	0.144
0.09	0.165	0.174	0.188

Table A.4. Decay of p-QM 3 photogenerated from QMP 3 (0.2 mM) in dilute aqueous phosphate buffer (pH7.04) containing various concentrations of 2-mercaptoethylamine hydrochloride (Thiol) at 25 ^{0}C.

[Thiol] M	**k_{Obs} s^{-1}**		
	Trial 1	**Trial 2**	**Trial 3**
0	0.00917	0.0099	0.00968
0.0005	0.01872	0.01642	0.01454
0.001	0.02105	0.02068	0.02133
0.0015	0.03362	0.03332	0.03362
0.002	0.03909	0.04387	0.04376

Table A.5. Decay of p-QM 3 photogenerated from QMP 3 (0.2 mM) in dilute aqueous phosphate buffer (pH 7.04) containing various concentrations of sodium azide at 25 ^{0}C.

[Sodium azide] M	**k_{Obs} s^{-1}**		
	Trial 1	**Trial 2**	**Trial 3**
0	0.00917	0.0099	0.00968
0.002	001731	0.017	0.01731
0.00265	0.023	0.02295	0.02409
0.005	0.04183	0.0423	0.041
0.007	0.0607	0.061	0.062

Table A.6. Decay of p-QM 3 photogenerated from QMP 3 (0.2 mM) in dilute aqueous phosphate buffer (pH 7.04) containing various concentrations of ethyl vinyl ether (EVE) at 25 ^{0}C.

[EVE] M	**k_{Obs} s^{-1}**		
	Trial 1	**Trial 2**	**Trial 3**
0	0.00917	0.0099	0.00968
0.005	0.00877	0.00833	0.00853
0.0075	0.00935	0.00979	0.01
0.015	0.009	0.00918	0.0099

B Polymer Mass Spectra

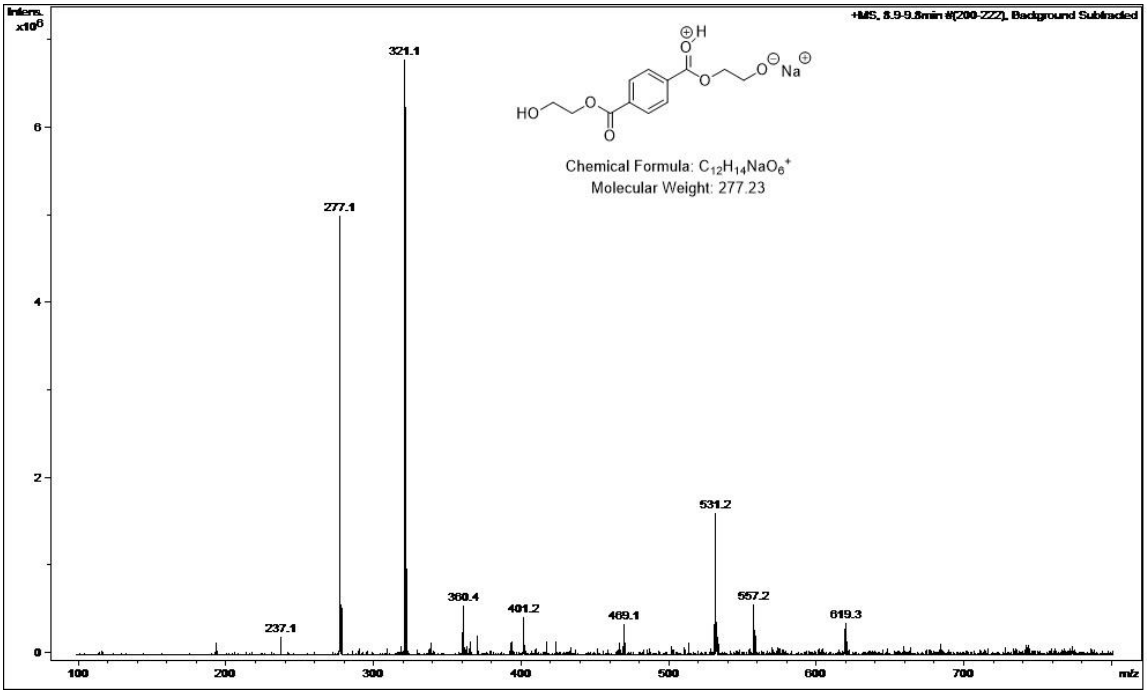

Figure B.1. ESI-MS of BHET.

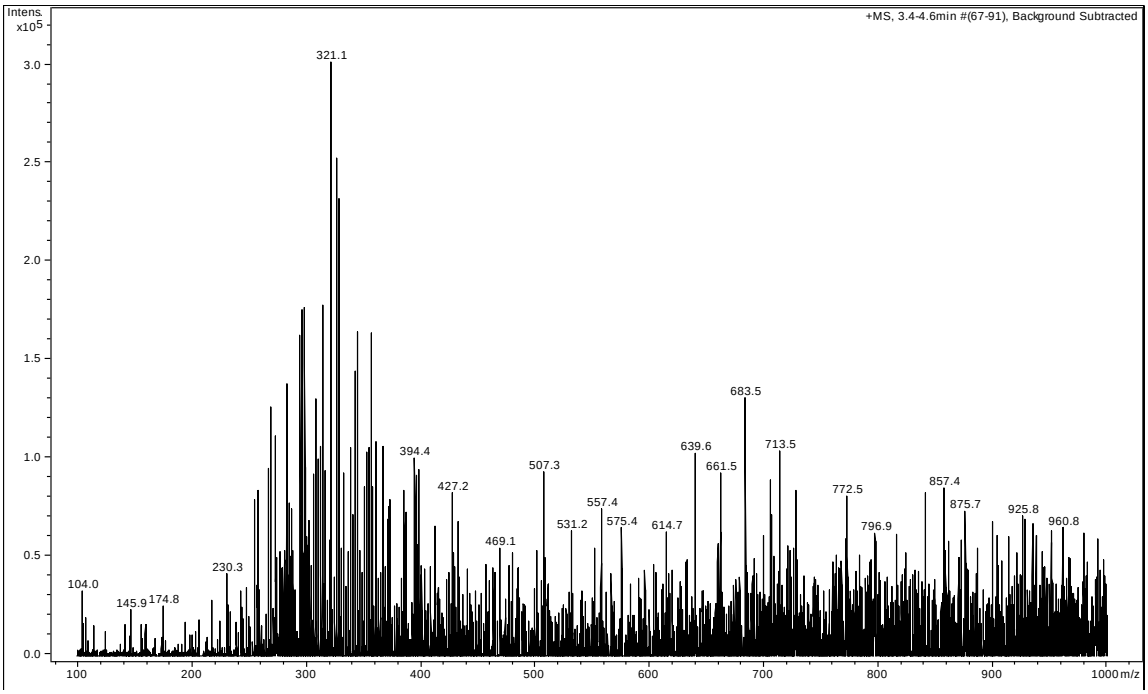

Figure B.2. ESI-MS of reaction mixture: BHET, EG, oNQMP monomer (Section 3.6.2).

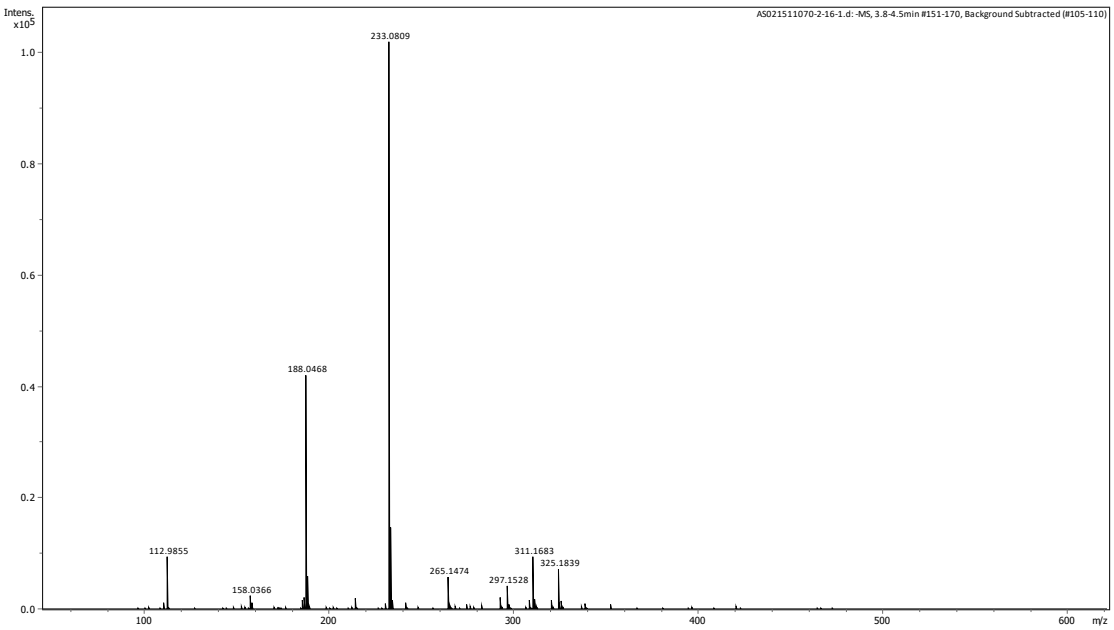

Figure B.3. HR-MS of oNQMP monomer.

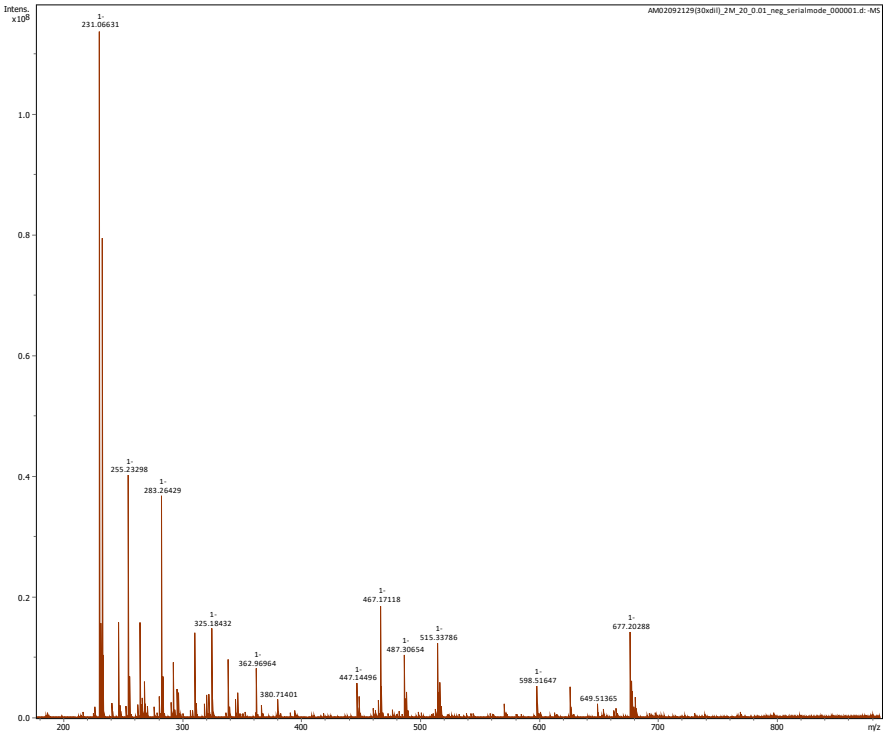

Figure B.4. HR-MS of oNQMP monomer solid state heating (Section 3.6.2).

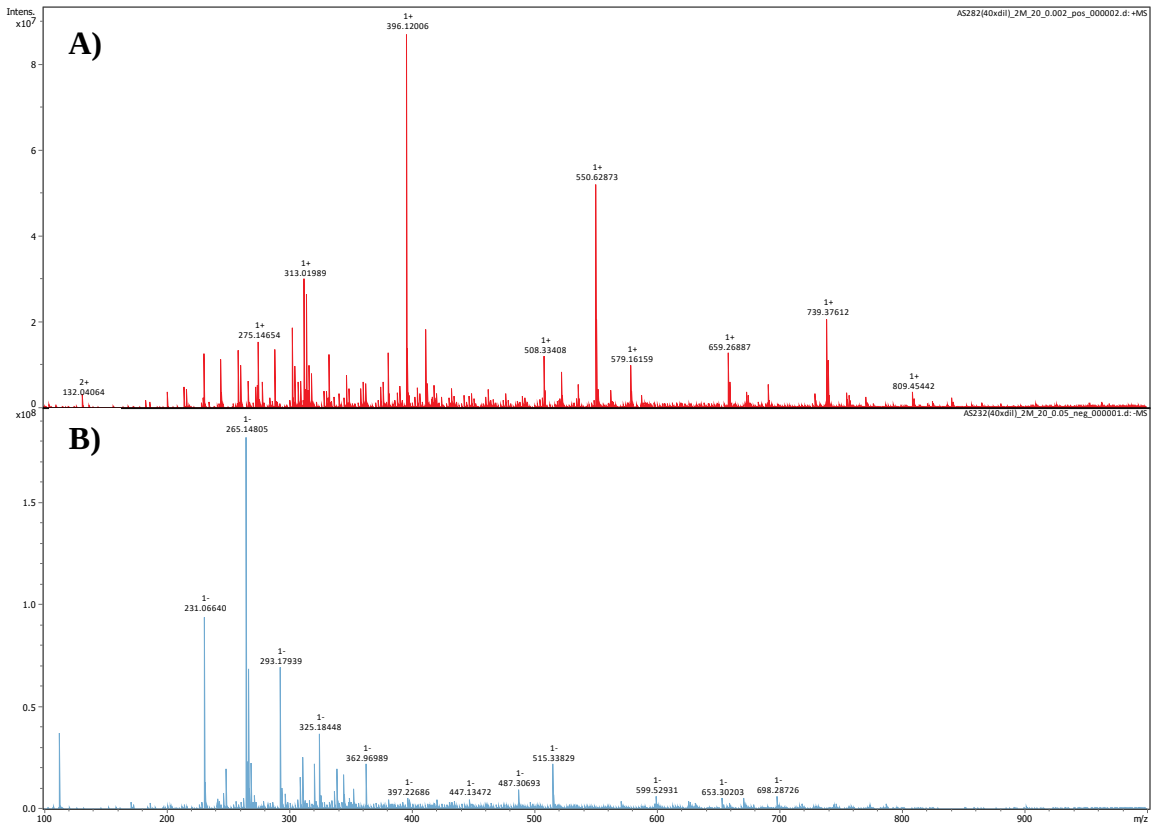

Figure B.5. MALDI-TOF of oNQMP monomer solid state heating (Section 3.6.2): A) Positive mode, B) negative mode.

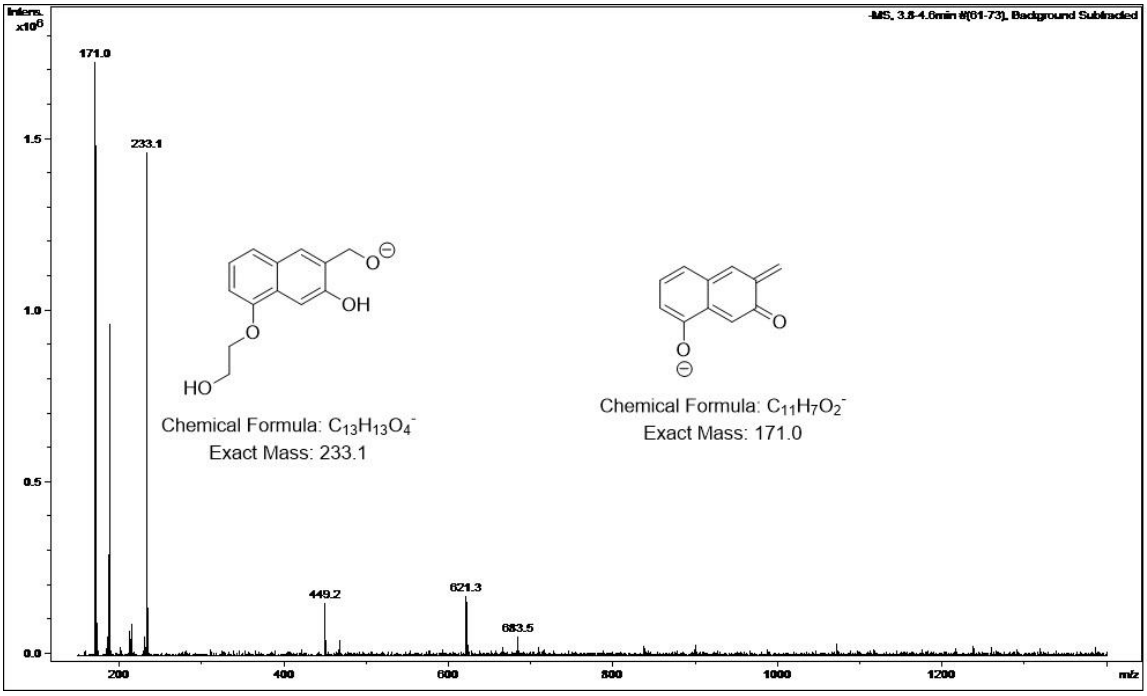

Figure B. 6. ESI-MS full spectrum oNQMP monomer heated in THF with pTSA catalyst.

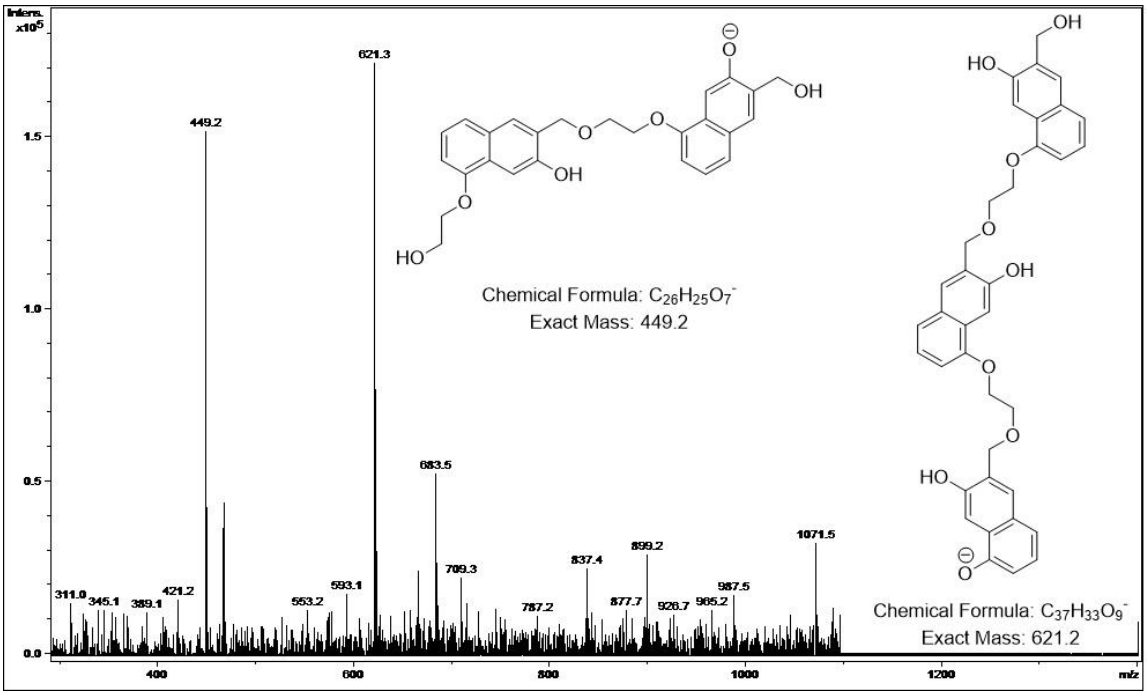

Figure B. 7. ESI-MS zoomed spectrum oNQMP monomer heated in THF with pTSA catalyst.

C ^{1}H AND ^{13}C NMR Spectra

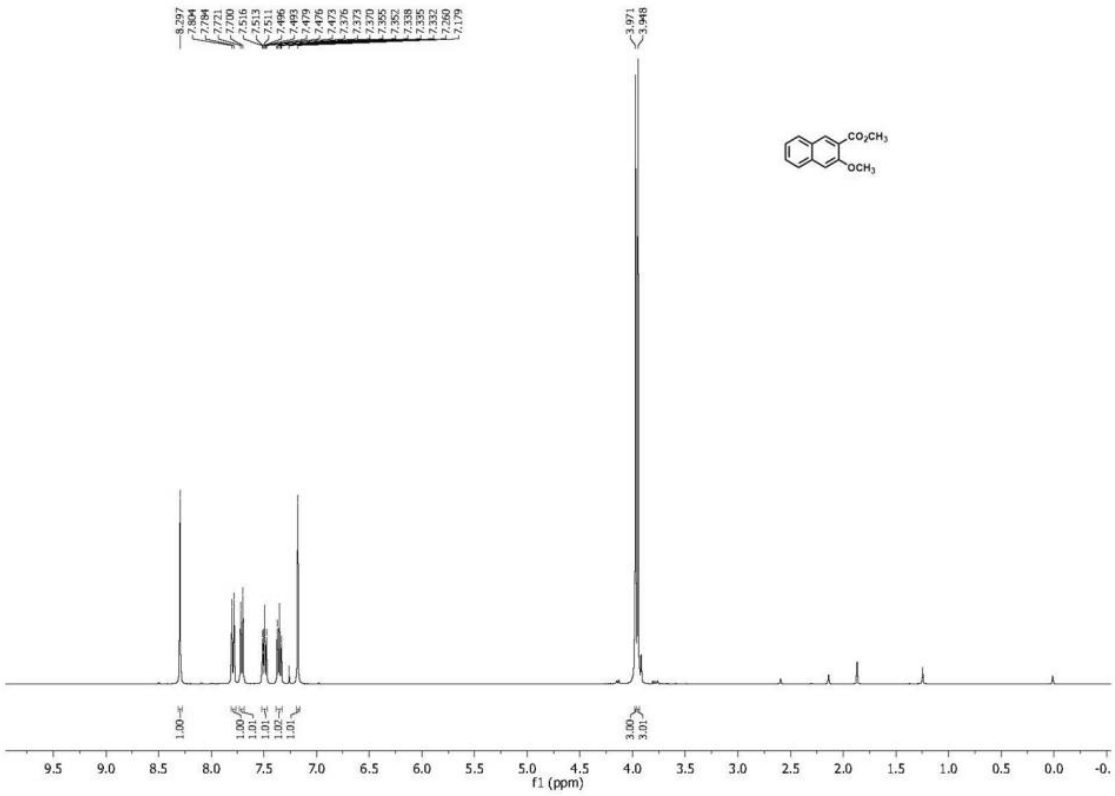

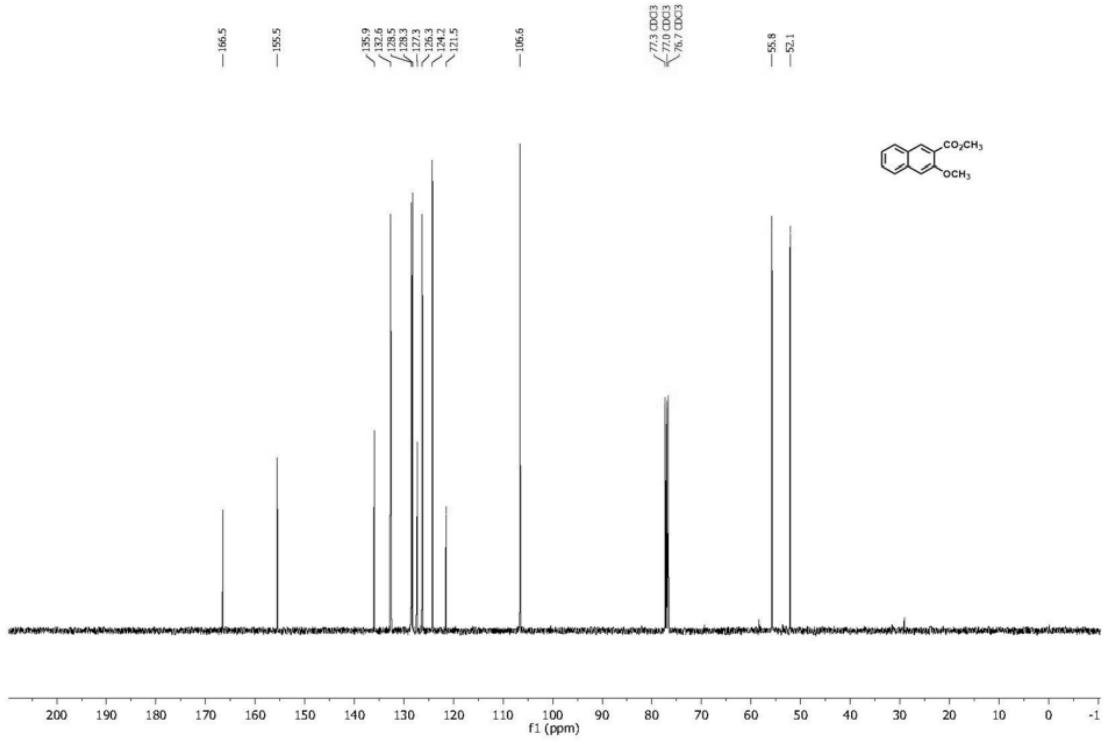
166.5
155.5
135.9
132.6
128.5
128.3
127.3
126.3
124.2
121.5
106.6
77.3 CDCl3
77.0 CDCl3
76.7 CDCl3
55.8
52.1
CO2CH3
OCH3
f1 (ppm)

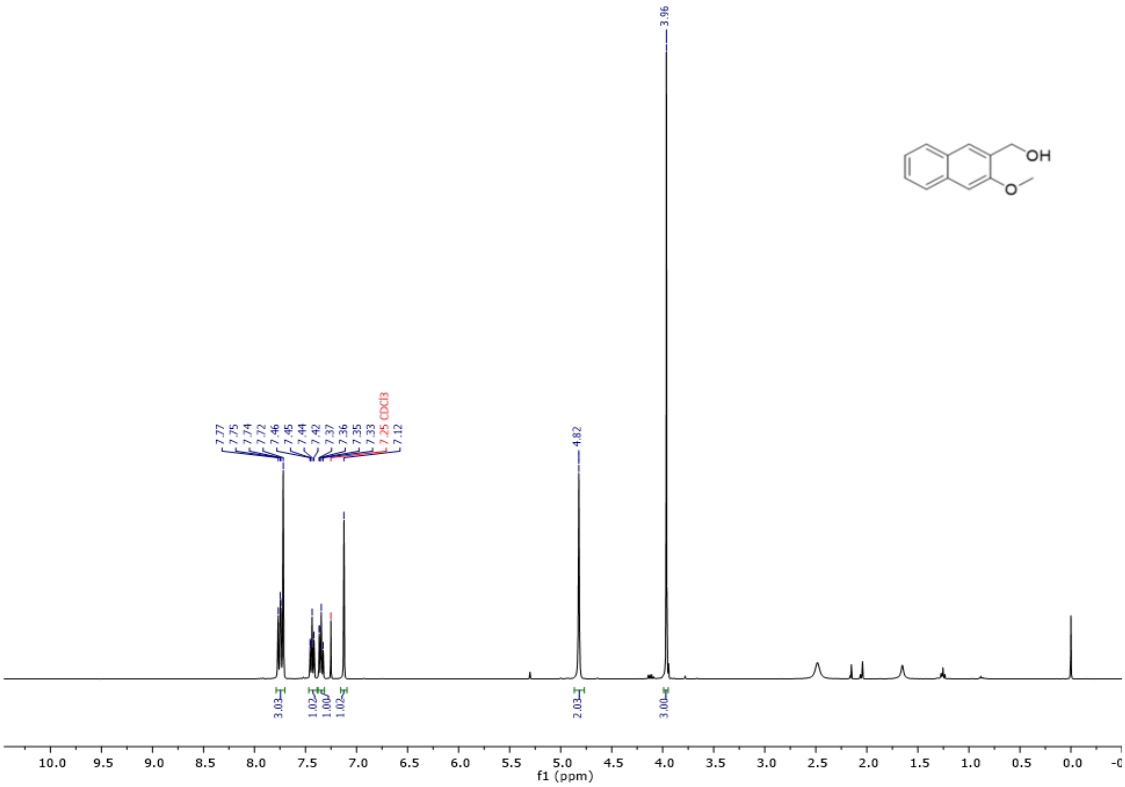
3.96
7.77
7.75
7.74
7.72
7.46
7.45
7.44
7.42
7.37
7.36
7.35
7.33
7.25 CDCl3
7.12
4.82
OH
3.03
1.02
1.00
1.02
2.03
3.00
f1 (ppm)

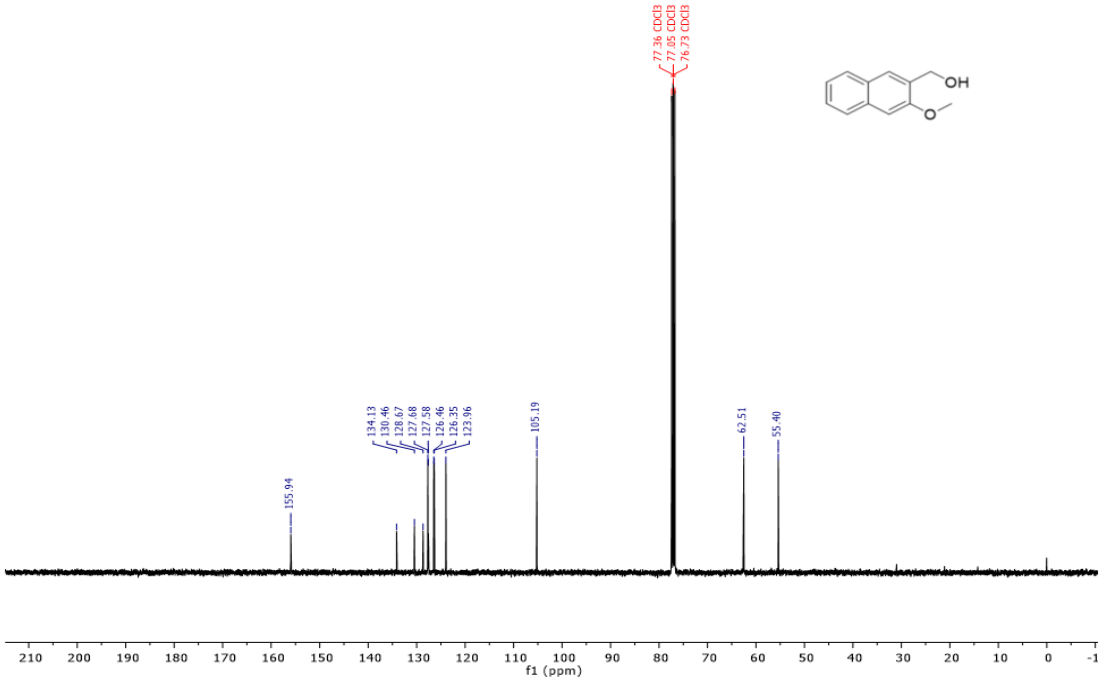
77.36 CDCl3
77.05 CDCl3
76.73 CDCl3
OH
O
134.13
130.46
128.67
127.68
127.58
126.46
126.35
123.96
155.94
105.19
62.51
55.40
f1 (ppm)

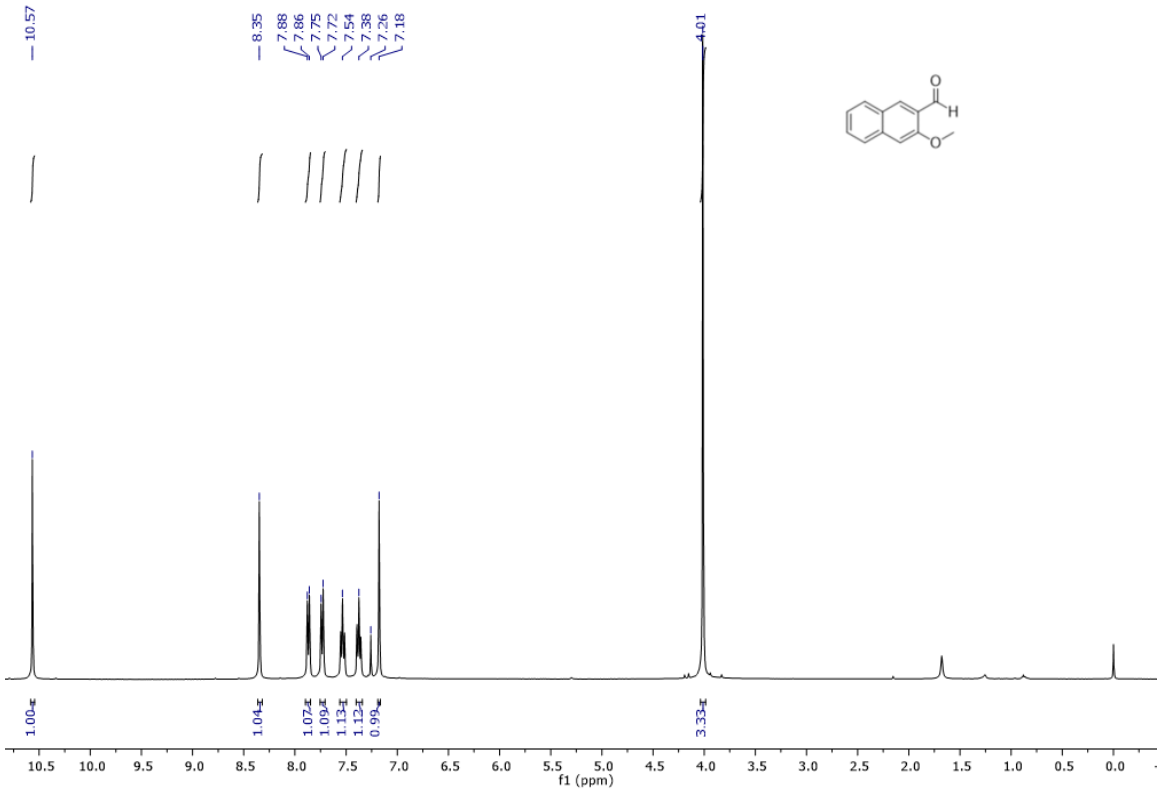
10.57
8.35
7.88
7.86
7.75
7.72
7.54
7.38
7.26
7.18
4.01
O
H
O
1.00
1.04
1.07
1.09
1.13
1.12
0.99
3.33
f1 (ppm)

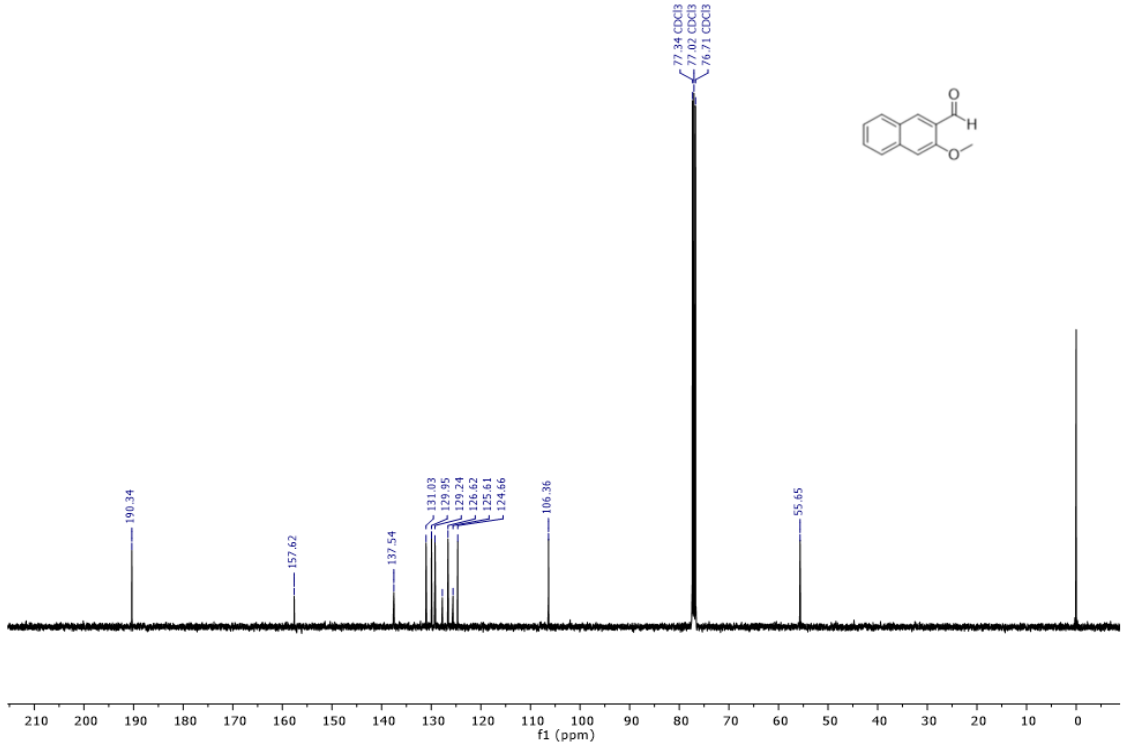
77.34 CDCl3
77.02 CDCl3
76.71 CDCl3
O
H
O
190.34
157.62
137.54
131.03
129.95
129.24
126.62
125.61
124.66
106.36
55.65
210 200 190 180 170 160 150 140 130 120 110 100 90 80 70 60 50 40 30 20 10 0
f1 (ppm)

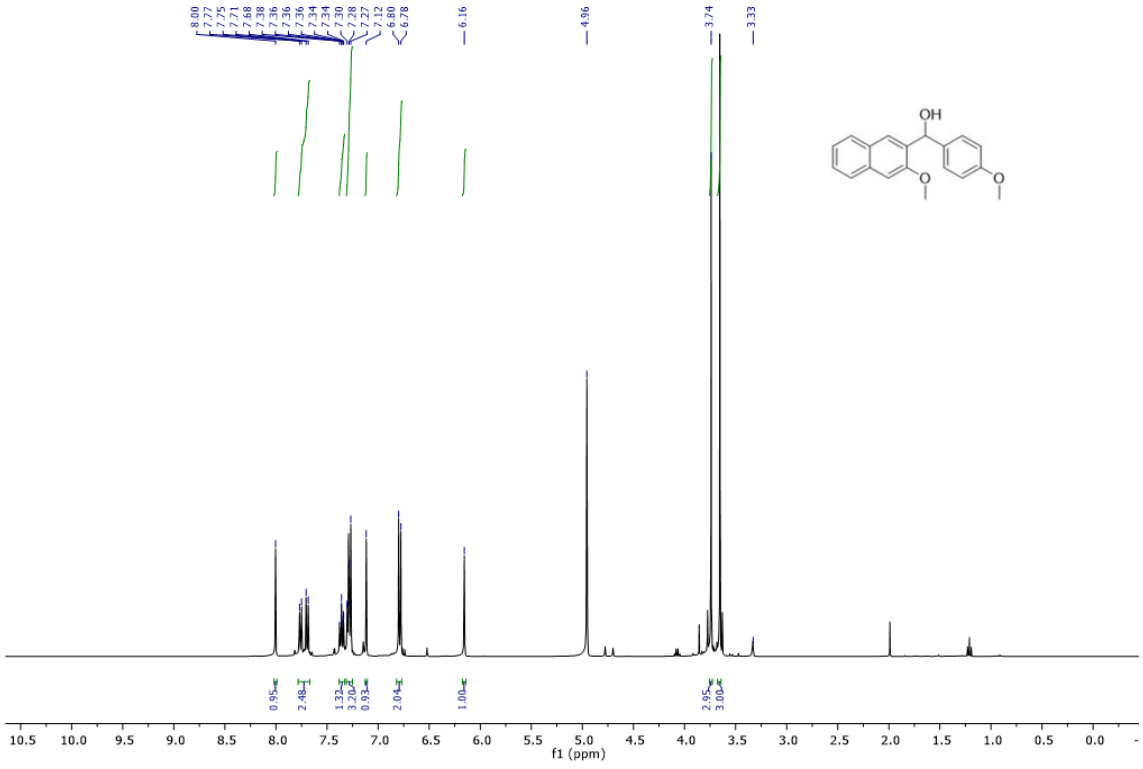
8.00
7.77
7.75
7.71
7.68
7.38
7.36
7.36
7.36
7.34
7.30
7.28
7.27
7.12
6.80
6.78
6.16
4.96
3.74
3.33
OH
O
O
0.95
2.48
1.32
3.20
0.93
2.04
1.00
2.95
3.00
10.5 10.0 9.5 9.0 8.5 8.0 7.5 7.0 6.5 6.0 5.5 5.0 4.5 4.0 3.5 3.0 2.5 2.0 1.5 1.0 0.5 0.0
f1 (ppm)

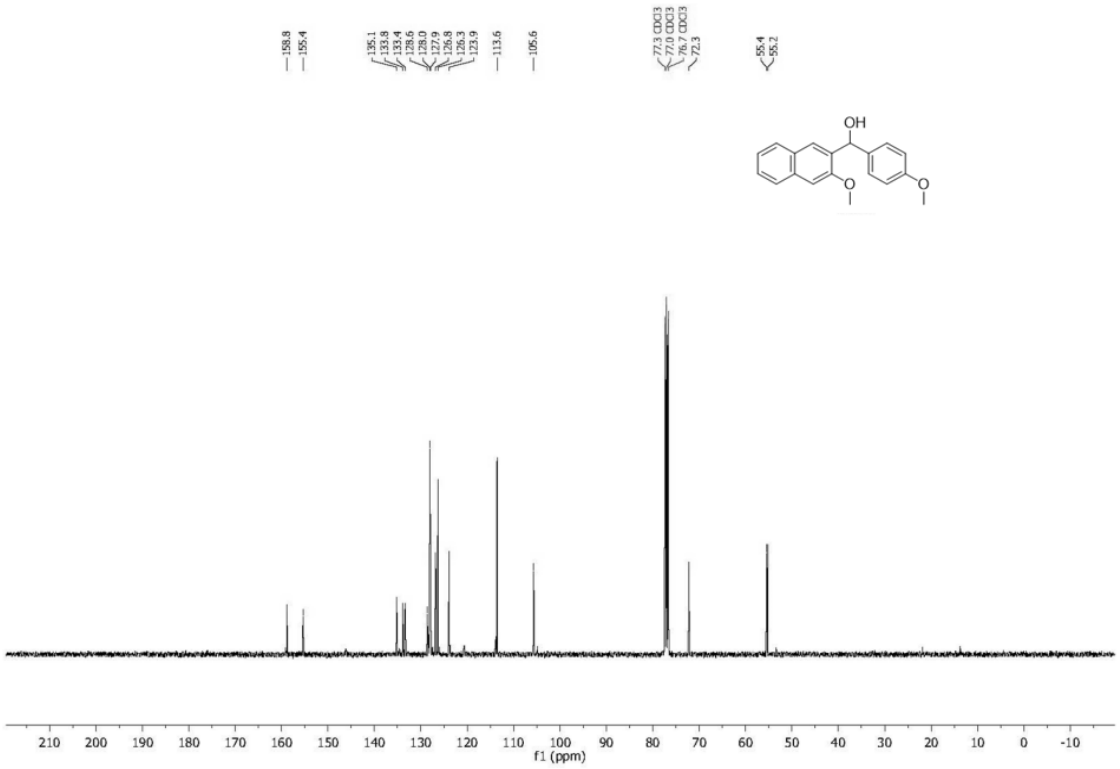
158.8
155.4
135.1
133.8
133.4
128.6
128.0
127.9
126.8
126.3
123.9
113.6
105.6
77.3 CDCl3
77.0 CDCl3
76.7 CDCl3
72.3
55.4
55.2
OH
O
O
f1 (ppm)

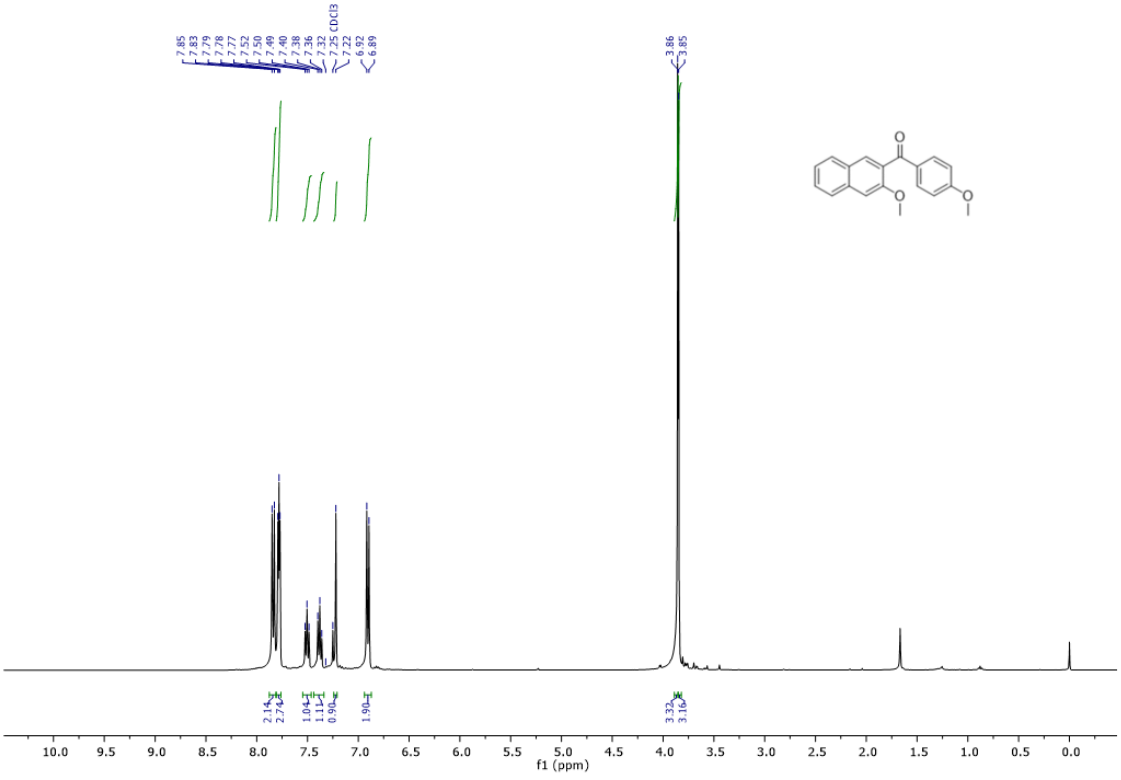
7.85
7.83
7.79
7.78
7.77
7.52
7.50
7.49
7.40
7.38
7.36
7.32
7.25 CDCl3
7.22
6.82
6.80
3.86
3.85
O
O
O
2.14
2.74
1.04
1.11
0.90
1.90
3.32
3.16
f1 (ppm)

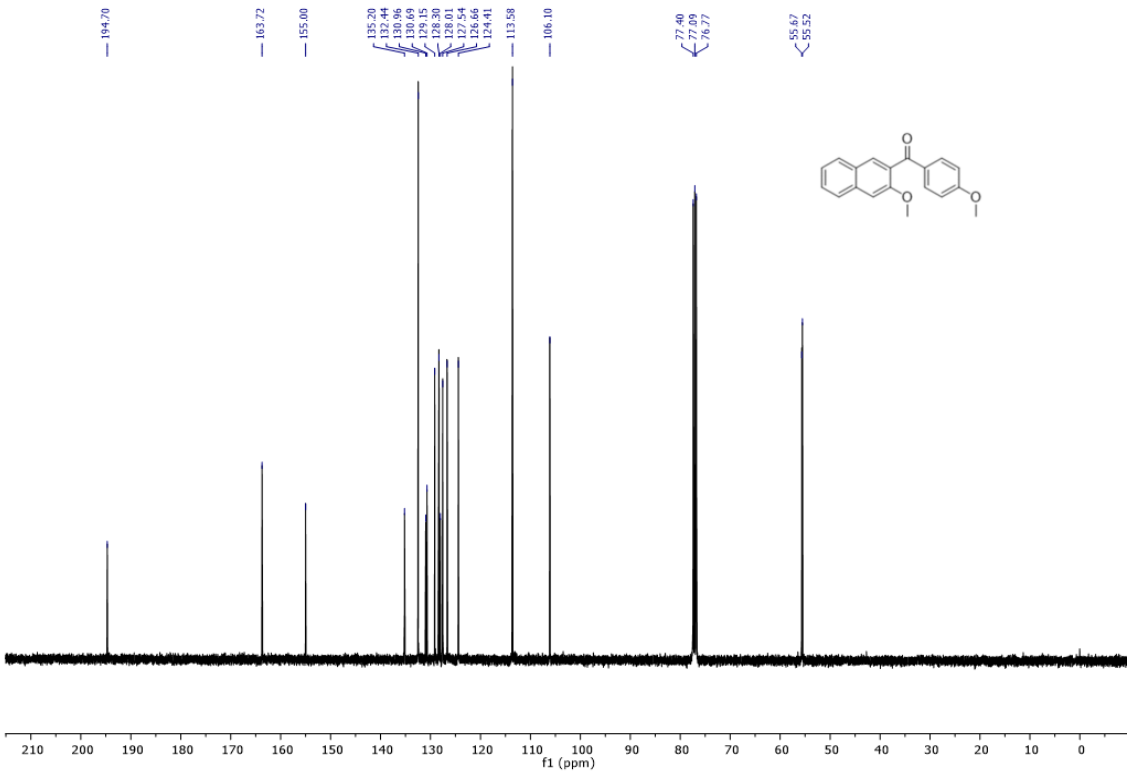
194.70
163.72
155.60
135.20
132.44
130.96
130.69
129.15
128.30
128.01
127.54
126.66
124.41
113.58
106.10
77.40
77.09
76.77
55.67
55.52
O
O
O
f1 (ppm)

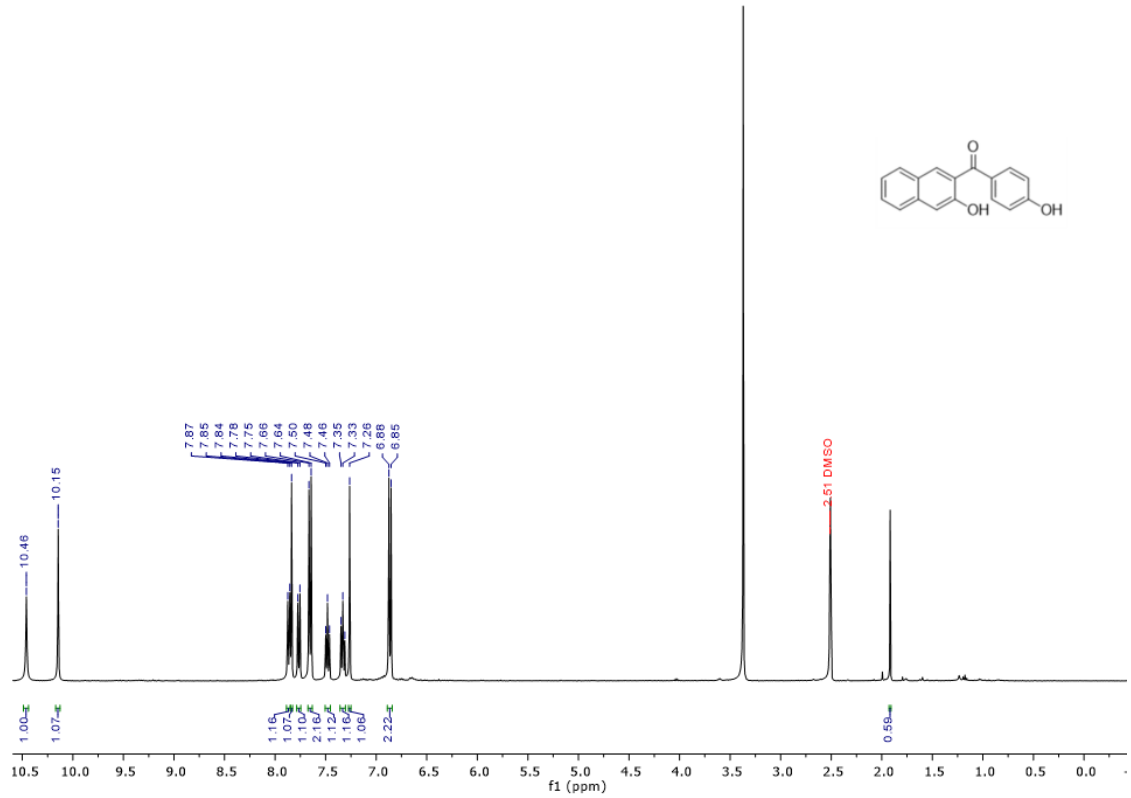
10.46
10.15
7.87
7.85
7.84
7.78
7.75
7.66
7.64
7.50
7.48
7.46
7.35
7.33
7.26
6.88
6.85
2.51 DMSO
O
OH
OH
1.00
1.07
1.16
1.07
1.10
2.16
1.12
1.16
1.06
2.22
0.59
f1 (ppm)

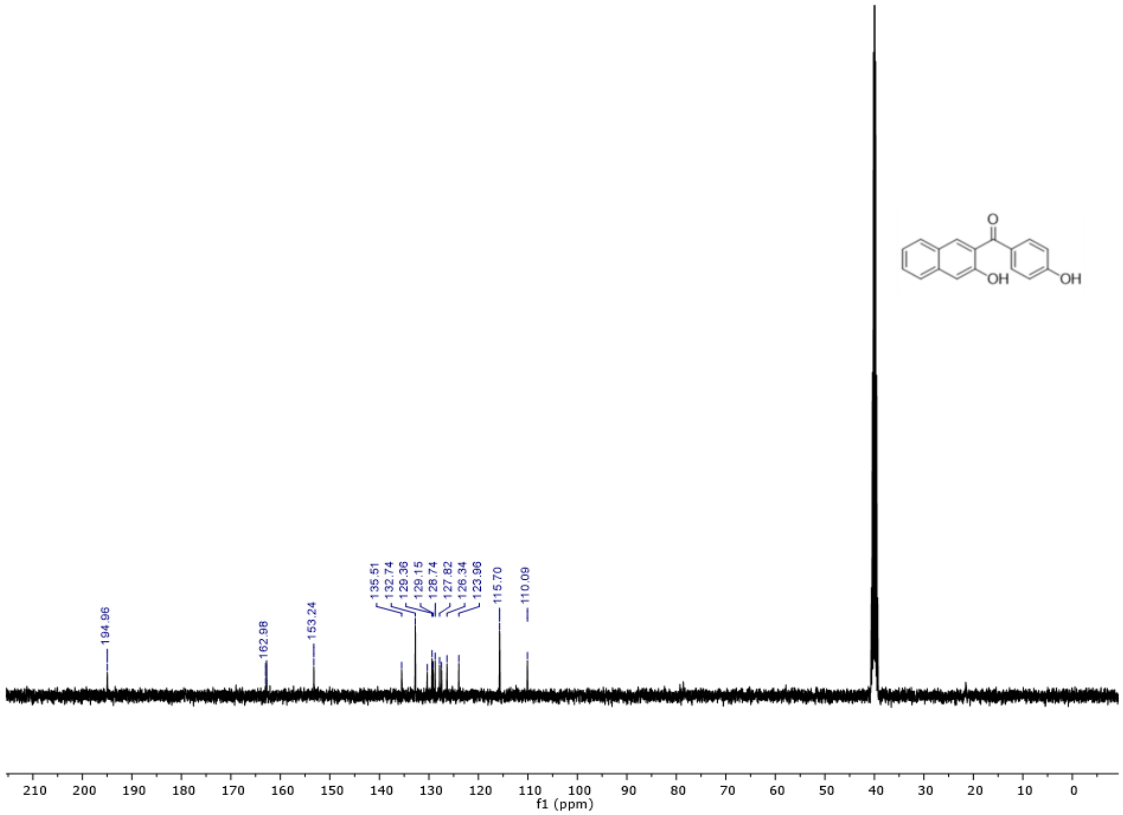
194.96
162.98
153.24
135.51
132.74
129.36
129.15
128.74
127.82
126.34
123.96
115.70
110.09
f1 (ppm)

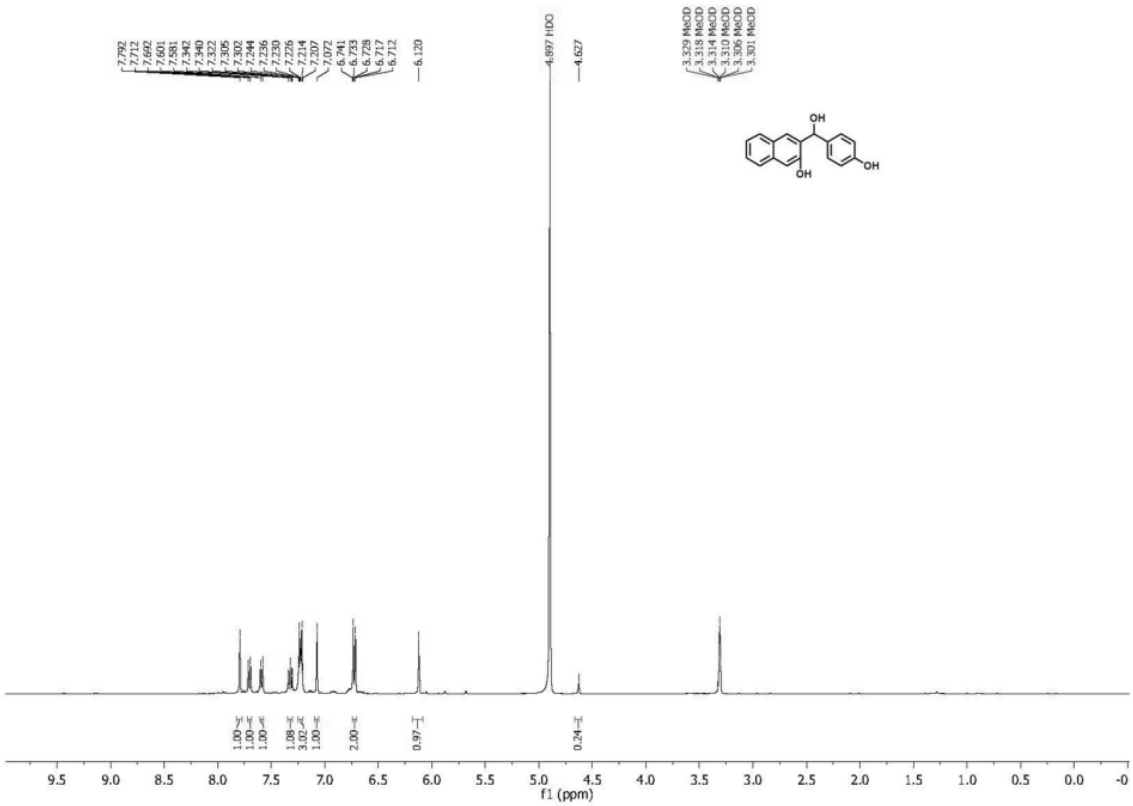
7.792
7.712
7.692
7.601
7.581
7.342
7.340
7.322
7.305
7.302
7.244
7.236
7.230
7.226
7.214
7.207
7.072
6.741
6.733
6.728
6.717
6.712
6.120
4.897 HDO
4.627
3.329 MeOD
3.318 MeOD
3.314 MeOD
3.310 MeOD
3.306 MeOD
3.301 MeOD
1.00
1.00
1.00
1.08
3.02
1.00
2.00
0.97
0.24
f1 (ppm)

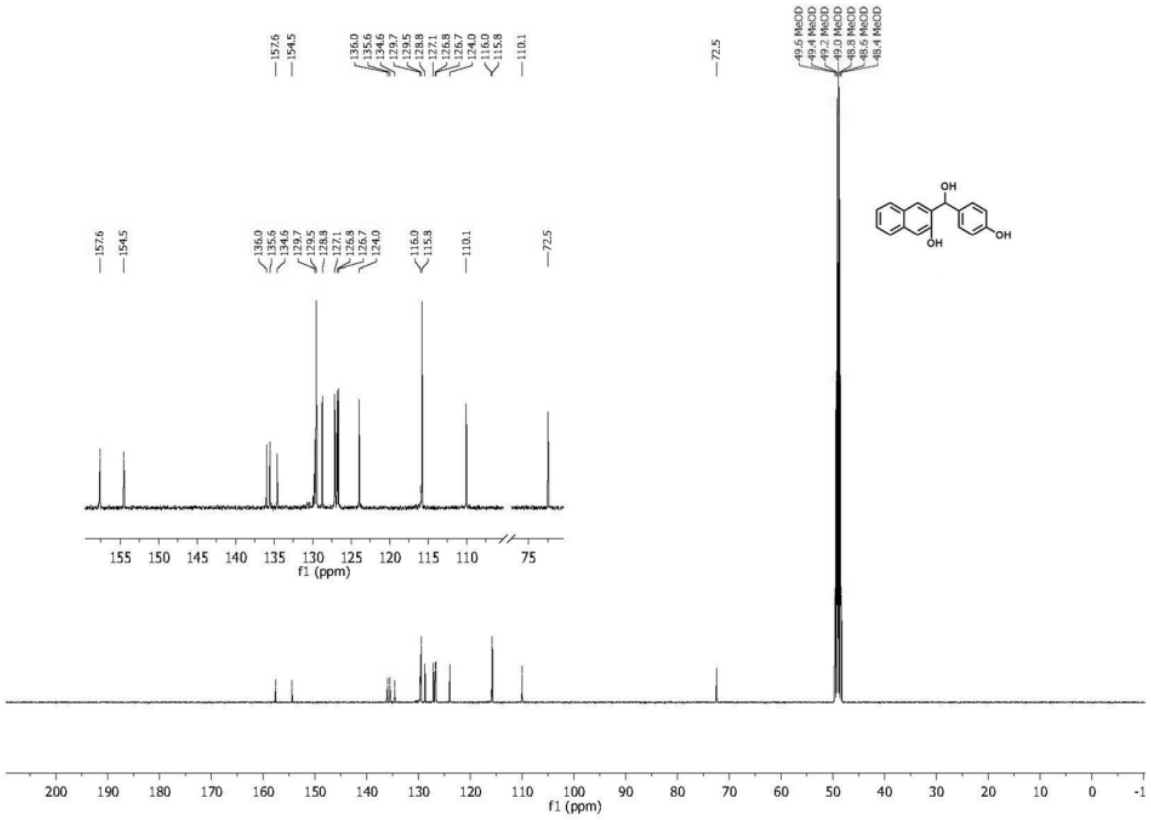
157.6
154.5
136.0
135.6
134.6
129.7
129.5
128.8
127.1
126.8
126.7
124.0
116.0
115.8
110.1
72.5
49.5 MeOD
49.4 MeOD
49.2 MeOD
49.0 MeOD
48.8 MeOD
48.6 MeOD
48.4 MeOD
OH
OH
OH
f1 (ppm)
f1 (ppm)

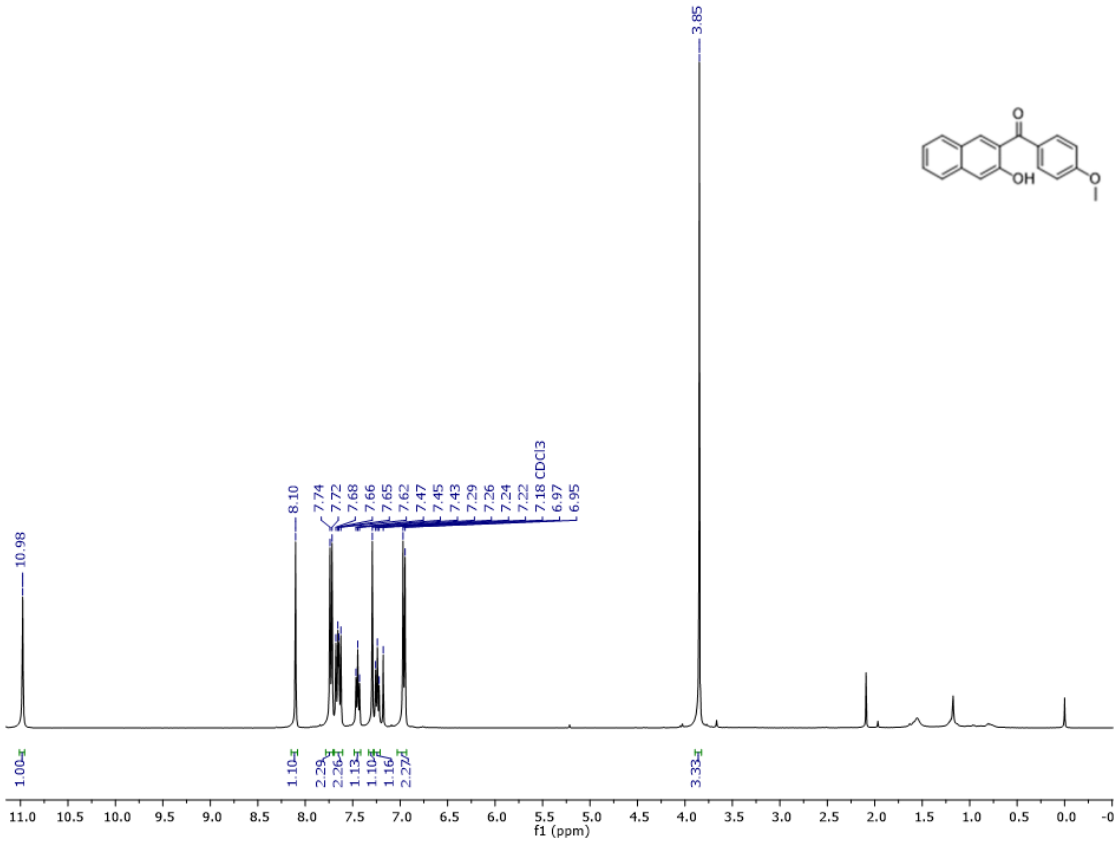
3.85
10.98
8.10
7.74
7.72
7.68
7.66
7.65
7.62
7.47
7.45
7.43
7.29
7.26
7.24
7.22
7.18 CDCl3
6.97
6.95
1.00
1.10
2.29
2.26
1.13
1.10
1.16
2.27
3.33
f1 (ppm)

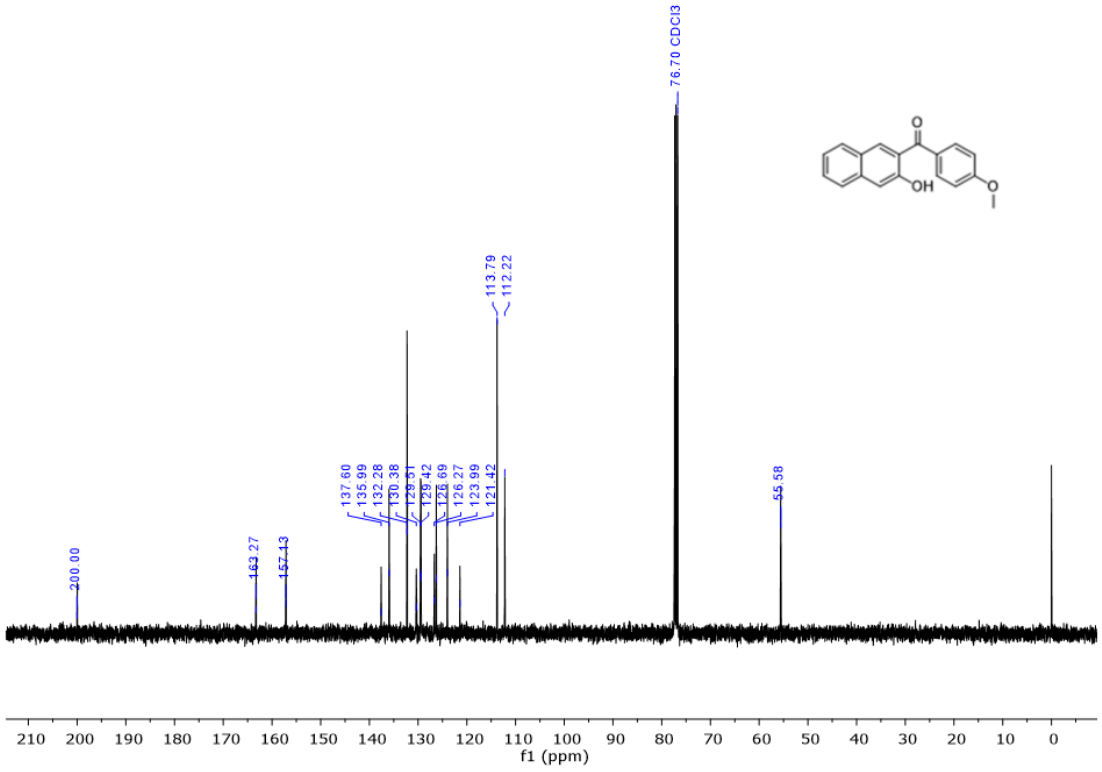
76.70 CDCl3
113.79
112.22
137.60
135.99
132.28
130.38
129.51
129.42
126.69
126.27
123.99
121.42
55.58
200.00
163.27
157.13
f1 (ppm)

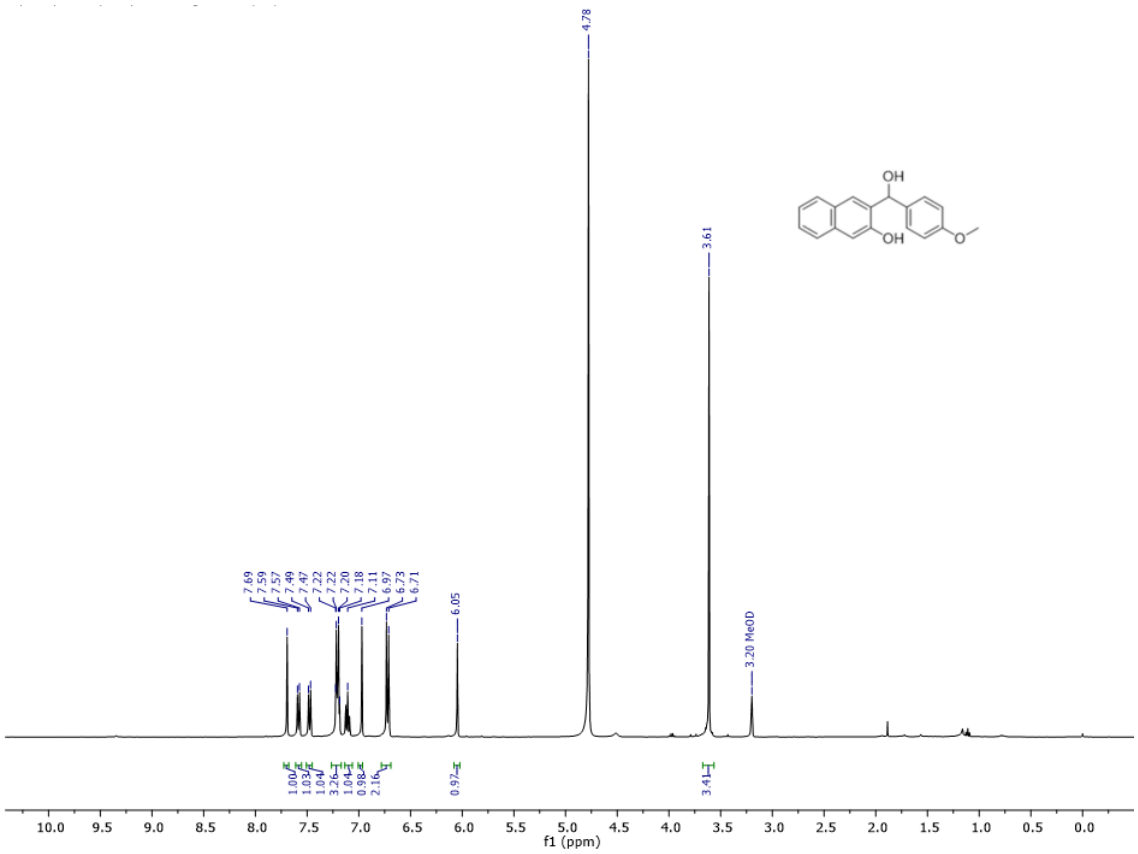
4.78
3.61
3.20 MeOD
6.05
7.69
7.59
7.57
7.49
7.47
7.22
7.22
7.20
7.18
7.11
6.97
6.73
6.71
OH
OH
O
1.00
1.03
1.04
3.26
1.04
0.98
2.16
0.97
3.41
10.0 9.5 9.0 8.5 8.0 7.5 7.0 6.5 6.0 5.5 5.0 4.5 4.0 3.5 3.0 2.5 2.0 1.5 1.0 0.5 0.0
f1 (ppm)

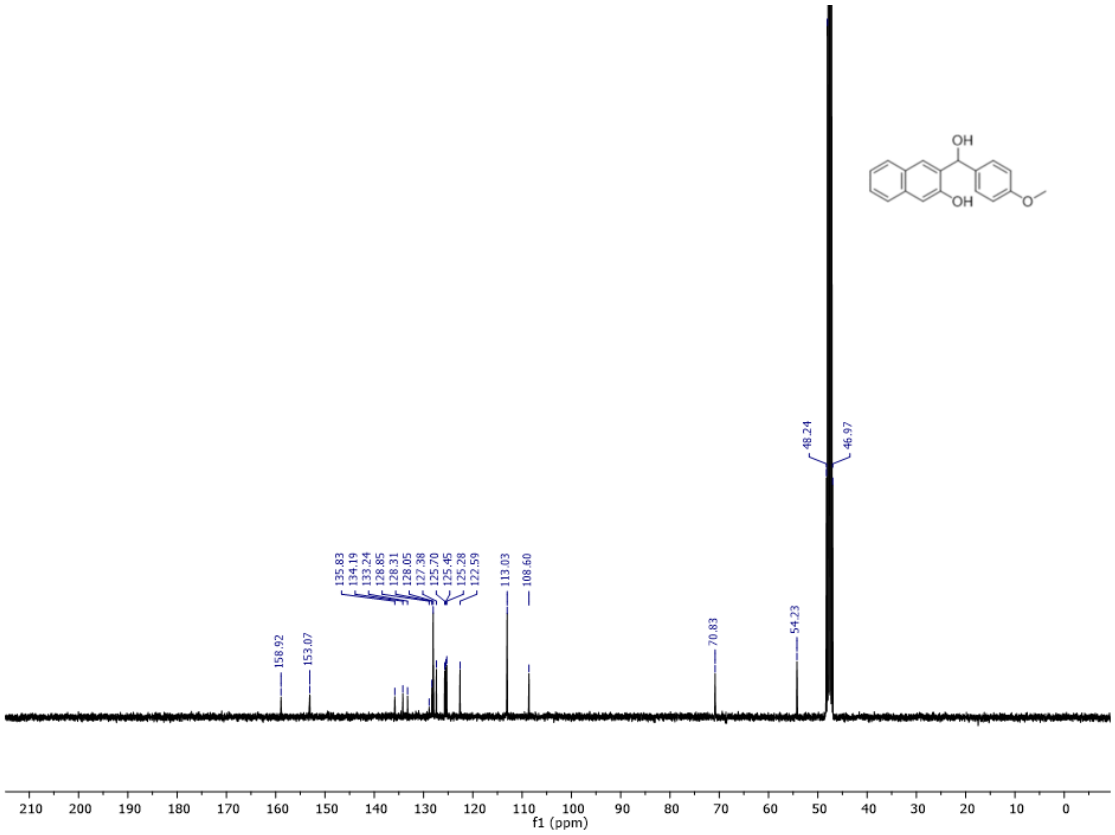
OH
OH
O
158.92
153.07
135.83
134.19
133.24
128.85
128.31
128.05
127.38
125.70
125.45
125.28
122.59
113.03
108.60
70.83
54.23
48.24
46.97
f1 (ppm)

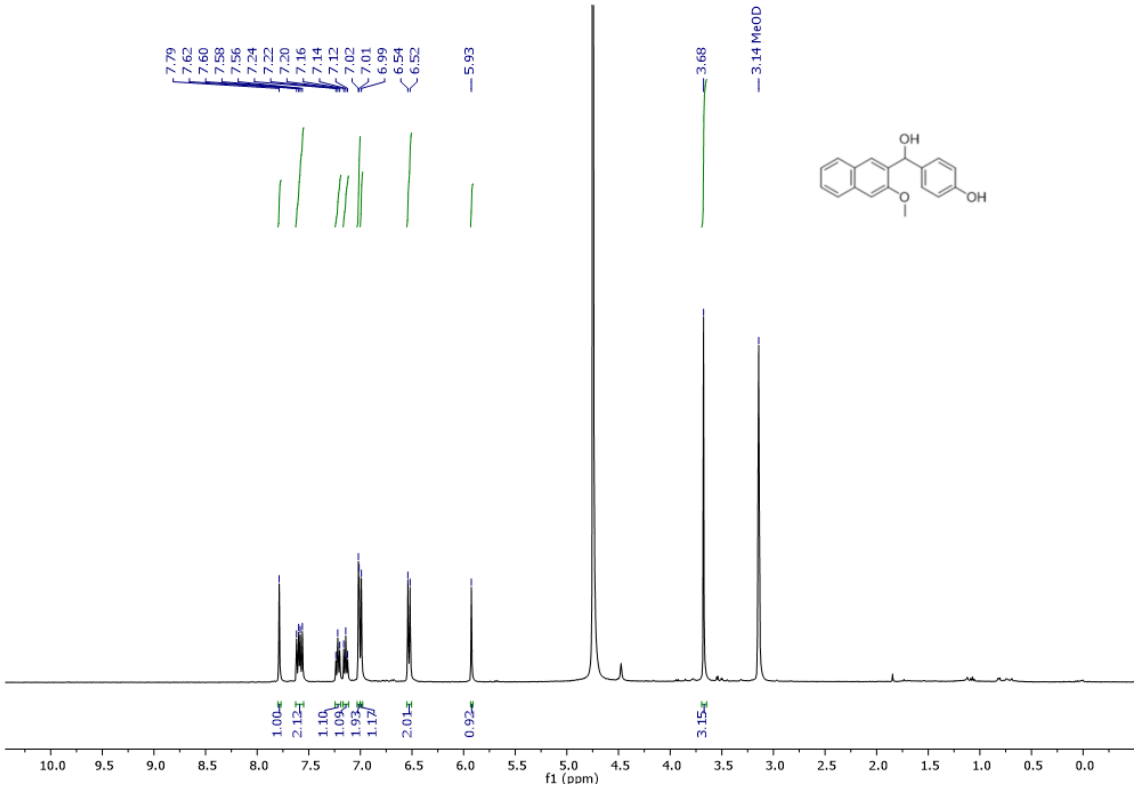
7.79
7.62
7.60
7.58
7.56
7.24
7.22
7.20
7.16
7.14
7.12
7.02
7.01
6.99
6.54
6.52
5.93
3.68
3.14 MeOD
OH
OH
O
1.00
2.12
1.10
1.05
1.93
1.17
2.01
0.92
3.15
f1 (ppm)

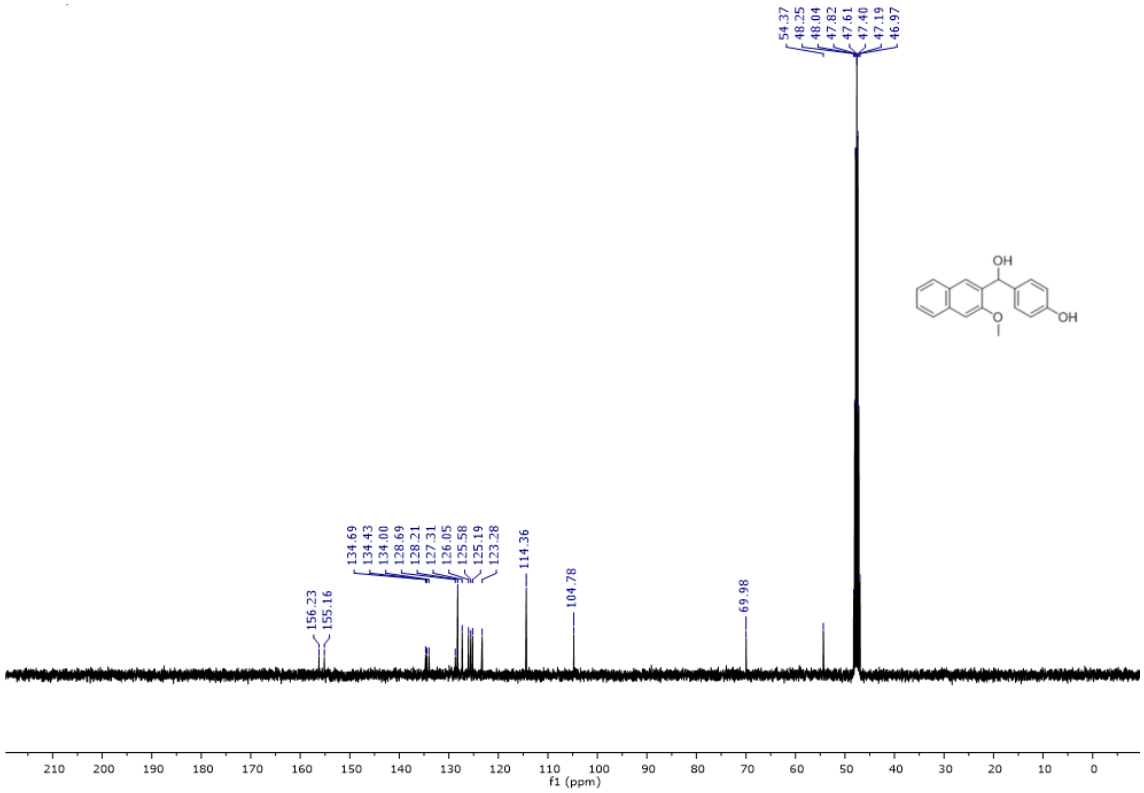
54.37
48.25
48.04
47.82
47.61
47.40
47.19
46.97
OH
OH
O
134.69
134.43
134.00
128.69
128.21
127.31
126.05
125.58
125.19
123.28
114.36
104.78
69.98
156.23
155.16
210 200 190 180 170 160 150 140 130 120 110 100 90 80 70 60 50 40 30 20 10 0
f1 (ppm)

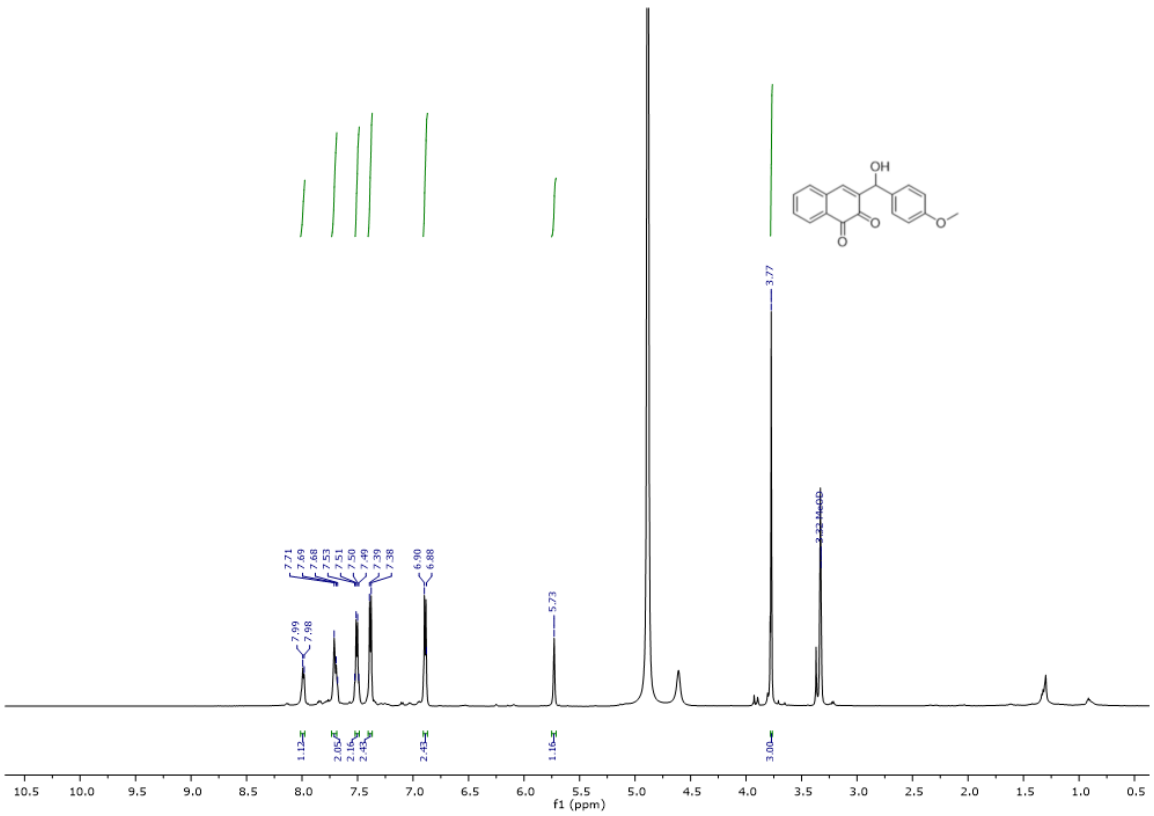
OH
O
O
3.77
7.71
7.69
7.68
7.53
7.51
7.50
7.49
7.39
7.38
6.90
6.88
7.99
7.98
5.73
1.13
2.05
2.16
2.43
2.43
1.16
3.00
10.5 10.0 9.5 9.0 8.5 8.0 7.5 7.0 6.5 6.0 5.5 5.0 4.5 4.0 3.5 3.0 2.5 2.0 1.5 1.0 0.5
f1 (ppm)

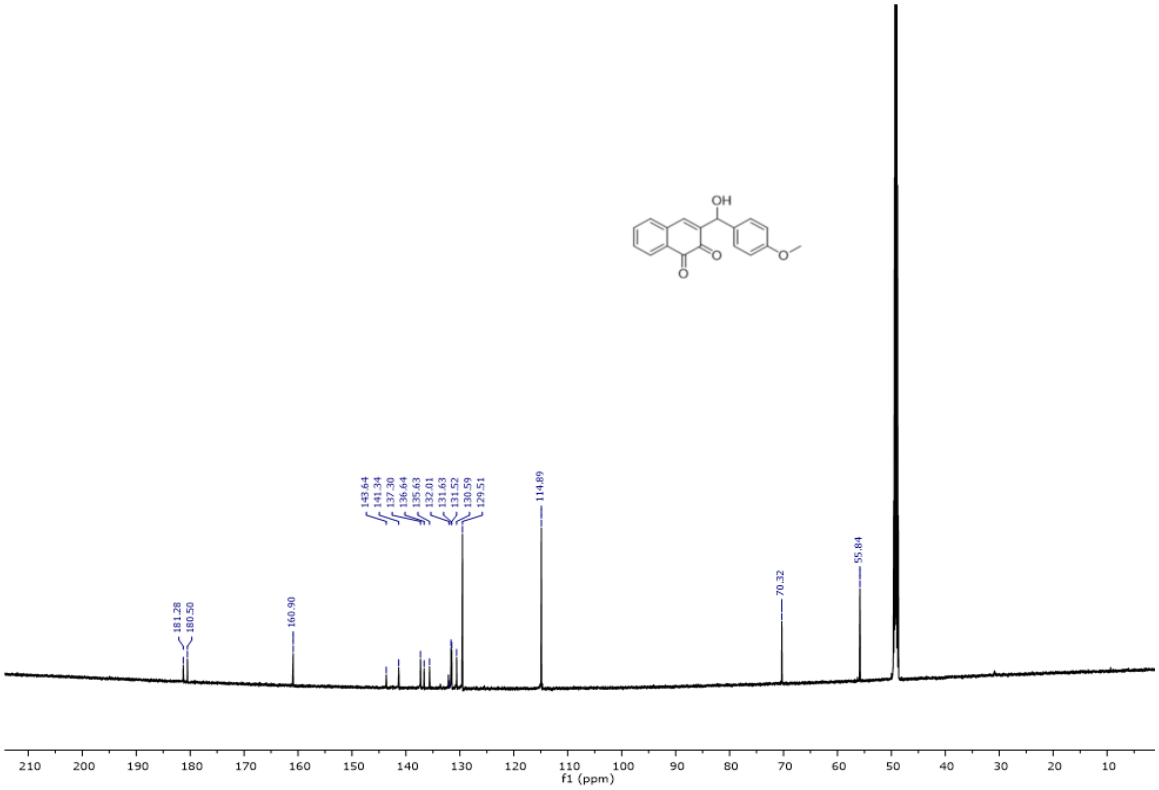
OH
O
O
O
143.64
141.34
137.30
136.64
135.63
132.01
131.68
131.52
130.59
129.51
114.89
70.32
55.84
181.28
180.50
160.90
210 200 190 180 170 160 150 140 130 120 110 100 90 80 70 60 50 40 30 20 10
f1 (ppm)

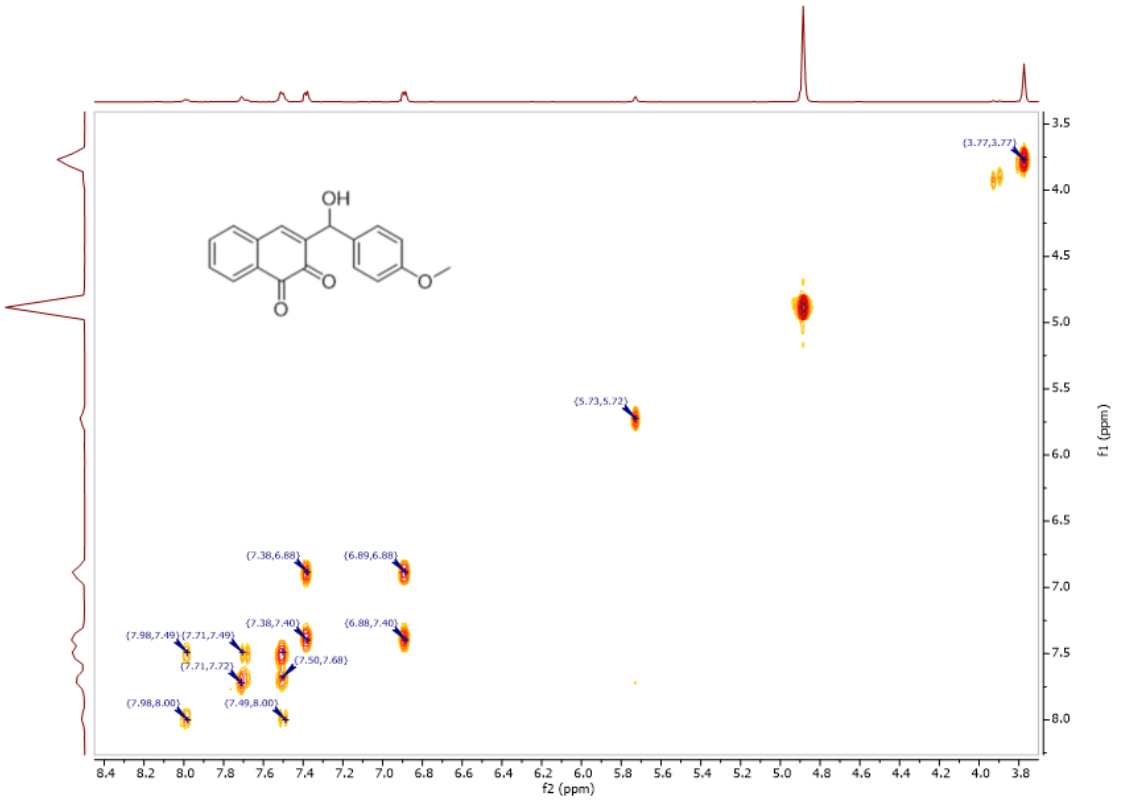
OH
O
O
{3.77,3.77}
{5.73,5.72}
{7.38,6.88}
{6.89,6.88}
{7.38,7.40}
{6.88,7.40}
{7.98,7.49}
{7.71,7.49}
{7.71,7.72}
{7.50,7.68}
{7.98,8.00}
{7.49,8.00}
3.5
4.0
4.5
5.0
5.5
6.0
6.5
7.0
7.5
8.0
f1 (ppm)
8.4 8.2 8.0 7.8 7.6 7.4 7.2 7.0 6.8 6.6 6.4 6.2 6.0 5.8 5.6 5.4 5.2 5.0 4.8 4.6 4.4 4.2 4.0 3.8
f2 (ppm)

C

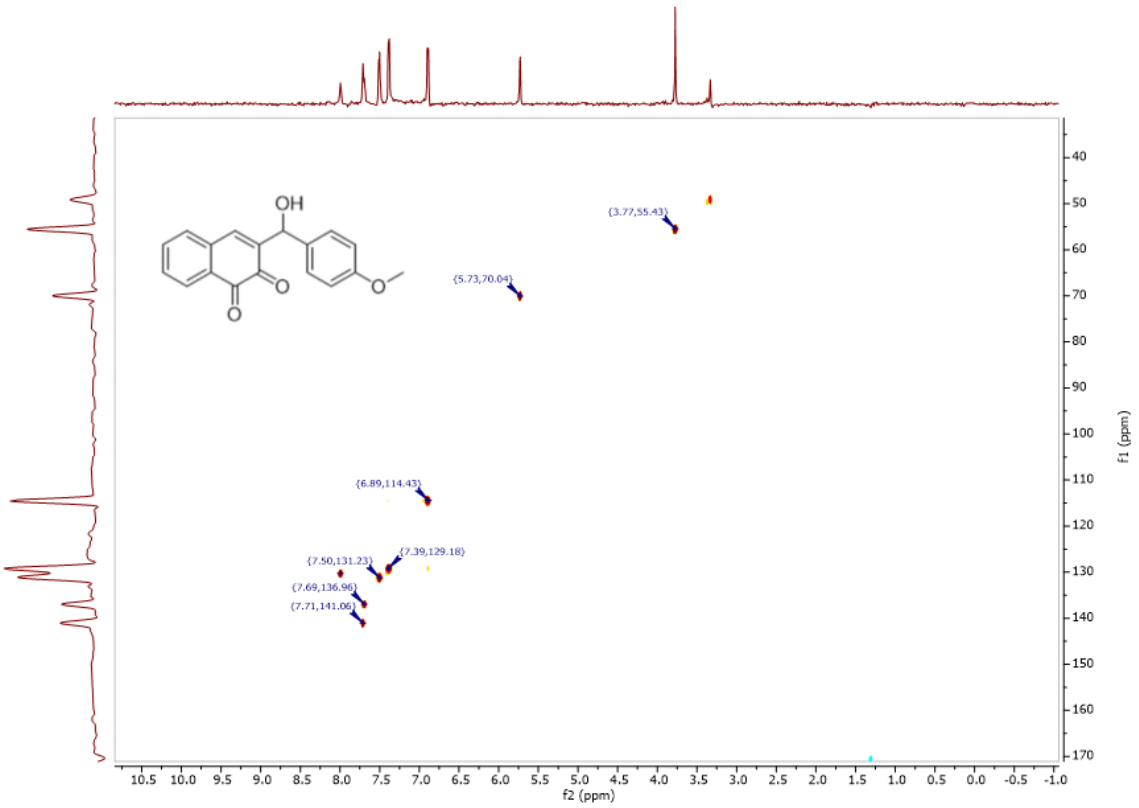
OH
O
O
O
{3.77,55.43}
{5.73,70.04}
{6.89,114.43}
{7.50,131.23}
{7.39,129.18}
{7.69,136.96}
{7.71,141.06}
f2 (ppm)
f1 (ppm)

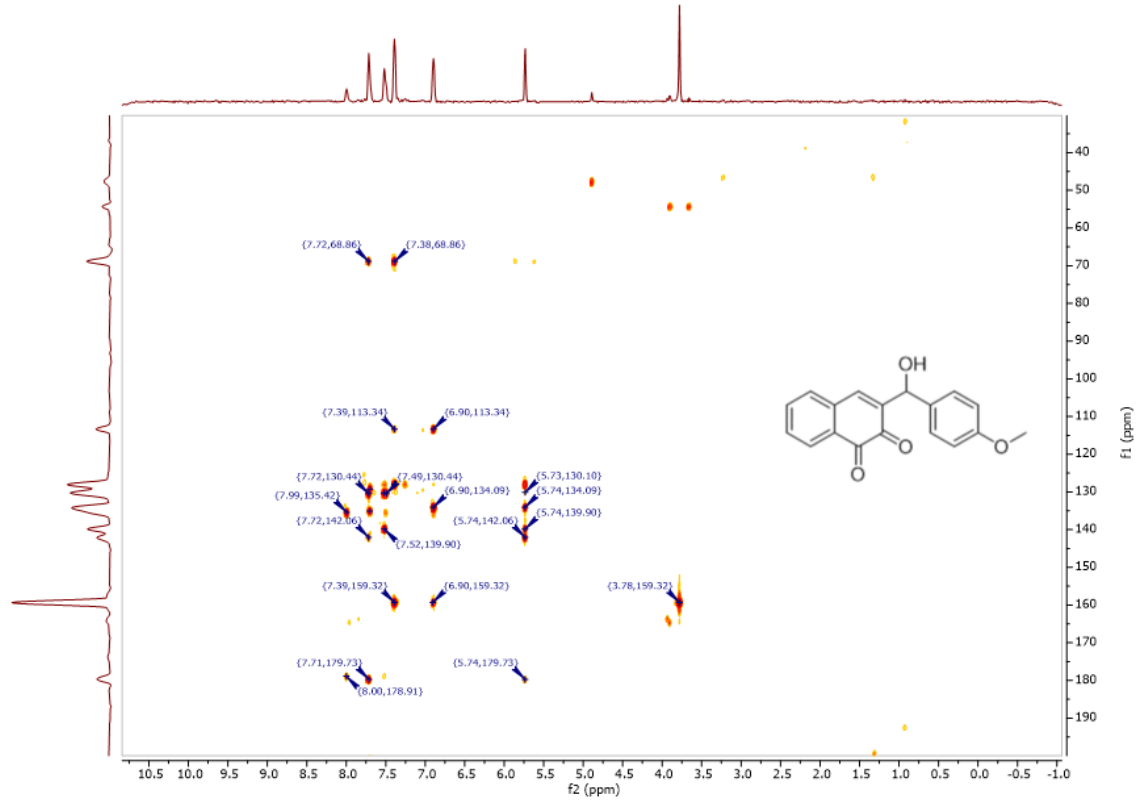
{7.72,68.86}
{7.38,68.86}
{7.39,113.34}
{6.90,113.34}
{7.72,130.44}
{7.49,130.44}
{5.73,130.10}
{7.99,135.42}
{6.90,134.09}
{5.74,134.09}
{7.72,142.06}
{5.74,142.06}
{5.74,139.90}
{7.52,139.90}
{7.39,159.32}
{6.90,159.32}
{3.78,159.32}
{7.71,179.73}
{5.74,179.73}
{8.00,178.91}
OH
O
O
f2 (ppm)
f1 (ppm)

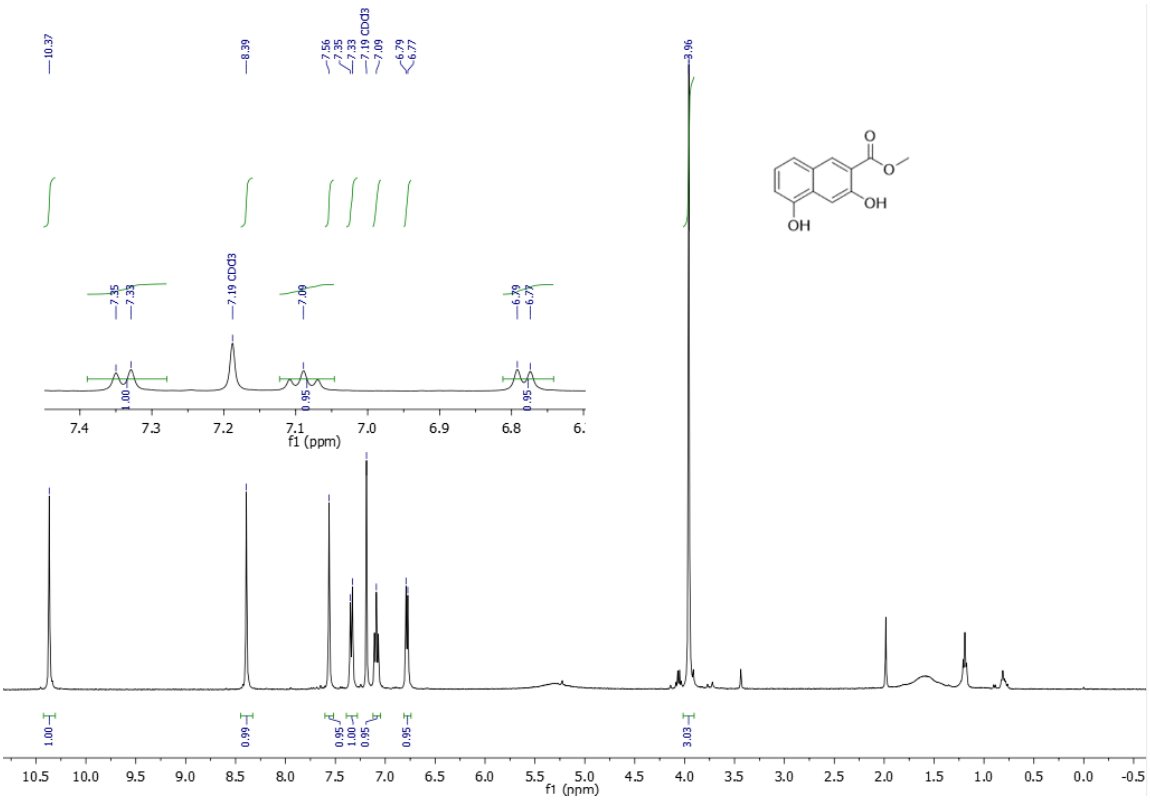
10.37
8.39
7.56
7.35
7.33
7.19 CDCl3
7.09
6.79
6.77
3.96
O
O
OH
OH
f1 (ppm)
f1 (ppm)

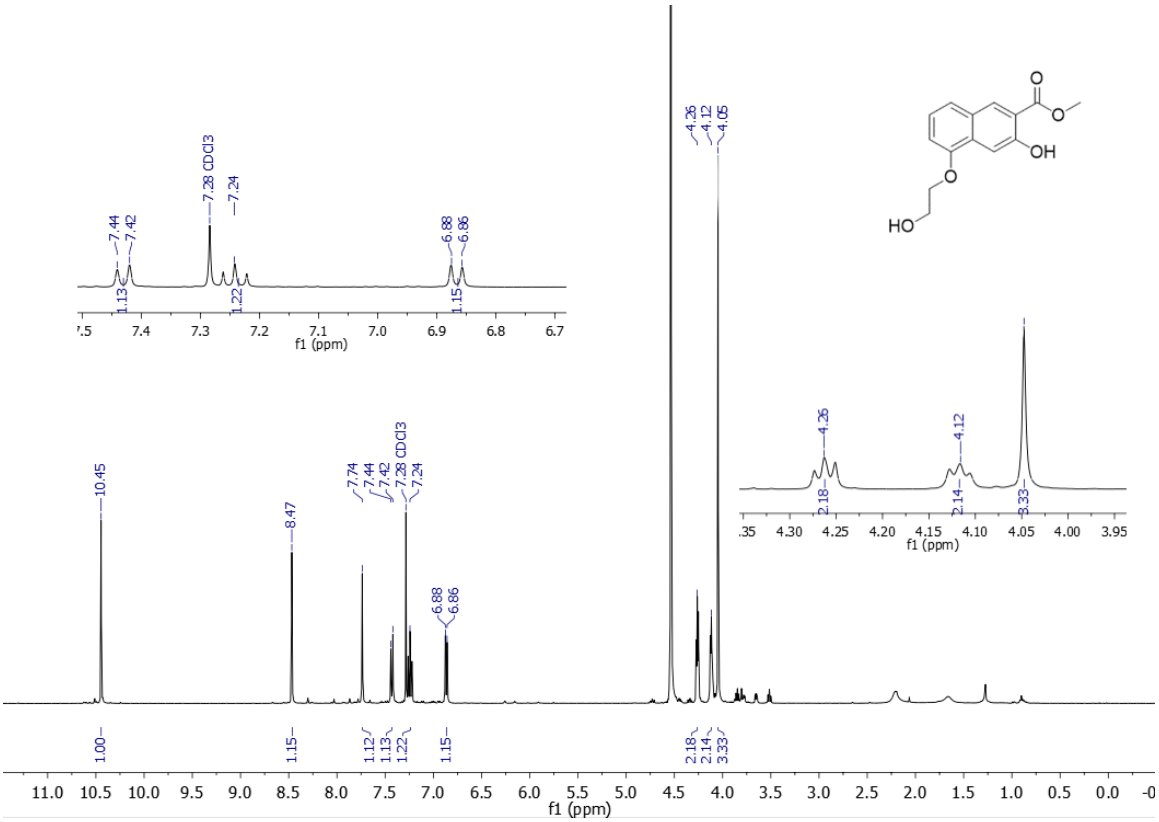
4.26
4.12
4.05
7.44
7.42
7.28 CDCl3
7.24
6.88
6.86
O
O
OH
HO
10.45
8.47
7.74
7.44
7.42
7.28 CDCl3
7.24
6.88
6.86
f1 (ppm)
f1 (ppm)

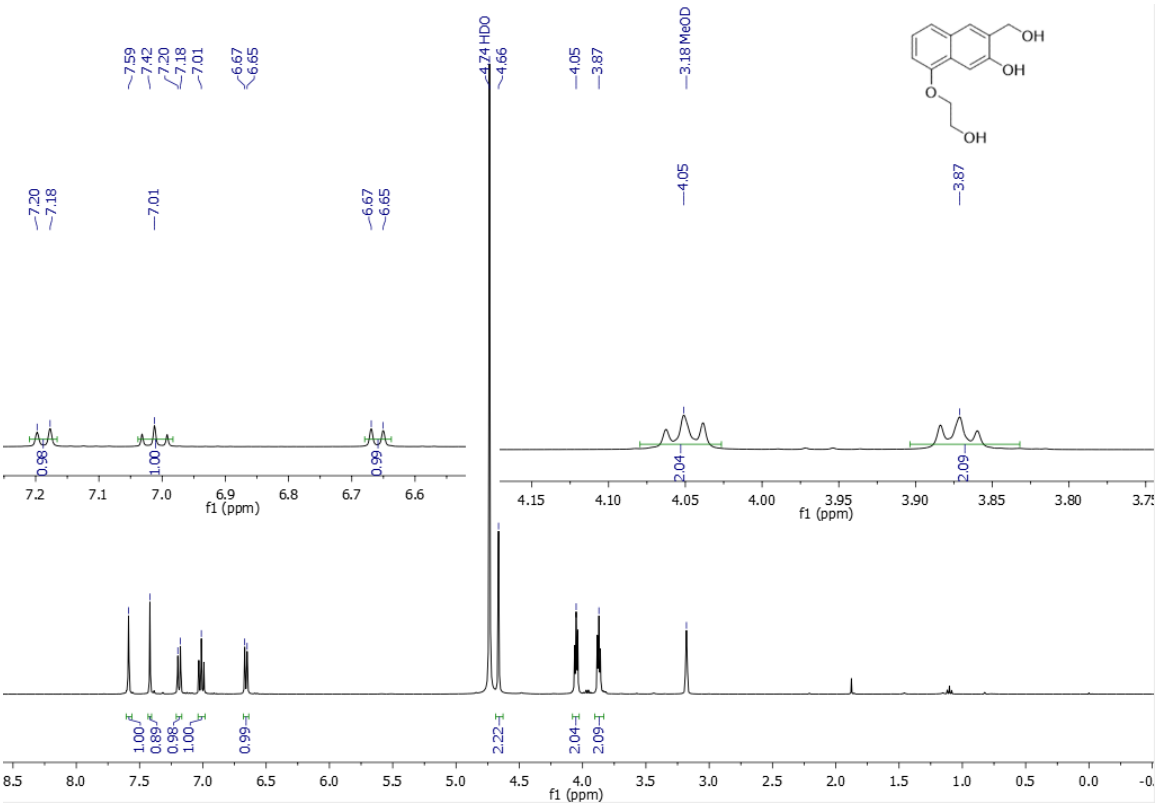
7.59
7.42
7.20
7.18
7.01
6.67
6.65
4.74 HDO
4.66
4.05
3.87
3.18 MeOD
OH
OH
O
OH
f1 (ppm)

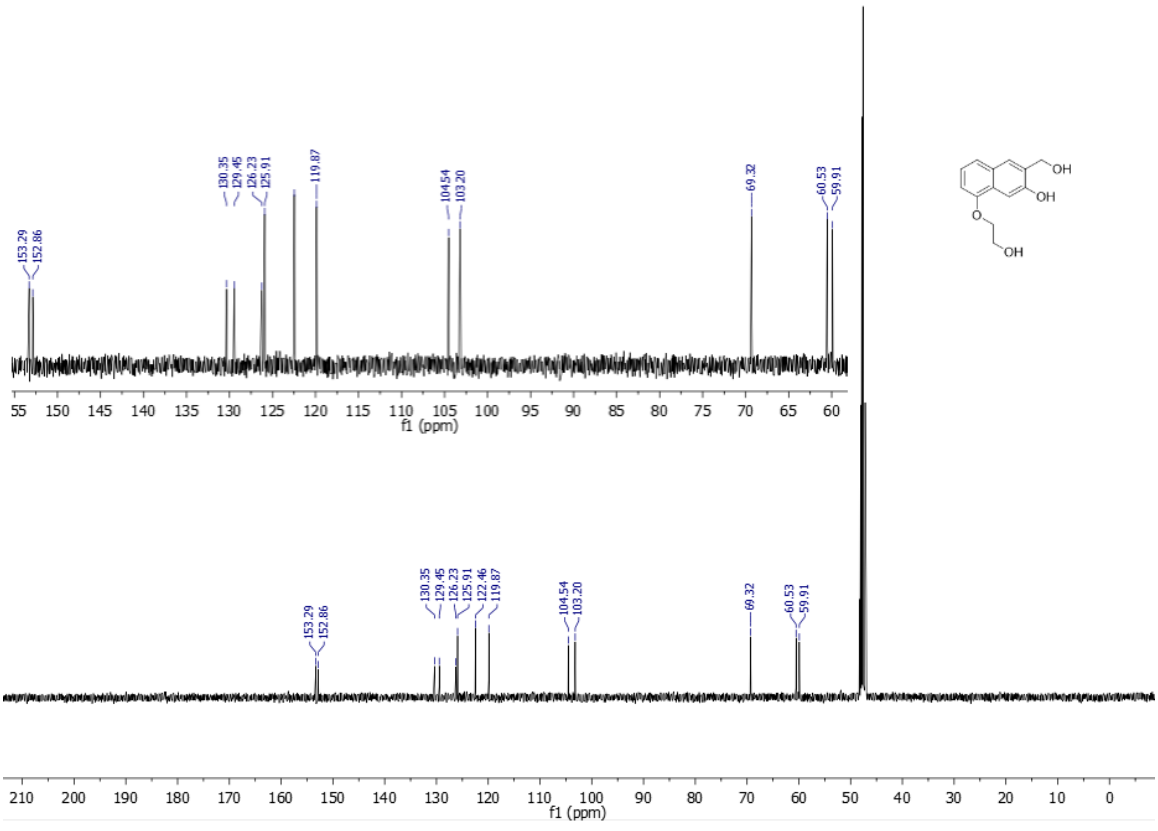
153.29
152.86
130.35
129.45
126.23
125.91
119.87
104.54
103.20
69.32
60.53
59.91
OH
OH
O
OH
f1 (ppm)

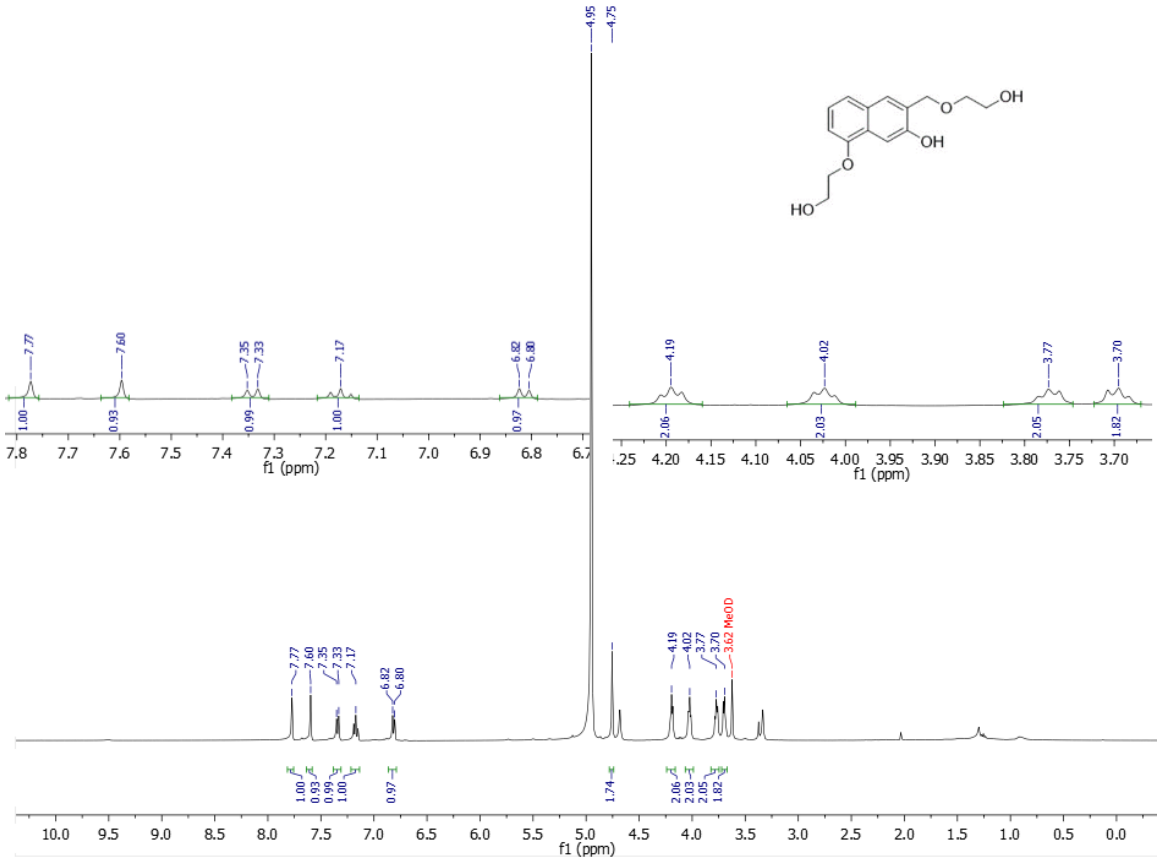
OH
OH
O
O
HO
4.95
4.75
7.77
7.60
7.35
7.33
7.17
6.82
6.80
4.19
4.02
3.77
3.70
3.62 MeOD
f1 (ppm)

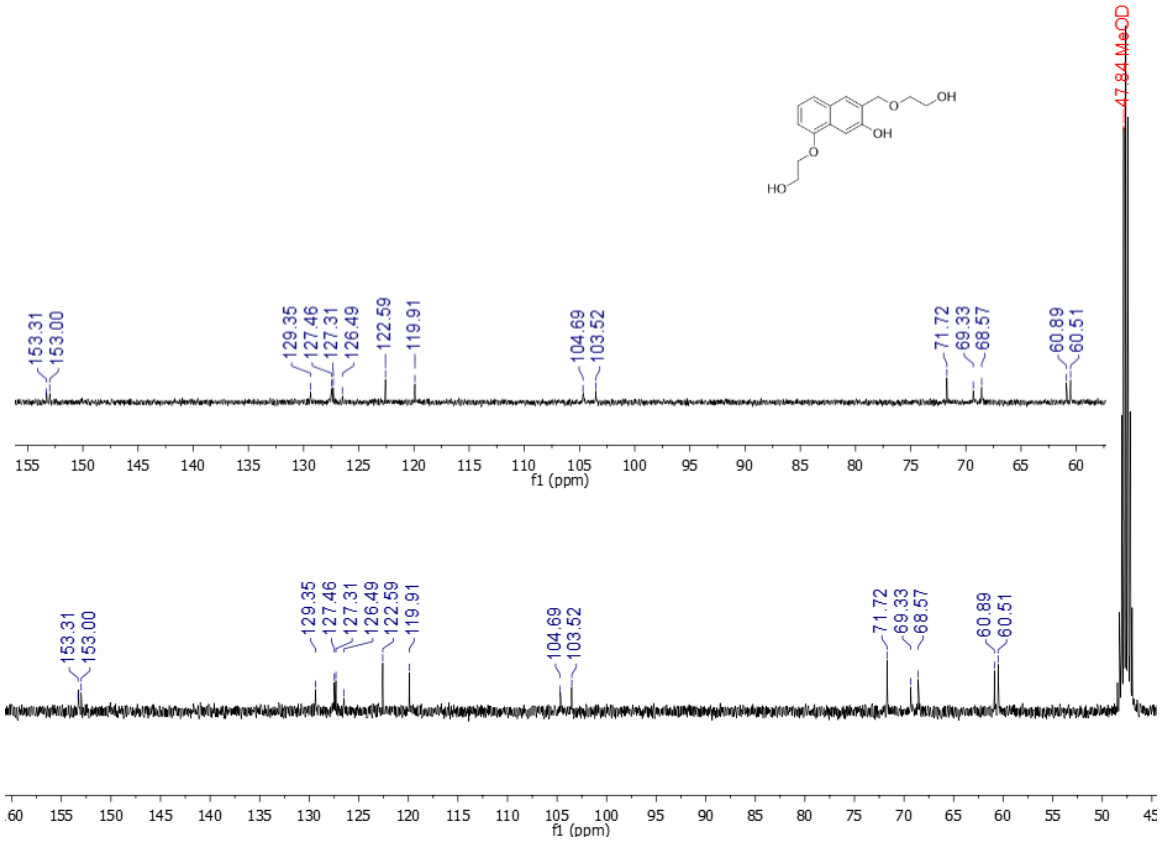
47.84 MeOD
153.31
153.00
129.35
127.46
127.31
126.49
122.59
119.91
104.69
103.52
71.72
69.33
68.57
60.89
60.51
f1 (ppm)
OH
OH
HO

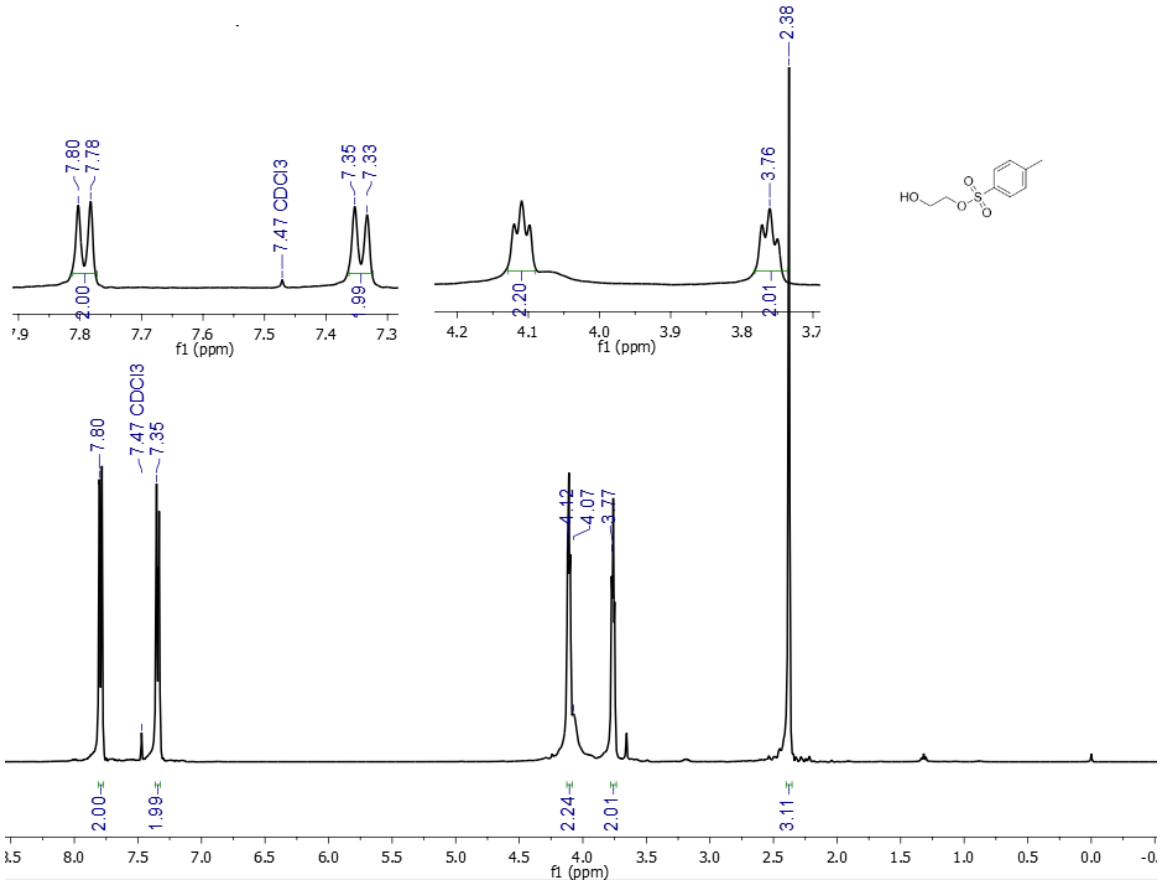
7.80
7.78
7.47 CDCl3
7.35
7.33
2.38
3.76
HO
2.00
2.20
2.01
1.99
f1 (ppm)
7.80
7.47 CDCl3
7.35
4.12
4.07
3.77
2.00
1.99
2.24
2.01
3.11
f1 (ppm)

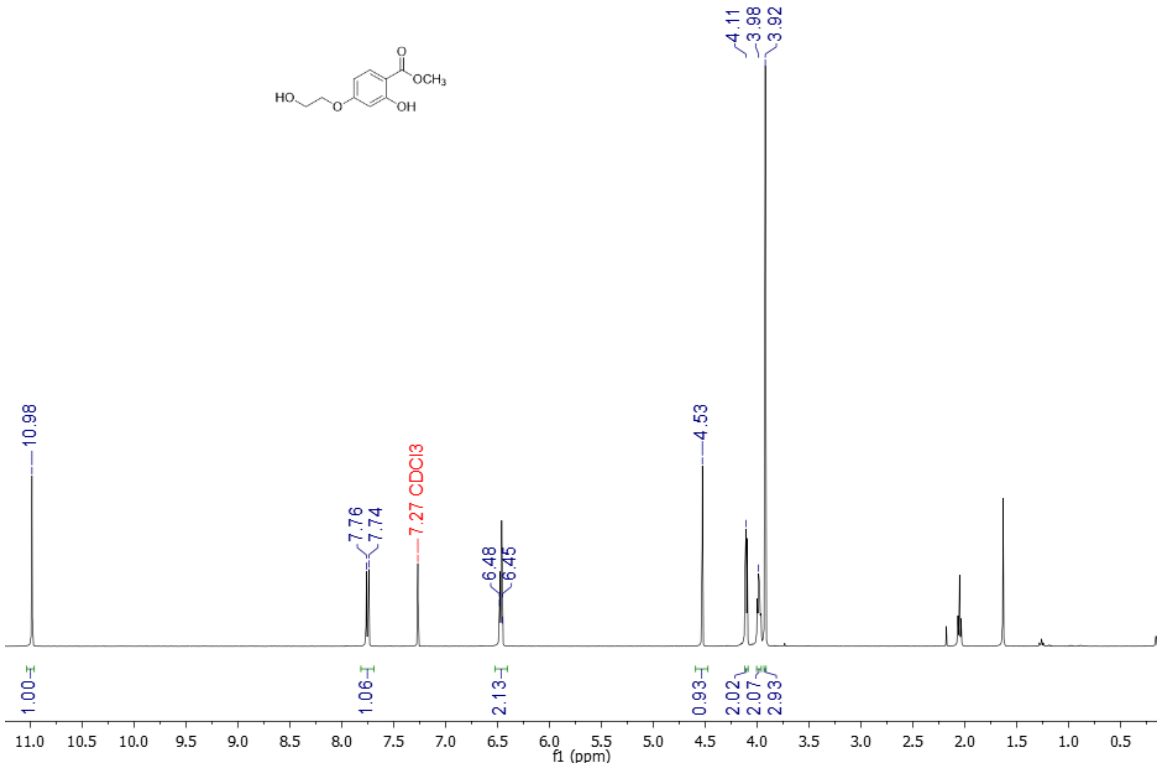
HO
O
O
OCH3
OH
10.98
7.76
7.74
7.27 CDCl3
6.48
6.45
4.53
4.11
3.98
3.92
1.00
1.06
2.13
0.93
2.02
2.07
2.93
11.0 10.5 10.0 9.5 9.0 8.5 8.0 7.5 7.0 6.5 6.0 5.5 5.0 4.5 4.0 3.5 3.0 2.5 2.0 1.5 1.0 0.5
f1 (ppm)

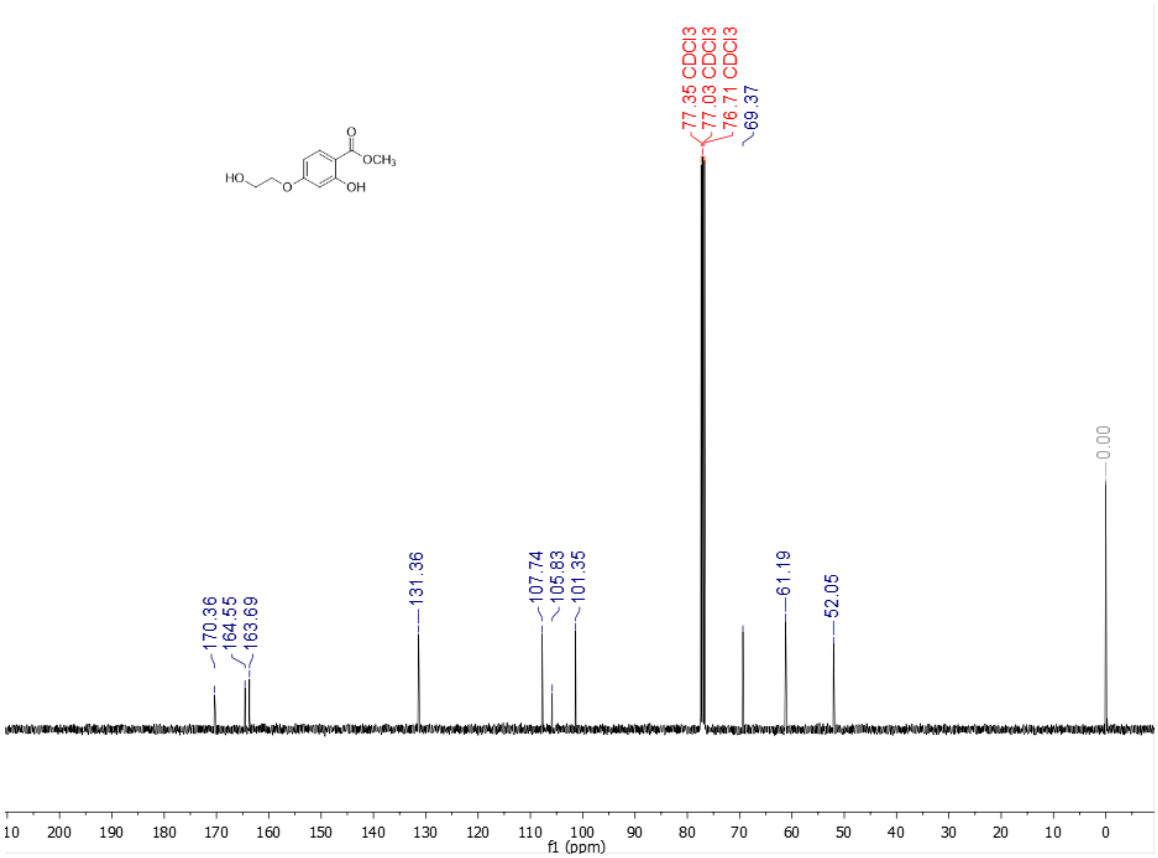
77.35 CDCl3
77.03 CDCl3
76.71 CDCl3
69.37
0.00
170.36
164.55
163.69
131.36
107.74
105.83
101.35
61.19
52.05
f1 (ppm)

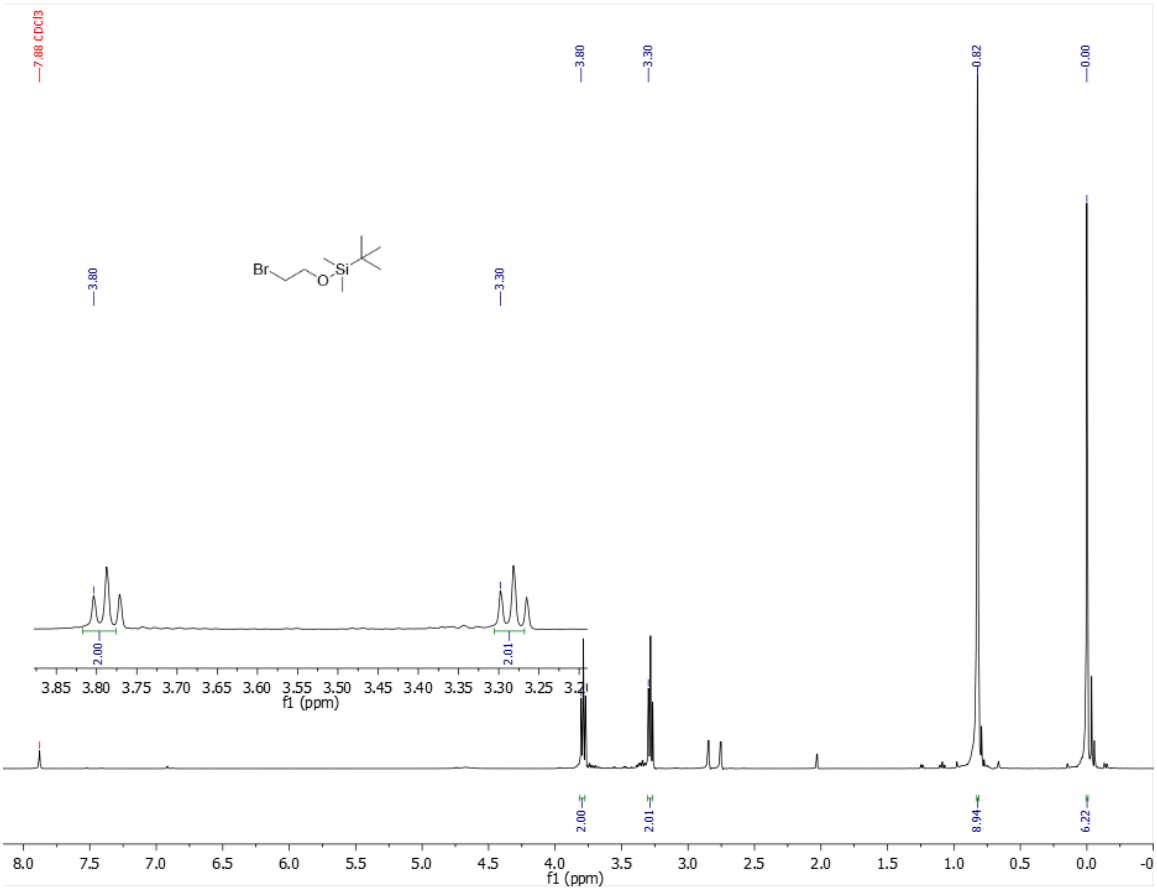
7.88 CDCl3
3.80
3.30
0.82
0.00
Br
O
Si
2.00
2.01
f1 (ppm)
8.94
6.22

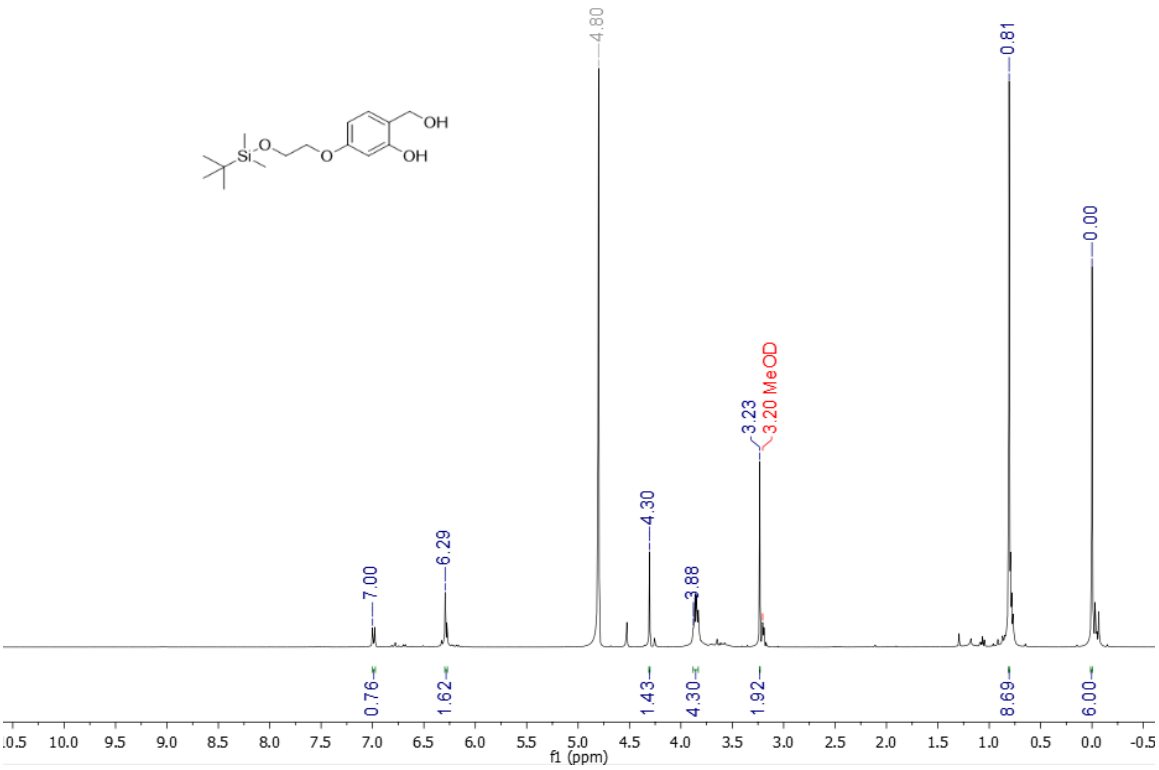
OH
OH
Si
O
O
4.80
0.81
0.00
3.23
3.20 MeOD
4.30
6.29
7.00
3.88
0.76
1.62
1.43
4.30
1.92
8.69
6.00
f1 (ppm)

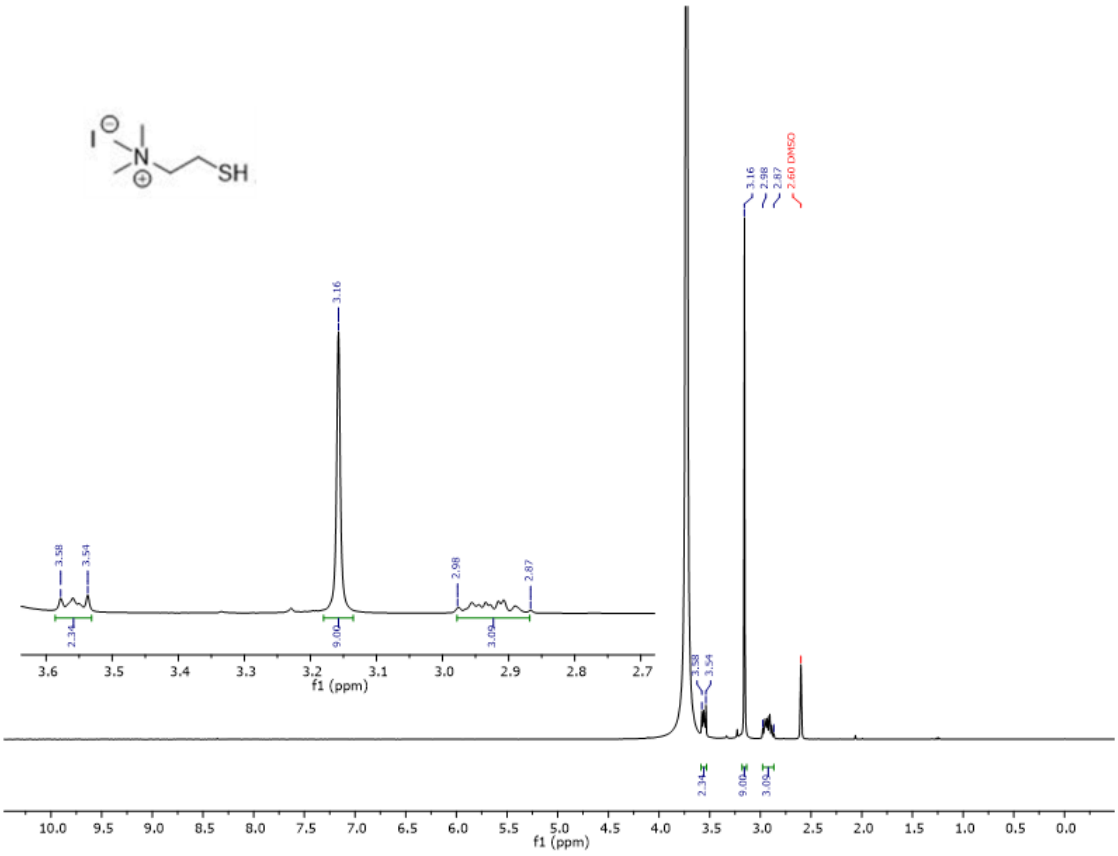
SH
3.58
3.54
3.16
2.98
2.87
2.34
9.00
3.09
f1 (ppm)
3.16
2.98
2.87
2.60 DMSO
2.34
9.00
3.09
f1 (ppm)

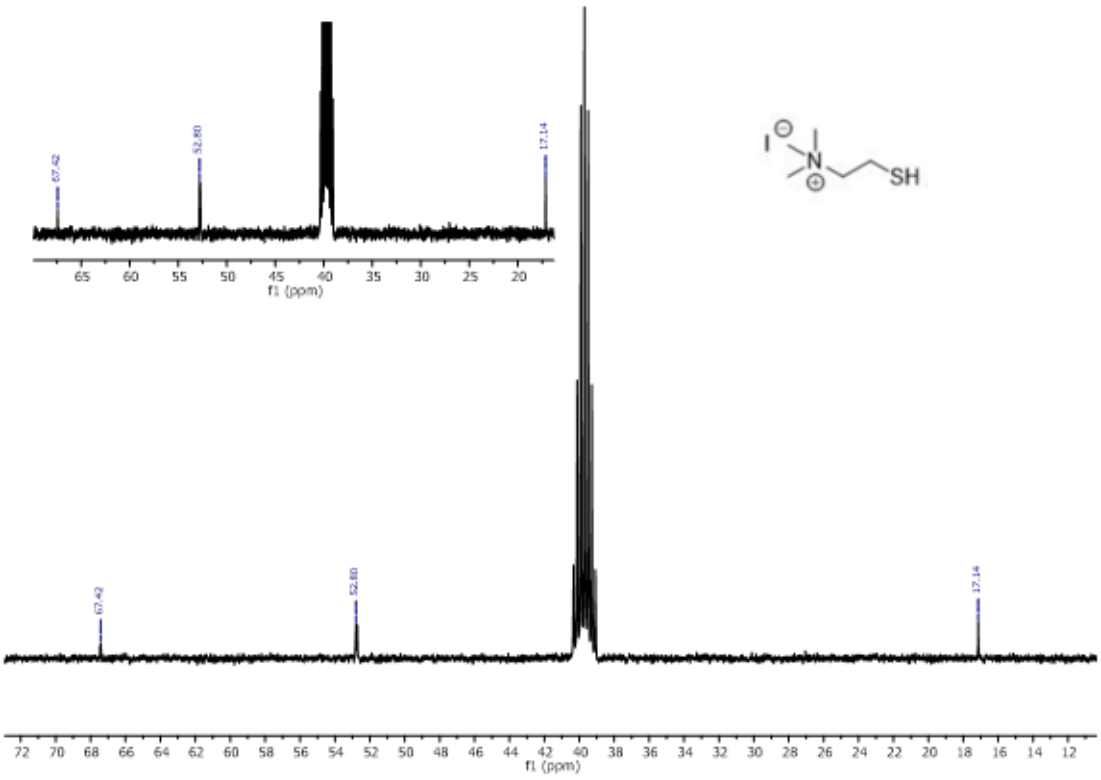
67.42
52.80
17.14
I
N
SH
f1 (ppm)